Universidade do Porto
Faculdade de Engenharia
FEUP

A General Framework for the Geomechanical Characterisation of Artificially Cemented Soil

Sara Rios da Rocha e Silva

Supervisor: António Viana da Fonseca

Co-supervisors: Nilo C. Consoli; Beatrice Baudet; Jorge Almeida e Sousa

A DISSERTATION SUBMITTED TO THE FACULTY OF ENGINEERING OF THE UNIVERSITY OF PORTO FOR THE DEGREE OF DOCTOR IN CIVIL ENGINEERING

DISSERTAÇÃO APRESENTADA À FACULDADE DE ENGENHARIA DA UNIVERSIDADE DO PORTO PARA A OBTENÇÃO DO GRAU DE DOUTOR EM ENGENHARIA CIVIL

SETEMBRO 2011

“The excellent map
misses no detail, but it is
as large as the world.”

Muir Wood (2004)

ABSTRACT

Artificially cemented soils are frequently used in line works for road and railway platforms to improve the natural characteristics of the soil. The mixture of Portland cement with soil has been used since the beginning of the last century, and it has become actual due to the progressive lack of natural materials and to account for environmental issues. However, conversely to concrete, the absence of a rational methodology leads to an empirical application of this technique. Moreover, their long term performance is often questioned especially, when subjected to transient loads.

The study of these mixtures in the laboratory enables the understanding of natural structured soils as well as defines the conditions in which artificially cemented soils can be used successfully in the field. In this work, an extensive laboratory program was developed to define a general framework for the comprehensive knowledge of an artificially cemented soil. For that purpose, a silty sand obtained by the weathered Porto granite and widely abundant in the north and central region of Portugal was selected. Since there was no experience in the use of this soil mixed with Portland cement to perform laboratory tests, the work has developed from very simple tests to more sophisticated experiments, and so, the cyclic characteristics of this material were evaluated after establishing the framework of the static behaviour. The experimental program comprised some preliminary tests from unconfined compression tests to seismic wave measurements; static triaxial tests at low and high pressures performed; as well as cyclic triaxial tests.

The performance of the porosity/cement ratio (n/C_{iv}) on the evaluation of some important features of these mixtures, such as compressive and tensile strength or dynamic and static stiffness, is one of the analysed issues. The results of the static triaxial tests were interpreted within the Critical State theory and, consequently, some topics are discussed such as the definition of the normal compression line and critical state line for uncemented and cemented specimens. The validity of the european standard for cyclic tests, developed for unbound materials, to study this cemented soil is also analysed, and then, the behaviour in long term conditions is characterised through cyclic tests with a great number of cycles. Finally, the results of the previous tests were used to calibrate a constitutive model for cemented soils, presenting the advantages and limitations of that model in the simulation of these mixtures behaviour.

RESUMO

Solos artificialmente cimentados são frequentemente usados em obras de linha para plataformas de estradas e de caminhos de ferro. A mistura de cimento Portland com solo tem sido usada desde o início do século passado, tendo-se tornado ainda mais actual com a escassez progressiva de materiais naturais, bem como por razões ambientais. No entanto, ao contrário do betão, a falta de uma metodologia racional levou a uma utilização empírica desta técnica. Por outro lado, o seu comportamento a longo prazo é frequentemente questionado, especialmente quando sujeito a passagens sucessivas.

O estudo destas misturas em laboratório permite compreender materiais naturais estruturados como também definir as condições em que solos artificialmente cimentados devem ser aplicados no terreno. Neste trabalho, um vasto programa laboratorial foi desenvolvido com vista à definição de um modelo geral de comportamento de um solo artificialmente cimentado. Nesse sentido, o solo residual do Porto, nas suas condições remoldadas, foi seleccionado por ser um solo bastante abundante na zona norte e centro de Portugal. Como não havia experiência no ensaio laboratorial de misturas deste solo com cimento, o trabalho partiu de ensaios muito simples para outros mais sofisticados e, da mesma forma, as suas características cíclicas só foram avaliadas depois de definido o modelo de comportamento em condições estáticas. O programa experimental inclui ensaios preliminares, desde ensaios à compressão simples até medições de ondas sísmicas, ensaios triaxiais estáticos a baixas e altas pressões, bem como ensaios cíclicos.

Uma das questões analisadas é a utilização do índice porosidade/cimento (n/C_{iv}) para o estudo de algumas importantes características destas misturas como a resistência à compressão e à tracção, ou a rigidez dinâmica e estática. Os resultados dos ensaios triaxiais estáticos foram interpretados através da teoria do Estado Crítico, discutindo-se, entre outros tópicos, a definição da linha de compressão normal e da linha de estado critico para o solo cimentado e não cimentado. A validade da norma europeia de ensaios cíclicos, desenvolvida para solos não cimentados, para o estudo deste solo cimentado é também analisada e, seguidamente, o comportamento a longo prazo é caracterizado através de ensaios cíclicos com um grande número de ciclos. Finalmente, os resultados dos ensaios anteriores foram usados na calibração de um modelo constitutivo para solos cimentados, onde se apresenta as vantagens e desvantagens deste modelo para a simulação do comportamento destas misturas.

RESUME

Sols traités au ciment sont fréquemment utilisés dans ouvrages en ligne pour plateformes de routes et chemins de fer. Le mélange de sol con ciment Portland est connu depuis le début du dernier siècle, étant plus actuel avec la réduction de matériaux naturels et pour raisons environnementaux. Néanmoins, au contraire du béton, cette technique est utilisée d'une façon empirique car il n'existe pas une méthodologie rationnelle. En adition, son comportement à long terme est fréquemment questionné, spécialement si soumis à successive passages cycliques.

L'étude de ce type de mélanges en laboratoire permet la compréhension des matériaux naturels structurés, aussi bien que les conditions d'application de sols traités au ciment. Dans ce travail, un grand programme expérimental a été développé pour la définition d'un modèle général de comportement d'un sol traité au ciment. Le sol résiduel du Porto, remoulé, a été choisi en raison de sa grande abondance dans la zone nord et centrale du Portugal. Comme il n'avait pas d'expérience dans les essais de laboratoire de mélanges de ce sol avec du ciment, le travail a commencé par des essais très simples jusqu'à des autres plus sophistiqués. De la même façon, ses caractéristiques cycliques ont seulement été évaluées après la définition du modèle de comportement en condition statique. Le program expérimental comprenait essais préliminaires (y compris essais de compression simples et essais d'ondes séismiques) essais triaxiaux statiques et essais cycliques.

L'utilisation de l'indice porosité/ciment (n/C_{iv}) a été une question adressée pour l'étude de quelques caractéristiques de ces mélanges comme la résistance à compression et à la traction, ou la rigidité dynamique et statique. Les résultats des essais triaxiaux statiques ont été interprétés par la théorie de l'Etat Critique, où la définition de la ligne de compression normale et la ligne d'état critique ont été dans les sujets discutés. La validité de la norme européenne des essais cycliques, développé pour des matériaux granulaires, pour l'étude de ce sol traité au ciment a été analysée et, puis, le comportement à long terme a été caractérisé par des essais cycliques avec un grand nombre de cycles. Finalement, les résultats des essais précédents ont été utilisés dans la calibration d'un modèle constitutive, pour lequel sont présentés ses avantages et limitations pour la simulation de ce sol traité au ciment.

ACKNOWLEDGMENTS

My special thanks go to my supervisor, Dr. António Viana da Fonseca, for his continuous support and advice during all this time and, especially, in the critical moments. Thanks are also due to my co-supervisors: Dr. Nilo Consoli, for the idea and first guidelines of this work and, for being there to answer all my questions; Dr. Beatrice Baudet, for making my stay in London possible, allowing the execution of high pressure tests, and helping me with the interpretation of the data giving a great improvement in the quality of the final work; and Dr. Jorge Almeida e Sousa for his revision of the model calibration part.

The financial support was provided by FCT (Portuguese Foundation for Science and Technology), through PIDDAC, by the PhD grant SFRH/BD/29346/2006 which is gratefully acknowledged. This research was also developed under the activities of FCT research unit CEC, in FEUP [PTDC/ECM/099475/2008], financed by the European Community (QREN/UE/FEDER), Operational Program for Competitive Factors "COMPETE". The contribution of Secil® for providing the cement used in the laboratory is also acknowledged.

Moreover, this work has profited from the collaboration of several institutions and persons to whom I would like to express my gratitude: to Javier Camacho-Tauta and Dr. Jaime Santos for receiving and helping me at IST (Lisbon) to perform the Resonant Column tests; to Dr. Giovanni Cascante for his advices on seismic wave tests; to Dr. Peter Sammonds, from the Earth Sciences Department at University College of London (UCL), for letting me use the Sediment Deformation Laboratory to perform the high pressure tests; to Professor Mathew Coop, for allowing the execution of the isotropic compression tests at Imperial College London (ICL) when time was pressing, for helping me with the apparatus, and for his experienced advices; and, to Nubia González and Dr. Marcos Arroyo for providing the cemented CASM constitutive model and helping me in the calibration.

I wish also to thank the technical teams of the three main laboratories where I have developed most of my work: at FEUP, to Mr. Armando Pinto, for his wisdom and experience and to Claudia, Daniela, Filipe, Luis and Sofia; at ICL to Dr. Steve Ackerley, Mr. Alan Bolsher and Mr. Graham Keefe for their precious help; and, at UCL, to Mr. Neil Hughes, Mr. Steve Boon and Mr. John Bowles for their kind assistance. Moreover, this work would not be possible without the help of my lab partners who have worked hard with me, namely Walid, Alonso, Osvaldo, Ana, and Marta, as well as, my colleagues for their convenient advices: Cristiana, Fatine, Ramtin, Agnese, Sheila, Eleonor, Miguel ... Finally, I cannot forget my family and friends who have supported me in all times. This list might be longer than the space but be sure I will not forget you. Thank you all !

CONTENTS

LIST OF FIGURES

LIST OF TABLES

NOMENCLATURE

Latin letters

A	cross-section area
C	cement content
c'	cohesion intercept
C_C	curvature coefficient
C_{iv}	volumetric cement content
C_u	uniformity coefficient
D_{50}	largest particle size in the smallest 50%
D_{max}	maximum particle dimension
E	stiffness modulus
e_0	initial void ratio
E_0	dynamic young modulus
E_r	resilient modulus
E_{sec}	secant stiffness modulus
E_{tb}	stiffness modulus(brazilian test)
E_{ti}	initial tangent stiffness modulus
E_{ur}	unload reload modulus obtained in load cycle
f	yield function
G	specific gravity
g	plastic potential function
G_0	maximum shear modulus
$G_0^{(hh)}$	maximum shear modulus (propagation and polarization in the horizontal direction)
$G_0^{(hv)}$	maximum shear modulus (horizontal propagation and vertical polarization)
I_D	density index
I_p	plasticity Index
k	slope of the swelling line
K	bulk modulus
K_0	coeficient of earth pressure at rest
M	stress ratio (q/p') at critical state
	membrane stiffness modulus
	constrained modulus
n	porosity
N	specific volume of the NCL when p' = 1 kPa
n	stress-state coeficient (cemented CASM parameters)
p'	mean effective stress
p'_0	initial effective consolidation pressure
p'_c	mean effective stress of the correspondent CSL used in the normalization
p'_e	mean effective stress of the correspondent NCL used in the normalization
p'_{ur}	average mean effective stress obtained in unloading and reloading
q	deviator stress
q_f	peak deviator stress
q_u	unconfined compression strength
r	spacing ratio (cemented CASM parameters)
R_t	tensile strength
R_{tb}	indirect tensile strength (brazilian test)
S	saturation degree
u	pore pressure
V	specimen volume
V_c	volume of cement
V_L	longitudinal wave velocity

V_P compressional wave velocity
V_{pp} peak to peak volts
$V_S^{(hh)}$ shear wave velocity (propagation and polarization in the horizontal direction)
$V_S^{(hv)}$ shear wave velocity (horizontal propagation and vertical polarization)
V_v volume of voids
w water content
w_L liquid Limit
w_P plasticity limit

Greek letters

γ unit weight
ψ dilatancy
ν Poisson ratio
Γ specific volume of the critical state line at p'=1kPa
τ shear stress acting on the shear plane failure
ρ mass density
η stress ratio (q/p')
ϕ' angle of shearing resistance
ϕ'_c angle of shearing resistance at critical state
σ'_c confining pressure
ϕ'_p peak angle of shearing resistance
σ'^{max}_v maximum vertical stress
γ_d dry density
τ_{oct} octahedral shear stress
γ_s particles unit weight
ε_a axial deformation
ε_p accumulated permanent or plastic deformation
ε_p^{rate} rate of the accumulated permanent or plastic deformation
ε_r elastic or resilient deformation
ε_s shear deformation
ε_v volumetric deformation
λ wave-length
gradient of the NCL and CSL
v specific volume
σ' normal stress acting on the shear plane failure
σ'_c effective confining pressure

Abbreviations

AASHO American Association of State Highway and Transportation Officials
AR Class of embankment
ASTM American Society for testing materials
BE Bender Elements
BP Back Pressure
CASM Clay and Sand Model
CBR Calibration Bearing Ratio
CBR_i Immediate Calibration Bearing Ratio
CEFEUP Faculty of Engineering of the University of Porto Experimental Site
CP Cell Pressure

CRD	One-dimensional compression tests at constant rate of deformation executed in oedometric cells
CSL	Critical State Line
CSW	Continuous Surface Wave
CT	Compression Transducers
DB	Deutsche Bahn
FD	Frequency Domain
FFT	Fast Fourier Transform
HCA	Hollow Cylinder Apparatus
ICL	Imperial College London
ICL_{iso}	Isotropic intrinsic compression line
IPI	Immediate Bearing Ratio
ISC'2	International Site Characterisation Conference
IST	Technical University of Lisbon
LCPC	Laboratoire Central des Ponts et Chaussés, Paris
LDT	Local Deformation Transducer
LVDT	Linear Variable Displacement Transducer
MASW	Multistation Analysis Surface Waves
MP	Modified Proctor
NCL	Normal Compression Line
PF	Platform of the earthworks
PN	Pore Pressure
PSR	Principal Stress Rotation
RC	Resonant Column
RCCT	Resonant Column Conventional Test
RCRN	Resonant Column Random Noise
SASW	Spectral Analysis Surface Waves
SEM	Scanning Electron Microscope
SETRA	Service d'études sur les transports, les routes et leurs aménagements
TD	Time Domain
UCL	University College London
UCS	Unconfined Compression Strength
UCT	Unconfined Compression Test
UGM	Unbound Granular Material

Chapter 1.
INTRODUCTION

1.1 Prologue

Soil improvement by the addition of cement has become an interesting alternative to traditional techniques in geotechnical engineering especially in road and railway platforms. The strength and stiffness are highly increased and consequently, in situ materials that did not fulfil the required mechanical properties can be now used.

Environmental issues are more and more important in an engineering design project. For that reason, this solution can be very attractive as it can minimize some of the impacts of road and railways construction. The use of in situ materials reduces in a great extent the transport distance of materials, which minimizes the damage of neighbouring roads, the pollution, the dust and the noise caused by trucks. Moreover, it minimizes the need of borrow and spoil areas which are usually a major problem. In fact, opening of new quarries is now more difficult, so if there is a mean to avoid the quantity of new materials this is definitely an advantage.

In Portugal, this technique was just applied in a few cases that can be explained by the lack of knowledge and experience in this area, and consequently, by some difficulties in the application on those few cases. There are no rational methodologies for the preparation of soil-cement mixtures as there is for concrete where the water/cement ratio has a major role in the achievement of the right strength.

The first dosage methodology based on rational criteria (porosity/cement ratio, taken as n/C_{iv}, where, n is the porosity and C_{iv} the volumetric cement content) was developed only recently by Consoli et al. (2007) and demonstrates that this ratio plays a fundamental role in the assessment of the target stiffness/strength. In recent researches the effects of soil-cement ratios have been investigated by numerous laboratory studies aimed at finding the minimum amount of cement that meets the target properties in terms of stiffness, strength

and durability [e.g. Horpibulsuk et al. (2003), Consoli et al. (2007)]. This approach results from the fact that soil-cement mixtures show a complex behaviour that is affected by many factors, for example the physical-chemical properties of the soil, the amount of cement, the stress level under which the cement was allowed to set, and the porosity and moisture content at the time of compaction [e.g. Clough et al. (1981), Consoli et al. (2000, 2003, 2006), Dalla Rosa et al. (2008)]. Of particular importance is the interaction between the density of the soil and the amount of cement used, both having a strong influence on the yield envelope and peak strength.

1.2 Historical overview

According to Lambe, T.W., (1962) soil stabilization with cement has began in 1917 when AMIES patented an initial procedure for improving soils by mixing them with variable proportions of Portland cement. Since then, the use of soil-cement, which is the name that has been adopted for this mixture, has extended throughout the world and it is becoming increasingly popular in highway engineering and particularly with pavement design and construction.

In 1935, engineers constructed the first experimental soil-cement pavement in State Highway 41 near Johnsonville, South Carolina which represented a significant development because it proved to be a long-sought means to stabilize local soils and provide good economic road base (PCA, 2005).

In Portugal, the first attempt was in the ex-colonies of Mozambique and Angola that the first experimental stretches were tested after the 2nd World War (Novais-Ferreira, 1981).

In France, this solution has been applied currently and developed enriching the existent know-how which has been published in some technical documents (e.g. GTS (2000) from LCPC/SETRA). In Spain, soil stabilization was almost insignificant in the final of the last century, however, the application of this technique has highly increased since then, being now generally used almost in all road platforms (Minguela, 2008).

1.3 Scope and objectives

In the scope of artificially cemented soils for transport platforms (roads, railway tracks, airport runways, port storage areas, etc ...), the aim of this work is to be a contribution to a better understanding of these materials in static and cyclic conditions. For this purpose an extensive laboratory experimental program has been conducted with the following main objectives:

- quantify the influence of the cement content, porosity and water content on the strength and stiffness of soil-cement mixtures;
- identify yield surfaces depending on the previous parameters and evaluate the stress-dilatancy behaviour;
- Evaluate the specificities of soil-cement behaviour when subjected to cyclic conditions bearing in mind their application in the referred transport platforms;

1.4 Organization of the thesis

This work is organised in ten chapters. After a brief introduction in Chapter 1, Chapters 2, 3 and 4 are related to the several issues comprised in this work, in terms of the existing knowledge on each subject. Then, chapters 5 to 8 follow, concerning the laboratory work and the corresponding obtained results. Both parts are related, which can be verified by the frequent references of the first chapters on the second part. In fact, the actual knowledge helps in the interpretation of the new data, and thus, only the combination of both can lead to new conclusions and research lines.

On the first part, the work develops from the practical point of view to a more theoretical one. Chapter 2 gives an idea of the actual technique of soil improvement with cement in terms of design, standards and specifications, construction procedures, etc... The next Chapter on the mechanics of cemented sands is divided in two parts. The first, concerns the factors that affect the cemented soil behaviour in static conditions, and the second is related to the existent knowledge on the cyclic behaviour. Chapter 4 is related to the critical state theory as a mean for the interpretation of the cemented soil behaviour. The concepts introduced in this part will be frequently used in the last chapters.

Chapter 5 includes a brief description of all the laboratory equipment used in the experimental program described in the following chapters. Chapter 6 focuses on the non triaxial tests performed in the experimental program, while Chapter 7 presents the static triaxial tests executed over uncemented and cemented samples. In both chapters the results are presented after the description of the experimental program. Chapter 8 includes the cyclic triaxial tests results where resilient and permanent deformations are investigated along with the fatigue phenomenon.

Finally, in Chapter 9 the great amount of experimental data is used to calibrate a constitutive model highlighting its advantages and limitations to simulate the tests performed before. The work finishes with Chapter 10 summarizing the most important conclusions and future developments.

Chapter 2.
SOIL IMPROVEMENT WITH CEMENT - APPLICATIONS IN LINE WORKS

2.1 Soil-cement and other cement-based pavement materials

After more than 70 years since the first time that soil-cement was used, experience has demonstrated that different kinds of soil-cement mixtures can be tailored to specific pavement applications. However, the basics always remain the same: soil-cement is the simple product of Portland cement blended with soil and/or aggregate, and water and compacted for use in a pavement structure.

Figure 2.1 illustrates how soil-cement compares to other cement-based pavement materials. Conventional concrete has a higher cement content and higher water content to form a paste that coats all the aggregates. With soil-cement, not all the soil particles are coated with a cement paste. The water content in soil-cement is determined from geotechnical engineering tests to find the best moisture level for compaction. Flowable fill is a controlled low strength material often used as backfill material. A material that is as strong as conventional concrete, but constructed similar to soil-cement, is roller-compacted concrete (RCC). RCC achieves its high strength because of the higher cement content and the use of properly selected and graded aggregates.

Cement-modified soil is used to improve the engineering properties and construction characteristics of silt and clay soils enhancing the compaction and strength of the material. 3-5% (by dry weight) of cement used to modify the soil improved it as a construction material. Cement-treated base is a general term that applies to all hardened soil-cement that meets the project specified minimum durability and strength requirements. The soil-cement can be mixed-in-place using on-site soils or mixed in a central plant using selected soils or aggregates. Cement-treated base needs more cement resulting in a strong, durable, frost resistant layer for the pavement structure. Typical cement contents in practical field applications range from 3 -10% cement, resulting in 7-day unconfined

compressive strengths from 2.1 – 5.5 MPa for common Portland cement. A special case of cement-treated base is full-depth reclamation (FDR), where aggregate for the cement stabilized base is obtained by pulverizing and recycling the old asphalt surface and base material. This construction procedure is very similar to mixed-in-place construction, except that there is an aggregate specification for the blend of the pulverized asphalt and old base material. FDR commonly uses 4 – 6% cement and results in 2.1 – 2.8 MPa unconfined compressive strengths in 7 days.

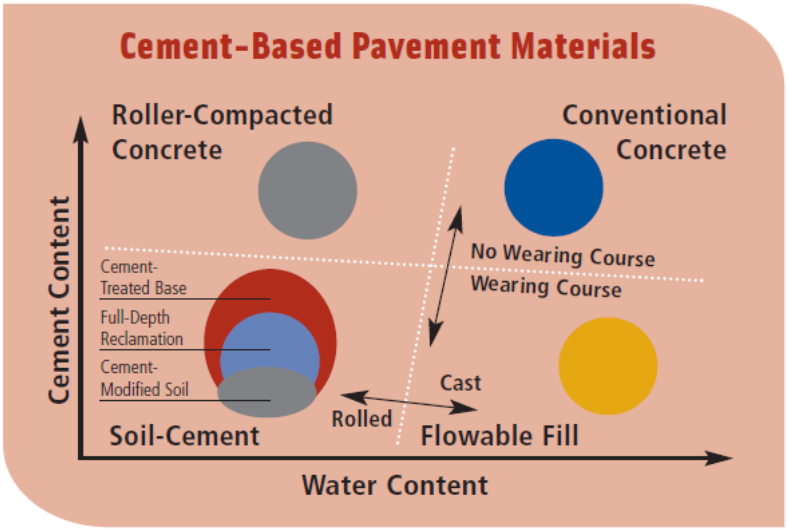

Figure 2.1 Soil-cement and other cement-based pavement materials (PCA, 2005).

Soil treatment and soil-cement are designations frequently confused. The soil treated with cement (also named as stabilized soil or modified soil) concerns a mixture with a low percentage of cement that enables the trafficability during work period but it breaks with the traffic becoming a granular material. Soil-cement is a mixture with higher cement content which presents good mechanical properties and durability after compaction assuring a long term bearing capacity and for that reason it is considered a structural material. In both cases, the aim is to improve the mechanical properties of the soil in order to be possible to use it. As it will be explained in section 2.3.2, depending on the cement content the material can be placed in different layers of the pavement.

2.2 Advantages and disadvantages of soil improvement with cement

The main advantages of this technique can be listed as following (Fortunato, 2008):

- to minimize economic and environmental costs derived from the exploitation of quarries and borrow areas to have adequate materials and from the need of spoil areas to deposit inadequate soils;

- to minimize social, economic and environmental costs resulting from the transport of borrow and spoil materials;
- to make possible the execution of earthworks even in bad weather conditions, which facilitates the accomplishment of deadlines;
- to make easier to build embankments in difficult access zones or with important geotechnical constraints.

It should be taken into account that in the costs derived from the transport, there are not only the costs from the trucks, but also the costs associated to the damaged roads, air pollution, noise and traffic congestion created by road interruptions. In railway lines, traffic interruption is even more problematic as usually the train cannot be switched to another track.

Some of the disadvantages that have limited the development of this technique are the following:

- high cost of cement;
- lack of experience by contractors;
- lack of required equipment, which needs a big investment;
- lack of specifications, standards and technical documents;
- economical reasons (in some places it is still easy to find adequate materials at low price; in small works the use of this technique might not be economically interesting);
- specific technical issues (in some places it may be impossible to apply this technique, for example, because of low temperatures, ice…);
- difficulties to attest the durability of the treatment;
- difficulties in assuring good quality of in situ soil treatment in very long line works where in situ materials can present high variability;
- unsuccessful experiences (reported problems lead to bad reputation due to wrong decisions).

More or less intensive and extensive application of this technique depends mainly on the legal and economic environment and on the knowledge that can be acceded. For example, in some African countries there is no systematic knowledge or adapted equipment but soil treatment is currently used as there are not much alternatives. Adequate natural materials are inexistent and in situ materials are applied with treatment making use of international knowledge brought by foreign consulting companies or contractors (Fortunato, 2008).

When it is important to have a high quality material, as it happens in transitions zones of high speed railway lines, quarry materials with good quality control and no variability can be treated with cement creating a very stiff material often named as cement-mixed gravel (Kongsukprasert et al., 2005).

2.3 Applications of soil improvement with cement in line works

2.3.1 Cement stabilizing mechanisms

The cementation of a granular soil mixed with cement is very similar to the cementation that occurs in concrete except for the fact that in a granular soil the cement paste does not fulfil the voids completely. The reaction products resulting from the combination of water and Portland cement are compounds of calcium-silicate-hydrate and calcium-aluminate-hydrate, as well as excess calcium hydroxide (lime) which generally is deposited. Cementation consists in adhesion forces between the surface of the soil particles and calcium silicates and aluminates.

Due to these stabilizing mechanisms, cement stabilization of foundation layers achieves the following performance improvements:

- the strength is increased including tensile strength;
- the stiffness modulus is increased;
- the stiffness to wet-dry and freeze-thaw is increased;
- the permeability is increased (except, if the treated soil is clay).

2.3.2 Line work applications

The soil-cement can be used successfully in road or airport pavements as well as railway platforms.

In the case of road or airport platforms, flexible and rigid pavements have to be distinguished (Figure 2.2). Soil-cement is usually applied in base layers of flexible pavements. Soil treated with cement is used in subbases and selected layers of sub-grade in flexible and rigid pavements.

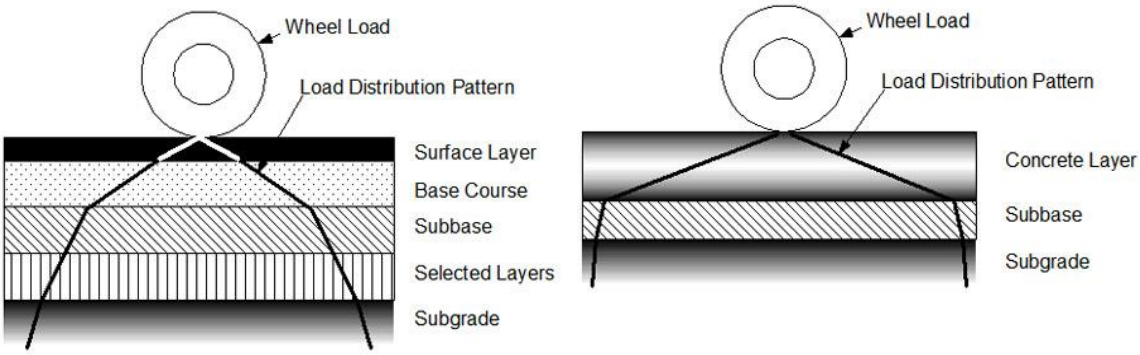

a) b)

Figure 2.2 Pavement layers: a) flexible pavement ; b) rigid pavement (SANRAL, 2011)

In railway lines, it depends whether it is a ballasted or non ballasted railway track (Figure 2.3). In a non ballasted railway track, a soil-cement layer is usually used as a transition between the rigid concrete slab and the subsoil as it is indicated in the figure. In a ballasted track, soil treated with cement can be used as a blanket layer of the sub-grade (it is not shown in the figure as it depends on the foundation quality).

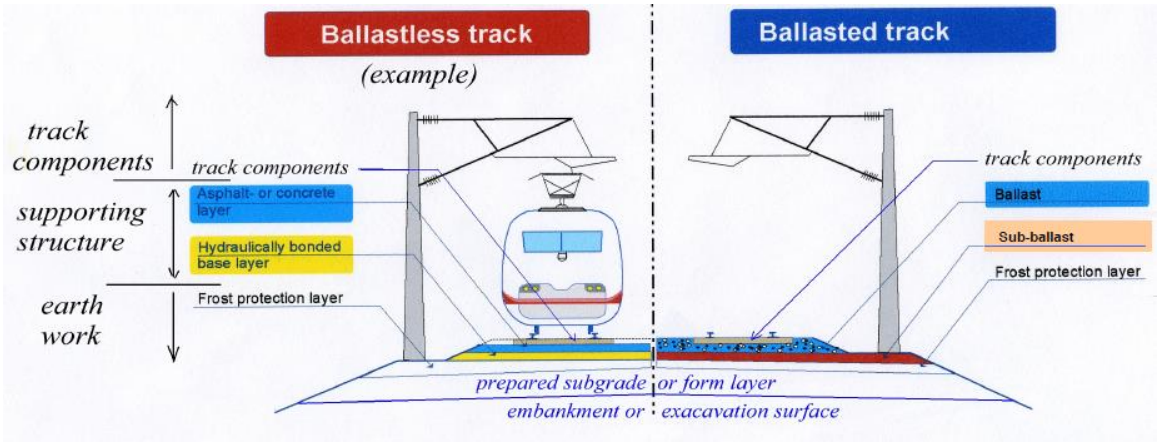

Figure 2.3 Comparison between permanent way systems: ballastless track and ballasted track (UIC, 2008)

2.3.3 Technical blocks

As was briefly expressed in section 2.2, hydraulic bonded layers can also be included in transition zones between embankments and viaducts, bridges or tunnels of road or railways lines where there is a high variation in stiffness (Figure 2.4). The main advantages of using this technique in transition zones are:

- reduced permanent deformations and high stiffness which enable a smooth transition between embankment and structure;

- the pressures over the structure are reduced due to the high stiffness of this material, and due to the drop of lateral pressures on the evolution of cementation;
- the availability to impose low compaction energies due to the high evolution of mechanical properties with curing facilitates compaction which is very important in difficult access zones.

In fact, soil-cement stabilization is a very attractive technique to perform the so called technical blocks. These areas include not only transition wedges but also difficult access zones where geometric or site conditions do not allow a good performance of the vehicles used in mixing and compaction of stabilized layers. Application examples of technical blocks are embankments around underground structures or support walls.

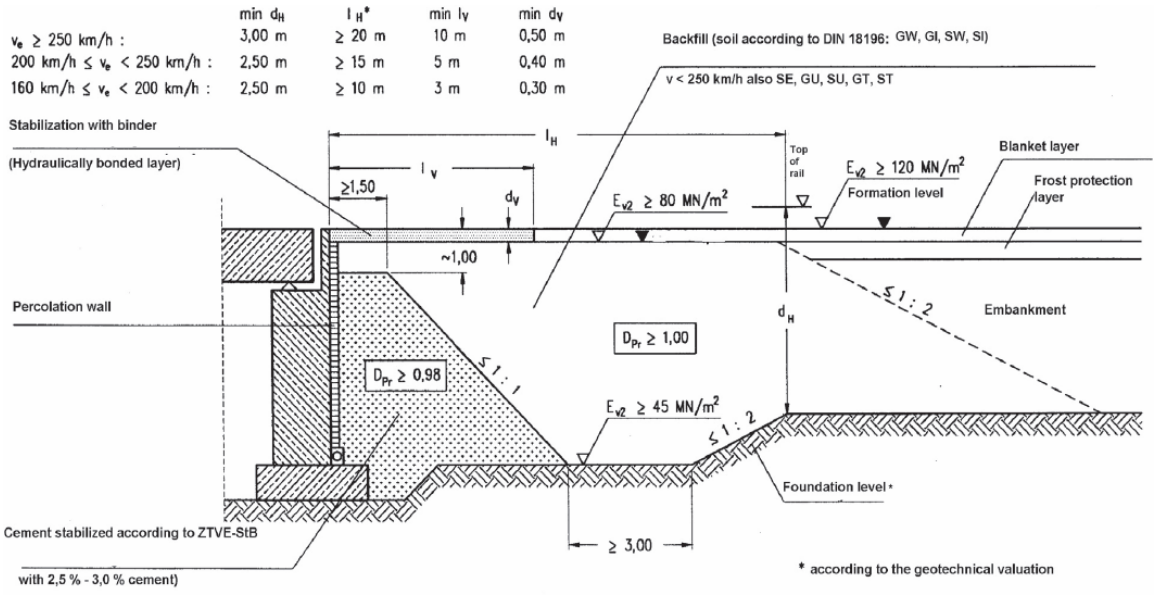

Figure 2.4 Transition between viaduct and embankment in a new railway line (DB: V > 160 km/h - UIC, 2008)

2.3.4 In situ and laboratory tests

Before application, soil-cement has to be well studied as each particular site conditions can influence the final result. First, the suitability of the soil has to be investigated; then, the mixture has to be tested either in laboratory, in experimental embankments or in situ.

Tests on non-treated soil

- grain size distributions curves;
- Atterberg limits;
- California Bearing ratio - CBR test;
- Sand equivalent test;
- Methylene blue test;

- Evaluation of organic matter content.

Laboratory tests on the treated soil

- Unconfined compression test over moulded samples;
- Tensile test (e.g., indirect tensile test or, as suggested by some, beam flexure tests) over moulded samples;
- Evaluation of the resilient modulus by cyclic triaxial tests.

Tests on the experimental embankment

- Plate load test;
- Falling weight deflectometer;
- Portable falling weight deflectometer;
- Portancemètre (Continuous measurement of capping layers bearing capacity equipment);
- Dynamic cone penetrometer;
- Dynamic probing light;
- Soil stiffness gauge;
- Ground penetrating radar;
- Surface wave methods (e.g. SASW, CSW and MASW);
- Unconfined compression test over specimens extracted from the embankment by sampling devices;
- Tensile test over specimens extracted from the embankment by sampling devices.

In situ tests for quality control

Quality control can be executed by performing water content and dry unit weight measurements. These can be done in several ways; the easiest is to use the nuclear densitometer (Figure 2.5).

Figure 2.5 Nuclear densitometer

2.4 Construction sequence

The construction sequence involved in the in situ stabilization of soils requires some new procedures. For this reason it will be briefly explained in this section the main steps of in situ stabilization, summarizing the large Spanish experience (Minguela, 2008).

The process follows these steps, illustrated in Figure 2.6:

- soil preparation;
- binder (cement) distribution and spreading;
- mixture;
- initial compaction;
- levelling;
- final compaction;
- cure and surface protection.

Before soil preparation, the organic matter should be taken out and, in the case of embankments, soil from other areas should be brought in place. Soil preparation includes disintegration, aeration and levelling through all the layer depth. The aim is to have an homogeneous soil to improve the binder action. First, the soil is disintegrated and scarified until the required grain size distribution curve is obtained. Then, the required moisture content should be evaluated. If the soil is slightly wet, aeration should be performed; if it is too dry some water has to be added to pre-wet the soil. Finally, the soil platform should be levelled before the application of the cement.

The next step consists in spreading the cement in the right dosage. In small works this is usually performed manually, placing cement bags in equal distance from each other to

achieve the right quantity per square meter. In large areas, mechanical vehicles are used working in two different ways: dry or wet way. In the first, the dry cement is spread by the vehicle into the soil and in the second the cement is mixed with water and then spread into the soil. In the dry way, care should be taken to avoid loss of cement by the wind that can cause some secondary problems. Although the wet method is usually more precise, the minimum cement content should not be too much reduced (lower than 2%) to assure a good homogeneity of the mixture.

A correct mixture of the binder is very important to obtain a homogeneous stabilization and consequently good performance layers. The productivity of the mixture and the speed of the process depend on the type of machines, thickness of the layer and type of soil. If the soil is too coarse the machines are easily damaged causing unacceptable delays.

The importance of good compaction in the quality of the final work is clear and well-known. In the case of cement stabilization, compaction should be performed just after mixing, due to two main reasons. First, it is not advisable to leave loose materials exposed to the weather agents, giving rise to moisture loss. On the other hand, taking into account that additional mechanical actions of the compaction equipment would damage the result of cementation in curing, the time to work with these materials has to be relatively short except when cement retarders are used.

If levelling is not well performed at this stage, rough surfaces caused by superficial defects have to be corrected by bituminous layers much more expensive. After an initial compaction with around 90-92% of the maximum density, levelling is performed removing the excess material. Usually, an additional thickness is considered at the beginning to compensate the removed material. The final compaction follows to achieve the required density.

Stabilized layers should be treated to avoid evaporation. Common practice is the application of a bituminous emulsion. If, for some reason, it is convenient to use the finish layer as a passage, light traffic should not be allowed on the first three days, and heavy traffic on the first 7 days.

Figure 2.6 Construction sequence of an in situ stabilized layer

2.5 Specifications and standards for the soil to be treated

2.5.1 Introduction

In general each country has its own specifications, standards, guidelines and other documents that help designers to select the best option for a particular case. In Portugal, the national specifications are usually based on international equivalent standards, specially Spanish and French documents, together with the national experience. For that reason, in sections 2.5 and 2.6 some of these countries standards and guidelines will be briefly described and compared. Section 2.5 will focus on the specifications for the soil (before treatment) and section 2.6 will be related to the mixture characteristics (after treatment).

2.5.2 Portuguese specification

Road specification

The old Portuguese specification from LNEC (1971), still valid, suggests the following recommendations for the soil:

- maximum organic matter content = 2%;
- maximum sulphate content = 0.2%;
- maximum particle diameter (D_{max}) = 75 mm;
- % passed on ASTM sieve nº 4 (4.75 mm) $\geq$ 45%;
- % passed on ASTM sieve 50 mm $\geq$ 80%;
- liquid limit (W_L) $\leq$ 45%;

The recommendations of the national institution for roads, *Estradas de Portugal, S.A*. EP (2009), express that if the treated material is to be applied in the selected layers below the base and sub-base pavement level - top of subgrade, the soil should satisfy the specifications expressed in Table 2.1. It is interesting to notice that distinction is made

between central plant treatment (Figure 2.7) and in situ treatment which is also adopted by the French specification as it will be described in section 2.6.4.

Table 2.1 Specifications that the soil should have to be treated with cement for the selected layers of the subgrade (EP, 2009) Note: I_p stands for plasticity index

Central plant treatment			In situ treatment	
D_{max}	% passed ASTM # nº200	I_p^{max}	D_{max}	I_p^{max}
50 mm	35%	12%	100 mm	12%

Figure 2.7 Central plant for soil-cement production

2.5.3 Spanish specification

Road specification

The Spanish standard called “Pliego de Prescripciones Técnicas Generales para Obras de Carreteras y Puentes” (PG3, 2004), present two different applications of soil with cement.

Soil stabilized in situ with cement can be used in the selected layers in the top of the subgrade giving rise to three types of subgrade: S-EST 1, S-EST 2 and S-EST 3. The first two can be stabilized with lime and/or cement while the third has to be stabilized only with cement.

Soil-cement with production in plant can be used as a pavement base course. There are two types proposed in this standard: SC20 and SC40, but in both cases the minimum cement content is 3%.

Table 2.2 summarizes the soil characteristics for in situ stabilization, distinguishing between the three types of final layers, while Table 2.3 refers to the soil-cement production in central plant. Furthermore, the Spanish standard presents the range of grain size distributions curves of the soil required to produce soil-cement (Figure 2.8).

Table 2.2 Soil specifications for the soil stabilized in situ according to PG3, 2004 (adapted from Minguela, 2008)

			S-EST 1	S-EST 2	S-EST 3
Grain size distribution	Dmax		80 mm		
	% passed in 63 µm	Lime	≥ 15		
	% passed in 63 µm	Cement	<50		<35
	% passed in 2 mm		> 20		
Plasticity	I_p	Lime	≥ 12	≥ 12 and < 40	-
	W_L	Cement	-	≤ 40	
	I_p		≤ 15		
% Organic material			< 2	< 1	
% Soluble sulphates			< 1		

Table 2.3 Soil specifications for the plant production of soil-cement according to PG3 (2004)

	Specifications for soil-cement	
	SC20	SC40
Dmax	< 50 mm	
% passed on sieve 2 mm	> 36%	> 17%
% passed on sieve 0.063 mm	< 35%	< 20%
Plasticity	I_p < 15% and W_L < 30%	
Organic matter content	< 1%	
Sulphates	< 1%	

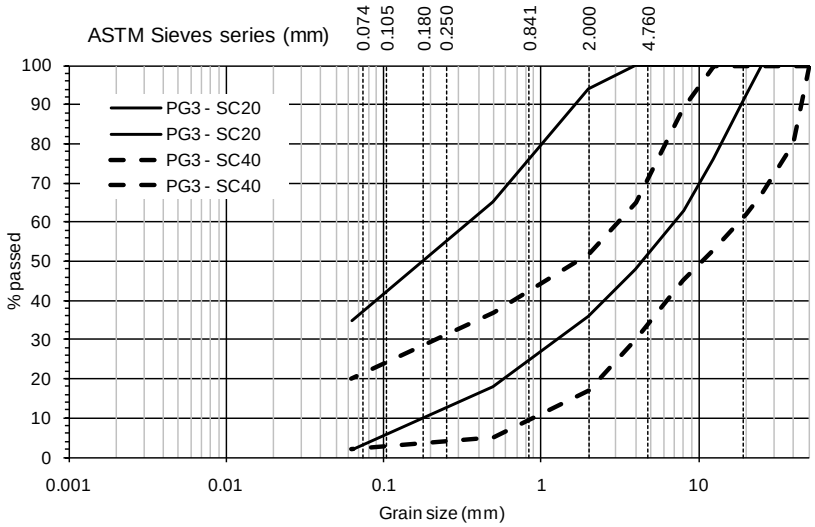

Figure 2.8 Range of grain size distribution curves of the soil required for soil-cement (PG3, 2004)

Railway specifications

The Spanish administration for railway infrastructures (ADIF, 2006) defines more strict recommendations to use hydraulically bonded materials:

- D_{max} between 80 and 400 mm (no more than 40% of the layer thickness)

- % passed on sieve 4 mm: between 20 and 50%
- % passed on sieve 40 mm < 30%
- % passed on sieve 0.08 mm < 8%

If the soil is to be applied in a transition zone some more recommendations are added:

- $I_p \leq 5\%$
- if the fines are non plastic, the fines content (% passed on sieve 0.08 mm) can go up to 15%
- cement content ≥ 3%

2.5.4 Standards comparison

Portuguese and Spanish specifications of the soil required to be mixed with cement were presented. Table 2.4 summarizes some of those parameters comparing the four standard documents available for road design in both countries. This table clearly evidences that all documents mainly agree in most of the values. As it would be expected the soil-cement specifications for bases of pavements are slightly more conservative than the requirements for soil stabilization in the selected layers of top of the subgrade: the maximum fines content is 20% for the higher quality soil-cement (SC40), the liquid limit is limited to 30% instead of 40% and the maximum dimension of the particle is 50 mm.

The Spanish recommendations for the railway design specified in the previous paragraph - ADIF (2006) - evidence the trend to be much more conservative than in road design.

Table 2.4 Summarized specifications for the soil to be treated with cement

	LNEC (1971)	EP (2009)	PG3 (2004)	
			S - EST3	Soil-cement
Maximum organic matter content	2%	-	1%	1%
Maximum sulphate content	0.20%	-	1%	1%
Dmax	75 mm	50 - 100 mm(2)	80 mm	50 mm
Maximum Liquid Limit (W_L)	45%	-	40%	30%
Maximum fines content (1)	-	35%	35%	20 - 35% (3)
Plasticity - maximum I_P	-	12%	15%	15%

(1) The fines content including clays and silts is in some cases defined by the ASTM sieve nº200 (0.075 mm), in some others by the sieve 0.08mm and also by the sieve 0.063 mm.

(2) The lower value corresponds to central plant treatment and the upper value to in situ treatment

(3) Depending on the type of soil-cement: 20% - SC40 and 35% - SC20

2.6 Specifications and standards for the required properties of the treated soil

2.6.1 Introduction

In this section the specifications and standards for the soil treated with cement will be presented. It should be noted that these recommendations refers to current Portland cements such as CEM I or CEM II, class 32.5.

2.6.2 The Portuguese specification

The old Portuguese specification E 304 (LNEC, 1974) suggests some abacus to evaluate the required cement content in order to achieve the minimum admissible uniaxial compression strength that the soil-cement mixture should have after 7 days of curing.

The national institution for roads (*Estradas de Portugal, S.A.* - EP, 2009) presents different recommendations depending on the future application of the cemented mixture: in the embankment or in selected layers below the base and sub-base pavement level.

For the treated soil applied in embankments, the suggestion concerns values of immediate CBR evaluated for 95% of Normal Proctor and for the natural water content, before and after the treatment as Table 2.5 expresses.

Table 2.5 Immediate CBR specification for the soil treated with cement applied in embankments (EP, 2009)

Type of soil	CBR_i	
	Before treatment	After treatment
S0	< 3	5
S2	3 to 5	5 to 15
S2	5 to 8	7 to 20

The recommendations for the soil treated with cement applied in the selected layers of the top of the embankment are summarized in Table 2.6. In the short term conditions, it is important to assure trafficability conditions, expressed by the uniaxial compression strength, as well as strength to immersion in water in the early ages. In the long term conditions a minimum value for the indirect tensile strength (by Brazilian diametral compression strength - CEN, 2003a) is imposed to assure strength to the formation of gel.

Table 2.6 Short and long term conditions for the soil treated with cement applied on the top of the embankment (EP, 2009)

Short term conditions	Long term conditions
R_c > 1.0 MPa	R_{tb} min = 0.25 MPa
R_{ci}/R_{c60} ≥ 0.80 if VA ≤0.5	R_c min =2.0 MPa
R_{ci}/R_{c60} ≥ 0.60 if VA > 0.5	

where,
R_c - unconfined compression strength
R_{ci} - unconfined compression strength at 60 days (28 days of normal curing plus 32 days inside water)
R_{C60} - unconfined compression strength at 60 days (normal curing)
R_{tb} - Brazilian tensile strength
VA - Sand equivalent value

2.6.3 The Spanish specification

Bearing in mind the difference between in situ stabilized soils for subgrade and plant produced soil-cement bases proposed by the Spanish specification as expressed before, the recommendations for the final mixture are now presented. In terms of in situ stabilized soils, specifications are presented concerning values of CBR and unconfined compression strength (UCS) at 7 days, as well as the suggestions for the modified Proctor density for each type of subgrade (Table 2.7). Concerning soil-cement bases it is recommended that the unconfined compression strength at 7 days should be between 2.5 and 4.5 MPa.

Table 2.7 Specifications for in situ stabilized soils (PG3, 2004 adapted from Minguela, 2008)

	Binder		At 7 days		Density
	Type	%	CBR	UCS	Modified Proctor
S - EST 1	cement or lime	≥ 2	≥ 6	-	97% (1)
S - EST 2	cement or lime	≥ 3	≥ 12	-	97%
S - EST 3	cement	≥ 3	-	≥ 1.5 MPa	98%

(1) 95% if it is not the top layer of the embankment

2.6.4 French and EN

In the French recommendations the main publication on stabilization of soils, GTS (2000), presents the same specification as *Estradas de Portugal* in EP (2009) presented in Table 2.6, as well as the minimum immediate bearing ratio - IPI (NF P 94-078 from AFNOR, 1997) that the mixture should have (Table 2.8) which is equivalent to Table 2.5.

Then, this guide suggests a classification chart (Figure 2.9) which plots the tensile strength (R_t) and the stiffness modulus (E) achieved at 90 days. E and R_t can be obtained directly by the direct tensile test (e.g, French standard NF P 98 232-2 from AFNOR, 1993) or indirectly by the Brazilian diametrical compression test (R_{tb} and E_{tb}) using the following relations:

$$R_t = 0.8\ R_{tb} \quad (2.1)$$

$$E = E_{tb} \quad (2.2)$$

Table 2.8 Minimum immediate bearing ratio - IPI of the treated material (GTS, 2000)

Type of soil based on GTR (2000)	IPI
A_3; C_1A_3	10
A_2; C_1A_2; B_6; C_1B_6	15
A_1; B_5; C_1A_1; C_1B_5	20
Remaining Classes	according to experience

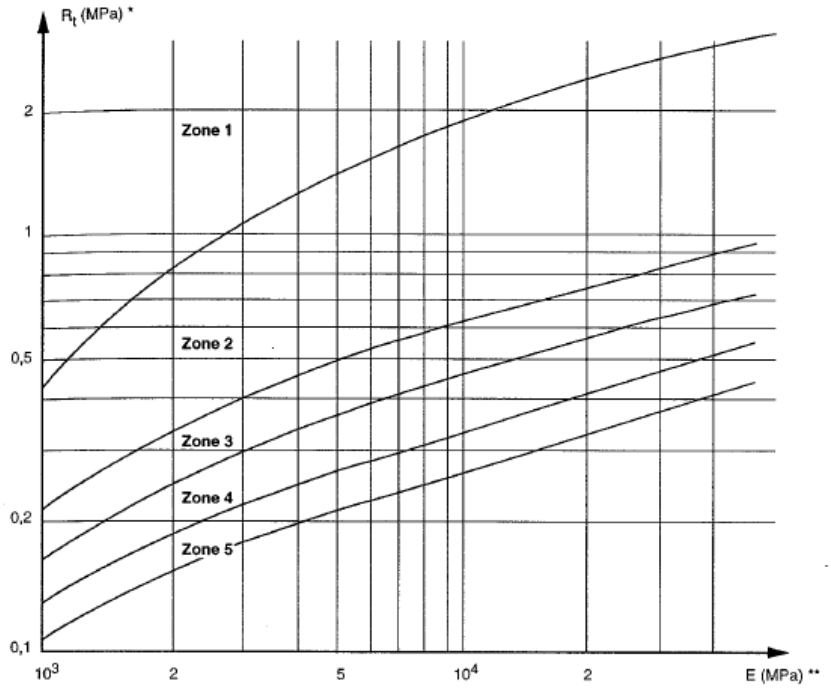

Figure 2.9 Classification zones in terms of tensile strength (R_t) and Stiffness modulus (E) - GTS (2000)

From this chart the mixture is located in one of the 5 zones, and then a mechanical class of the material can be obtained by Table 2.9 depending if the mixture is executed in situ or in a central plant. It should be noted that these specifications concern stabilized soils for the top selected layer of the subgrade. Depending on the class of the embankment (AR) and on the thickness and class of the stabilized soil, the platform of the earthworks (PF) gets a classification which is related to its stiffness modulus.

Table 2.9 Evaluation of the mechanical class of the material due to the execution method (GTS, 2000)

Central plant treatment	In situ treatment	Class of the material
Zone 1		1
Zone 2	Zone 1	2
Zone 3	Zone 2	3
Zone 4	Zone 3	4
Zone 5	Zone 4	5

A more recent European Standard EN 14227-10 (CEN, 2006) related to cemented treated soil also presents a similar classification to GTS (2000). For the soils stabilized with cement a classification based on the CBR is proposed. The mixtures of soil-cement can be classified by the unconfined compression strength (Rc) measured in cylindrical samples with a ratio H/D = 2. In addition, a classification chart based on the tensile strength (R_t) and stiffness modulus (E) similar to Figure 2.9 is presented (Figure 2.10). However, while EN 14227-10 (CEN, 2006) explicitly indicates that the stiffness modulus can be obtained either by direct tensile test, Brazilian test or in uniaxial compression, in GTS (2000) there is any reference to the use of the unconfined compression strength to obtain such modulus, so there is an assumption that it should be defined in tensile action.

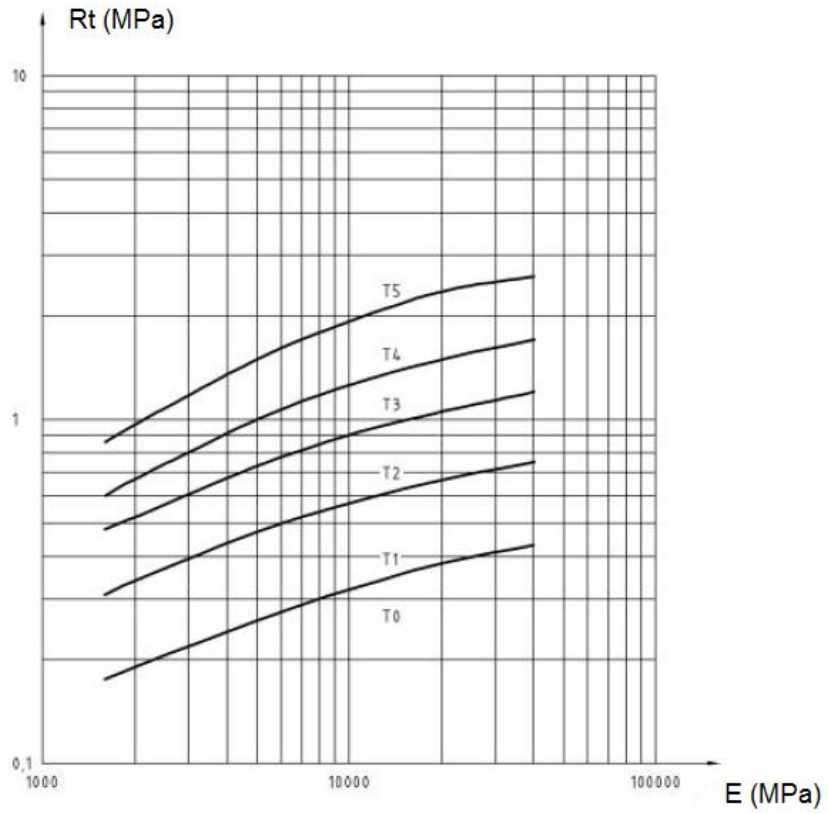

Figure 2.10 Classification chart proposed by the EN 14227-10 (CEN, 2006).

It is interesting to notice that these two classification charts (Figure 2.9 and 2.10), which seem quite similar, are in fact totally different, as the classes T0 to T5 are not comparable to Zone 1 to 5. In Figure 2.11 the two classification systems are plotted for comparison where the lines represent the lower bound of the corresponding zone.

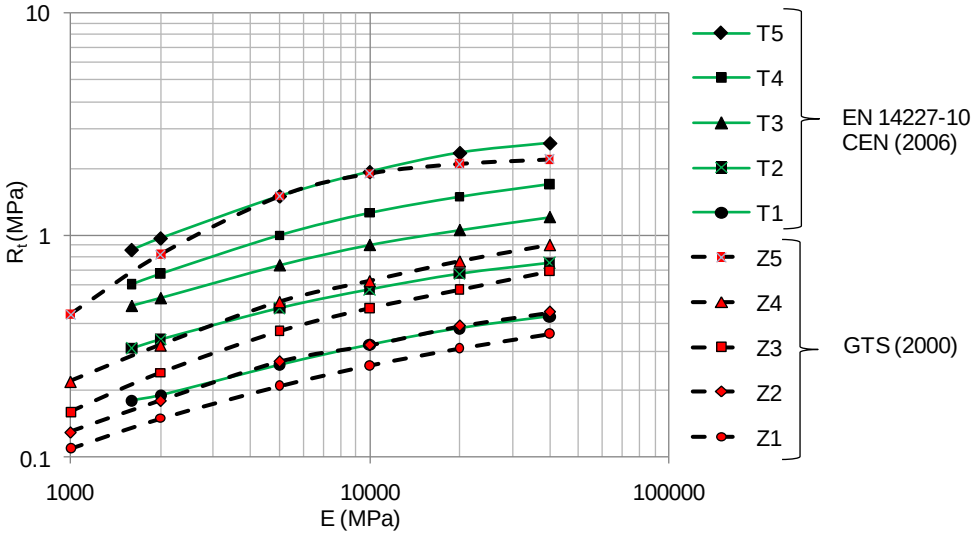

Figure 2.11 Classification systems from CEN (2006) and GTS (2000) based on the tensile strength (R_t) and on the stiffness modulus (E).

Even being more recent the European standard (CEN, 2006) seems more generic. Applying to soil treated with cement for roads, aerodromes and airports, and other circulation zones this standard is not inserted in any specification that could help the road designer on the calculation of each layer thickness. On the other hand, GTS (2000) provides all design details, relating to the class of the embankment (AR), the class of the stabilized soils and class of the platform of the earthworks (PF) giving rise to its stiffness modulus. Having these design tables together with some more details about the construction of embankments, GTS (2000) classification is much easier to follow than the CEN (2006).

2.6.5 Comparison

Specifications from Portugal, Spain and France together with reference to the European standard were presented. These documents refer only to road design. Railways specific standards for soil treated with cement are not so fully developed in Portugal and Spain possibly due to the lack of systematic recording of experiences results and are generally more conservative due to the high performance expected in railway lines.

The reported data allows the following comparison:

- The CBR_i and IPI values seem to be quite in agreement in all the documents ranging between 5 and 20, depending of the type of soil used in the treatment;
- In terms of unconfined compression strength at early ages, the Portuguese specification suggests a minimum value of 1MPa to assure trafficabilly while the Spanish standard requires a minimum value of 1.5 MPa for the high quality in situ stabilization (S-EST 3) and 2.5 MPa for soil-cement bases;
- In short term conditions both Portuguese and French specifications are in full agreement;
- In long term conditions the Portuguese specification suggests a minimum unconfined compression strength at 28 days of 2 MPa and a tensile strength of 0.25 MPa while the French and European standard recommend the graphs, shown in Figure 2.11, that relate to tensile strength and corresponding stiffness modulus. The introduction of the stiffness modulus is possibly to avoid the risk of cracking by fatigue of very stiff soil-cement layers.

2.7 Examples of soil improvement with cement in Portugal

Since the eighties that soil-cement has been applied in Portugal in some roads, especially in order to fulfil the following aims:

- increase the bearing capacity of old pavements in order to assure enough support for the actual traffic;
- provide a convenient subgrade in zones with low quality foundation soils;
- decrease the thickness of granular bases and sub-bases where there is a lack of appropriate quarries.

This technique has also other advantages as described in section 2.2, but unfortunately, it is not so widespread because it is still possible to find granular materials at relatively low cost and there is a lack of contractors that have the appropriate equipment. In the next sections some Portuguese examples will be briefly presented, showing different solutions for distinct problems.

2.7.1 IP 6 - Abrantes/Mouriscas (Caspurro and Dias, 2008)

In this case, the lack of granular materials was the main reason to decide for soil improvement with cement. A specific soil classified as a SC in the Unified Classification System (ASTM, 1998a) was used for the mixture with cement. A laboratory study with unconfined compression tests and indirect tensile tests was performed to find the best cement content, which was considered 3%.

The pavement structure adopted for this road included 3 layers:

- 5 cm of asphalt concrete 0/14 mm;
- 14 cm of asphalt concrete 0/32 mm, and;
- 25 cm of in situ soil-cement base.

2.7.2 IC 3 - Alternative road in Tomar (Caspurro and Dias, 2008)

The lack of foundation soils with the required design properties lead to the use of a soil-cement subgrade that allowed also the reduction in the thickness of the granular layers. Due to the low quality of in situ soils, a borrow zone was found with appropriate soils to be stabilized with cement. For this soil, classified as a SC (ASTM, 1998a), Normal Proctor curves were obtained, as well as the bearing capacity at short and long term by the CBR_i and CBR values. The soil mixed with cement was also tested at different cement contents with evaluation of the Proctor curves, CBR_i, unconfined compression strength and indirect tensile strength. In this case 6% of cement content was applied.

The pavement structure adopted for this road was the following:

- 5 cm of asphalt concrete 0/14 mm;
- 9 cm of asphalt concrete 0/20 mm;
- 11 cm of asphalt concrete 0/32 mm;
- 20 cm of well graded granular material for the base, and;
- 25 cm of in situ soil-cement subgrade.

2.7.3 Highway A11 between Braga and Barcelos

The solution for this road comprised a sub-base in soil-cement performed in situ whose structural role was very important due to the low quality of the foundation soils, mainly from schist and granite, presenting low values of CBR around 5 and 8%. In this case, a thin layer of fine grained asphalt concrete was used to avoid the propagation of fissures from the soil-cement to the bituminous layers.

The pavement structure was the following:

- 4 cm of porous asphalt;
- 5 cm of asphalt concrete 0/14 mm;
- 9 cm of asphalt concrete 0/20 mm;
- 2 cm of asphalt concrete 0/4 mm, and;
- 30 cm of in situ soil-cement.

Chapter 3.
MECHANICS OF CEMENTED SOILS

3.1 Introduction

Cemented soils are currently focused in the literature with the aim of understanding natural formations that by physical-chemical bonding, cementation or fabric show a mechanical behaviour that is not only explained by stress history or in situ density. In some cases it is possible to collect natural undisturbed samples allowing the understanding of in situ soil (Cuccovillo and Coop, 1997 and 1999; Qadimi and Coop, 2007). Conversely, in other conditions in situ analysis is not reliable due to the high variability of properties giving rise to non-representative sampling and to weak structure partially destroyed during sampling process (Huang and Airey, 1993; Dalla Rosa et al., 2008). This subject of how to evaluate the impact of such effect of sampling disturbance in the geomechanical properties of residual soils deducted in laboratory tests is discussed in Viana da Fonseca (1996, 1998, 2003), Viana da Fonseca et al. (1997), Viana da Fonseca and Coutinho (2008) and, Ferreira et al. (2011). According to Leroueil and Vaughan (1990) cemented soils (from natural structured clays to weak rocks or artificially cemented soils) show a similar pattern of behaviour where density and bonding strength seem to be the most important parameters. Being so, it is expected that both natural and artificial cemented soils have a similar behaviour as it has been demonstrated in the literature (e.g. Vaughan et al., 1988, Boey, 1990, Ismail et al., 2004). Relying on this idea, several authors have been performing laboratory tests in artificially cemented samples to understand naturally cemented formations, analyzing the effects of structure on their behaviour (recently a thorough work was developed by Cruz, 2010). As an example, there is the great number of investigations in natural carbonate soils in the coast of Australia whose knowledge is very important to the foundation of offshore structures (Allman and Poulos, 1988, Huang and Airey, 1993, Ismail et al., 2002 and Sharma and Fahey, 2004).

3.2 Factors affecting cemented soil behaviour

There are several parameters that influence the behaviour of cemented soils. Several authors (Acar and El-Tahir, 1986; Huang and Airey, 1993; Zhu et al., 1995; Consoli et al., 2000; Schnaid et al, 2001; Kongsukprasert et al, 2005, Khan et al, 2006, among others) have pointed out the parameters that influence the behaviour of artificially cemented soils such as type of cement and cement content, curing time and stress, water content and porosity. In the following items these parameters will be analysed in detail.

3.2.1 Influence of the type of soil

Almost every type of soil can be treated with cement, although the treatment can be disadvantageous by economic reasons if the quantity of cement to be introduced is very high. In general, the cement content increases with the quantity of fines, being inadvisable for fat clays where the treatment with lime is more convenient. On the other hand, as cementation occurs between particle contact points, in a well graded soil the cementation is more effective and so the quantity of cement needed to achieve the same strength is lower than in an uniform sand.

3.2.2 Influence of type and cement content

Ismail et al. (2002, 2004) have studied the influence of several types of cementing agents on the small-strain stiffness of a carbonate sand. Four cementing agents were used as following: calcite using the process called CIPS (Calcite In situ Precipitation System); 6% Portland cement; 5% epoxy and 12% gypsum. The results in terms of the shear wave velocity are presented in Table 3.1. First, it can be observed, as expected, that the effect of cementation has a significant increase in the shear modulus, irrespectively of the type of cementing agent. Furthermore, it can be seen that the different types of cementing agents have different results in the stiffness behaviour of the soil.

Table 3.1. Results of V_s and G_0 obtained after curing of each cement (Ismail et al., 2004)

Cement	$V_{S\ (hh)}$ (m/s)	$V_{S\ (hv)}$ (m/s)	$G_{0\ (hh)}$ (MPa)	$G_{0\ (hv)}$ (MPa)
Calcite (CIPS)	812.9	821.3	1030.9	1052.3
6% Portland cement	908.7	717.7	1189.2	741.8
5% epoxy	829.9	728.1	1074.3	827.89
12% gypsum	728.7	827.1	828.1	1066.9
Uncemented LP sand (*)	467.7	493.9	315	351.4

(*) at σ'_v = 215 kPa

The cement content used in the mixture is also of major importance as reported by numerous authors (Huang and Airey, 1993; Zhu et. al, 1995 or Schnaid et. al., 2001). As an example, some results of Schnaid et al. (2001) are plotted on Figure 3.1. The soil used in this work is a residual soil from sandstone mixed with Portland cement. As the plot indicates, the addition of small quantities of cement has a significant influence of the stress-strain-volumetric behaviour of the soil which changes from ductile to brittle behaviour, being brittleness increased when more cement is added. As the cement content increases both peak and initial stiffness are increased. These results also suggest an existence of an ultimate state where the deviatoric stress remains constant, independently of the cement content. The discussion of a unique critical state line irrespectively of the cement content will be discussed later in this work in the light of the obtained experimental results.

In addition some results from Huang and Airey (1993) are also presented where is clear the effect of the cement content on the yield surface of an artificially cemented soil.

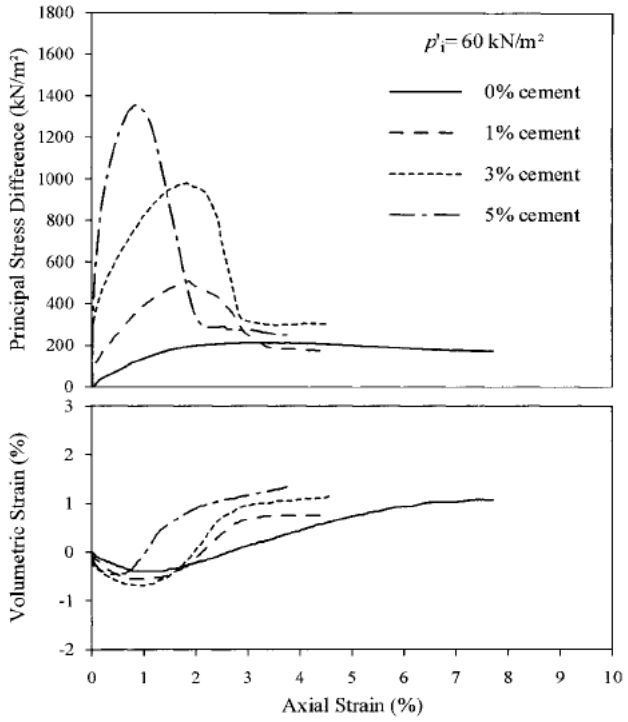

Figure 3.1. Stress-strain-volumetric response for different cement contents (Schnaid et al., 2001)

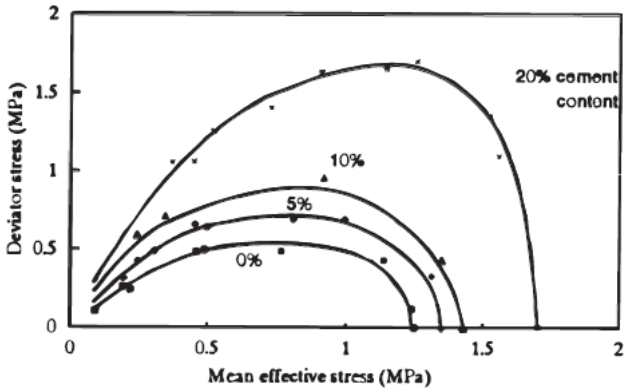

Figure 3.2 Influence of cement content on the yield locus of the cement for an artificially bonded soil (Huang and Airey, 1993).

3.2.3 Influence of curing time and stress

Depending on the type of cement the time to achieve the maximum strength of the mixture will also be different. It seems obvious that, when the mixture is tested before the end of that curing period the mixture behaviour will be influenced by the time of curing.

On the other hand, the effect of curing stress is less obvious on the final behaviour. Consoli et al. (2000) have analysed that issue reporting that while the specimens cured without stress show a decrease in the initial stiffness with increasing confining stress, the specimens cured under stress show an increase in stiffness as the stress level increases. Considering the volumetric behaviour the specimen cured without stress exhibits highly compressive behaviour in higher stress levels while the specimens cured under stress show less compressibility being even dilatant in the intermediate confining stress (Figure 3.3). This is an obvious consequence of the progressive destructuration of the cemented structure, when formed in conditions free of stress, subjected to post-curing yield when subsequently loaded.

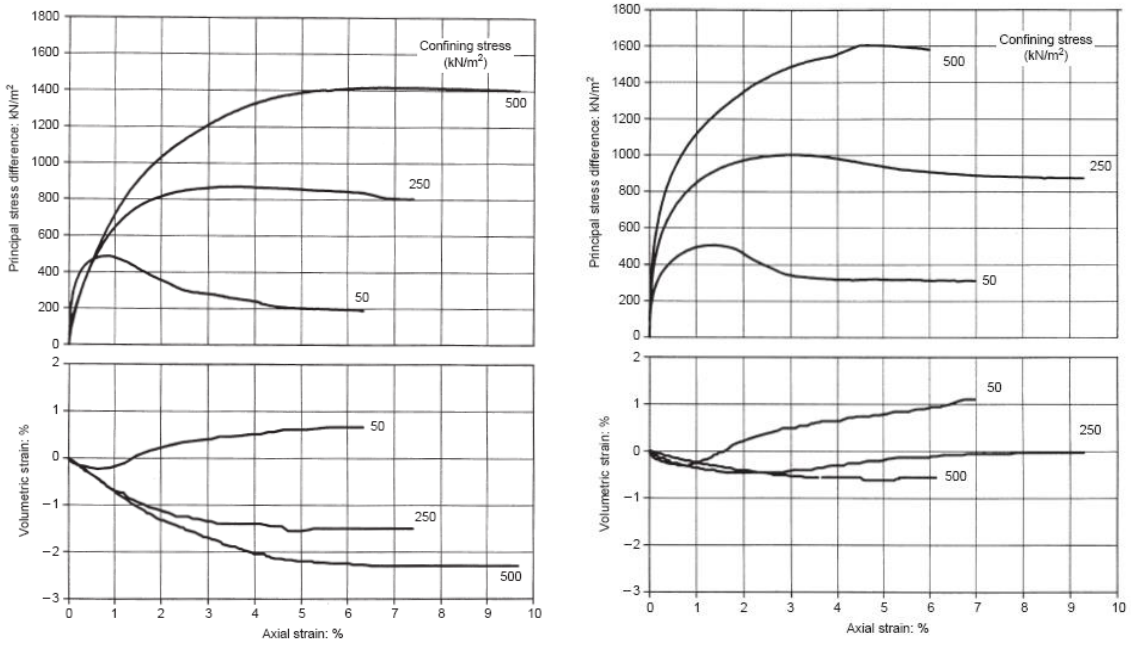

Figure 3.3. Stress-strain behaviour of cemented soil. (a) cured without stress. (b) cured under stress (Consoli et al., 2000)

More recently, Dalla Rosa et al. (2008) used the same soil as Consoli et al. (2000) to perform triaxial tests on cemented samples cured under confining pressures of 50, 250 and 500 kPa corresponding the last two stresses to points on the isotropic normal compression line for the uncemented soil also referred to as isotropic intrinsic compression line (ICL_{iso}). As Figure 3.4 expresses the samples cured at confining pressures of 50 kPa have higher normalized yield and state boundary surfaces. However, for samples cured on the isotropic intrinsic compression line a single state boundary surface was determined independently of the curing stress and shearing confining pressure.

Dif (2007) performing cyclic triaxial tests on artificially cemented Porto residual soil from granite concluded that there was a significantly influence of the curing stress on the reduction on the final permanent deformation observed during the cyclic loading although it was lower than the effect of initial void ratio. The influence on the resilient modulus was not so relevant.

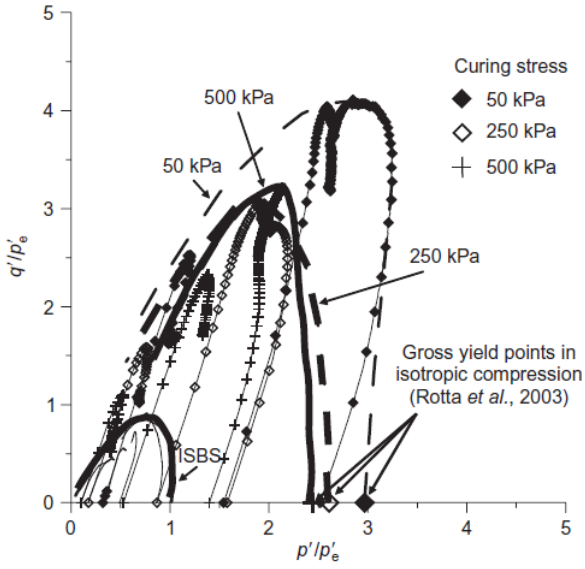

Figure 3.4 Effect of curing stress on the size of the state boundary surface (Dalla Rosa et al., 2008)

3.2.4 Influence of water content

The water content is very important to hydrate the cement giving better consistency to the mixture and facilitating the compaction. After Gomes Correia and Neves (1999) a complete hydration of the cement is assured with a quantity of water of about 20% of the weight of cement. According to GTS (2000) the water content taken by the cement hydration is around 0.3 to 0.5% per 1% of cement. Being so, the water content specified by the Proctor test is more than enough to hydrate the cement, as it was discovered in 1935 when this test was first applied to soil-cement samples.

The influence of the water content on the strength or stiffness behaviour of a soil-cement mixture needs to take into account the grain size distribution of both the uncemented soil and the cemented mixture. It is well know that the fines content has a significant influence on the behaviour of a soil and especially on the influence of the water content on its behaviour. Being a fine material, the cement can increase the fines content of the soil. So, if a comparison is established between an uncemented soil and the same soil plus cement then, the grain size distribution of the two soils will not be the same, as the mixture of soil-cement has higher fines content. Several authors have performed tests in such conditions (e.g., Khan et. al., 2006) and so they have found that the influence of the water content increases with the cement content as Figure 3.5 indicates.

Some other authors (Coop and Atkinson, 1993) have added fines to the uncemented soil so it could be comparable to the cemented soil as both soil and mixture would have the same grain size distribution. Finally, some other works (Consoli et al., 2009) have been

performed in soil-cement mixtures where a quantity of fines equal to the amount of cement to be introduced was taken out from the soil before mixture.

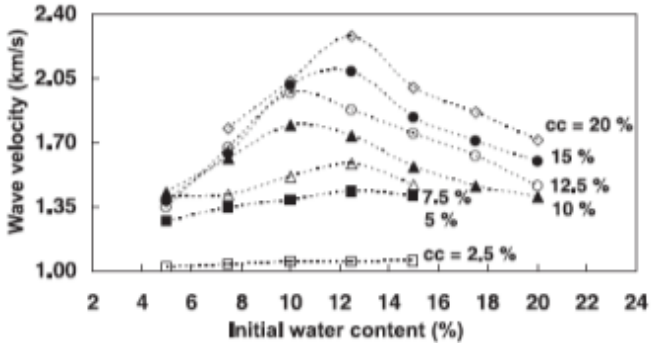

Figure 3.5 Effect of the initial water content (Khan et al., 2006)

3.2.5 Influence of porosity

The porosity of the mixture of soil-cement is also a parameter to take into account as it will be discussed further below on section 4.4.1. It should be noted that the analysis that is presented herein concerns only the cases where compaction took place before the curing of the cementing agent so that compaction procedures do not break the cementing bonds.

Consoli et al. (2007) observed that the unconfined compression strength increases exponentially with the reduction in porosity of the compacted mixture (Figure 3.6a) due to the increase in the number of contact points between particles. The same data can be plotted in a different way (Figure 3.6b) showing that the rate of strength gain increases with density, which proves once more that the effectiveness of cementation is enhanced by a reduction in porosity.

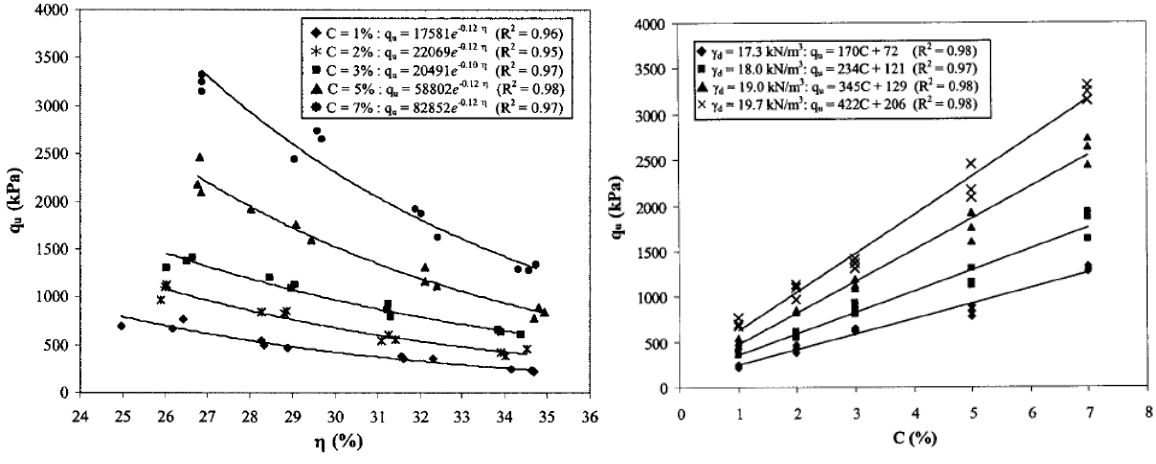

a) b)

Figure 3.6. Variation of unconfined compression strength with a) porosity; b) cement content (Consoli et al., 2007) Note: For these authors, η stands for porosity.

3.2.6 An index ratio

Seeking for a ratio that would reflect the influence of some of these parameters Consoli et al. (2007) presented an index property defined as the ratio of porosity to the volumetric cement content, called porosity/cement ratio (n/C_{iv}). Some previous attempts have been made, such as the degree of cementation proposed by Chang and Woods (1992) that concerns the percentage of voids filled with cement, being this parameter developed for sands. Lorenzo and Bergado (2004) have also presented the ratio of the after curing void ratio to the cement content (e_{ot}/A_w) proving to be quite interesting for clay mixtures with high values of water and cement content. Additionally, Kasama et al. (2006) have also presented some indexes to describe the strength of several cemented treated soils.

Another available parameter is the water/cement ratio used for concrete. However, soil-cement mixtures are usually cured in a non saturated condition, which makes the previous ratio inadequate in the analysis of these mixtures behaviour. The main difference between soil-cement mixtures and concrete (besides the cement content) is that during the curing of concrete all voids are completely full of water and therefore concrete stress-strain behaviour is not dependent on the void ratio but on the water content. In opposition, soil-cement mixtures currently executed in embankments and transport platforms have a curing water content lower than the saturation water content and so their compressibility will be related to its porosity. Moreover, while concrete has an almost linear behaviour for a wide range of deformations, soil-cement mixtures have a clear non-linear behaviour since very small strains as a result of the progressive degradation of the cemented structure. Being so, even if the soil-cement mixture is saturated after the maximum strength has been achieved (i.e. after curing) the curing void ratio still has a very important role on the mechanical behaviour of the mixture.

The convenience of the porosity/cement ratio was first analyzed in terms of unconfined compression tests (Consoli et al., 2007) followed by triaxial compression tests and stiffness properties investigation (Consoli et al., 2009) where it has revealed quite adequate, and finally, more recently, in the stress-dilatancy relationship of an artificially cemented sand (Consoli et al., 2011a).

Figure 3.7 shows a very good agreement between unconfined compression strength and the porosity/cement ratio. In Figure 3.8 results from triaxial compression tests are shown, where a trend was established between porosity/cement ratio and the peak strength parameters, namely the cohesion intercept and angle of shearing resistance which show high values of the coefficient of correlation. It should be noted that this ratio can be also written as the volume of voids to the volume of cement (V_v/V_c) at it appears in the Figures.

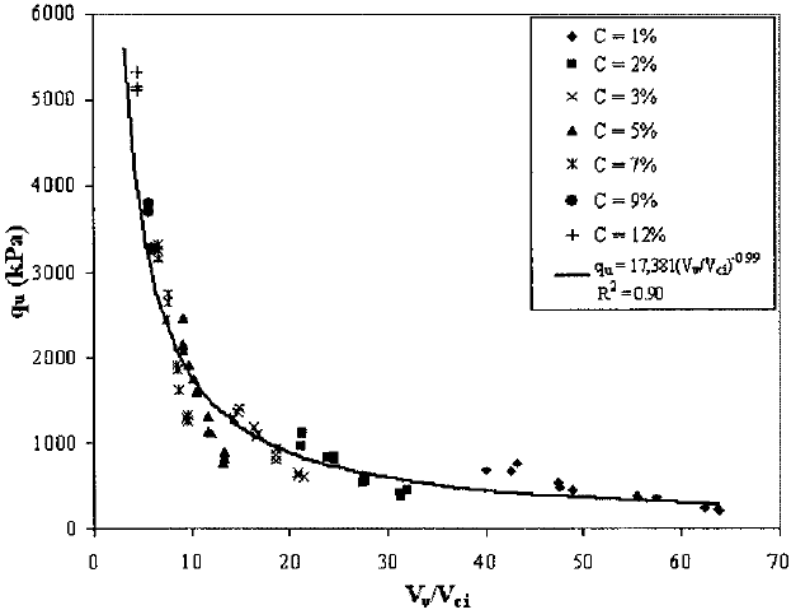

Figure 3.7 Variation of the unconfined compression strength with the porosity/cement ratio (Consoli et al., 2007)

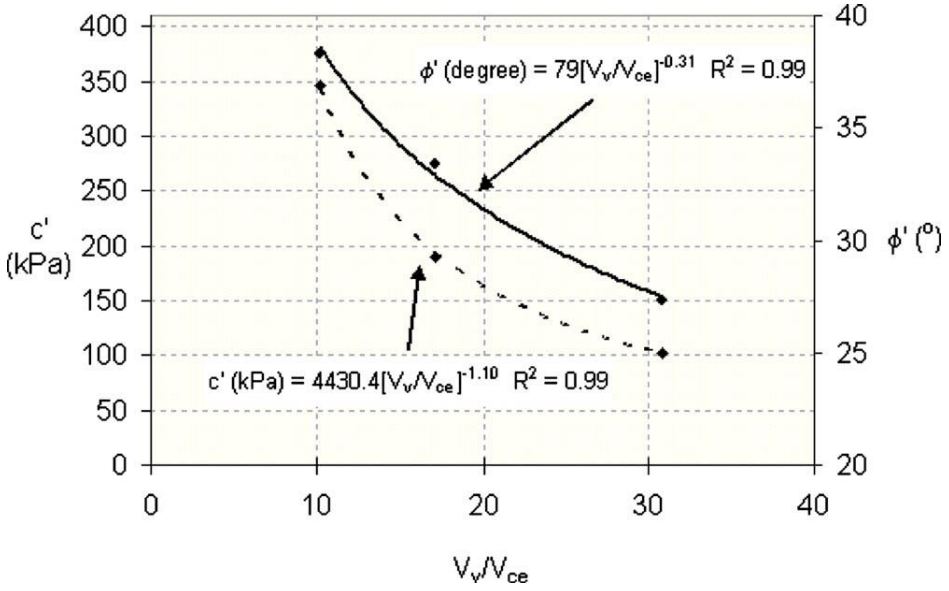

Figure 3.8. Relationship of the porosity/cement ratio with peak effective strength parameters: cohesion intercept and angle of shearing resistance (Consoli et al., 2009)

3.3 Characterization of the cyclic behaviour of cemented soils

3.3.1 Introduction

Artificially cemented soils for transport platforms subjected to cyclic loading are not usually seen in the literature. Some data concerning loose cemented and uncemented sands is available with the aim of analyzing the liquefaction phenomenon (Seed and Idriss, 1971,

Idriss and Boulanger, 2006, Viana da Fonseca et al., 2011; Carrera et al., 2011; Dash et al., 2011). Additional data about natural cemented carbonate sands is also found due to the great interest of these studies in the petroleum industry (Airey, 1993, Yeoh and Airey, 1994 and 1998, Sharma, 2004). Furthermore, there are some other interesting works about the cyclic behaviour of unbound granular materials (UGM) to be applied in transport infrastructures (Werkmeister, 2003). It should be noted that the materials studied in the scope of this work are highly compacted, generally compacted over than 90% of the Modified Proctor, and consequently their behaviour can be a bit different from loose cemented sands or natural cemented sands with higher void ratios.

For this reason, the cyclic behaviour of artificially cemented soils was analysed in two parts: first, the static behaviour of artificially cemented soils was studied and then the cyclic behaviour of uncemented soils was pursed in order to estimate the possible behaviour of cemented soils in cyclic conditions. In the previous section (section 3.2) the static behaviour of cemented sands has been highlighted specially in terms of the most important parameters. In this section the issue of cyclic loading conditions will be introduced focusing on the main relevant works in this area even if most of them are not directly related to cemented soils.

3.3.2 Cyclic loading

Under the passage of a moving wheel load, an element of material in the track substructure or in the pavement subgrade is subjected to a complex regime of vertical, horizontal and shear stresses, as shown in Figure 3.9, leading to principal stresses rotation (Lekarp et al., 2000a; Werkmeister, 2003; Burrow et al., 2004, Momoya et al., 2005, Gräbe and Clayton, 2009 among others). Currently, the most suitable equipment to simulate in situ conditions subjected to a moving load is the Hollow Cylinder Apparatus (HCA) which, unlike conventional triaxial apparatus, allows normal and shear stresses to be controlled. Gräbe and Clayton (2009) showed that the axial permanent deformation obtained without the principal stress rotation effect, as is the case of cyclic triaxial loading, may be underestimated when compared to the HCA results considering the principal stress rotation (PSR). According to these authors the ratio of the rate of increase of permanent strain per log of loading cycles with PSR divided by the corresponding rate without PSR, for the same material, can be as much as between 1.5 and 3.8 depending on the clay content. In fact, the clay content seems to have a significant effect because when it was reduced, the permanent deformation resulting from PSR increased. Furthermore, the difference induced by PSR was greater at higher peak effective principal stress ratios.

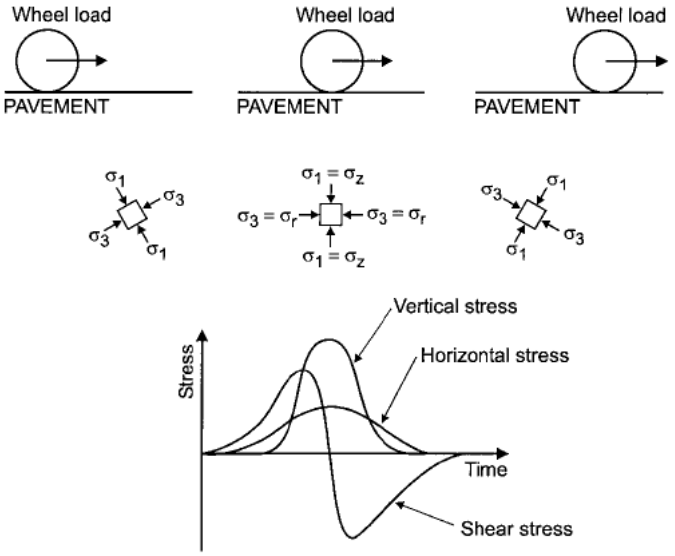

Figure 3.9 Stresses induced under a moving wheel load (Lekarp et al., 2000a)

3.3.3 Permanent and resilient deformation

In the case of road pavement design the criteria applied in current (analytical) design methods are intended to avoid excessive permanent deformation originating within the subgrade and cracks initiating at the underside of the bound layers due to the cyclic resilient deformation (fatigue) (Figure 3.10).

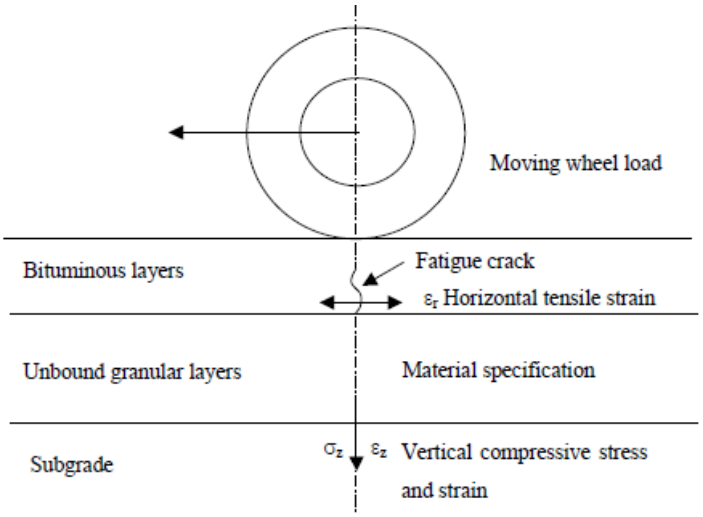

Figure 3.10 Critical strains and stress in a three layer system considered for routine design of road pavements (Powel et al., 1984).

In railway track systems computer models have become of interest for characterizing the resilient response and thus analysing track performance, being the subgrade resilient modulus an essential property in these models (Li and Selig, 1994).

The resilient modulus is, in fact, a parameter to assess and characterize the elastic stiffness of soils and aggregates. However, this in not a constant property but it depends upon many different factors as described by Li and Selig (1994), Lekarp et al. (2000a), Konrad and Nguyen (2006) among others:

- loading condition or stress state;
- soil type and its structure (including compaction method and energy);
- soil physical state (moisture content and dry density).

In the first, the most important is usually the deviator stress but others factors are included such as confining stress, number of cycles and their sequence.

Figure 3.11, illustrating the typical stress-strain relationship in cyclic loading, allows the definition of resilient and permanent deformations as well as the resilient modulus referred above. During one load cycle there are elastic and plastic deformations, in the sense that only part of the deformation is recovered (ε_r - elastic or resilient deformation). The remaining part is considered as a permanent or plastic deformation - ε_p. In most cases the permanent deformation of just one load cycle is insignificant; however the accumulation of plastic deformations through a great number of cycles can be very important. For that reason, the permanent deformation is usually quantified in terms of the sum of permanent deformations occurred in a number of cycles n (ε_p^n), which corresponds to the deformation at the end of cycle n (assuming zero deformation in the beginning of cycle 1). According to the European standard (CEN, 2004a) the resilient deformation is the deformation recovered during the unloading part of the cycle obtained by the difference between the deformation when the load is maximum and the deformation at the discharge of the unload branch of the cycle. To estimate the resilient modulus it is assumed that a resilient behaviour has been established independent of the number of cycles, i.e, after some cycles the permanent deformation has stabilized or has reduced significantly and the resilient deformation is approximately constant. In ASTM (1996a) a closure error (Δ_c), defined as the deformation between two successive peaks (Figure 3.11), is limited to 0.0001 in (0.00254 mm) so that the evaluation of the stiffness (“resilient”) modulus can be considered valid. If some permanent deformation is still present, the resilient modulus should be determined in the unloading part of the curve, in agreement with the previous definition of the resilient deformation, as shown in Figure 3.12.

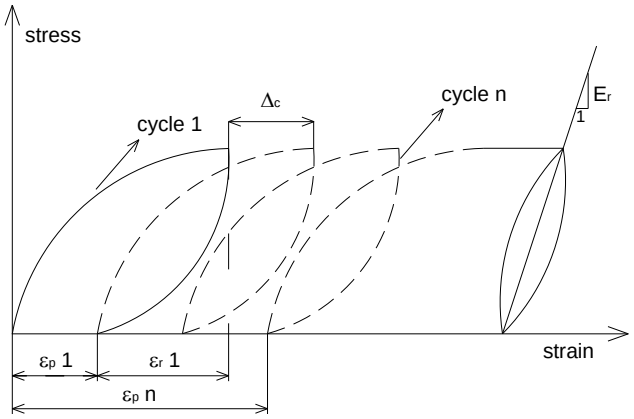

Figure 3.11 Typical stress-strain relationship in cyclic loading

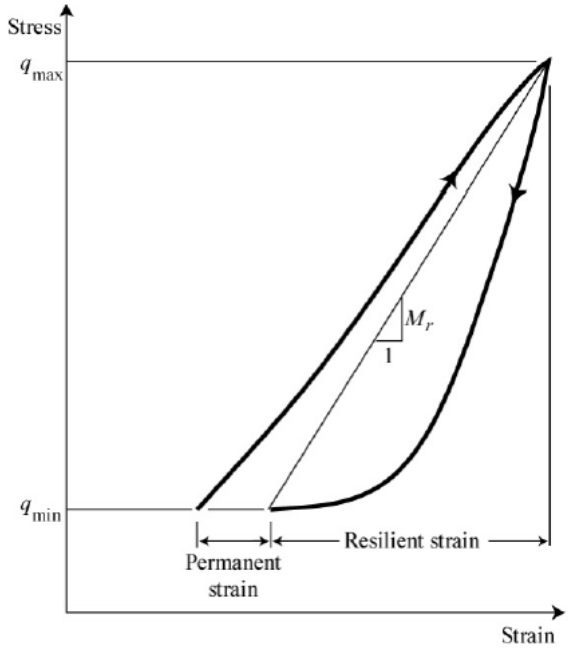

Figure 3.12 Definition of the resilient modulus (Konrad and Nguyen, 2006) Note: The M value was used by the authors instead of the Young Modulus due to the nonlinear elastic response of granular materials

There are some models to estimate the permanent deformation associated to a given number of cycles, and also more complex expressions relating the permanent strain with respect to stress level. Traditionally, the foundation layers of pavements or railway tracks were always constructed with granular materials. Consequently, most of the studies in the scope of the cyclic behaviour of foundation layers involved unbound granular materials. Table 3.2 summarizes some of the approaches presented by Lekarp et al. (2000b) and Werkmeister (2003) for the estimation of the permanent deformation in terms of the number of cycles.

Table 3.2 Approaches to estimate the permanent deformation with respect to the number of load application (after Lekarp et al., 2000a and Werkmeister, 2003)

Reference	Authors proposal
Khedr (1985)	$\varepsilon_p = NAN^{-b}$
Barksdale (1972)	$\varepsilon_p = a + b\log(N)$
Svere (1990)	$\varepsilon_p = aN^b$
Wolff and Visser (1994)	$\varepsilon_p = (cN + a)(1 - e^{-bN})$
Paute (1996)	$\varepsilon_p^* = A\left(1 - \left(\frac{N}{100}\right)^{-B}\right)$
Huurman (1997)	$\varepsilon_p = A\left(\frac{N}{1000}\right)^B + C\left(e^{D\frac{N}{1000}} - 1\right)$

where,

- ε_p is the accumulation of permanent deformation after N cycles
- ε_p^* is the accumulation of permanent deformation after N cycles, excluding the first 100 cycles
- N is the number of cycles
- a, b, c, A, B, C and D are constants

The resilient deformation was object of more attention through the last decades and it is often analysed through the resilient modulus which has also been reviewed by Lekarp et al. (2000a) and later summarized by Konrad and Nguyen (2006) from which Table 3.3 resulted. As the table evidences the models are based on the loading stress level, in terms of confining pressure (σ_3 in Table 3.3), reference mean stress (p_0 in Table 3.3), bulk stress (θ in Table 3.3), octahedral shear stress (τ_{oct} in Table 3.3), mean stress (p) and deviator stress (q).

Table 3.3 Existing models to predict the resilient response of unbound granular materials (Konrad and Nguyen, 2006) Note: The M value was used by the authors instead of the Young Modulus due to the nonlinear elastic response of granular materials

Reference	Authors proposal
Dunlap (1963); Monismith et al. (1967)	$M_r = k_1 \sigma_3^{k_2}$
Brown and Pell (1967); Seed et al. (1967)	$M_r = k_3 \sigma_3^{k_4}$
Uzan (1985)	$M_r = k_5 p_0 \left(\frac{\theta}{p_0}\right)^{k_6} \left(\frac{q}{p_0}\right)^{k_7}$
Witczac and Uzan (1988)	$M_r = k_8 p_0 \left(\frac{\theta}{p_0}\right)^{k_9} \left(\frac{\tau_{oct}}{p_0}\right)^{k_{10}}$
Andrei (1999)	$M_r = k_{11} p_0 \left(\frac{\theta - 3k_{14}}{p_0}\right)^{k_{12}} \left(\frac{\tau_{oct}}{p_0} + k_{15}\right)^{k_{13}}$
Tam and Brown (1988)	$M_r = k_{16} \left(\frac{p}{q}\right)^{k_{17}}$
Johnson et al. (1986)	$M_r = k_{18} \left(\frac{J_2}{\tau_{oct}}\right)^{k_{19}}$
Itani (1990)	$M_r = k_{20} p^{k_{21}} q^{k_{22}} \sigma_3^{k_{23}}$
Pezo and Hudson (1994); Garg and Thompson (1997)	$M_r = k_{24} q^{k_{25}} \sigma_3^{k_{26}}$

Note: k_i, material parameters for each model

3.3.4 Strength and Shakedown theory

The cyclic behaviour of the soil is often approached in the literature by the evaluation of the cyclic strength of the soil and the number of the cycles to failure. The cyclic strength was defined by Sharma and Fahey (2003a) as the cyclic stress that can cause failure of the sample after a specific number of cycles. Other authors, like Li and Selig (1996), had considered the dynamic strength of the soil defined as the critical level of repeated deviator stress above which the soil plastic deformation increases rapidly with cyclic loading.

The Li and Selig (1996) approach is in agreement with the shakedown theory included in the concept of the European standard EN 13286-7 - Cyclic load triaxial test for unbound mixtures (CEN, 2004a). It is interesting to notice that even the European standards still lack a correspondent standard for hydraulic bound mixtures.

This concept of shakedown was definitely developed for unbound granular soils, and it may not be applicable to cemented soils, however, being the reference of most works found in the literature (including the European standard for cyclic triaxial tests) it is worth going through some detailed explanation. According to Yu et al. (2007a), the basic assumption of this theory is that below a certain load (termed the ‘shakedown load’) the structure will

eventually shakedown, i.e. the ultimate response will be purely elastic (reversible), that is there is no more accumulation of plastic strain. If the applied load is higher than the shakedown load, the structure will fail in the sense that the structural response is always plastic (irreversible) in spite the number of load cycles applied. In fact, as stated by Werkmeister et al. (2001, 2005), the shakedown concept has been used to describe the behaviour of conventional engineering structures under repeated cyclic loading. The possible use of the shakedown concept in pavement design was first introduced by Sharp (1983) and Sharp and Booker (1984) justified with results of the AASHO-Road-Tests (Kent, 1962) where, in some cases, the deformation was reported to stabilize after a finite number of load applications. The original concept provides four categories of material response under repeated loading as illustrated in Figure 3.13:

- purely elastic (0 in Figure 3.13)
- elastic shakedown (1 in Figure 3.13)
- plastic shakedown (2 in Figure 3.13)
- incremental collapse or ratchetting (3 in Figure 3.13)

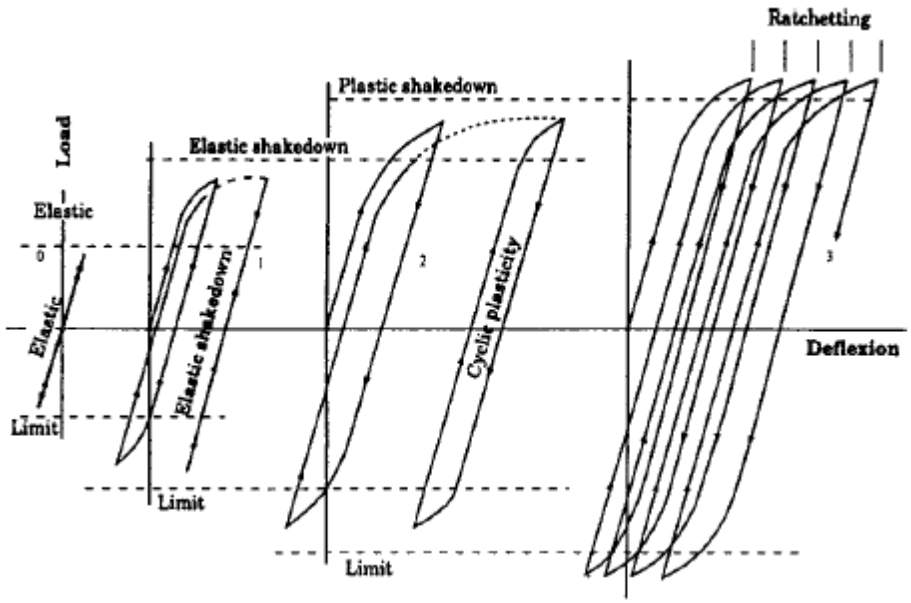

Figure 3.13 Classical elastic/plastic shakedown behaviour under repeated cyclic compression and tension (Johnson, 1986)

However, Werkmeister et al. (2004), having studied in detail the cyclic behaviour of unbound granular materials (UGM), stated that this behaviour does not relate in a straightforward manner to what was observed in laboratory testing of UGM and thus, another modified set of possible responses was defined in shakedown terms. Instead of Figure 3.13, these authors suggest the idealized behaviour illustrated in Figure 3.14 introducing three types of behaviour:

(A) plastic shakedown;

(B) intermediate response-plastic creep;

(C) incremental collapse.

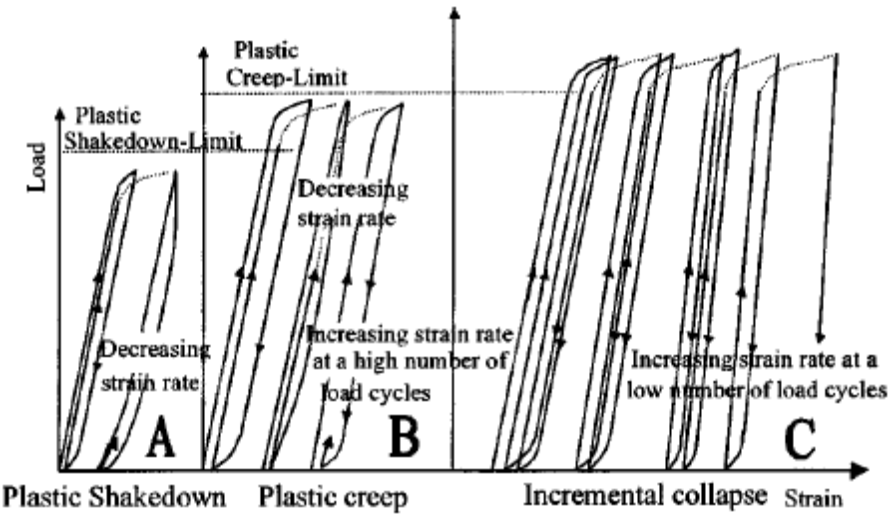

Figure 3.14 Idealized behaviour of granular materials under repeated cyclic pressure load (Werkmeister et al., 2001, 2005)

It should be noticed that the original concept presented in Figure 3.13 assumes that the material is loaded equally in tension and in compression. Werkmeister et al. (2004) clearly noticed that the UGM cannot sustain tensile strains in the same way as compression strains and thus, it is unlikely that the hysteresis loop will be symmetrical. On the other hand, none of the test results presented by these authors showed “Range 0 - purely elastic” (Figure 3.13) leading to the conclusion that probably this type of response does not occur in pavements UGM’s due to the permanent and resilient deformations always observed in the first cycles (indicated by the authors as postcompaction strain as a result of particle orientation).

In the plastic shakedown range (Range A in Figure 3.14) the response is plastic for a finite number of load applications but after the postcompaction period the response becomes entirely resilient and no further permanent strain occurs. It is said to “shake down”.

In the incremental collapse (Range C in Figure 3.14) there is a continuing of incremental plastic deformation with each load cycle and the permanent strain rate decreases very slowly or not at all (Figure 3.15a).

In the Intermediate response (Range B in Figure 3.14) the behaviour is characterised by a decrease of the high level of plastic strain rate during the first load cycles to a low nearly constant level. Although the behaviour may seem to stabilize, failure could occur if cycling

at the same load level is continued long enough. The distinction between Range B and C is usually clear plotting the vertical permanent strain rate against the vertical permanent strain (Figure 3.15a). In cases where this procedure is not enough the analysis of the resilient strain with the number of cycles can be very useful (Figure 3.15b).

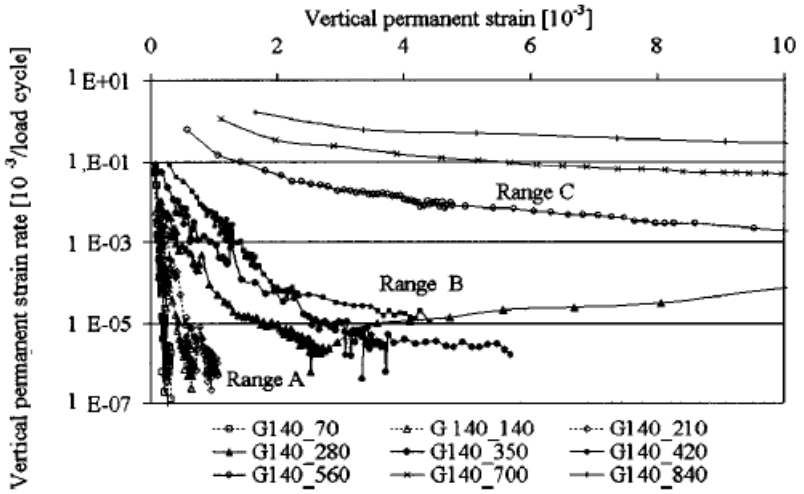

a)

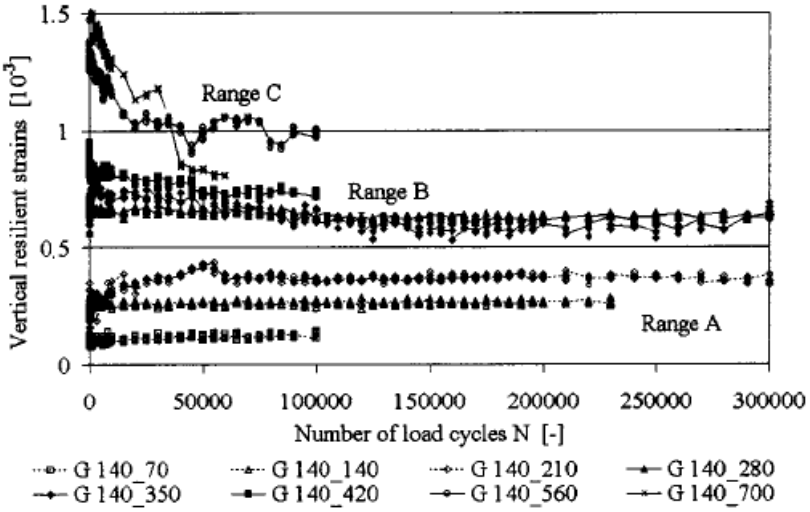

b)

Figure 3.15 Plots to distinguish between the different ranges: a) vertical permanent strain rate against vertical permanent deformation; b) vertical resilient strain against the number of cycles (Werkmeister et al., 2004)

The referred ranges A, B and C may be compared with the responses provided in the original shakedown concept (Figure 3.13) as following: ranges A and B correspond to behaviour type 2 and 3 except that they do not enter tensile space, and range B corresponds to an intermediate behaviour between type 2 and 3.

3.3.5 European standard

The European standard also supports these classification ranges, as well as the permanent deformation limits obtained by Werkmeister (2003) from plots like Figure 3.15. The classification ranges proposed in the European standard, illustrated in Figure 3.16, are the following:

- Plastic shakedown – range A (stable deformation behaviour);
- Plastic creep – range B (failure at high number of load cycles);
- Incremental collapse – range C (failure at low number of load cycles).

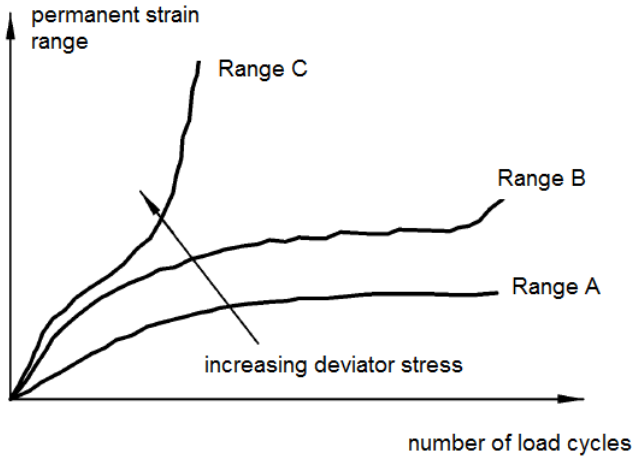

Figure 3.16 Deformation behaviour of unbound granular materials (adapted from CEN, 2004a)

The idea underlying in the standard is to create a model where the shakedown limit of each material is known and for each case the suitability of the material for a pavement layer can be easily checked (Figure 3.17).

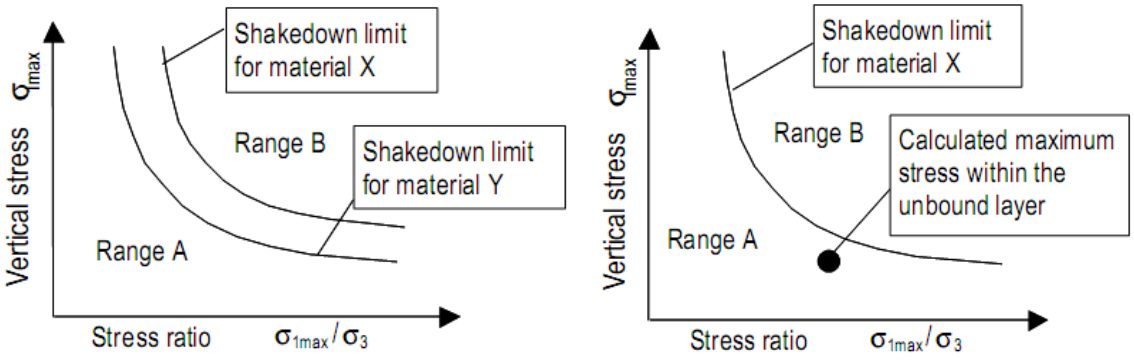

Figure 3.17 Ranking of materials and application to unbound pavement layers (adapted from CEN, 2004a)

In that model equation (3.1) should represent the plastic shakedown limit of the material:

$$\sigma_{1max} = \alpha \times \left(\frac{\sigma_{1max}}{\sigma_3}\right)^{\beta} \quad (3.1)$$

where,

- σ_{1max} is the maximum value of the vertical stress (kPa),
- σ_3 is the constant cell pressure (kPa),
- α is a model constant (kPa),
- β is a model constant.

To find out these constants, it is suggested to conduct permanent deformation tests at a minimum of three different confining stresses. For each confining pressure the specimen should be subjected to increasing deviator stress levels according to Table 3.4 until the following strain is reached:

$$\varepsilon_p{}^{5000} - \varepsilon_p{}^{3000} > 0.04\% \quad (3.2)$$

where,

- $\varepsilon_p{}^{5000}$ is the vertical accumulated permanent deformation at 5000 load cycles,
- $\varepsilon_p{}^{3000}$ is the vertical accumulated permanent deformation at 3000 load cycles.

Table 3.4 Possible stress levels for the permanent behaviour ranking test (Single-Stage Tests / Multi-Stage Test) - CEN (2004a)

Confining stress, σ_3 kPa	**Deviator stress**, σ_D kPa	**Stress ratio**, σ_D/σ_3 (–)
constant	min	max
20	0	1; 2; 3, 4; 5; 6; 7 … n
50	0	1; 1,5; 2; 2,5; 3 … n
70	0	1; 1,.5; 2; 2,5; 3 … n
150	0	1; 1,5; 2; 2,5; 3 … n

On the basis of Werkmeister (2003), the European standard suggests that the Plastic Shakedown limit is defined by the following strain value:

$$\varepsilon_p{}^{5000} - \varepsilon_p{}^{3000} = 0.0045\% \quad (3.3)$$

and the Plastic Creep Limit is defined by:

$$\varepsilon_p{}^{5000} - \varepsilon_p{}^{3000} = 0.04\% \quad (3.4)$$

Subjecting a specimen to stress levels which generate strains a little larger than these values, will allow the exact Plastic Shakedown and Plastic Creep Limits to be interpolated.

3.3.6 Other significant issues in cyclic conditions especially in cemented soils

There are several issues such as strain rate effects, fatigue or creep that may affect the soil behaviour in cyclic conditions.

Rate effects are related to the velocity of the loading, and are conceptually quite simple to understand as explained by Matesic and Vucetic (2003) for monotonic loading. If the velocity of loading and straining is low, more time is allowed for the soil to creep and relax, allowing the development of larger deformations at a given load increment and larger shear stresses at a given strain increment. The final result is that the stress-strain curves plots lower, which means that the strength is increased when the velocity is higher.

In cyclic conditions rate effects depend on the loading frequency. For six soils varying from clean sand to high plasticity clay, Matesic and Vucetic (2003) have shown the cyclic secant modulus to rise with increasing strain rate. In clays, this increase was relatively significant while in sands it was much smaller. Yeoh and Airey (1994 and 1998) also agree that in granular soils rate effects are not so significant, but in cemented soils, like in artificially cemented carbonate sand, the number of cycles to failure has changed with frequency. These authors have concluded that increases in frequency cause significant increases in the number of cycles to failure and that these increases are more marked at higher stress levels where rate effects and creep are likely to be more significant. Furthermore, the initial modulus also increased with frequency for a given stress level revealing to be associated to lower strain amplitude and reduced creep.

The cyclic fatigue phenomenon is observed when the material fails at a stress level lower than its static strength. Yoshinaka and Osada (1995) reported this behaviour when working with soft sedimentary rocks, observing that the dynamic strength is smaller than the static strength obtained in monotonic tests. From these findings it is expected that the same phenomenon would be observed in cemented soils.

However, the stress history of soils and the drainage conditions may have a significant influence in their dynamic strength. In a normally consolidated clay, for example, the dissipation of pore-water pressure, caused by repeated loading, will lead to reconsolidation and thus to a settlement that makes the soil more resistant to further cyclic loading. For this reason, Yeoh and Airey (1998) reported that in drained conditions the number of cycles to failure is expected to be higher than in undrained conditions. However, draining conditions

in laboratory, for instance in a cyclic triaxial test, may be difficult to implement when high frequencies are applied if the pressure-volume control is not able to respond fast enough.

The creep effect is reported by Werkmeister et. al. (2004), expressed in Figure 3.18, which has separated the effects of elasticity and creep looking at a hysteresis loop experienced by a granular material during one load cycle. During one loading phase the curve is initially stiffening (typical of deformation behaviour within Ranges A and B), then, increasing the stress level, softening is observed probably on the transition to Range C where creep is associated with permanent deformation. At the beginning of the unloading there is no, or only very small, recovery. Then, the elastic recovery continues at a much slower rate than the next phase called elastic creep.

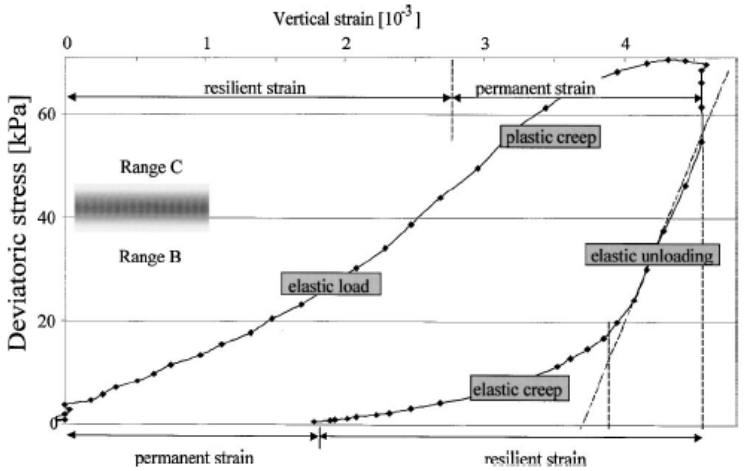

Figure 3.18 Hysteresis loop in a Range C material (Werkmeister et. al., 2004)

Chapter 4.

CEMENTED SOILS WITHIN THE CONTEXT OF CRITICAL STATE SOIL MECHANICS

4.1 Introduction

In soils, the term structure was first introduced by Mitchell (1976) but was described by Burland (1990) as the combination of cementation and fabric. Cementation results from bonding between particles and fabric refer to the distribution of the particles and their relative position.

Most natural soils and soft rocks are structured, i.e. at a given void ratio they can sustain higher stresses than could the same material non-structured. Leroueil (2003) summarizes the main differences between structured and non-structured soils saying that the former has higher preconsolidation pressure, undrained strength and stiffness. For this reason state alone has been considered insufficient to characterize those features.

Although critical state soil mechanics has been first established for clays, the behaviour of non-structured and structured sands can be analysed in terms of the critical state theory following the framework proposed by Cuccovillo and Coop (1999) and Coop and Airey (2003). First, a framework for non-structured sands is established and then, having the intrinsic behaviour of the sand as a reference, the effects of structure can be identified and a framework for the structured sand defined.

In this chapter, an overview of the soil behaviour by the critical state soil mechanics will be presented to highlight some basic concepts that will be useful in the subsequent sections.

4.2 Basic principles of the critical state theory

4.2.1 Introduction

Critical state soil mechanics departs from classical soil mechanics by dealing with the volumetric behaviour of the soil together with the stress analysis. Roscoe et al. (1958) stated that the shear behaviour of reconstituted soils is solely controlled by the state of the soil defined as the combination of deviator stress (q), mean effective stress (p') and specific volume (v). Strain softening and strain-hardening modes of shear behaviour are associated with volumetric compression and dilation, respectively, and are therefore controlled by the volumetric changes experienced by the soil in moving from its initial state to critical state.

4.2.2 Isotropic compression

Soil behaviour during isotropic compression is primarily caused by rearrangement of the grains and so the stiffness will increase from loose states to dense states. The mechanisms of volume change in soils due to rearrangement of the grains accounts for the non-linear bulk stiffness behaviour. The unloading-reloading stiffness of the soil during isotropic compression is higher than the initial first loading stiffness because the grains will obviously not "un-rearrange" themselves on unloading. In the same way, soils which have weak grains that fracture on loading, will not "unfracture" on unloading (Atkinson, 2008).

The conventional representation of isotropic compression is the specific volume v plotted against the mean effective pressure p'. The first loading is known as the *normal compression line (NCL)* and is given by:

$$v = N - \lambda \ln p' \tag{4.1}$$

where λ is the gradient and N is the value of v when p'=1 kPa. This representation is similar to the typical curve obtained from oedometer tests in function of void ratio and vertical effective stress:

$$e = e_0 - C_c \ln \sigma'_v \tag{4.2}$$

The unloading line is usually called *swelling line* and is given by:

$$v = v_k - \kappa \ln p' \tag{4.3}$$

where κ is the gradient. There are infinite swelling lines and therefore infinite values of v_k defined as the value of v when p' = 1 kPa (Figure 4.1). However, the parameters λ, k and N

remain always constant for a given soil and so they are regarded as important parameters of a particular soil.

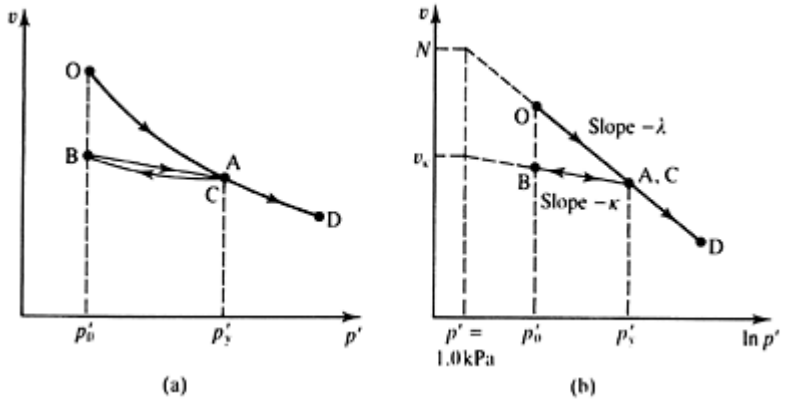

Figure 4.1 Isotropic compression and swelling: a) non logarithmic scale; b) logarithmic scale (Atkinson, 2008).

According to the theory of critical state soil mechanics (Roscoe et al., 1958) the state of the soil can reach any point below and to the left of the NCL by unloading, but the state cannot reach the region above and to the right. Hence the NCL is a boundary to all possible states for the isotropic compression.

4.2.3 Peak and ultimate strength

In simple terms the strength of a material is the maximum shear stress that it can sustain; materials loaded just beyond the maximum stress will fail. Failure may be sudden or it may lead to a very large plastic straining. Typical stress-strain curves for soils according to the critical state framework are presented in Figure 4.2.

Two types of behaviour can be seen depending on the state of the soil before shearing as expressed by Figure 4.3. Soils consolidated on the wet side of critical can be normally or lightly overconsolidated clays or loose sands (marked W on Figure 4.2) and soils on the dry side are generally heavily overconsolidated clays or dense sands (marked D on Figure 4.2).

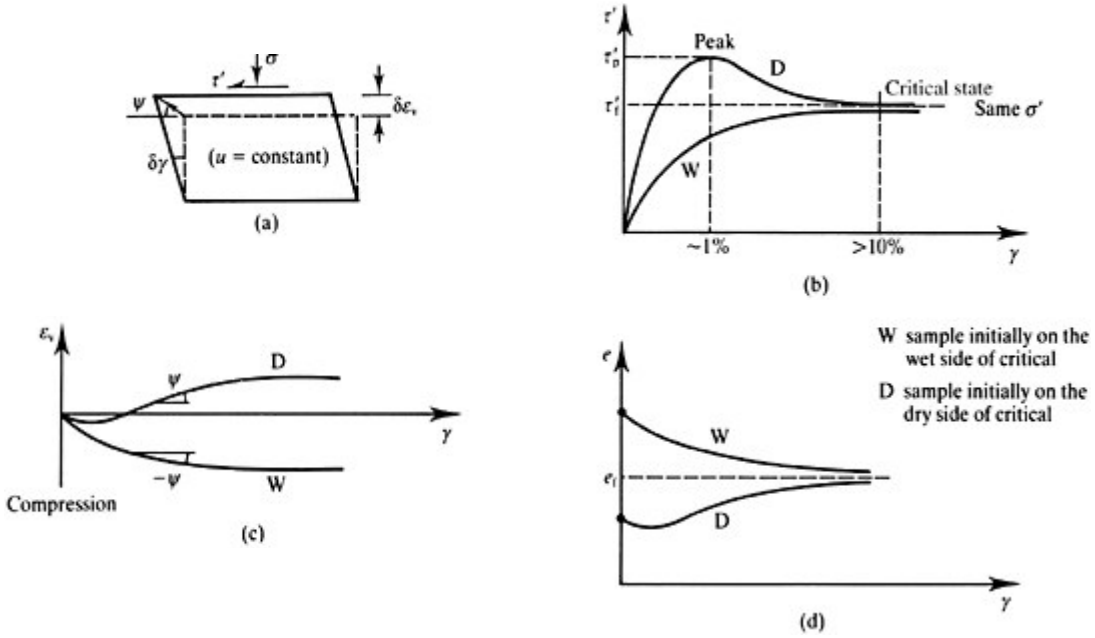

Figure 4.2. Typical behaviour of soils in drained triaxial tests (Atkinson, 2008)

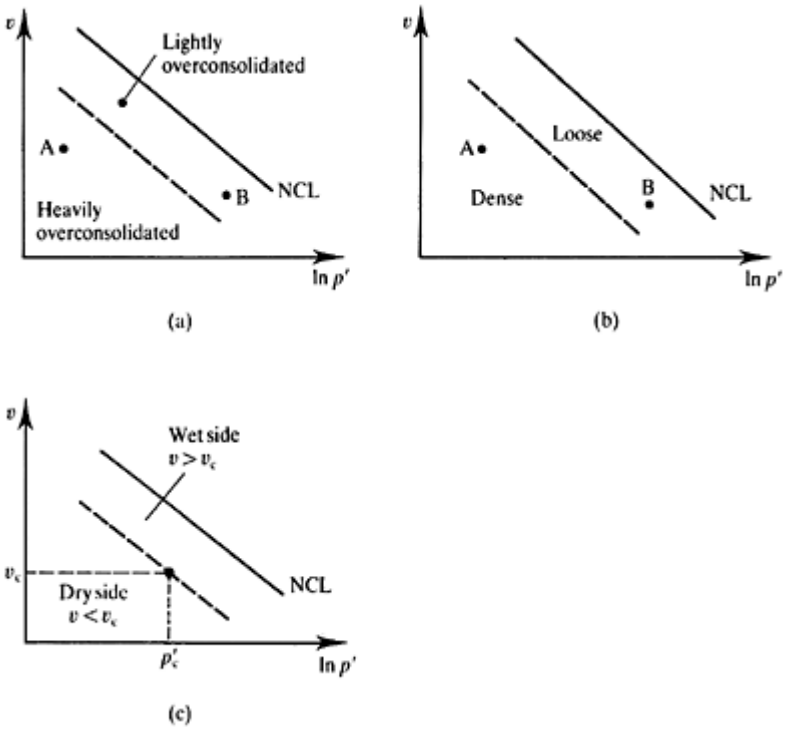

Figure 4.3 States of soils on the wet side and on the dry side of critical (Atkinson, 2008)

Soils on the wet side compress as the shear stresses increase while soils on the dry side dilate (expand) after a small compression. Soils on the dry side reach peak shear stresses before reaching the ultimate state. In reconstituted soils the peak state coincides with the point of maximum rate of dilation, defined as the gradient of the volume deformation

towards the axial deformation. Soils on the wet side compress throughout shearing up to the ultimate state and there is no peak.

Critical state can be defined as the ultimate state of the sample in which the mass is continuously deforming at constant volume and constant vertical effective stress. This state is reached after at significant strain level (usually higher than 10%) and at that point there is an unique relationship between the shear stress, the normal stress and the voids ratio represented by the critical state line (CSL) given by:

$$v_f = \Gamma - \lambda \ln p'_f \quad (4.4)$$

$$q'_f = M\, p'_f \quad (4.5)$$

where f denotes ultimate failure at the critical states. The gradient of the critical state line in the plot deviatoric stress (q) against mean effective stress (p') is M and can be related to the critical friction angle ϕ'_c. The CSL and NCL are parallel in the plane v against p' and the gradients are λ (Figure 4.4).

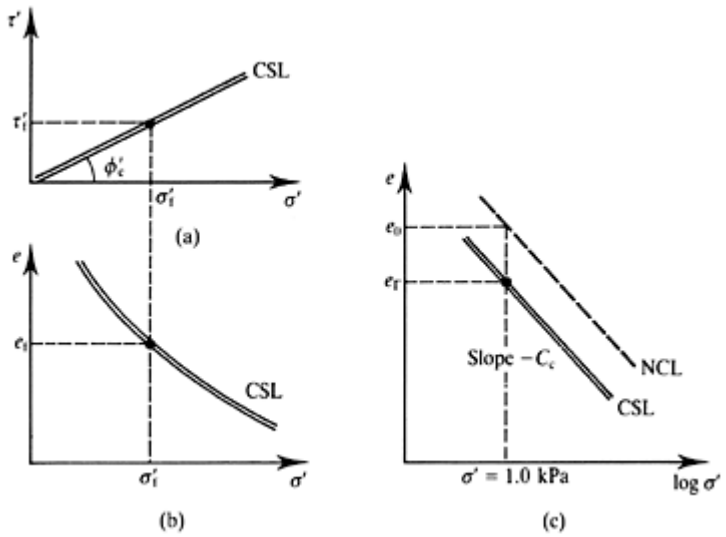

Figure 4.4 Critical states of soils (Atkinson, 2008).

The essential features of critical states are that, during shear, all soils will ultimately reach their critical states which are independent of the initial states. As express before in Figure 4.2, soils on the wet side compress and soils on the dry side dilate but they both will ultimately reach the CSL as is shown in Figure 4.5 in terms of v against p'.

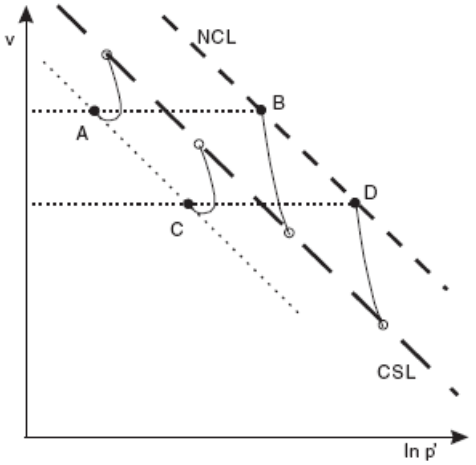

Figure 4.5. Schematic illustration of the influence of state on volumetric change (Coop and Airey, 2003)

Peak states from shear tests on samples with different values of normal effective stress, overconsolidation ratio and voids ratio generally fall within the region OAB of Figure 4.6 which is above the critical state line. At effective stresses lower than those normally applied in routine soil tests (i.e. at high overconsolidation ratios) the peak state line is markedly curved towards the origin.

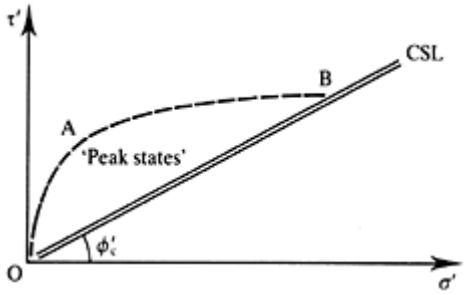

Figure 4.6 Region of peak states (Atkinson, 2008).

One way to examine the peak state is to make use of the Mohr-Coulomb equation - Eq. (4.6) - with an apparent cohesion intercept and a peak friction angle (ϕ'_p). Although with normalized axis (which will be explained in detail in the following section), Figure 4.7 illustrates this peak envelope.

$$\tau_p = \sigma'_p \tan(\phi'_p) + c'_p \quad (4.6)$$

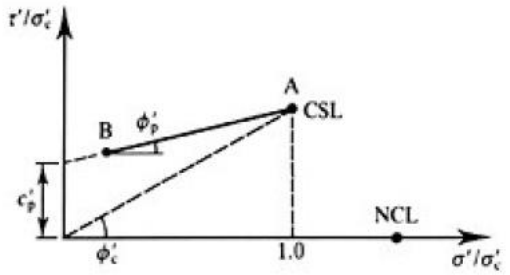

Figure 4.7 Normalized peak and critical states for shear tests. (Atkinson, 2008).

In cohesionless soils another approach is more commonly used, which considers no cohesion intercept being the peak friction angle the combination of the critical state friction angle (ϕ'_c) and dilatancy (ψ). A first proposal, illustrated in Figure 4.8 and expressed in (4.7), was derived from the stress-dilatancy relation of Taylor (1948). Another proposal was later presented by Bolton (1986) - Eq. (4.8) - based on Rowe's stress-dilatancy equation (Rowe, 1962).

$$\tau_p = \sigma'_p \tan(\phi'_c + \psi) \tag{4.7}$$

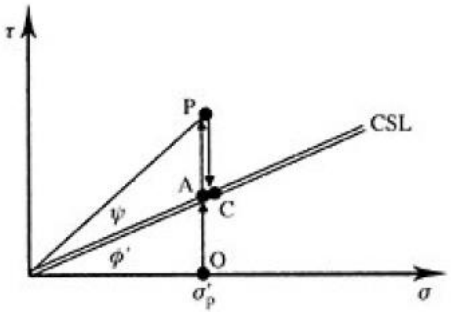

Figure 4.8. Peak strength of dilating soil (Atkinson, 2008)

$$\tau_p = \sigma'_p \tan(\phi'_c + 0.8\,\psi) \tag{4.8}$$

4.2.4 Normalization

Using a method of normalizing voids ratios or specific volumes, all specimens (for a given soil) with the same history and state should ideally have the same behaviour after normalization. The stress path v:q:p' can be normalized for the effect of volume becoming q/p'_e and p'/p'_e being p'_e the normalizing parameter. This means that all the points over the same line such as NCL or CSL or even another one parallel to these will be represented by a single point after normalization (Figure 4.9).

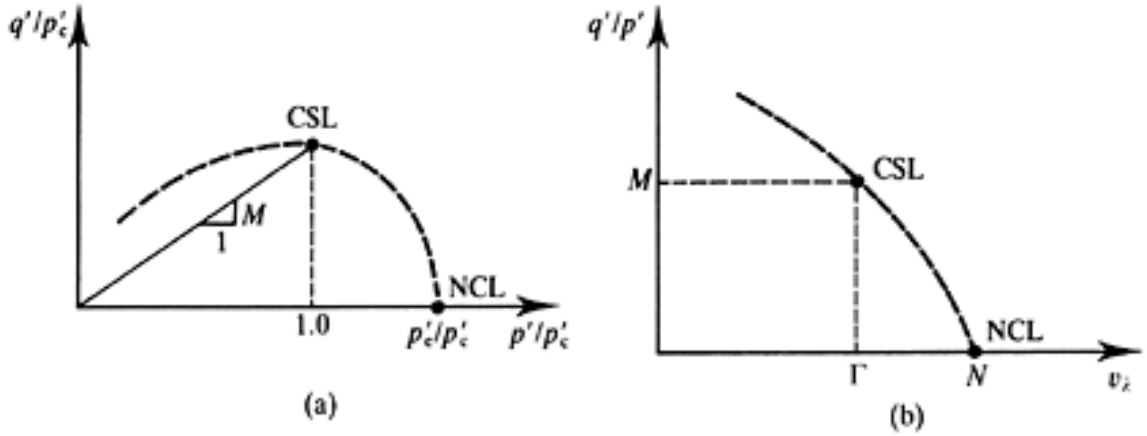

Figure 4.9 Normalized critical state and normal consolidation lines (Atkinson, 2008).

There are different ways of normalization and thus different normalizing parameters. The most common is to consider the equivalent pressure on the normal compression line (p'_e) or on the critical state line (p'_c) as normalizing parameters (Figure 4.10). Each value of the stress-path is normalized by the correspondent normalizing parameter obtained by the NCL or CSL equation for the specific volume (v) of the point that is being normalized as following,

$$p'_e = \frac{\mathrm{N} - v}{\lambda} \tag{4.9}$$

$$p'_c = \frac{\Gamma - v}{\lambda} \tag{4.10}$$

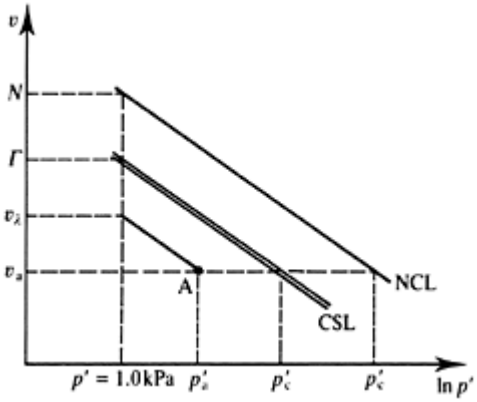

Figure 4.10 Parameters for normalizing triaxial test results (Atkinson, 2008).

The equivalent pressure on the isotropic normal compression line p'_e is often used as a normalizing parameter for triaxial tests, especially when the critical state line is not so well defined. Otherwise, the p'_c normalization is preferred as the critical state line is unique for a given soil, while there are different NCL for isotropic and one-dimensional compression and the position of the NCL of natural soils can be influenced by cementing, structure and other effects (Atkinson, 2008).

Another way or normalization is based on the state parameter ψ defined by Been and Jefferies (1985) as the vertical distance of the initial state from the critical line for the same mean effective stress p'. However, in some soils (in particular sands) the CSL may be curved in the lower stresses and so this parameter becomes less useful as Figure 4.11 expresses.

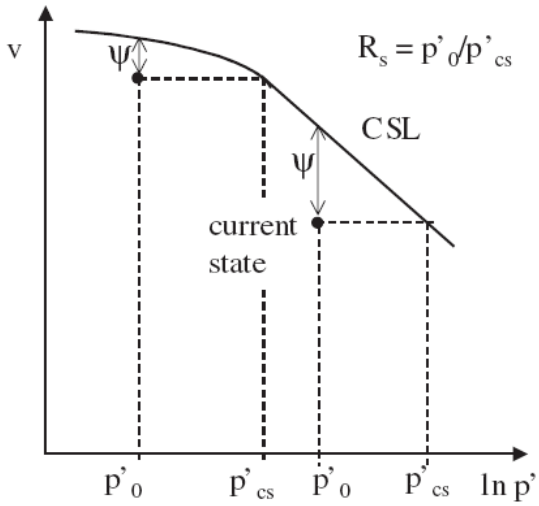

Figure 4.11. Definition of normalizing parameters (Been and Jefferies, 1985)

4.2.5 State boundary surface

There are cases where the possible states of soils are limited: the isotropic normal compression line represents a boundary to all possible states of isotropic compression; and similarly, the peak envelope must also represent a boundary to all possible states.

The peak state line corresponds to one specific volume. There will be other peak state lines corresponding to other volumes and together these will form a peak state surface that can be reduced to a single line by normalization. The peak state surface is a boundary on the dry side of the critical. The remaining part of the state boundary surface links the NCL and the CSL represented by single points in the normalized plot.

However, it should not be forgotten that the line of the state boundary surface which has normalized axes is really a three-dimensional surface in the set of axes q':p':v (Figure 4.12). This surface is rather difficult to draw, which is why it is easier to normalize the results first.

The part of the state boundary surface on the wet side of critical (i.e. between the NCL and the CSL) is sometimes known as Roscoe surface and the part on the dry side corresponding to peak states is sometimes known as Hvorslev surface. Since uncemented

soils cannot sustain tensile (negative) effective stresses, this also represents a limit to possible states. The surface is called the tension cut-off and it limits the Hvorslev surface where the mean effective stress p' is close to zero. By definition, the state cannot exist outside the surface, although there are cases of cemented soils where unstable states outside the boundary surface are possible. If a soil with a state on the surface is unloaded the state moves inside the surface and on reloading the state will be back to, but not outside, the surface. Thus, the state boundary surface can also be a yield surface.

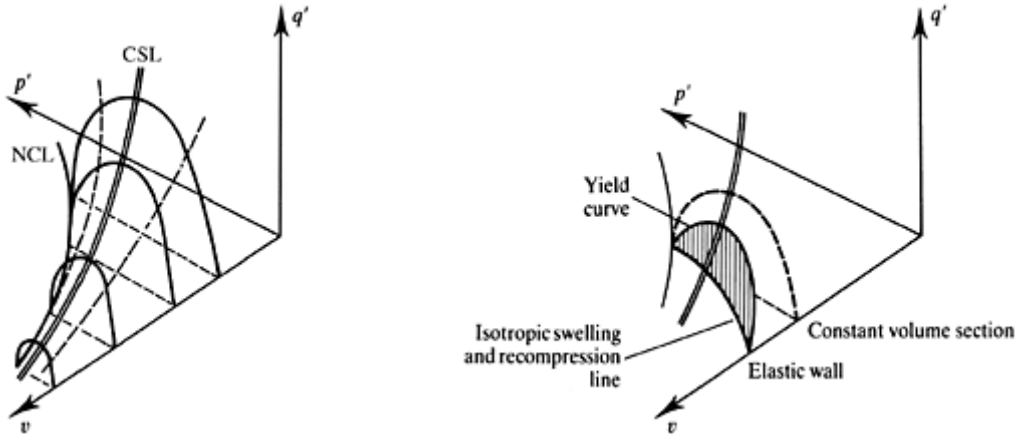

a) b)

Figure 4.12 A state boundary surface for soil (a); Elastic wall and yield curve (b). (Atkinson, 2008)

4.3 The behaviour of sands

As mentioned before the understanding of uncemented sands behaviour within the critical states soil mechanics is very important because the effect of cementation can be analysed by comparison of the same sand in uncemented and cemented conditions.

Although the critical state theory was first developed for clays, this model can generally be applied for sands, if some of their particular features are taken into account. The framework proposed by Coop (2003) for uncemented sands is similar to the critical state framework used for clayey soils in using normal consolidation and critical state lines and describing the sand behaviour in terms of its state relative to NCL and CSL (equivalent to an overconsolidation ratio). However, departures from the critical state framework occur at low stresses because the behaviour is controlled by the depositional void ratio. A consequence of this is that there are a range of paths by which a soil can reach a given initial state without reaching the NCL, and there are a wider range of possible behaviours than for clays.

The main features of sands behaviour will be summarized as follows (Coop, 2003, Qadimi, 2005):

- the plastic volumetric strain observed in isotropic compression is associated with particle breakage which is gradual so the first yield is indistinct;
- yield in isotropic compression is controlled by the strength of the particles as well as by the initial density which determines the number of inter-particle contacts and hence the contact stresses;
- yield of sands in first loading occurs at very high stresses, so within the engineering stress range most sands will not reach their NCL, and therefore, their behaviour will then depend on the depositional density;
- in contrast to clay, for which the in situ specific volume is a unique function of the current stress, stress history and structure of the soil, for sands it may also depend on the density with which the soil is deposited;
- critical states can be very difficult to define for sands as large strains have to be reached during shear, typically over 30% shear strain;
- especially in the low strains, critical state line can be difficult to determine, leading some authors (example, Verdugo and Ishihara, 1996) to consider that this line may be curved towards the horizontal at lower stress levels. This problem also results from the maximum void ratio that exists in granular soils due to the particles packing. As a consequence, problems may arise in the application of the state parameter methods of normalization using the original definition of state parameter defined by Been and Jefferies (1985) – see Figure 4.11 of section 4.2.4;
- the behaviour of the sand is controlled by its initial grading and not by its current grading because of particle breakage and so, therefore, interpretation of an in situ sand behaviour from tests on reconstituted samples can be very difficult if the sand has experienced any particle breakage during its geological history;
- sands can reach a given initial state by a varieties of paths as they can be overconsolidated or follow a first loading after an initial compaction, meaning that the particle breakage suffered by the sample in each case is different which has an impact on their subsequent shearing behaviour.

4.4 Structured soils in volumetric compression

4.4.1 Stress-volumetric behaviour in isotropic conditions

Following experimental evidences Vaughan (1988) and Leroueil and Vaughan (1990) have demonstrated that structured soils can exist at void ratios greater than are possible for the destructured material. In Figure 4.13 there are two void ratio-stress spaces: the space bonded by the line that defines the loosest possible packing for the destructured soil; and

the space outside this line in which the soil can only exist due to structure. The experimental evidence of such behaviour leads to the following consequences:

- large plastic strains are unlikely while a soil sustain its cemented structure;
- only structure will allow the soil to exist in the structure permitted space;
- the soil will remain stiff until yield (point Y in Figure 4.13);
- large compressive strains will develop when yield occurs in structure-permitted space which will depend on the void ratio and on the difference in void ratio between point Y and the curve limiting the structure permitted space. This behaviour is more compressible than in the remoulded condition and therefore, is called meta-stable.

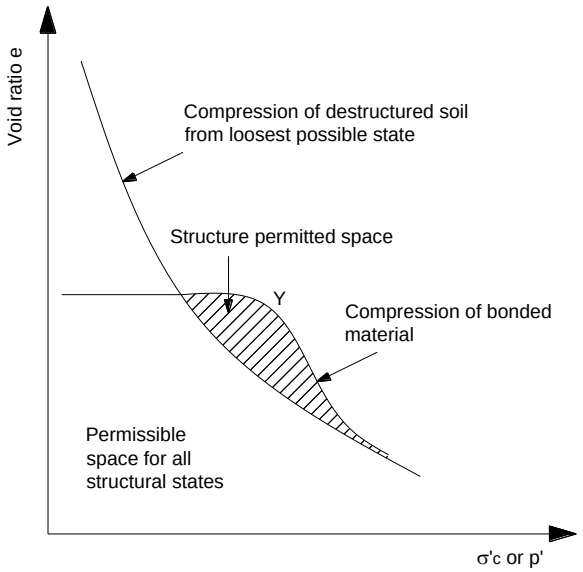

Figure 4.13 Comparison between structured and destructured behaviour in compression (adapted from Vaughan, 1988)

After that many other authors (Burland, 1990; Coop and Atkinson, 1993; Airey, 1993; Viana da Fonseca, 1988, 1996, 1998, 2003, Asaoka et al., 2001, Rodrigues, 2003, Rotta et al., 2003; Baudet and Stallebrass, 2004; Gasparre et al, 2007, among others) have showed the same type of behaviour in other soils.

Working with artificially cemented calcareous sands Cuccovillo and Coop (1999) have proposed two different types of behaviour depending on the nature of cementation distinguishing between strong and weak bonding. For weakly bonded sand, yield of the cement bonds occurs prior to reaching the NCL of the uncemented soil, being the only effect of bonding to increase the pre-yield stiffness. In opposition, strong bonding shows the

pattern presented by Vaughan (1988), allowing the cemented sand to reach states outside the uncemented NCL (Figure 4.15a).

Coop (2003) stated that yield in isotropic compression of sands is associated with the onset of particle breakage. Being so, if cemented sands are reaching states outside the NCL, as in strong type of bonding, this means that the cement is carrying some of the confining stress and preventing breakage, at least partially. However, after yielding the degradation is much higher than what would be expected without cementation as a characteristic of meta-stability. Degradation of the cement bonds turn to be dominant with the onset of particle breakage at the yield point. In reverse, in weak bonded soils the yield of cement occurs before the onset of particle breakage so that the cement yield is less indistinct and a second yield point or "gross yield" will be associated with the start of particle breakage.

Thus, it is expected that both cemented and uncemented normal compression lines will join together at some point even if high stresses are required. As soon as there is degradation of the cement bonds, particle breakage will start and both lines will eventually converge. This is also according to the model proposed initially by Vaughan (1988) as presented in Figure 4.13. Viana da Fonseca (1996, 1998) presented a set of one dimensional compression curves of cemented and remoulded natural silty sand where this was clear, while Rotta et al. (2003) have also shown isotropic compression curves of both artificially cemented and uncemented samples. In this case, the maximum confining pressure used in these tests (around 7MPa) was not enough to show clearly that both NCL on uncemented and cemented samples were coincident, however they seem to converge and the authors believed they would be coincident for higher pressures (Figure 4.14).

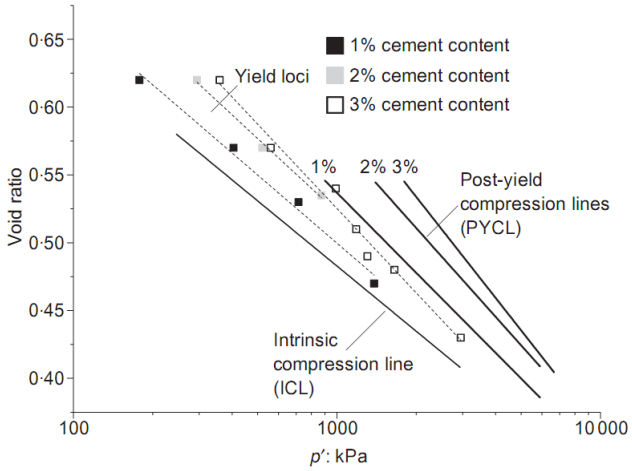

Figure 4.14 Summary of primary yield points, yield loci, and post-yield compression lines (Rotta et al., 2003)

The difference between weak and strong patterns depends on the strength of the bonds compared to the soil strength which is given not only by the individual strength of the grains but also by soil density derived from particles arrangement. Figure 4.15 shows the factors that define the type of behaviour which are not only the strength of bonds but also the location of the NCL and the initial density of the sands. Coop and Airey (2003) report that the weak pattern of behaviour is typical of denser cemented sands including quartz sandstones that can have cement bonding which is relatively weak compared to their particles.

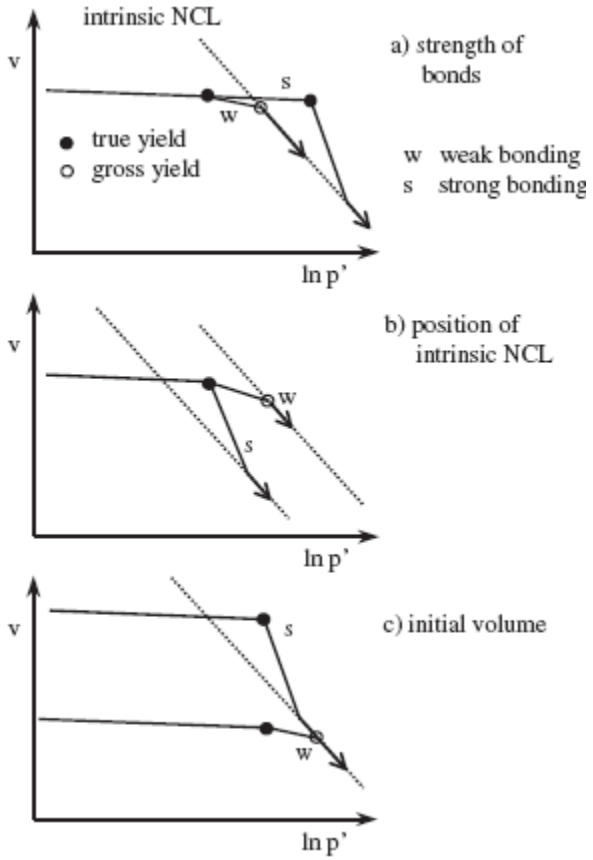

Figure 4.15. Schematic representation of the factors that might influence the effect that inter-particle cementing has on behaviour of a sand (Coop and Airey, 2003)

Alarcon-Guzman et al. (1988) have reported that when the cementation is stronger than the particles, the yielding is only related to the degradation of cementation, and not with the breakage of particles. In this case, the consolidation yield stress is well defined and the consolidation curves of the treated and untreated material can be distinguished easily.

The effect of void ratio on the behaviour of a cemented soil can be approached in different ways. As expressed above, and in agreement with the work of Huang and Airey (1993), the

higher the density, the less is the influence of cementation on the overall behaviour of the soil and fabric becomes more important than bonding. On the other hand, as expressed by Zhu et al. (1995), higher density of soil-cement mixtures will increase the number of bond contacts and therefore the effectiveness of cementation. This fact is corroborated by the work of Chang and Woods (1992) which have defined the degree of cementation in terms of percentage of voids filled with cement in sands. This determinant influence of the voids in the effectiveness of the generalization of the bonding bridges of cementation is revealed in ratios that relate porosity and cement content. The ratio n/C_{iv} presented before will be explored further down in this work for different materials with the possibility of playing with more or less compaction energies. Generally, it will be recognised that the exponent factoring used to fit the experimental results (x in n/C_{iv}^{x}) will be a sign of how porosity becomes relevant in the cementation result when soils are more or less easily compacted such as the well graded soils.

4.4.2 Stress-volumetric behaviour in oedometric conditions

Futai et al. (2004) have performed one-dimensional tests executed in oedometric cells and isotropic compression tests in triaxial cells, over natural samples of a tropical residual soil. These authors realised that there were differences between the preconsolidation pressure obtained on both types of tests, pointing this fact to the coefficient of earth pressure at rest (K_0).

In their reference work, Leroueil and Vaughan (1990), have pointed out the effect of structure on the coefficient of earth pressure at rest (K_0) of natural soils and weak rocks reporting that while the structure is not damaged the K_0 is lower and then, after yielding, the K_0 increases to the value given by Jaky's equation (4.11) for the non-structured material where the behaviour is solely governed by friction.

$$K_0 = 1 - \sin \phi' \tag{4.11}$$

where ϕ' is the angle of shearing resistance.

In Figure 4.16 the evolution of the stress-path followed during the test is shown. The slope of the stress-path is given by Eq. (4.12) which means that when the slope decreases, K_0 increases, which is what happens when the structure is broken.

$$\frac{\Delta q}{\Delta p'} = \frac{3(1+K_0)}{2K_0+1} \tag{4.12}$$

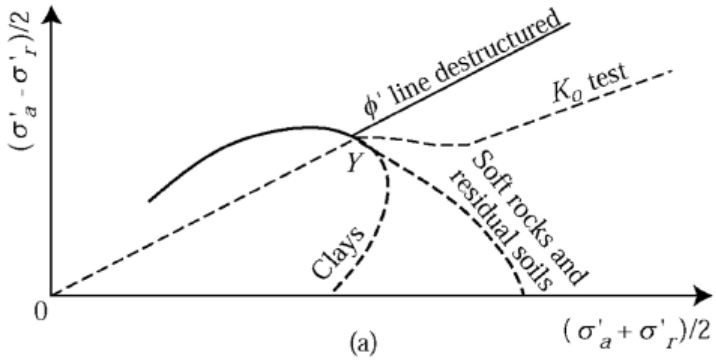

Figure 4.16. Evolution of the stress-path on a K_0 test (Leroueil and Vaughan, 1990)

This was corroborated by Viana da Fonseca (1996) which has performed K_0 tests in undisturbed samples of residual soil from granite, similar to the soil that has been used in this work (Figure 4.17). Viana da Fonseca and Almeida e Sousa (2001) have reported K_0 values around 0.41 in remoulded conditions, while on undisturbed samples values of 0.35 to 0.38 were found, deduced from SBPT tests and triaxial tests over high quality samples. However, regional experience indicate that K_0 values are usually low for high weathering degrees (W6 to W5 rock masses) where K_0 values range from 0.35-0.50, becoming higher in moderate weathering levels (W4 to W3 rock masses) with K_0 values close to unity preserving the stress states of the parent rock.

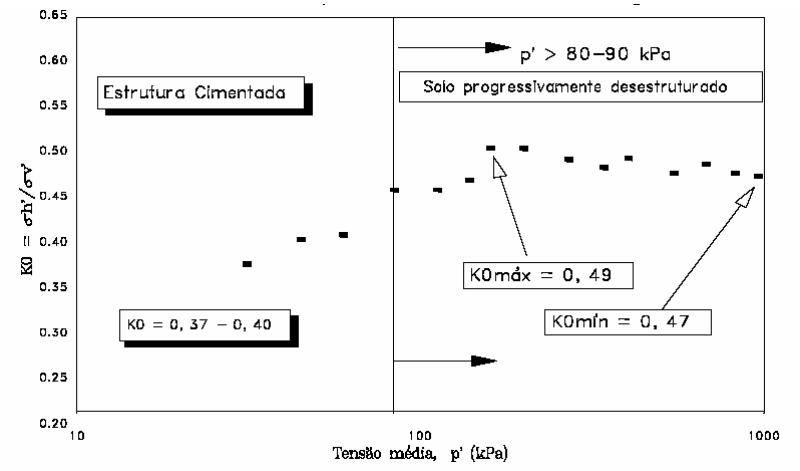

Figure 4.17. K_0 variation with mean effective stress p' in a K_0 test of an undisturbed sample (Viana da Fonseca, 1996)

Structure in artificially cemented soils has a major importance as it is not only due to the fabric but also, and most of all, from bonding due to the cementation. For this reason it is expected that the K_0 variation observed on natural structured soils can be found on artificially cemented soils as well.

Zhu et al. (1995) have reported some important features of the at-rest lateral stresses in artificially cemented sands by performing tests in a modified oedometer ring capable of measuring the at-rest lateral stresses. The authors have reported that the at-rest lateral stress significantly decreases with the cement content for a certain density, thus, the K_0 becomes significantly lower with increasingly cementation. On the other hand, K_0 of cemented sands is influenced not only by the cement content but also by the vertical stress if capable of destroying part of the structured bonds. As Figure 4.18 expresses the higher the vertical stress the greater the K_0 because with higher vertical loads the cementing bonds will progressively break and so the effect of cementation in the K_0 becomes reduced. This fact is more evident in weakly cemented sands with cement contents less than 2% due to the high sensitivity of this weak structure to induced stress, where at-rest lateral stress are significantly influenced by vertical stress, especially at low strain levels. In opposition, highly cemented samples with around 8% of cement content did not show any variation of their low K_0 (around 0.1) for the range of vertical stresses applied (up to 1 MPa).

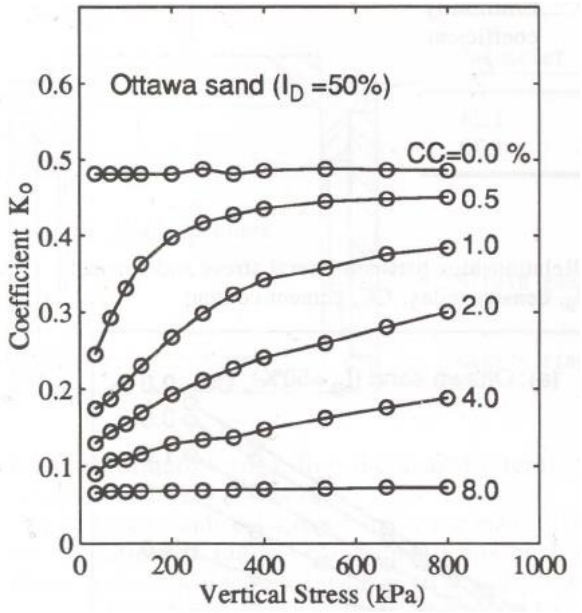

Figure 4.18 Relationship between K_0 and vertical stress (I_D – density index) - Zhu et al. (1995)

4.5 Structured soils in Shearing

4.5.1 Introduction

In section 4.4.1 the difference between weak and strong type of bonding was expressed in isotropic compression. In this section the two patterns of behaviour will be analysed in shearing conditions following the framework proposed by Coop (Coop and Airey, 2003 and Coop, 2003) for structured sands based on critical state soil mechanics and having as a

reference the intrinsic behaviour of reconstituted samples, so the effect of structure (and the separate effects of bonding and fabric) can be conveniently identified.

4.5.2 Peak and ultimate strength

As defined before, the difference between strong and weak bonding is that the former reaches states outside the NCL of the uncemented soil while the weak bonded soil yields before reaching the NCL. On the other hand, Cuccovillo and Coop (1999) have observed that in strong bonded soils the intact isotropic boundary is not parallel to the CSL, due to the progressive degradation of bonding after yield, so references to states on the “dry” or “wet” side of the critical state become meaningless for distinguishing different modes of behaviour. In Figure 4.19, the typical pattern of shearing of “strong” bonding is shown, where behaviour depends on the initial state of the soil. For lower stresses (point 1), the behaviour is elastic up to peak where yield occurs being entirely cohesive and not associated with dilation, followed by pronounced strain-softening back towards the frictional strength at critical state. At intermediate pressures (point 2) yield occurs before the ultimate/uncemented strength is reached so no peak strength was seen and failure was essentially frictional. In this case, the effect of bonding was essentially to have higher initial stiffness but not the strength. At higher stresses (points 3 and 4) the bonds have already yielded in isotropic loading having little effect in shearing so the stress-strain behaviour is mainly ductile just as the uncemented behaviour.

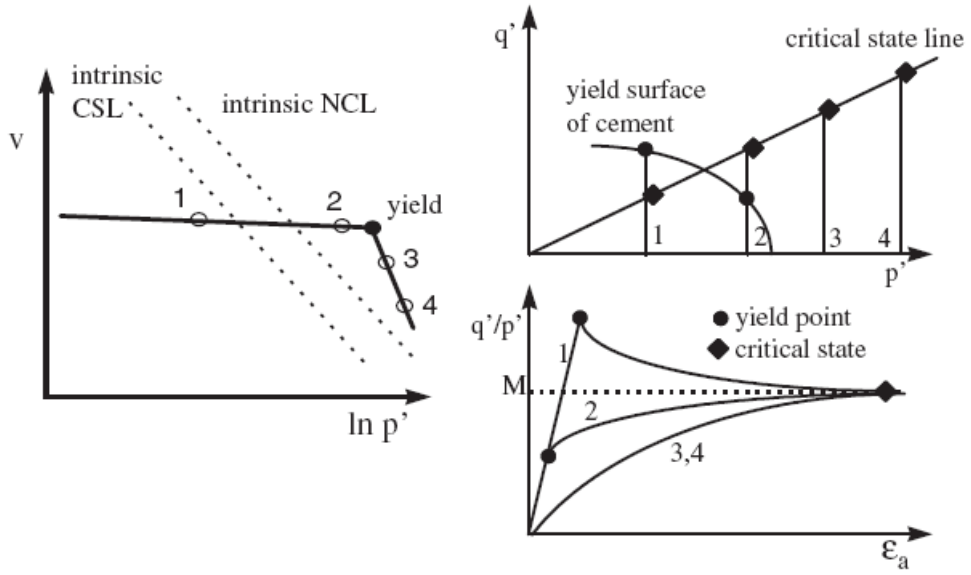

Figure 4.19. Typical patterns of shearing behaviour of “strong” bonding (Coop and Airey, 2003)

Figure 4.20 presents the idealised behaviour of the weak bonding. The main difference between strong and weak type of behaviour in shearing is that in weak bonded soils at

intermediate stresses, even beyond the yield of cement, the soil still has a peak strength resulting from dilation on shearing, so that the peak strength envelope is not restricted to the yield locus of the cement.

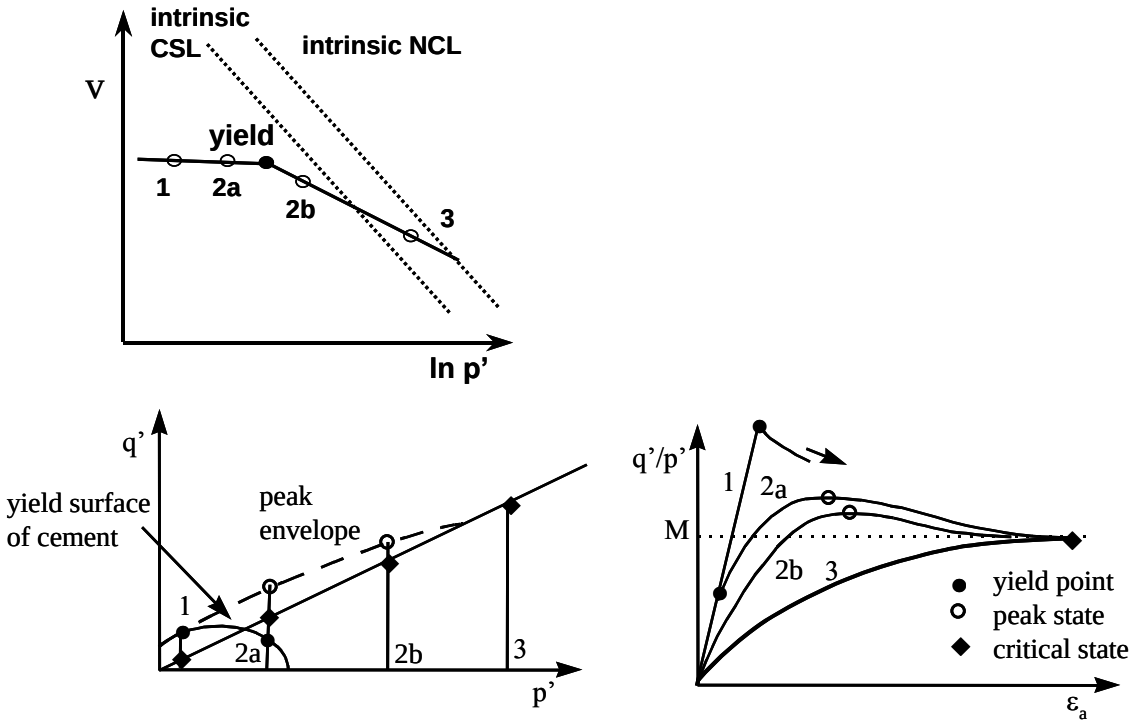

Figure 4.20. Idealised stress-strain behaviour for weak bonding (Coop, 2003)

In what fabric concerns, the behaviour of natural sands may be significantly affected by fabric resulting from a high interlocking that reconstituted sands cannot achieve. However, this cannot be analysed in artificially cemented soils. Being uncemented and cemented samples moulded in the same way it is assumed that they would have the same fabric. Thus, the comparison between uncemented and cemented soil only allows the evaluation of the effect of bonding and not of the fabric.

4.5.3 State boundary surface

The same two types of bonding (weak and strong) can be analysed in terms of the state boundary surface, if the test data is normalised for the effect of volume.

The work of Coop and Airey (2003) for strong type of bonding is plotted in Figure 4.21 where the q' vs p' stress-paths normalised with respect to the preconsolidation pressure (cementing threshold) are presented. This plot shows that the cemented soil reaches states outside the intrinsic state boundary surface on both wet and dry side of critical, so the yield surface of the cemented soil is larger than the intrinsic state boundary surface. However,

for states beyond yield in isotropic compression (points 3 and 4 of Figure 4.19) the normalized shearing path collapses back towards the intrinsic state boundary surface.

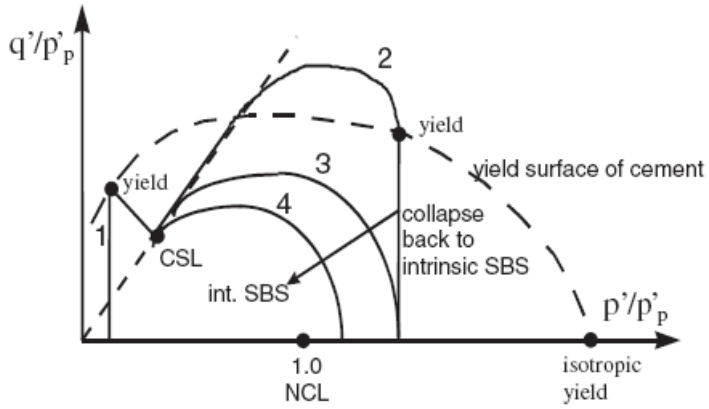

Figure 4.21. Characteristic normalized shearing behaviour of "strongly" bonded sand (Coop and Airey, 2003)

The same normalized plot for weak type of bonding is presented in Figure 4.22, showing that the yield locus of cement occupies only a small part of the intrinsic state boundary surface and states outside the intrinsic state boundary surface are only reached on the dry side of critical at low stresses.

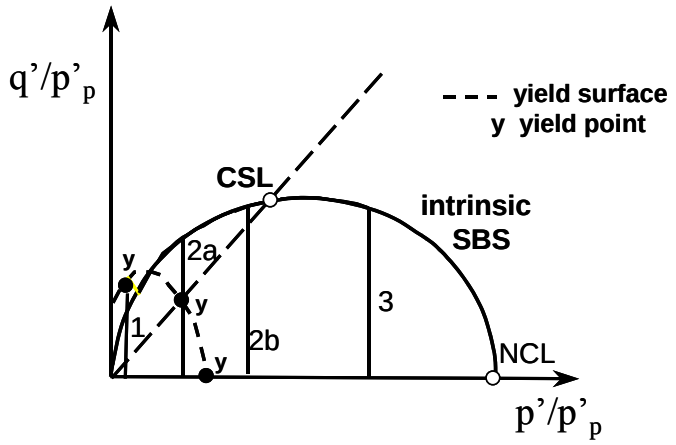

Figure 4.22. Characteristic normalized shearing behaviour for a weak bonding (Coop, 2003)

4.5.4 Stress-dilatancy

An alternative approach to understanding the peak states is to recognize that during shearing of a dilating soil the shear stresses must both overcome friction between the grains and lift the normal loads. For a given normal stress the peak shear stresses will increase with increasing rate of dilation. Moreover, the peak angle of dilation rises with increasing compaction and overconsolidation ratio, when presented in alternative. During drained shearing, two samples of the soil compacted to different void ratios (and consequently, to different overconsolidation ratios) dilate and both ultimately reach the

same critical state. Being so, they necessarily have different dilation rates and different volume changes.

Stress-dilatancy analysis can also be very useful to determine the critical state condition in uncemented samples that have not reached critical state, for example, when the axial strain was not enough to define clearly the ultimate steady state, or there was strain localization. As Figure 4.23 expresses, there are two points D and F where the rate of volume change ($\delta\varepsilon_v/\delta\varepsilon_s$) is zero and q/p' = M. Consequently by plotting soil test data as q/p' against $\delta\varepsilon_v/\delta\varepsilon_s$ the position of the critical state point F can be found even if the loading is terminated before the samples have reached their critical states.

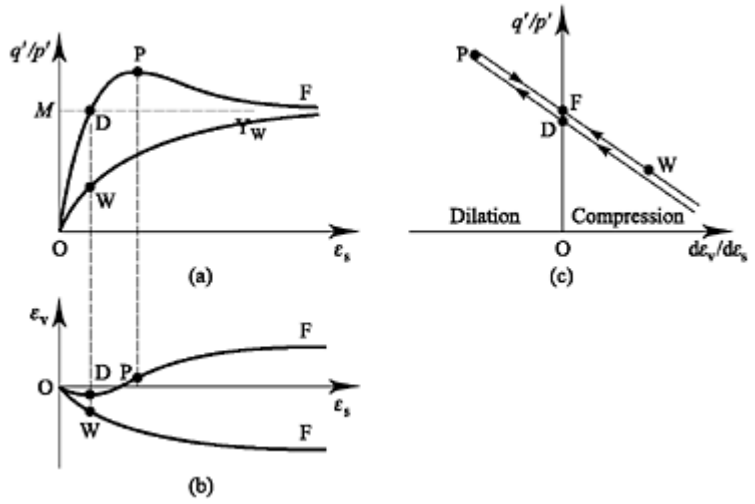

Figure 4.23. Stress ratio and dilation of soil (Atkinson, 2008)

This analysis is normally done by using Eq. (4.13), which indicates that the stress ratio q/p' is the sum of the friction component M and a component due to dilation.

$$q/p' = M - \delta\varepsilon_v/\delta\varepsilon_s \quad (4.13)$$

This approach was first presented and theoretically justified by Roscoe et al. (1958) and Schofield and Wroth (1968) being expressed in representing such dual answer with good results in sands (Figure 4.24a), but also in cemented soils (Figure 4.24b) by Coop and Wilson (2003), which have worked with several uncemented sands and sandstones, such as Castlegate sandstone. In the tests plotted in Figure 4.24a) an expected linear trend is seen as showed schematically in the previous figure. In reverse, Figure 4.24b) shows a different pattern. As mentioned before, in this weak type of bonding the peak does not correspond to the breakage of the cement, which happens before the peak, and therefore the peak strength is solely frictional. As the cement yields, the soil starts to dilate and as a consequence of the dilation having been delayed by the presence of cement, when it starts

the rate of dilation is much higher than it would be otherwise. After the peak the soil strain softens, apparently following the straight line of frictional trend on the stress-dilatancy plot, but as the stress ratio reduces, strain localization occurs so that the rate of dilation reduces more rapidly than the stress ratio, bringing the path inside the frictional relationship. The value of M given by the stress-ratio of the frictional trend at critical state (zero rate of dilatancy) is 0.9 which corresponds to an angle of friction of 23°.

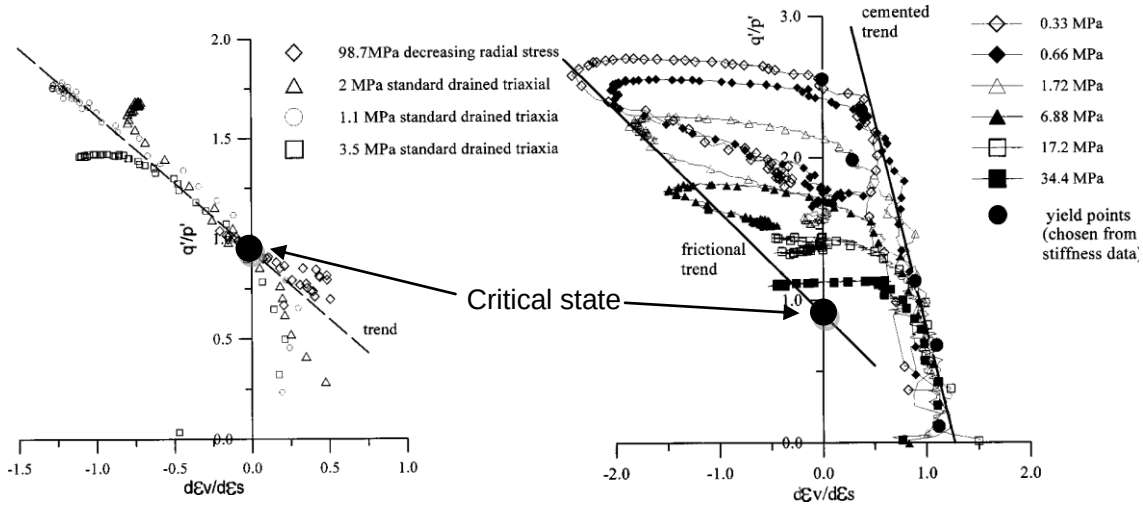

Figure 4.24. Stress–dilatancy data for shearing of: a) sand; b) Castlegate sandstone (Coop and Wilson, 2003)

Consoli et al. (2011a) show some results of stress-dilatancy plots of tests in a mixture of Portland cement with an uniform sand (Osorio sand). The general pattern of behaviour is similar to Castlegate sandstone showing a great increase in the rate of dilation after yield and reaching a maximum at, or shortly after, the peak stress, before strain softening. However, in this case, the initial part of the dilatancy behaviour is dominated by the cement and the paths are more vertical than in granular soils as little or no volume change is observed. There is then a well defined yield point where the path deviates. The intercept of the frictional trend corresponds to a value of M of 1.2 which means an angle of friction of 30º.

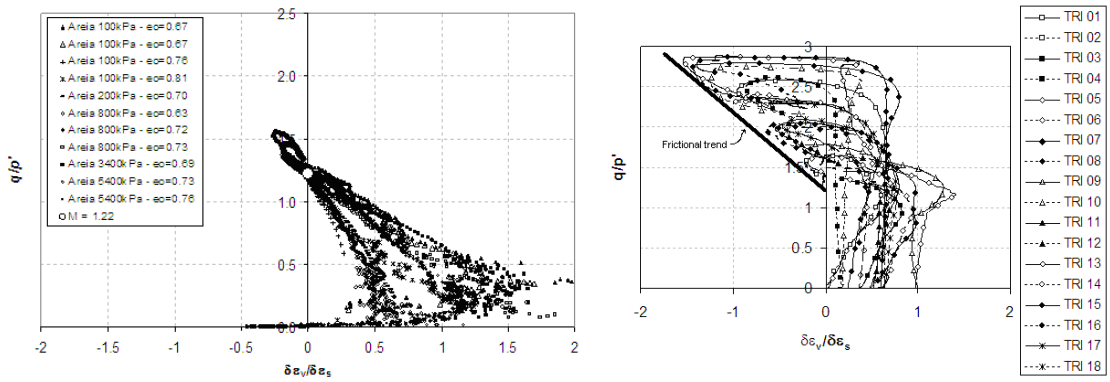

a) b)

Figure 4.25. Stress-dilatancy analysis for uncemented (a) and cemented (b) Osorio sand (Consoli et al., 2011a)

It should be noticed that in cemented soils the peak stress does not always correspond to the rate of maximum dilation as it happens in most uncemented sands. In strong bonded soils, the rate of maximum dilation is often after the peak, indicating that the peak is influenced by the cementation, being yield a consequence of bond degradation, while after that break a most probable generation of coarser aggregated group of cemented particles impose higher energy to lift one particle over the other.

4.5.5 Development of slip surfaces

An important feature of straining soils at relative large strains is the development of strong discontinuities, or slip surfaces. These are not really slip surfaces but thin regions of intense shearing through material that is essentially rigid on either side. Once slip surfaces have developed soil is no longer homogeneous and the shear and volumetric strains are highly non-uniform, so that measurements of strain made at the boundary of a test sample will not properly measure the strains and specific volume in the soil, which is straining in the slip surfaces. Consequently, once a slip surface has developed in soil samples, conventional measurements of strain and specific volume are not reliable anymore.

If a soil is on the dry side of critical state it will dilate on shearing absorbing water and becoming weaker so when a slip plane starts it will tend to grow. However, if the soil is on the wet side of critical it will compress during shearing and if a slip plane starts to form, the soil will strengthen and the slip plane will stop growing. For this reason, slip planes are most often seen in soils whose states are on the dry side of critical. As there must be some drainage of water into the slip plane from the surrounding soil, volumetric strains and water contents measured in the usual way at the boundaries of the sample are different from those in the soil inside the slip plane. The quantity of this local drainage depends on the permeability of the soil and on the rate of shearing in the test.

Figure 4.26 illustrates the behaviour of a sample of soil in an undrained triaxial compression test. If the soil was fully undrained it would follow the path O-Y-F_u, and if it was fully drained it would follow the path O-Y-F_d. As there is local drainage into the slip plane from the nearby soil, the soil follows an intermediate path such as O-Y-F_{pd}, showing a peak where it should not be if the soil went through O-Y-F_u as was expected. The critical state of the sample at F_{pd} is less than it would have been if there was not partial drainage, but we would plot it at F_{um} at the measured value of p' and at a specific volume equal to the initial specific volume, giving rise to a wrong estimate of the critical state line.

To overcome this problem some authors, like Carrera et al. (2011), have reported that in cases where the sample seemed to have reached a stable state before localisation, that state has been considered to be representative of the Critical State. The results from such tests were generally in good agreement with those from other tests and so this procedure was considered valid.

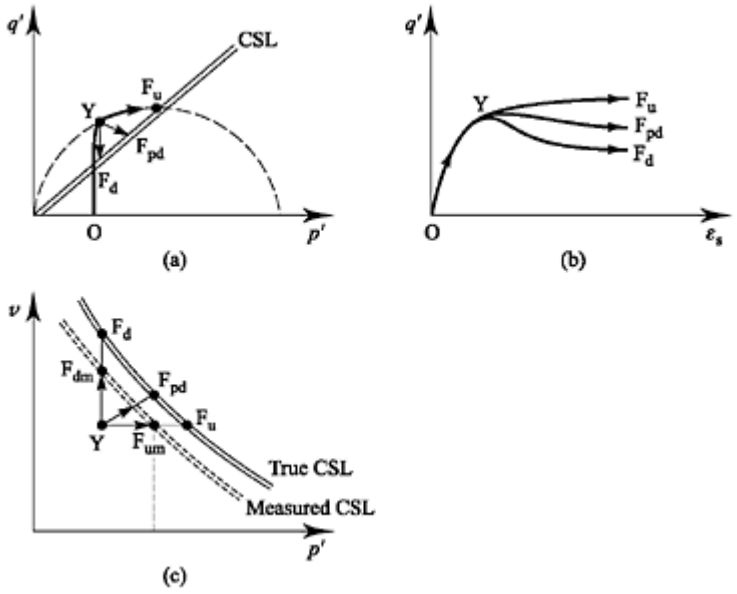

Figure 4.26. Influence of slip planes on critical state lines measured in tests (Atkinson, 2008).

4.6 Structured soils at small strains - Stiffness

According to critical state soil mechanics the state boundary surface is a yield surface, thus, while the state is on the surface there are simultaneous elastic and plastic strains, but if the state is brought inside the boundary surface, by unloading, the strains are assumed to be purely elastic. In this idealized model, the soil is considered isotropic and elastic, shear and volumetric effects are decoupled and, the volume changes are related only to changes of p' and are independent of any change of q.

However, this is simple an idealization. In fact, there are plastic strains within the limit state boundary. Jardine et al. (1991), Jardine (1992), Hight and Higgins (1994) and Tatsuoka et al. (1997) schematized this behaviour shown in Figure 4.27 as described by Leroueil (2003):

- There is the outer yield curve (surface) Y3 that is associated with a change in fabric and coincident with the limit state curve. Soils experiencing stress paths that reach this curve undergo large plastic strains. Inside Y3, strains are small to moderate;
- Within the inner yield curve Y1 surrounding the current effective stress conditions (zone 1), the behaviour is linear-elastic and characterized by very small strain elastic properties, in particular the small strain shear modulus G_0;
- When the stress path crosses Y1, but remains inside zone 2 limited by the yield curve Y2 (between A and B), the behaviour is nonlinear elastic;
- Between Y2 and Y3 (between B and C in zone 3), soil develops plastic strains. As indicated in Figure 4.27c), the ratio of plastic to total strain progressively increases as the stress path approaches C on Y3. Passage through Y2, point B, also corresponds to the strain at which, in undrained conditions, pore pressures start to build that is certainly the case of high strain rate tests such as vibratory tests (resonant column or cyclic triaxial tests);
- When Y1 and Y2 are crossed by the effective stress path, they are dragged with the effective stress state.

When the stress conditions in a soil element move out of zone 1, the stress-strain behaviour becomes non-linear and subsequently non-elastic when out of zone 2. According to Leroueil (2003), the non-linearity depends on several factors including the type of soil, previous stress and strain history, stress path, strain rate and degree of cementation (Viana da Fonseca and Coutinho, 2008, Cruz, 2010). However, there are several aspects of stress-strain behaviour that seem to be general.

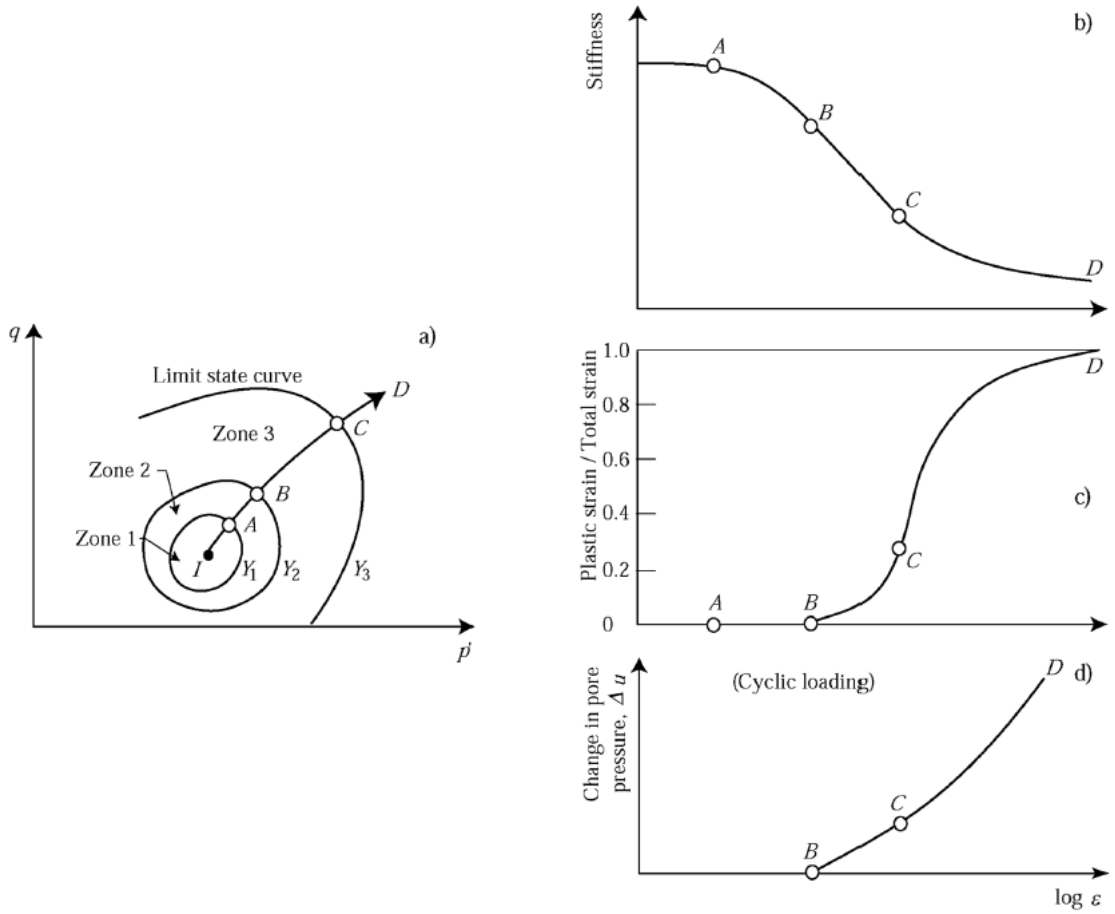

Figure 4.27. Scheme of multiple yield surfaces and soil response (modified by Leroueil, 2003 after Jardine et al., 1991; Jardine, 1992; and Hight and Higgins, 1994).

Several moduli can be defined to describe soil stiffness as shown in Figure 4.28a). Monotonic loading enables to define, at a point such as P a secant modulus G_s and a tangent modulus G_t. In case of cyclic loading, these moduli are relevant only to the loading part of the first cycle. For the subsequent cycles, the defined shear modulus is implicitly the equivalent shear modulus G_{eq}. As a consequence, the relationship between shear modulus and shear strain defined in monotonic loading test may be different from the equivalent curve defined in a cyclic loading test (Figure 4.28b). Regarding the influence of strain rate, this phenomenon could be increased by strain rate effects. This difference between cyclic and monotonic loading is also clear in Figure 4.29 not only for a granular soil (Toyoura sand) but also for Porto residual soil from granite.

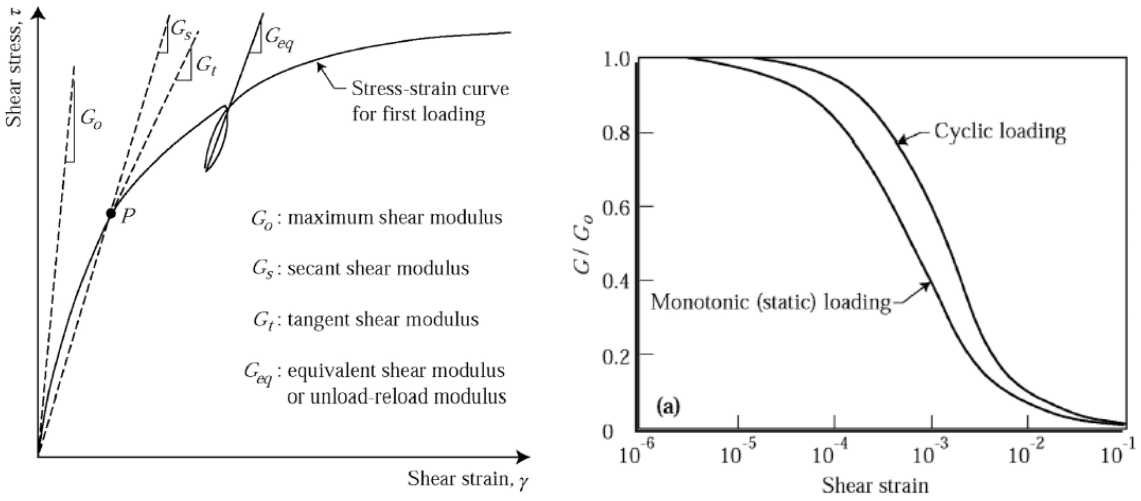

a) b)

Figure 4.28. a) Definition of soil stiffness; b) schematic representation of the relationship between shear modulus and shear strain obtained from monotonic loading and cyclic loading tests (Leroueil, 2003).

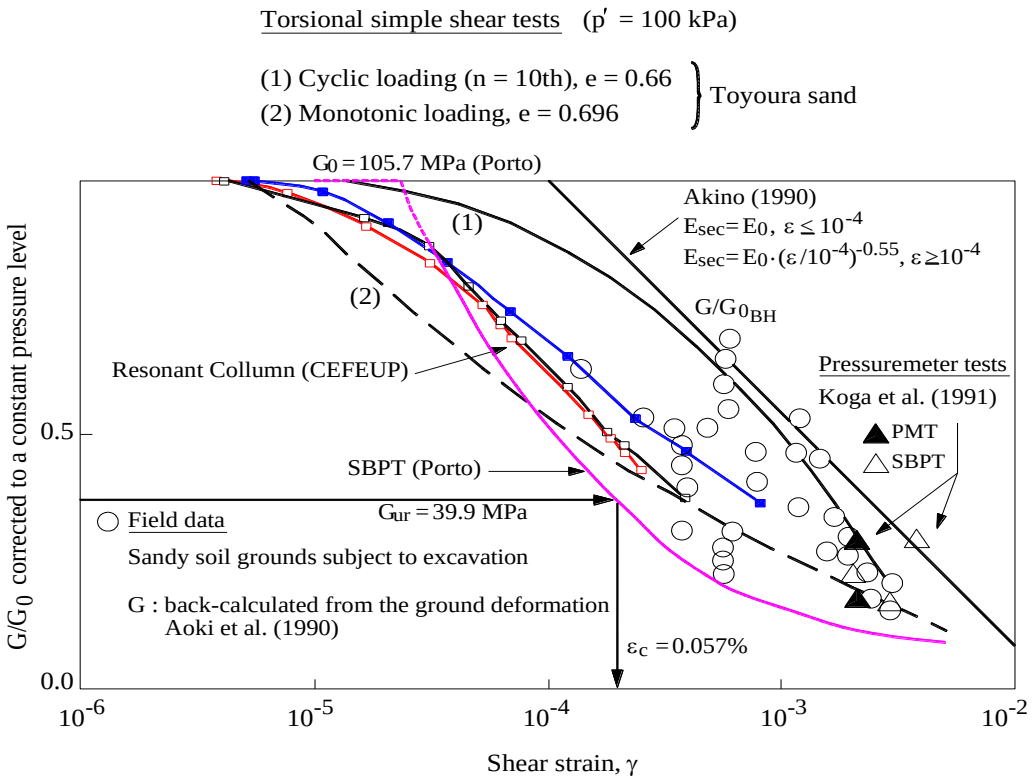

Figure 4.29. Comparison of secant shear modulus as function of shear stress level: results of resonant column results in residual soils from granite of Porto versus data from other testing conditions in sandy soils (Viana da Fonseca and Coutinho, 2008).

Stiffness can be highly increased by the effect of cementation for a given confining pressure. However, the soil behaviour becomes also more brittle and the stiffness

degradation on cemented soil is faster than in the same soil uncemented. Sharma and Fahey (2003b) have shown these features on their work on a cemented calcareous soil. Figure 4.30 presents the comparison of stiffness degradation for cemented and uncemented samples consolidated to 200 kPa of effective confining pressure. The secant shear modulus was increased almost 10 times by the effect of cementation but it rapidly decreased when the cement started breaking.

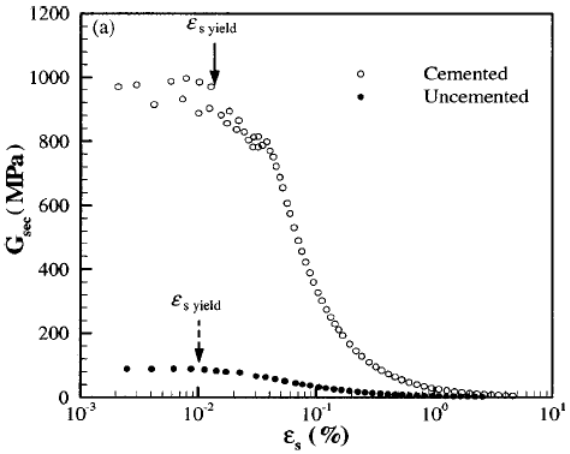

Figure 4.30. Comparison of degradation of stiffness G_{sec} with deviatoric strain for cemented and uncemented samples at p'_0 = 200 kPa (Sharma and Fahey, 2003b)

Cuccovillo and Coop (1997) have observed that in sands where the influence of structure arises predominantly from bonding, the values of the shear stiffness after the first yielding decrease as the bonding degrades, even if the mean effective stress and density increase. However, in sands where the influence of structure arises from an interlocking fabric the values of the shear stiffness remain high despite bond degradation, and even increase when the mean effective stress and density increase.

Another effect of cementation is that the stiffness becomes less dependent on the confining pressure (Acar and El-Tahir, 1986; Baig et al., 1997; Fernandez and Santamarina, 2001, among others). In uncemented soils, stiffness tends to increase with confining pressure due to the increase in the number of contact points between the particles which improves the strength of soil to deformation. Obviously, this is valid up to a certain level of confining pressure which assures that the particles are not being broken by a big increase of effective stress. In the same way, in cemented soils confining pressure does not have a significant effect on the shear modulus, unless the pressure necessary to break the cementation bonds is not exceeded. In fact, this difference in behaviour is not only a consequence of breakage of cementation due to an increase of confining pressure, but also the relative importance of the energy necessary to disconnect the contacts of the particles,

towards the cement strength. This explains the change between strain softening and strain hardening behaviour with increasing confining pressure as the behaviour becomes more frictional and the dilatancy of the soil is more significant than cementation. Viana da Fonseca (1996, 2003) presented some modelling of this different stiffness behaviour of naturally cemented soils and the same remoulded to equivalent void ratios.

In Figure 4.31, the effect of confining pressure on shear wave velocities is presented for uncemented sand and the same sand mixed with Portland cement. The difference in absolute values in both cases is notorious (which lead the author to use different scales) but the effect of confining pressure is only observed in the uncemented sand, while the cemented soil does not seem to change. The work of Baig et al. (1997) on Ottawa sand is presented in Figure 4.32 showing that this effect is clearer when the cement content is increased.

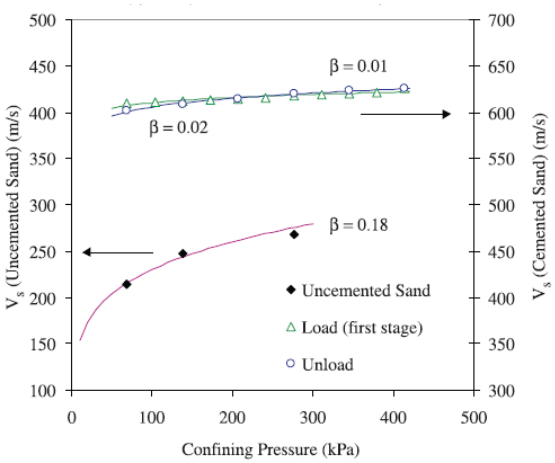

Figure 4.31. Evolution of shear wave velocities with confining pressure for cemented and uncemented sands (Fernandez and Santamarina, 2001)

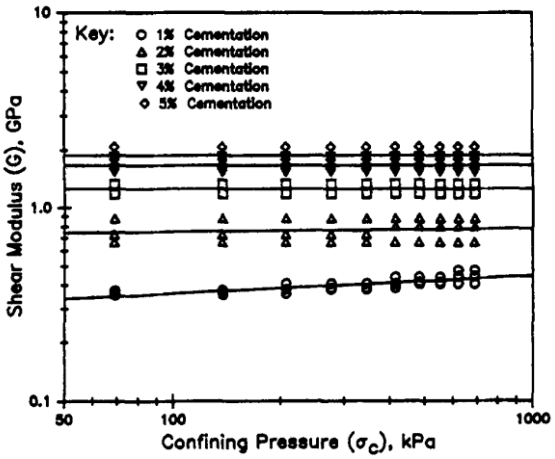

Figure 4.32. Influence of confining pressure on the shear modulus measured by bender elements in samples with different cement contents (Baig et al., 1997)

4.7 Destructuration

Destructuration consists on the degradation of the soil structure, by the breakage of the bonds between particles or aggregates, which leads to a remoulded or reconstituted soil. In this work, all these words: destructured, remoulded or reconstituted, will be used with the same meaning. This is mainly a progressive process that is achieved when the stress state reaches the yield surface.

Destructuration can be caused by unloading, sampling, installation of in situ devices, during construction, or just by the application of compression, tensile or shear stresses in lab tests.

The main effects of destructuration are: decrease in stiffness of the soil inside the limit state curve; decrease in the peak shear strength and in the preconsolidation pressure, as well as shrinkage of the entire limit state curve, decrease in the compression index.

The effects of destructuration were studied by Santamarina (2001) in terms of the shear wave velocity evolution with increasing effective stress (Figure 4.33). As reported in the previous section, while the structure of the soil is kept intact, the soil stiffness (related to the shear wave velocity) remains constant with increasing effective stress. On the contrary, if the imposed stresses are enough to cause a progressive degradation of the soil structure, the shear wave velocity increases with the stress level.

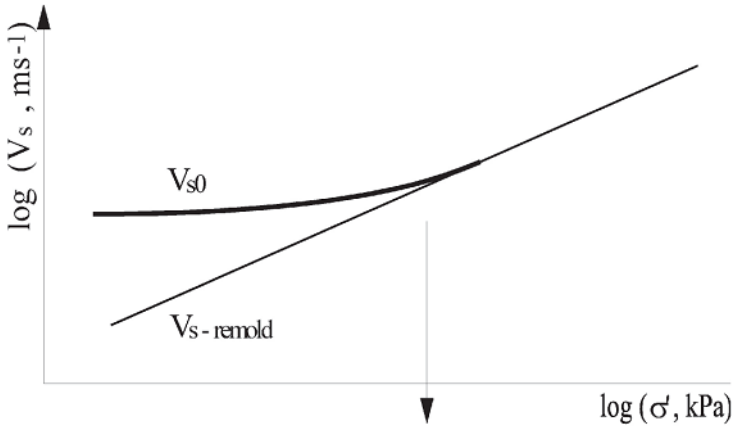

Behaviour	No debonding $\Delta\sigma' < \Delta\sigma'_{debond}$	Debonding $\Delta\sigma' > \Delta\sigma'_{debond}$
Cement-controlled: $V_{S0} > V_{S\text{-remold}}$	No sampling effect (sandstone at shallow depth)	stress reduction during sampling affects the measured properties
Stress-controlled: $V_{S0} \approx V_{S\text{-remold}}$	No sampling effect (weakly cemented soil at depth)	No sampling effect (soil debonds, behaviour determined by σ')

Figure 4.33. Skeletal forces vs. cementation strength – sampling and debonding (Santamarina 2001 cited by Viana da Fonseca and Coutinho, 2008).

Chapter 5.
EQUIPMENT AND PROCEDURES

5.1 Introduction

A great part of this research program involved experimental tests. For that reason, it seemed important to include an entire chapter with the description of the equipment as some apparatus are not conventional in a Soil Mechanics Laboratory. Most of the tests were conducted at the Geotechnical Laboratory of FEUP - Faculty of Engineering of the University of Porto (www.fe.up.pt/labgeo/), although other tests were also performed in Lisbon and London.

First some identification tests were conducted like grain size distribution analyses or Atterberg limits that do not require a specific equipment description. Then, some simple mechanical tests were performed like unconfined compression tests, indirect tensile tests or constant rate deformation tests. Although these conventional tests do not need a detailed description of their equipment some brief notes will be left concerning the size of the specimens, range of deformation transducers and rate of the test. There will also be made a brief description of other equipments to perform the QicPic test and the scanning electron microscope.

Being the triaxial test the most used equipment throughout this work, a detailed description of the each equipment will be made. First, low pressure triaxial tests were performed, then cyclic triaxial tests and finally, high pressure triaxial tests could be executed due to an important collaboration of two universities in London.

5.2 QicPic test

The QicPic test performed in this work used the equipment of the Geotechnical Laboratory of the Imperial College London (ICL) and consisted on the particle size and shape calculation by image analysis. The basic concept is the combination of well established powerful disperser with dynamic image analysis (Figure 5.1). A well dispersed particle flow

is led through the image plane. Due to the dispersion the particles are separated from each other by the transportation fluid and overlapping particles are widely avoided, and thus, high particle numbers per image frame can be captured (Sympatec, 2008). As the camera and the light source are able to operate at any speed from 0 to 500 frames per second, very high counts of particle are acquired in short time: with 100 particles per frame (due to a good dispersion) and 500 frames per second, 1,000,000 particles are acquired in 20 seconds (the normal time of the test). Figure 5.2 shows some photographs of the equipment.

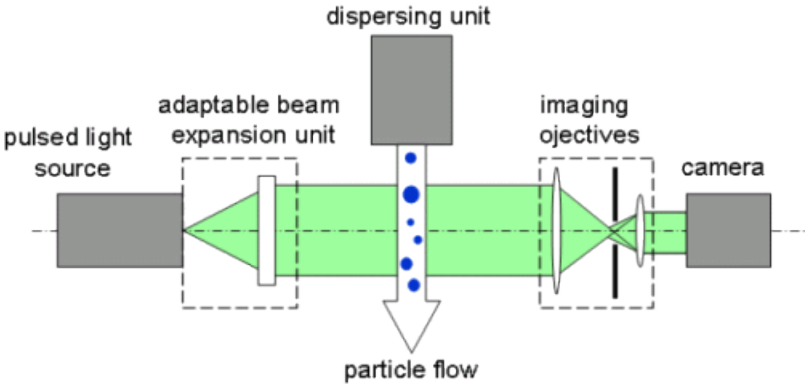

Figure 5.1 QicPic test configuration

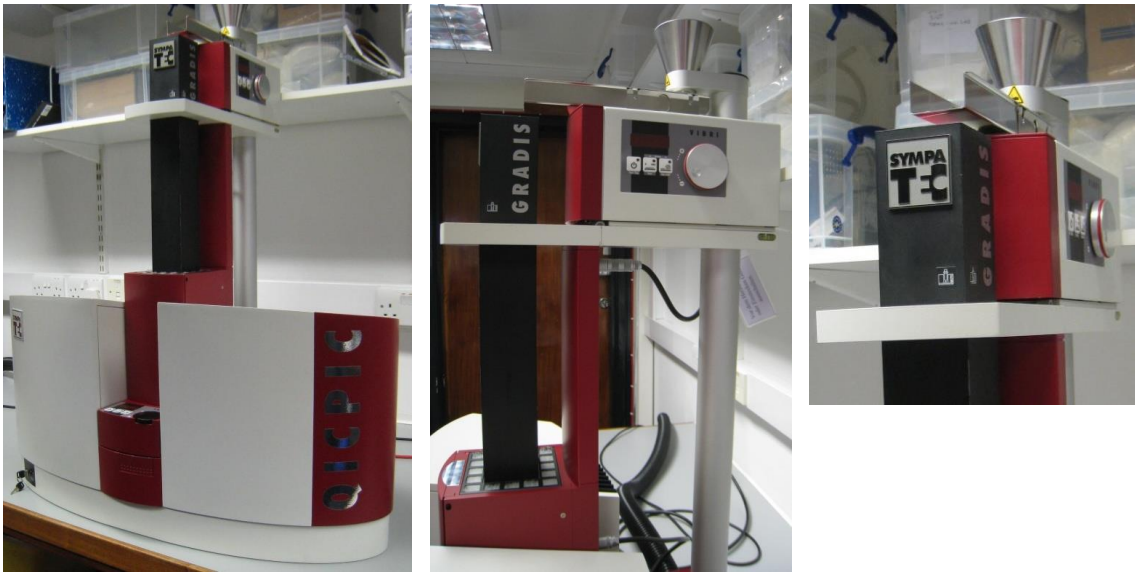

a) b) c)

Figure 5.2 Qic Pic equipment: a) front view; b) lateral view; c) zoom of the dispersing unit

5.3 Scanning Electron Microscope

Scanning electron microscope (SEM) micrographs were taken on fractions of uncemented and cemented specimens already tested in isotropic compression at high pressures and air dried. The tests were performed using a high resolution field emission SEM in the Natural History Museum in London, under collaboration with ICL.

As the name suggests, in the scanning electron microscope, the area to be examined is irradiated with a finely focused electron beam (Figure 5.3). The types of signals produced when the electron beam impinges on a specimen surface include secondary electrons, backscattered electrons, auger electrons, characteristic x-rays and photons of various energies. These signals are obtained from specific emission volumes within the specimen and can be used to examine many characteristics of the specimens (composition, surface topography, crystallography, etc...). In SEM the signals of greatest interest are the secondary and the backscattered electrons, since they vary due to differences in surface topography as the electron beam is swept across the specimen. Secondary electrons are produced as a result of interactions between energetic beam electrons and weakly bound conductions electrons. Backscattered electrons are beam electrons that were scattered out of the specimen, instead of expending all their energy in the interaction volume and being absorbed by the target.

The secondary electron emission is confined to a volume near the beam impact area, permitting images to be obtained at relatively high resolution. The three dimension appearance of the images is due to the large depth of field of the scanning electron microscope as well as due to the shadow relief effect of the secondary electron contrast. Other signals are available proving to be similarly useful in many cases (Goldstein et al., 1981).

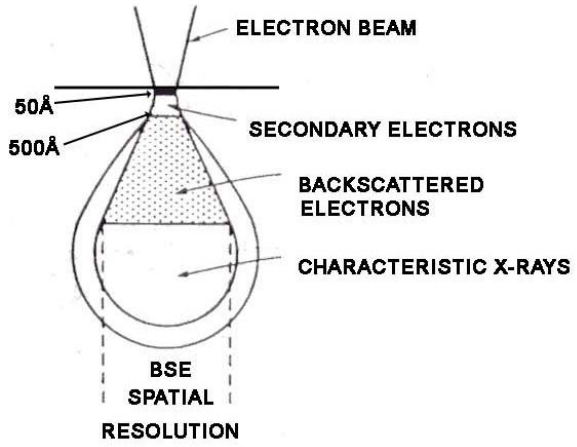

Figure 5.3 Electron beam

The preparation of the specimens for SEM testing includes mounting the specimens onto stubs and coating them with gold. The test consists in taking micrographs at different magnifications and from different points of view, and, by means of specific software it is also possible to obtain the chemical composition of some points of the specimen, which provides the basis for particle identification. The results presented herein were obtained by the Back Scattered Electron Microscope Analysis that revealed to be more adequate to analyze this material with and without cement.

5.4 CRD tests, Unconfined compression and Tensile tests

The tests stated in the section title were all executed in the Geotechnical Laboratory of FEUP.

One-dimensional compression tests at constant rate of deformation were executed in oedometric cells of 75 mm of diameter and 30 mm of height. The deformation of the specimen was measured by a Linear Variable Displacement Transducer (LVDT) of 5 mm of range and 0.02 mm of resolution.

The specimens for the unconfined compression test were 70 mm of diameter and 140 mm high and the deformation was measured by LDT's - Local Deformation Transducers (Goto et al., 1991).

The specimens for the indirect tensile tests (also known as Brazilian tests) were 70 mm of diameter and height and since the only purpose of strength evaluation, no strain transducers were used.

All these tests were executed at 0.1 mm/min in an automatic loading machine of 100 kN of capacity together with a load cell with the same capacity and resolution of 0.006 kN. Figure 5.4 shows the specimens being tested in each of the tests. The strain rate of loading was adapted from ASTM (1996b) and the Portuguese (LNEC, 1972a) standard for compressive strength of soil-cement specimens that suggest 1 mm/min. A slower speed was used considering that this soil has a significant percentage of fines (thus, not so permeable) and that the stiffer specimens (with 7% cement content) would fail within a very short period (less than 10 min) if 1 mm/min was considered.

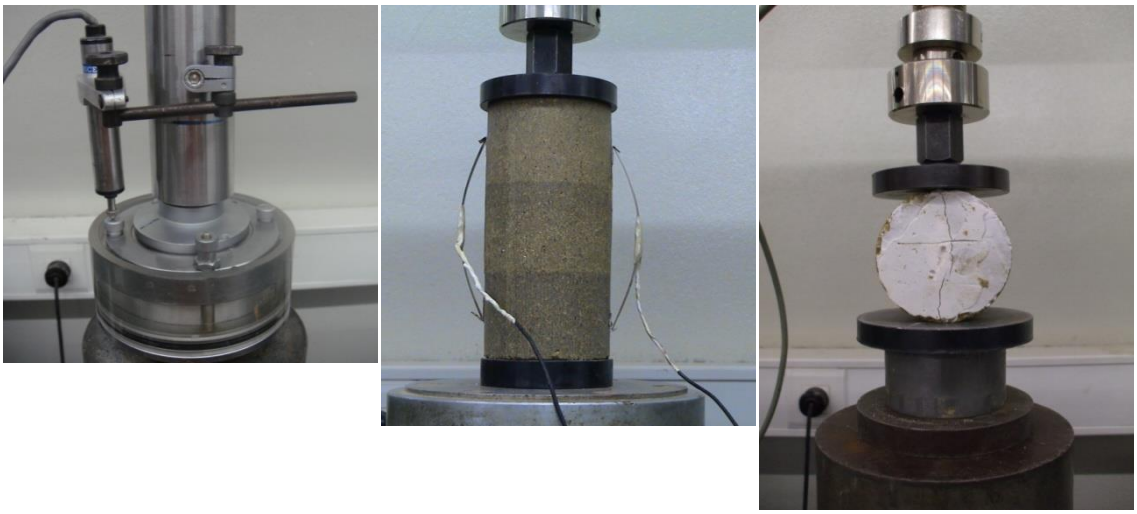

a) b) c)

Figure 5.4 a) CRD test b) unconfined compression test c) indirect tensile test

5.5 Seismic wave velocities measurements

5.5.1 Introduction

Seismic wave velocities measurements were performed in three main setups, the first two at the Geotechnical Laboratory of FEUP. A first set of specimens especially moulded for this purpose was tested with bender elements and compression transducers. Then, some tests were also performed with ultrasonic transducers and finally, resonant column tests were performed in the Technical University of Lisbon.

5.5.2 Bender elements and compression transducers

The laboratory equipment used for the first set of seismic wave measurements involved a triaxial cell with two different types of piezoelectric transducers, although the tests were performed without confinement. It included a single pair of compression transducers and a single pair of bender elements, respectively, for compression and shear wave measurements - see Figure 5.5b). Therefore, compression waves were measured independently from shear waves. This system comprised an ISMES-Enel.Hydro multiplexer/amplifier which is a single box containing both a power amplifier and an output amplifier. It amplifies the input signal by 40 times (though the maximum input frequency from the function generator is 2.5 Vpp) and the output 10 times (1000%). This capability of amplifying the input signal is very important as it improves the signal-to-noise ratio. The signal was created by a programmable function generator (TTi, model TG1010® Programmable 10 MHz DDS Function Generator, 0 Hz up to 10 MHz) capable of

generating an electrical signal with various user-defined configurations, though in this work only sinusoidal waves were used. Both input and output signals were displayed in a dual-channel oscilloscope (Tektronix, model TDS220® two channel digital real-time oscilloscope 100 MHz) for visualizing and directly identifying the travel time (time domain method - TD). For signal acquiring, the oscilloscope was connected with a PC where data was transferred using specific software program and stored in different formats for post processing and interpretation. For the frequency domain methods, FD, a low-cost oscilloscope and FFT-based spectrum analyser (PicoScope ADC-216) were used. This FFT-based spectrum analyser digitises the signal using an A/D converter and the stored values are then processed using the Fast Fourier Transform (FFT) algorithm. Figure 5.5a) shows the testing setup with all components used in this work. A better description of this equipment is done by Ferreira (2008).

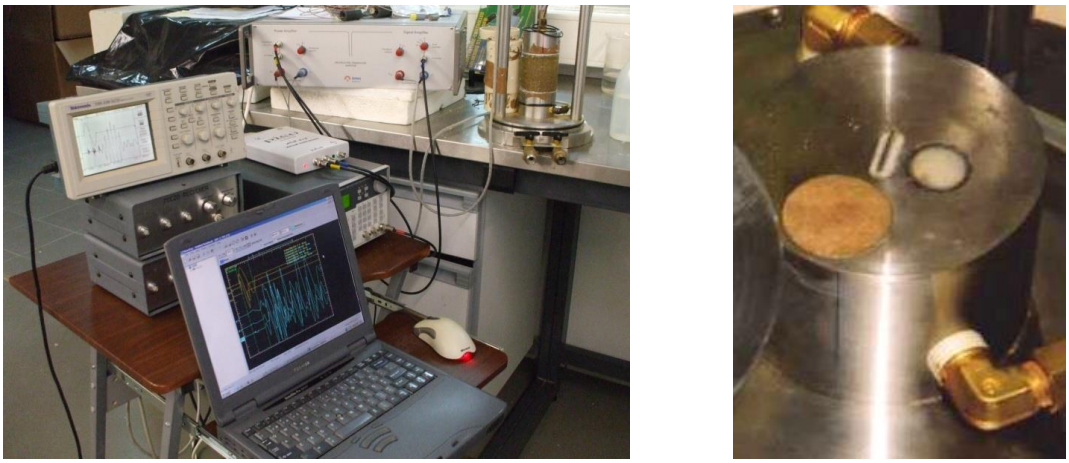

a) b)

Figure 5.5. Laboratory equipment used for seismic wave measurements: a) testing setup; b) detail of the bottom base with bender element, compression transducer and porous stone.

5.5.3 Ultrasonic transducers

The piezoelectric ultrasonic transducers used are part of a seismic wave velocities equipment from Pundit®. Their nominal frequency is 50 kHz and their polarity is in the direction of their height, which means that the wave obtained in the receiver is independent of the relative position of the transducers. The longitudinal waves (compression waves) are generated by a compressive strain derived from an electric potential difference (Amaral, 2009).

The instrumentation consists of a function generator, two ultrasonic transducers (transmitter and receiver), a digital oscilloscope and a data acquisition system, interfaced with a desktop computer as schematically represented in Figure 5.6 and shown in the

photo of Figure 5.7. In this method, pulses are emitted by the transmitter and travel through the material, being detected by a receiver, placed on the opposite face of the test object. The travel time of the first arriving pulse is precisely measured and recorded with electronic equipment. Two types of waves were used and compared: a square wave (f=50 kHz) and a sinusoidal pulse (f=25, 50, 75 kHz). This method is described in the ASTM standard C 597-02 (ASTM, 2002) and by Khan et al. (2006). To improve coupling between the specimen and the transducer high vacuum grease (Figure 5.7b) was used as suggested by Professor Giovanni Cascante (University of Waterloo, Canada).

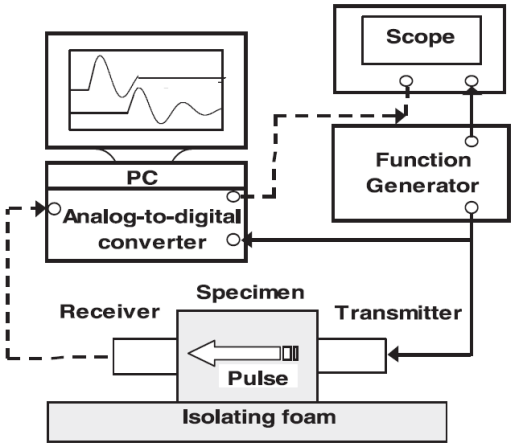

Figure 5.6 Experimental setup (Khan et al., 2006)

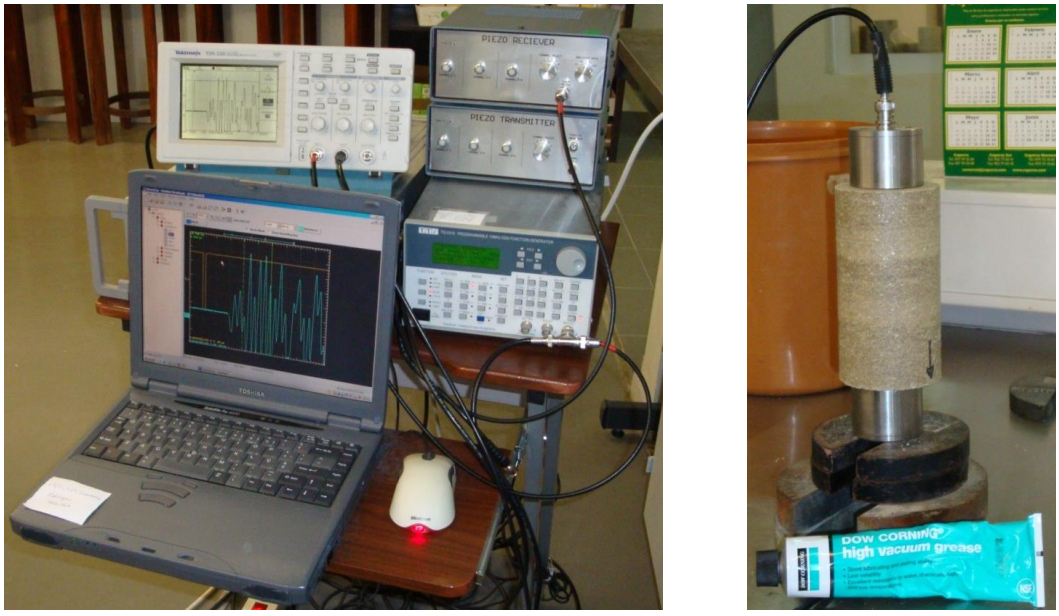

a) b)

Figure 5.7 Instrumentation for ultrasonic wave measurements (a) and detail of the specimen being tested

5.5.4 Resonant column tests

The resonant column tests were carried out in the Technical University of Lisbon at IST (Instituto Superior Técnico) with the very kind assistance of PhD student Javier Camacho-Tauta and collaboration of Dr. Jaime Santos.

The IST resonant-column equipment is a Drnevich-type manufactured by Seiken Inc. in 1992. It consists of three subsystems: pneumatic, electro-mechanic and electronic. The pneumatic subsystem provides the pressure to the application of cell pressure, backpressure and axial force; the electro-mechanical subsystem allows the torsional vibration and the electronic subsystem provides the input signal and measures the response of the system.

The system was recently adapted (Camacho-Tauta, 2010) to perform resonant column random noise tests and bender elements measurements besides the conventional resonant column test (ASTM, 2000). For this purpose, the resonant-column apparatus was improved by replacing the internal sinusoidal generator with an arbitrary function generator. A PC oscilloscope was used to acquire both input current in coils and vibration response of the system. Both generator and oscilloscope can be computer controlled by means of a specific software developed in LabVIEW®. This software controls the equipment, acquires data and then processes the information, which along with the calibration parameters and specimen information, allows the computing of the dynamic properties of the soil.

Each end (at the top and base cap) is equipped with two bender elements orthogonally oriented (T-shaped style) encapsulated into a metallic encasement. In Figure 5.9 a general view of the equipment is shown.

Figure 5.8. IST modified resonant-column/bender element apparatus (Camacho-Tauta, 2010).

Resonant column devices are generally classified by the boundary conditions at the specimens ends. This system, illustrated in Figure 5.9, consists of a modified case of the "fixed-free" as described in detail by Camacho-Tauta (2010). The top active platen has a rotational mass inertia J_A and is partially restrained by a spring with constant K_A and a dashpot with constant ξ_A. Therefore, torsional stiffness and damping was added to the system. This alteration produces a better distribution of the rotation angle, while the system is able to apply up to medium shear strain levels. Additionally, the application of anisotropic or isotropic stresses is possible, by use of an actuator to apply axial loads.

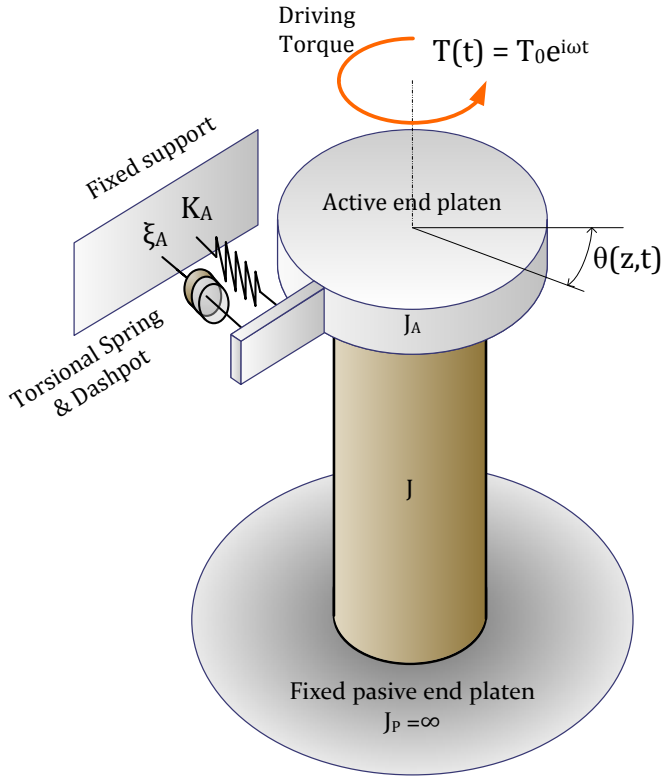

Figure 5.9 Modified Fixed-Free Resonant-Column System: the top base is partially restrained by a spring and dashpot (Camacho-Tauta, 2010)

5.6 Low pressure triaxials - FEUP

5.6.1 Introduction

Low pressure triaxial tests were performed at the Geotechnical Laboratory of FEUP. From low pressures it is intended that the maximum cell pressure that can be achieved in those cells is 1700 kPa. Four types of different apparatus were used, which will be described in the following sections.

5.6.2 ISMES - Enel.Hydro system cell

The ISMES - Enel.Hydro system includes a triaxial cell prepared for specimens of 70 mm of diameter. In opposition to most triaxial cells, in this apparatus the cell pressure is controlled by the pressure of the air applied directly to an air/water interface in the top of the chamber (the cell is not fully filled with water leaving some air in the top). This apparatus is equipped with an internal load cell of 25 kN of capacity, local deformation transducers - LDT's (Figure 5.10c and d) as well as bender elements and compressions transducers for S and P independent wave measurements (Figure 5.5b). The tests were manually controlled and data acquisition was performed through a data logger linked to a computer with TRIAX® software.

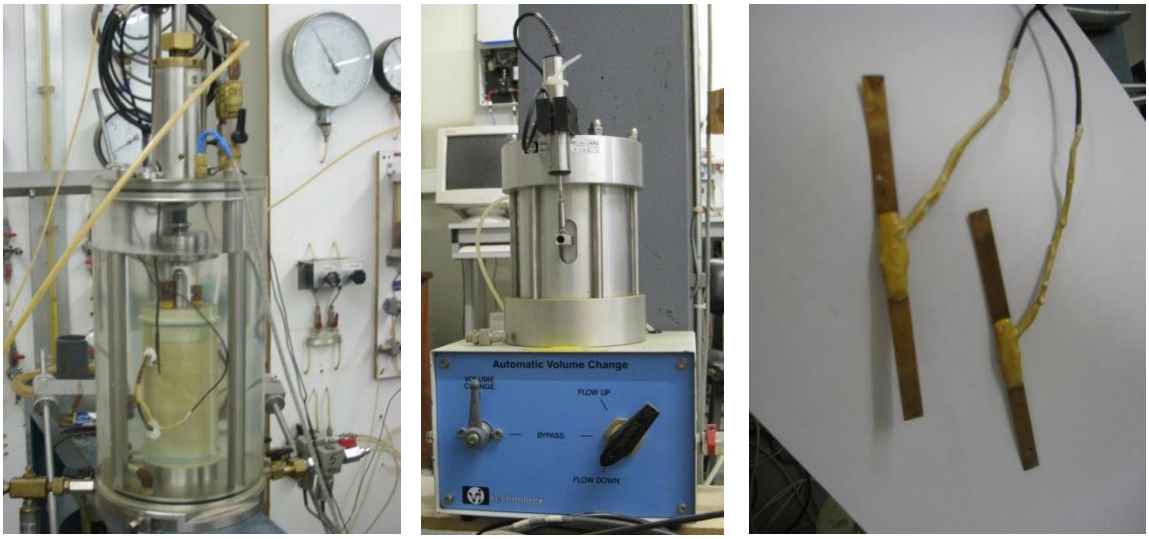

a) b) c)

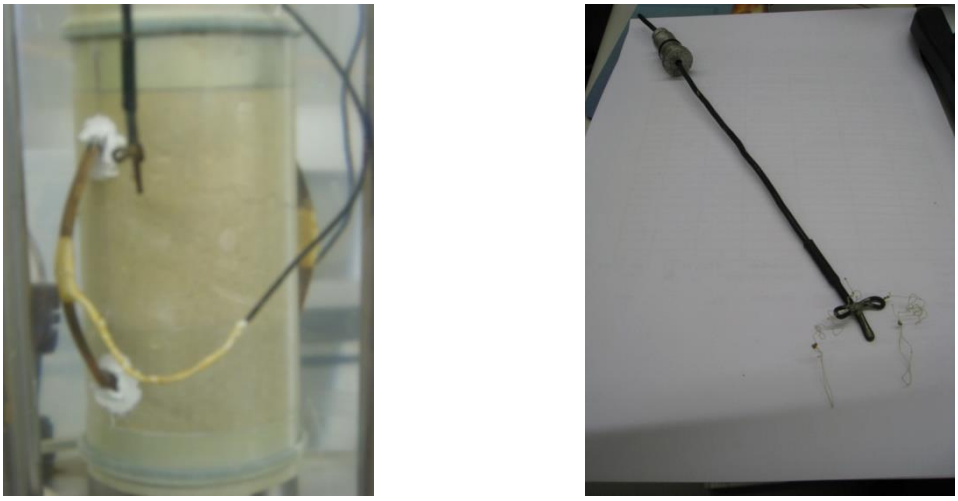

d) e)

Figure 5.10 ISMES Enel.Hydro system a) test setup; b) volume gauge; c) LDT's; d) specimen with LDT's; e) device to take out the LDT's

The LDT's are very important in the first stage of the test to read the initial deformation of the specimen more accurately. However this device is quite sensible and can be damaged when high strains are imposed to the specimen so it is essential to provide a way to take them out of the specimen anchors. This was achieved by a simple tool shown in Figure 5.10 d) and e) which is linked to the LDT's by very thin (almost invisible) wires. When the LDT's range is about to reach its limit, this tool is twisted several times by the user so that the thin wires are rolled pulling the LDT's out of their supporting anchors.

To evaluate the volume change of the specimen by measuring the quantity of water that flows in and out all of the specimen, most triaxial apparatus of the FEUP Geotechnical Laboratory use a volume gauge of 100 cm^3 of capacity associated to a valve system capable of changing the flow direction, which increases the capacity of the volume gauge (Figure 5.10b).

5.6.3 Bishop-Wesley stress-path cell

In FEUP Geotechnical laboratory there are two Bishop Wesley stress-path cells allowing tests in specimens of different sizes from 38 mm to 100 mm. In these systems the axial strain is applied hydraulically using computer controlled stepper motors or motorised Bishop rams and thus it does not require a separate load frame. Both cell and pore pressures are computer controlled through TRIAX® software. The apparatus can carry out routine strain controlled triaxial tests or tests in which the axial stress is controlled and it can change from stress control to strain control during a test with little disturbance. The cells are equipped with standard transducers for the measurement of strain, pore pressure and volume change as well as an internal load cell. The internal load cells were chosen for each set of tests depending on the expected peak strength of the soil. Local measurements of deformation were possible in these apparatus by using LVDTs, for axial and radial deformation (Figure 5.11b).

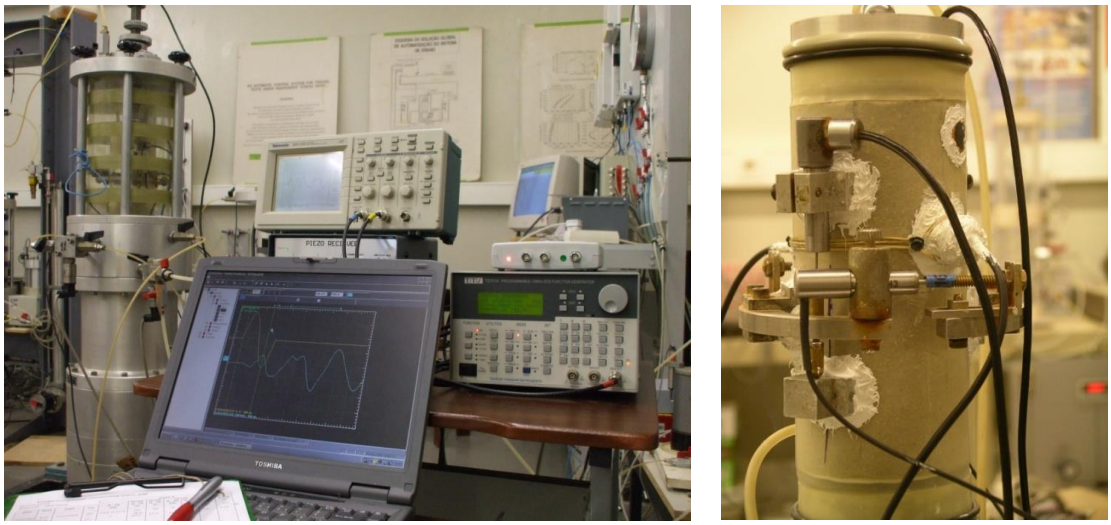

a) b)

Figure 5.11 Bishop Wesley stress-path cell: a) setup; b) axial and radial LVDT's

5.6.4 Conventional triaxial cell with bender elements

This apparatus is a conventional triaxial cell that was adapted to include T shape bender/extender elements (Ferreira, 2008). It has the advantage of being computer controlled for saturation and consolidation stages with a LabView® software developed in FEUP. It is equipped with Hall Effect transducers (Clayton et al., 1989) that enable axial and radial local deformation measurements. Figure 5.12 shows the general setup of the equipment (a), the Hall Effect transducers (b) and the T shape bender/extender elements (c). For higher confining pressures such as 750 kPa a GDS was used to apply the cell pressure because the pressure regulators were unable of keep a constant pressure as the backpressure for the pneumatic pressure system is limited to 8-10 bars. As the specimens tested in this apparatus were all uncemented, an internal load cell of 5 kN was used. The dimensions of the specimens tested in this apparatus were 70 mm of diameter and 140 mm high.

a) b)

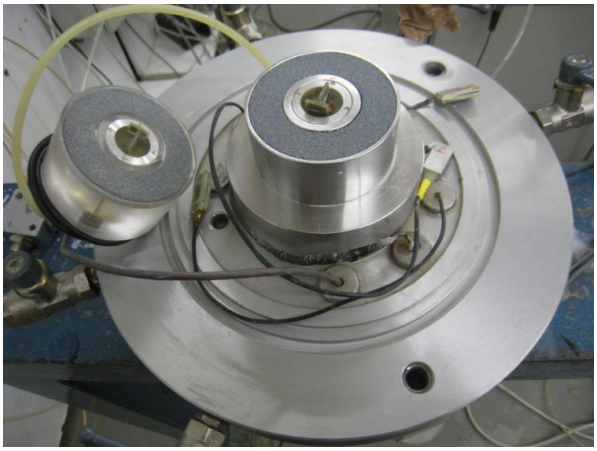

c)

Figure 5.12 Conventional triaxial cell with BE: a) setup; b) axial and radial Hall Effect transducers; c) bottom platen and top cap with BE

5.6.5 Conventional triaxial cell

Finally, a simple conventional triaxial cell was also used to perform some of the tests. Initially the tests were performed only with LDT's for local axial deformation measurements but as soon as it was possible Hall Effect transducers were installed and calibrated to enable radial deformation measurements as well. Most of the apparatus of the Geotechnical Laboratory of FEUP work with internal load cells and this one was no

exception. In fact, as this equipment replaced ISMES (described in section 5.6.2), when it became damaged the load cell was kept the same being 25 kN of capacity. For that reason, the tests were manually controlled and data acquisition was performed with a data logger linked to a computer installed with TRIAX® software just as with the ISMES equipment. This apparatus is prepared for specimens of 70 mm of diameter so the work with the same specimens could be pursed without major problems.

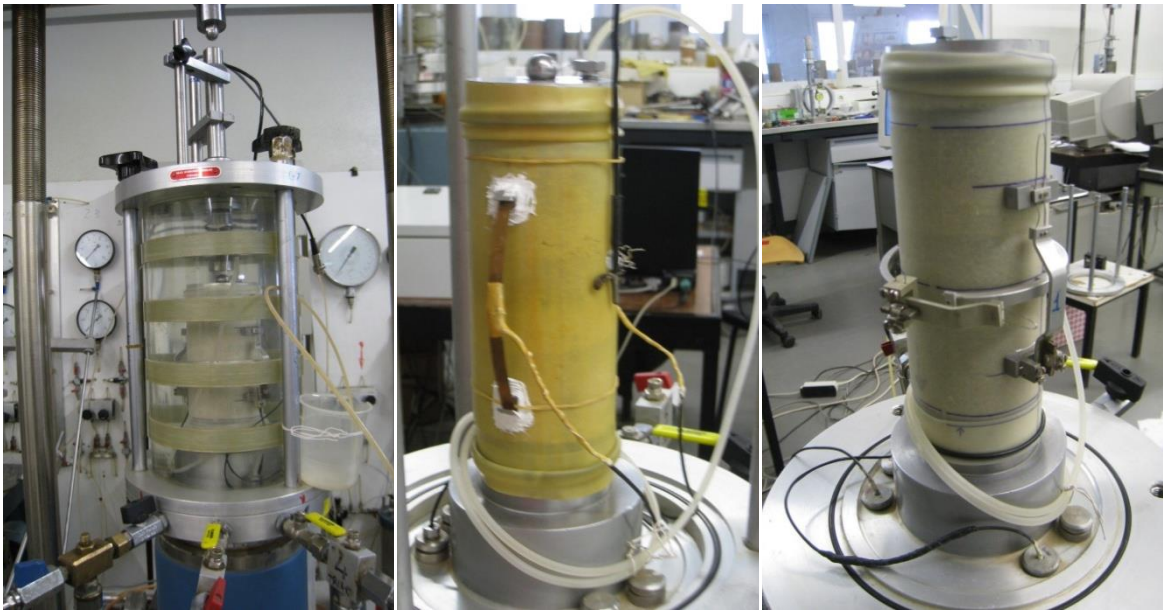

a) b) c)

Figure 5.13 Conventional triaxial cell: a) setup; b) specimen with LDT's; c) specimen with Hall-Effect transducers

5.6.6 Test procedures of the low pressure triaxial tests

All the uncemented and cemented specimens tested in the apparatus described above followed the same test procedures. After moulding, the specimen was placed in the triaxial chamber and water was allowed to percolate during at least 24h or twice the volume of voids of the specimen in order to eliminate part of the air bubbles trapped in the soil and in the tubing system of the cell.

The saturation of the specimens then started until a back pressure of 500 kPa was achieved. In the manual control equipment both cell and pore pressure were increased by steps, smaller at the beginning and higher at the end. Providing that there was a pore pressure transducer linked to the top of the specimen each step was left to stabilise until the pore pressure at the top was equal to the bottom imposed back pressure. This method enabled the calibration of the automatic control where a certain rate of pressure increment had to be introduced (around 30 kPa/h). After reaching the final pressures, the specimen

was left to stabilize with those pressures for some time, usually one night or, at least, 5 hours.

The isotropic consolidation followed by increasing the cell pressure while maintaining the pore pressure constant. The consolidation rate was defined to avoid excess pore pressures, and so an enough slow rate was considered (between 30 and 60 kPa/h). Finally, the specimen was left to stabilize for some hours before shearing even if no apparent volume change was observed.

Drained and undrained shearing was conducted by strain control at a constant rate of 0.01 mm/min. At this speed it was expected that drained tests would not have pore pressure generation, and that strain rate effects were reduced in both drained and undrained tests. All the tests were conventional compression tests where the radial pressure was left constant during shearing and the axial stress was increased by a moving piston associated to a load frame.

5.7 Cyclic triaxial apparatus - FEUP

The cyclic triaxial tests were performed in an apparatus developed by the Institute of Mechanical Engineering and Industrial Management of the University of Porto (INEGI), under specifications of the Geotechnical Laboratory of FEUP. The cyclic triaxial apparatus with all its components is illustrated in Figure 5.14.

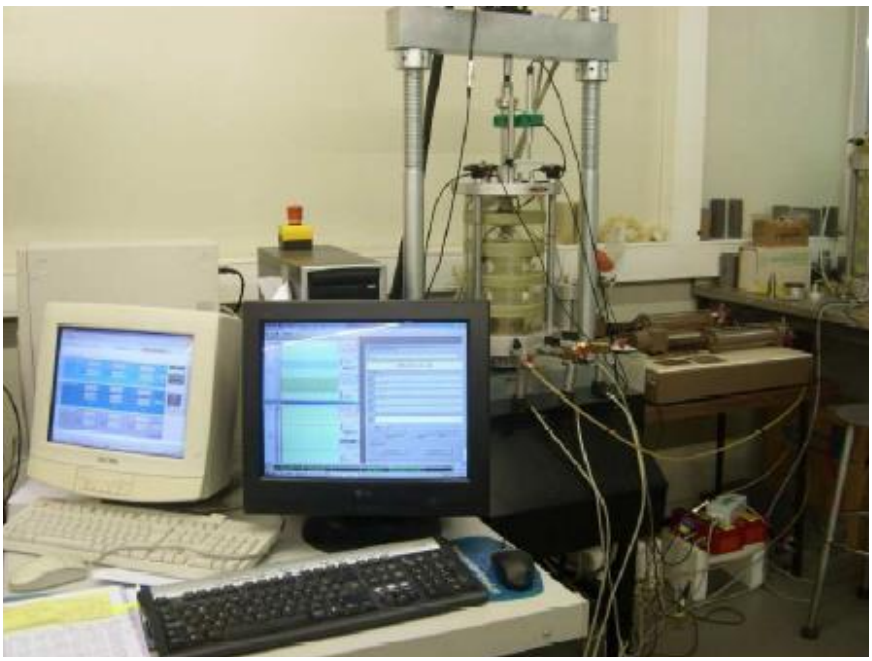

Figure 5.14 Cyclic triaxial apparatus

The cell is a conventional triaxial cell just as described in section 5.6.5 prepared for specimens up to 100 mm of diameter, where specimens of 70 mm by 140 mm were installed for this work. For the present program of tests an internal load cell of 10 kN of capacity was used for the purpose of assuming a good readability of the cyclic loads. This apparatus is able of applying cyclic loads solely in the axial direction. Another apparatus was recently developed in the Geotechnical Laboratory of FEUP to apply both axial and radial cyclic loads.

In terms of the hardware needed to apply a cyclic loading the following components were installed:

- a motor and an hydraulic pump with a maximum pressure of 250 bar allowing the execution of static tests with a maximum load of 50 kN and cyclic tests up to 10 kN;
- an hydraulic unit and a servo actuator that contains an hydraulic cylinder with a displacement transducer and a load transducer (that permits introducing cyclic load with a frequency between 0.001 and 2 Hz);
- an electrical panel with the protection of the motor and an emergency button.

The frame piston was fixed to the actuator (Figure 5.15), so that the real loading curve could follow as close as possible the sinusoidal shape of the load curve chosen for the experimental task.

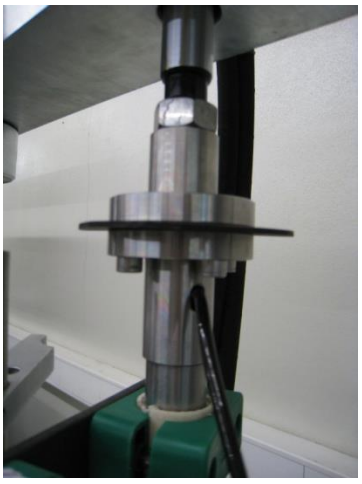

Figure 5.15 Detail of the attachment of the piston to the actuator

The system includes also a data acquisition system with 16 x 2 bits where several channels are available to connect all the transducers and the load cell. A specific software (Dyna tester) was designed to control the system and for data acquisition during the test. Although the tests performed in this apparatus were all stress-controlled, the system also enables strain-controlled tests. The main transducers installed in this equipment were:

- internal load cell;
- Cell Pressure transducer (CP) placed outside the cell;´
- Back Pressure transducer (BP) placed outside the cell to measure the pressure at the bottom of the specimen;
- Pore Pressure transducer (PN) placed outside the cell to measure the pressure at the top of the specimen;
- axial displacement transducer measuring the internal displacement of the piston attached in the top of the load frame;
- external LVDT with 50 mm or 5 mm range placed in parallel to the piston, which measures the relative displacement between the load piston and the triaxial chamber;
- two internal LVDT, sustained by two aluminium brackets glued onto the membrane and with a pivot in the specimens at a distance of 72 mm, which enables an accurate calculation of stiffness modulus to be made (Figure 5.16);
- volume gauge of 100 cm^3 of capacity of the same type as shown in Figure 5.10b), to measure the flow of water after saturation of the specimens. Sometimes this measurement was also performed by the GDS® digital pressure/volume controller;
- two GDS® pressure/volume controllers were used to apply both cell and pore pressure to the specimen during saturation and consolidation controlled automatically by another computer with a specific LabView® software (Costa, 2008). During cyclic shear the pressure regulators were considered more suitable than GDS® as their response is much faster.

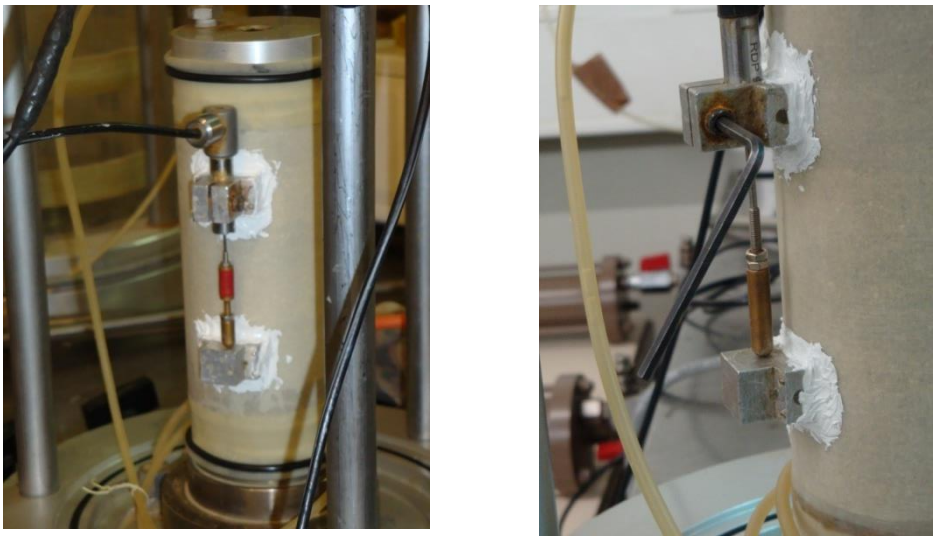

a) b)

Figure 5.16 LVDT's for local axial deformation measurements

5.8 High pressure triaxial

5.8.1 Introduction

In order to study the fundamental mechanics of soils for a broad range of stresses, high pressure testing is necessary. As the volumetric behaviour of soils is logarithmic, a more complete understanding of their behaviour often requires testing at stress levels some orders of magnitude greater than those involved in geotechnical structures (Cuccovillo and Coop, 1999).

In artificially cemented soils, as those studied herein, the stresses applied go up to 50 MPa in order to obtain a clearer understanding of the influence of structure on the mechanical behaviour, the high pressure being used essentially to induce different levels of destructuring in the soil. First, some isotropic compression tests were performed in one of the high pressure apparatus of Imperial College Geotechnical Laboratory. The following work, developed at the University College of London, involved high pressure triaxial tests with shearing by axial compression after an isotropic consolidation. In both laboratories uncemented and cemented specimens were tested.

The most notorious difference between high pressure tests and conventional triaxial tests is that the specimen cannot be seen during the test as the chamber is made from stainless steel, which has been anodized to avoid corrosion. This fact is quite an important issue as in conventional tests simple procedures like filling the chamber or positioning of the piston can be observed and checked. In this case, it is not possible, for example, to see if the piston is touching the specimen or not. However, this can be easily overcome by carefully measuring the cell dimensions and then taking into account the axial displacement during the movement of the piston. This makes the external axial displacement transducer calibration much more important than in other apparatus because if the transducer is not moving in its linear range the consequences may be significant.

Another particular feature of this apparatus is that the confining liquid is oil and not water. The use of oil is justified as water submersible LVDTs cannot be used at the operation pressures of this equipment and therefore non-submersible LVDTs with exposed contacts are used, which require a non-conductive medium, (Cuccovillo and Coop, 1998). Having oil as confining liquid, natural latex membranes cannot be used as they are deteriorated with oil, being replaced by neoprene membranes.

The drainage system is similar to other conventional apparatus, except for the stainless steel lines that are used in order to reduce the compliance of the drainage system as higher

pore pressures are expected and for safety in case of membrane puncture. All the others lines, namely for cell pressure, are also, of course, in stainless steel.

5.8.2 Imperial College London equipment

General Overview

This apparatus used at the Geotechnical Laboratory of Imperial College (ICL) is prepared to test specimens of 50 mm of diameter by 100 mm high and it is able to reach a maximum cell pressure of 70 MPa.

The cell bodies and motorised loading frames were manufactured by Wykeham Farrance Engineering, Ltd. Although the original design of the cell by Wykeham Farrance was suitable only for standard tests carried out in conventional rock mechanics, this cell, produced at that time for City University (Taylor and Coop, 1990), suffered several modifications. The computer control program is an updated version of the original code written by Coop (1991). The program monitors all the pressure and displacement transducers and records and prints their readings. It can also control the stresses. Figure 5.17 gives an overview of the equipment. The main components of the system that were important in performing isotropic tests will be described in detail below.

Figure 5.17 General view of the 70MPa high pressure apparatus

Pressure control system

The system has three pressure control units: cell pressure, axial pressure and back pressure. An air compressor provides air supply to these three units at a maximum pressure of 800 kPa. The air pressure from the regulators is delivered to either by an air/water or by an air/oil interface respectively for the back-pressure and for the axial and cell pressure respectively.

For the back pressure the air/water interface is provided by a volume gauge, with which the volume changes of the specimen are measured. The maximum back pressure is therefore 800 kPa which is usually enough for the saturation of the specimen. To achieve high pressures within the cell chamber and in the axial loading system two hydraulic circuits are built in parallel with the standard pressure control units represented in Figure 5.18.

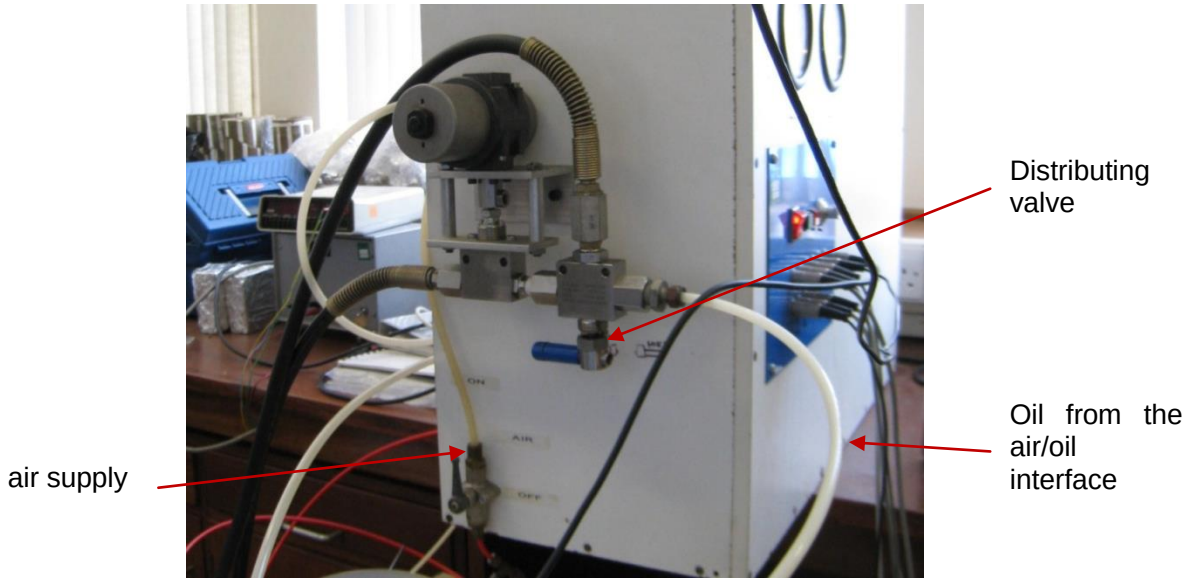

Figure 5.18 Distributing valve that switches between the low or high pressure system. This distributing valve is automatically shut when the security switch on the volume gauge is activated should a membrane puncture occur (see Safety measures).

For example, the cell pressure can be applied either by a low pressure or a high pressure system. The low pressure system, which operates up to 800 kPa, consists of an air-oil interface connected to the regulated air supply, as referred above, and provided with an oil outlet which feeds a two-way distributing valve connected to the cell by a high pressure tube. The high pressure system consists of a 1:100 ratio piston pump fed with the same air supply used for the low pressure system on one side of the piston chamber. The other side of the piston chamber is connected both to an oil reservoir and to a high pressure outlet tube. During operation, the pressurized air displaces the piston down towards the oil bearing side of the piston chamber (oil chamber) generating an amplified pressure which is

then transmitted to the high pressure outlet (Alvarado, 2007). In Figure 5.19 there is a schematic diagram of the control system of the high pressure.

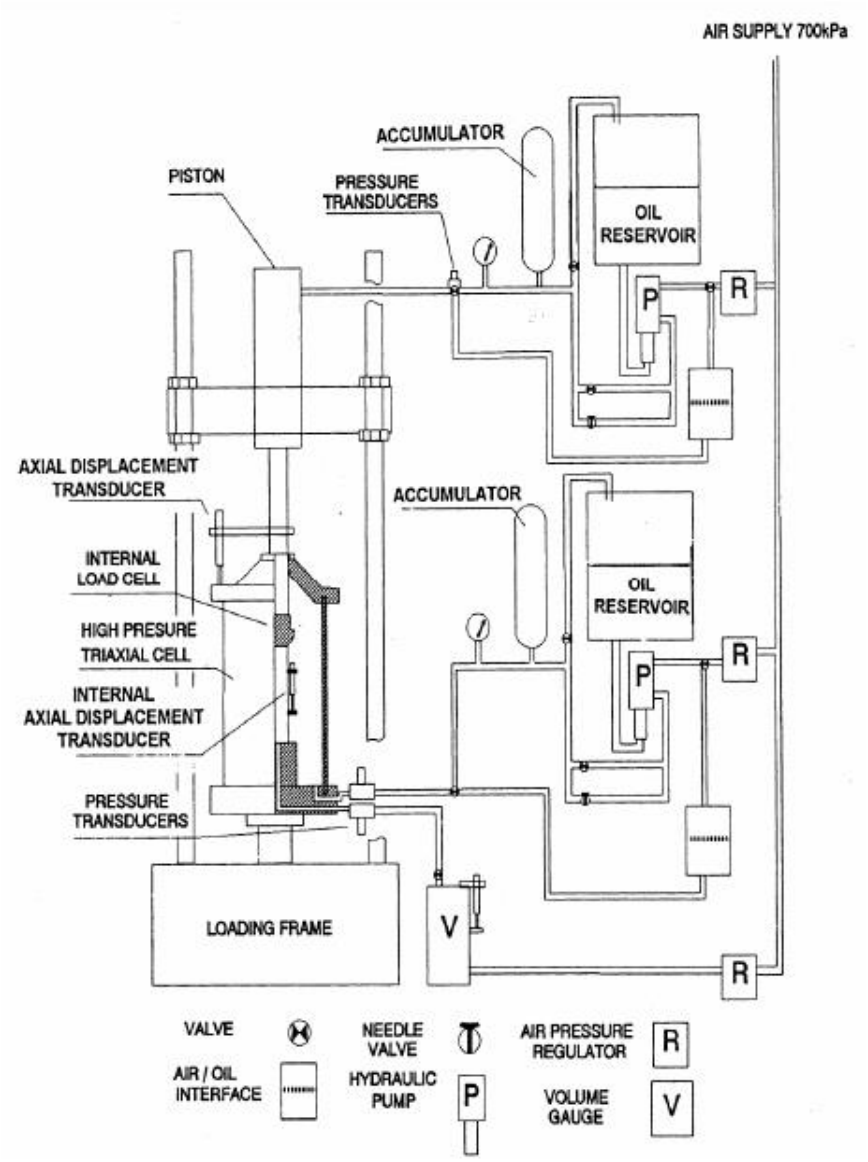

Figure 5.19 Schematic diagram of the control system of the high pressure (Cuccovillo and Coop, 1998)

Safety measures

Due to the high pressures used in such an apparatus some safety had to be included. The main risk that may arise during testing is the membrane puncture. In that case, the cell pressure oil at very high pressure would go into the specimen and from there to the volume gauge damaging it. To minimize the consequences of this problem, a micro switch (Figure 5.21a) located at the base of the volume gauge would be triggered disconnecting the power to the pressure regulators while a safety valve in the system vents the pressure in the

volume gauge to atmosphere. At the same time another safety valve (Figure 5.18) placed between the accumulator and the cell closes, preventing the high pressures still present in the hydraulic circuit from reaching the cell chamber and consequently the volume gauge.

Transducers and gauges

Axial displacements are measured externally by means of a LVDT with a maximum range of 50 mm which is fixed to the frame.

The internal measurements of the specimen height are measured by two axial local LVDTs from RDP® of the type D5/200. These LVDTs can be referred as "oil-submersible" and they can support high pressures by having a small pressure-relieving hole drilled in the body of the LVDT to allow the oil to flow freely in and out (Cuccovillo and Coop, 1998). Their range is ± 5 mm. The wires that connect the LVDTs inside the chamber are very sensible, being easily broken, as they are made of solid cooper (Figure 5.20).

Figure 5.20 Local "oil-submersible" LVDT

A ICL volume gauge with 50 cm^3 of capacity was used for measuring the volume changes of the specimen. The volume gauge (Figure 5.21a) can be filled with a Screw Ram seen on Figure 5.21b). The security switch referred above can be seen in Figure 5.21a) at the base of the volume gauge movement.

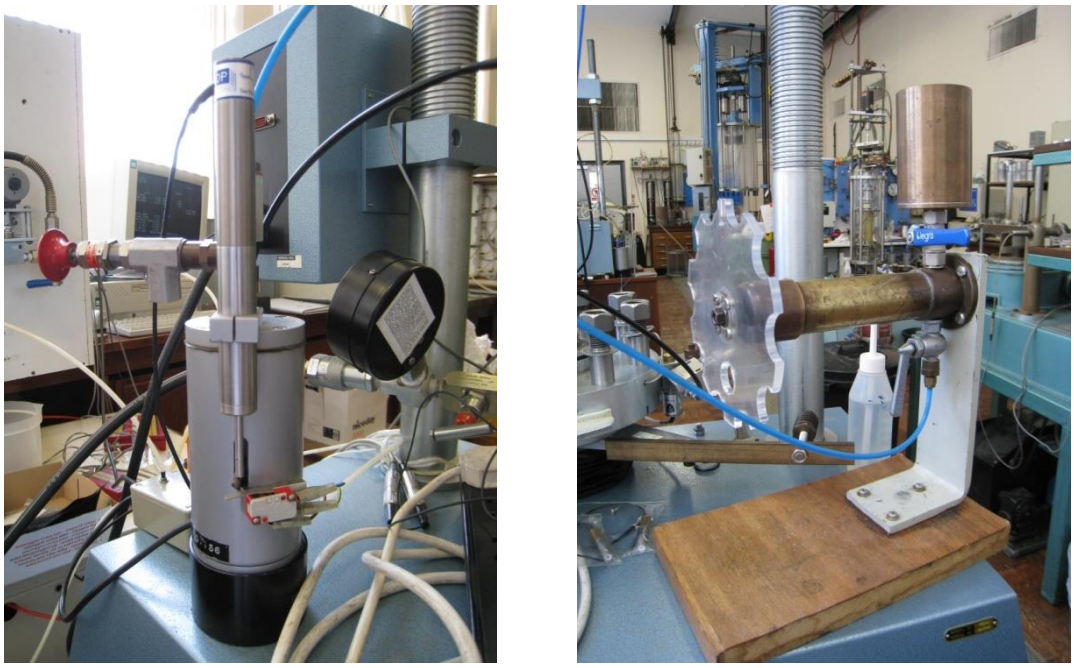

a) b)

Figure 5.21 Volume gauge (a) and Screw Ram (b)

Cell and back pressure are measured by two pressure transducers of 70 MPa of capacity placed between the specimen and the corresponding valve. This means that if the valves are closed, the applied pressures cannot be measured. However, the pressure of the air supply that feeds both air/water or air/oil interface can be checked by some pressure gauges shown in Figure 5.22.

Figure 5.22 Pressure gauges of the air supply to the different units.

The apparatus is prepared to use bender elements measurements during tests. However, bender elements are used only when the tests are performed up to 25 MPa as to avoid

leaks through the top bender element connection. As the pressures used in the isotropic compression tests performed in this apparatus went up to 50 MPa no bender elements measurements could be done (Figure 5.23).

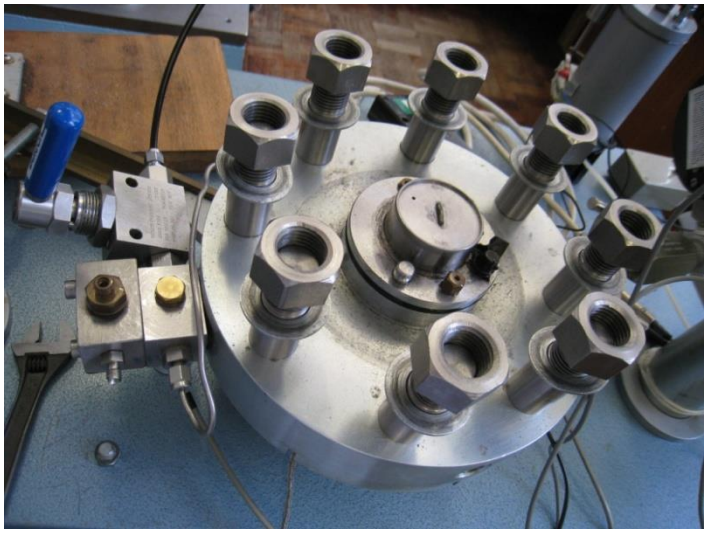

Figure 5.23 Bender elements in the base platen of the cell

In the following table, the capacity of the instrumentation used in this apparatus is presented.

Table 5.1 Capacity of instrumentation

Transducer	Type of measurement	Capacity
Pressure transducers	cell and back pressure	70 MPa
Volume gauge	volumetric strain	50 cm^3
LVDT	external axial displacement	50 mm
Local LVDTs	local axial displacement	10 mm

5.8.3 University College of London equipment

Comparison with Imperial College apparatus

The equipment used in the University College of London (UCL) belongs to the Earth Sciences Department and it is located in Kathleen Lonsdale Building on the Sediment Deformation Laboratory.

The apparatus (Figure 5.24) is similar to the Imperial College London (ICL) one being the maximum pressure of 70 MPa as well, although the specimen size is of 38 mm of diameter by 79 mm high.

Figure 5.24 General view of the equipment

The apparatus consists on a Wykeham Farrance Engineering Ltd original design cell and load frame, prepared to work with oil. At ICL hydraulic oil of the type Tellus 37 from Shell® was used in the cell; in opposition, at UCL silicone oil was used. The cell, the drainage system as well as the local LVDTs and membranes are similar to ICL apparatus described above as they both have to support high pressures.

This type of stainless steel cells is quite heavy which means that some lifting system has to be provided. In UCL the cell was moved by a hoist (Figure 5.25a) fixed to the main structure of the apparatus which holds the load frame where the cell can be attached (Figure 5.25b). In ICL a crane was used to lift and lower the cell.

a) b)

Figure 5.25. View of the hoist used to lift the cell (a) cell being held by the load frame (b)

Pressure control system

The main differences between the apparatus of two laboratories are on the pressure system. In UCL, both the cell and pore pressures were provided by intensifiers, which means that in this system the pore pressure can be increased as much as the cell pressure and it is not limited to 800 kPa as in ICL apparatus. For this reason, a volume gauge is not used and instead the volume change of the specimen is measured by the movement of the piston in the pore pressure intensifier. The whole system is not computer controlled being adjusted by the operator in the control panel shown in Figure 5.26. The data acquisition is done through a Labview® software.

Figure 5.26. Control panel for the pressure system

Transducers and gauges

Conversely to ICL where no shear tests were conducted, at UCL a load cell had to be calibrated in order to perform the desired shear tests. For that reason, an external load cell (Figure 5.27) with 250 kN of capacity was calibrated. The axial displacement is measured by an external LVDT fixed to the piston as seen in the same Figure 5.27 and by local LVDT's similar to the ones at Imperial College described above. The capacity of the main transducers and gauges is presented in Table 5.2.

Figure 5.27 External load cell

Table 5.2 Capacity of instrumentation

Transducer	Type of measurement	Capacity
Pressure transducers	cell and back pressure	70 MPa
Load cell	deviatoric load	250 kN
LVDT	external axial displacement	25 mm
Local LVDTs	local axial displacement	10 mm

5.8.4 Test procedures of the high pressure triaxial tests

Introduction

The installation of the specimens in the low pressure triaxial cells is widely well known, and for that reason the test procedures have been briefly expressed just in terms of the test sequence, applied pressures and employed rates. However, in the high pressure apparatus this installation of the specimens is slightly different from the low pressure procedure and thus it seems important to do a more detailed explanation of the main steps involved in the setup of a high pressure triaxial test. As reported above, two types of apparatus have been used with two distinct test procedures. First the test procedure followed at ICL geotechnical laboratory for isotropic tests will be described and then, the key points that distinguish the methodologies of both laboratories will be expressed focusing on the UCL laboratory method.

Imperial College procedures

The cemented specimens tested at ICL were tested within 9 days of curing period, remaining in this period involved in plastic bags to avoid loss of humidity. Before the test they were placed in water for one night (around 15 hours) to achieve saturation and then 40 min more submerged in water in a vacuum chamber (Figure 5.28a), together with the porous stones. This procedure allowed a degree of saturation of 90% measured by the weight of the specimen before and after being placed in water. The specimen was then placed in the cell with one neoprene membrane and two o'rings: one at the base platen and the other with a special top cap prepared for vacuum. As the specimen is almost saturated by that time, when the vacuum is applied in the top, some water comes out from the specimen along with the air that is being sucked from the specimen (Figure 5.28c). Careful had to be taken to avoid water to go into the vacuum pump (Figure 5.28b), so this process took no more than 20 min.

The uncemented specimens are obviously not submerged in water before the test, thus, some water had to be allowed into the specimen during the application of the vacuum as

shown in Figure 5.28c). However, to avoid destroying the structure of the compacted specimen by the water, a splitting mould was placed around the specimen and so the specimen geometry was not changed. On the other hand, the water allowed into the specimen had a very small pressure around 30 kPa (this pressure is insignificant in a high pressure apparatus). To take out the mould some vacuum had to be applied in the bottom of the specimen until the cell was filled with oil. In the first isotropic test (ISO(0)_14.7) this problem was not taken into account, the splitting mould was not placed around the specimen, and so the initial void ratio might be slightly different from the moulded one.

a) b) c)

Figure 5.28 a) Vacuum chamber; b) vacuum pump; and c) vacuum being applied to the specimen

The remaining procedure is similar to both types of specimens (cemented and uncemented). The acrylic top cap was taken out and replaced by a metal one with a smaller height. Then, another neoprene membrane was placed where the local LVDTs anchors were glued (Figure 5.29). The anchors were positioned with a distance of 50 mm to allow the full range of the LVDTs to be used.

Figure 5.29 Local LVDTs glued to the neoprene membrane

Finally, the chamber was closed and filled with oil and the saturation process could begin. The saturation was done by increasing both cell and back pressure up to 700 kPa of back pressure, keeping a constant effective stress of 50 kPa. The specimen was left with the maximum back pressure for some time, at least one day, until the parameter B was higher than 0.9.

The isotropic compression of the specimen by increasing the cell pressure was done in a quite unusual way. The cell pressure valve was closed and then, by moving the piston down so as to apply axial stress but without touching the specimen, the cell pressure increased. As the piston can be moved with a constant speed it was expected that the cell pressure would increase linearly. Although it may be so for low pressures and for low speed, if the piston was moved faster the pressure would start increasing faster with an exponential law (Figure 5.30). So, careful had to be taken during this process, checking the pressures and the movement of the piston with time, so as to avoid touching the specimen or destroying the equipment by pushing the piston too far.

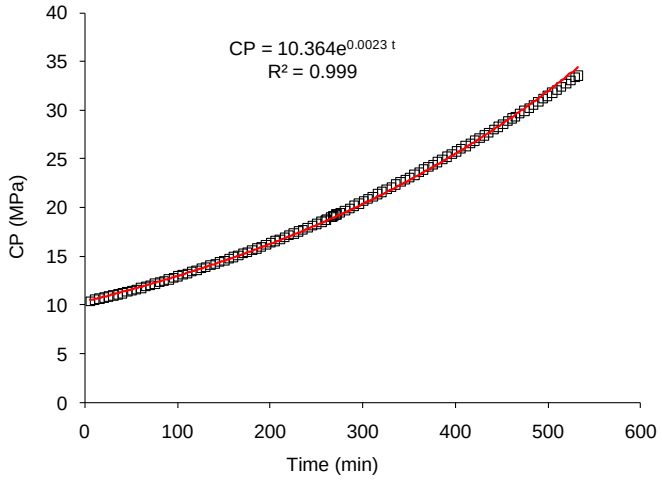

Figure 5.30 Evolution of the cell pressure with time

Comparison between Imperial College and UCL procedures

The specimens tested at the UCL Sediment Deformation Laboratory were cured for more than 28 days involved in plastic bags not to lose any moisture. In order to achieve a faster saturation a similar procedure, as described above, was carried out being the specimen left in water for at least 15 hours and then placed in a dessicator linked to a vacuum pump (or vacuum chamber) together with the porous stone. The saturation stage was executed at high pressures up to 4 MPa of back pressure and so the vacuum applied to the specimen in the cell, as done in ICL, was not performed here.

In the same way as in ICL, two neoprene membranes were used and fixed with o'rings to the bottom platen where a deaired porous stone was placed before. The top cap was placed above the specimen and the two membranes were fixed with two more o'rings. It should be pointed out that the o-rings were placed after the two membranes and none of them was folded back towards the o-rings as this created a leak. A second top cap, which was convex to the first, was then placed and the two pieces were joined together with anti seize compound. The aim of these two pieces was to allow them to move one over the other so that any misalignment would not be transferred to the specimen. The LVDT's anchors were glued to the membrane and all the wires were fixed with rubber bands not to be damaged when the cell was lowered (Figure 5.31).

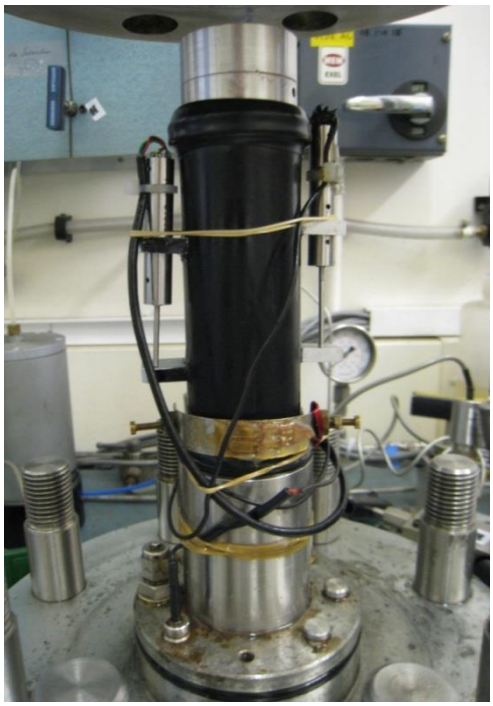

Figure 5.31. Setting of the specimen

The cell held by the load frame and moved by the hoist should be lowered carefully, just enough to make the vessel in contact with the base platen, so that the piston would not hit the specimen. The load frame was then held by the side securing nuts and the attachment to the cell was only taken out at the end of consolidation when the high pressure inside the cell avoided the piston to fall (Figure 5.31a). Before shearing, the external load cell would be placed above the cell (Figure 5.31e and f). Figure 5.32 summarizes the test setup during several stages.

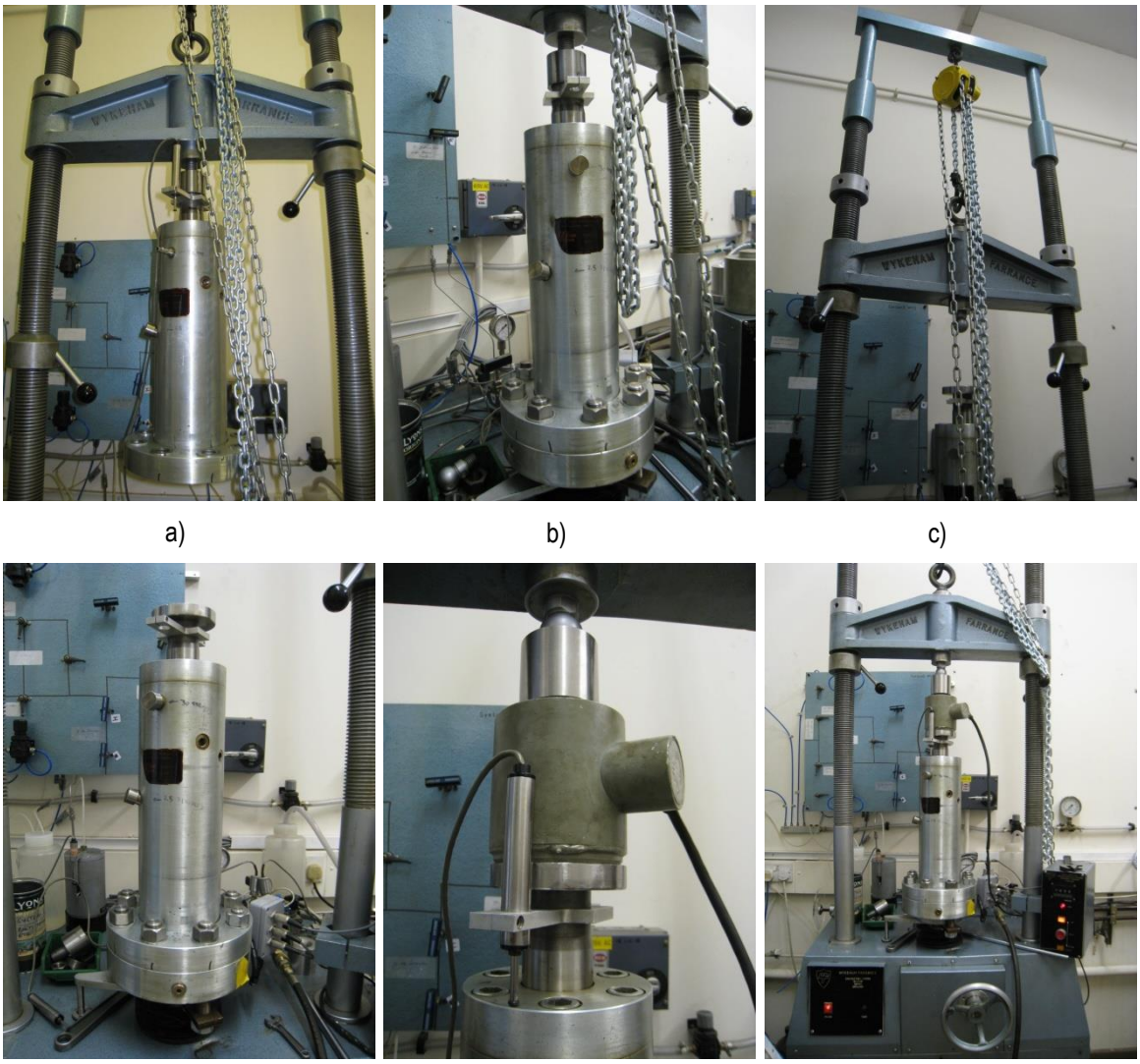

Figure 5.32. Test setup: a) movement of the cell; b) test setup during saturation and consolidation; c) cell separated from the load frame and lift of the load frame; d) cell; e) external load cell placed over the cell; f) test setup for shearing

Both the cell and the cell pressure intensifier were filled by a manual pump which had to be filled with oil before each test. After closing the cell, the specimen was left to saturate with 4 MPa of pore pressure and 4.4 MPa of cell pressure.

The consolidation stage was done manually by increments of cell pressure and in each step the volume change was stabilized before applying a new increment. The strain rate of the shear stage was 0.01 mm/min, similarly to the others tests performed in FEUP.

To empty the oil out of the cell, compressed air was used that enabled a much faster procedure than in ICL laboratory where the oil was left flowing by gravity during the night.

Chapter 6.
PRELIMINARY TESTS

6.1 Introduction

This chapter is the first of a set of three chapters related with the extensive experimental program developed in this research work. Under the name of “Preliminary tests”, chapter 6 comprises the description of the soil used in this work (including conventional and non conventional identification tests), the preparation of the specimens to be tested subsequently, as well as all the non triaxial tests performed in this experimental program.

This set of data includes a wide type of tests from very simple ones, such as Proctor tests or suction measurements by the paper filter method, to more sophisticated tests to evaluate the elastic stiffness by wave velocities measurement such as Bender Elements (BE) or Resonant Column (RC) tests. The high number of different test methods was justified from the lack of knowledge about artificially cemented materials in CEC/FEUP research group, and especially, the lack of information in the literature about the behaviour of a mixture of Portland cement with a very well graded soil with around 30% of fines. Some of these tests were later found to be inadequate for the study of cemented materials, but even though, their description in this chapter was considered important as the obtained experience provided new research lines that can be followed in the future with a better outcome. Some others, although simple and conventional, were very important to the definition of the triaxial tests experimental program described in the next chapters.

For each test, the number of specimens tested and their conditions will be first presented and, then, the test results will be given as well.

6.2 Description of the soil

6.2.1 Classification

The soil used in this research program is a remoulded residual soil from granite taken from the Faculty of Engineering of the University of Porto experimental site (CEFEUP) described by Viana da Fonseca et al. (2006) and widely studied in 2004, in its natural conditions, by the time of the International Site Characterisation Conference (ISC'2) in Porto (http://www.fe.up.pt/ISC-2). Residual soils from granite are very frequent in Portugal where this type of rock is very abundant especially in the north and central region. The grain size distribution of this formation can change within a certain range illustrated by Viana da Fonseca (2003) in Figure 6.1.

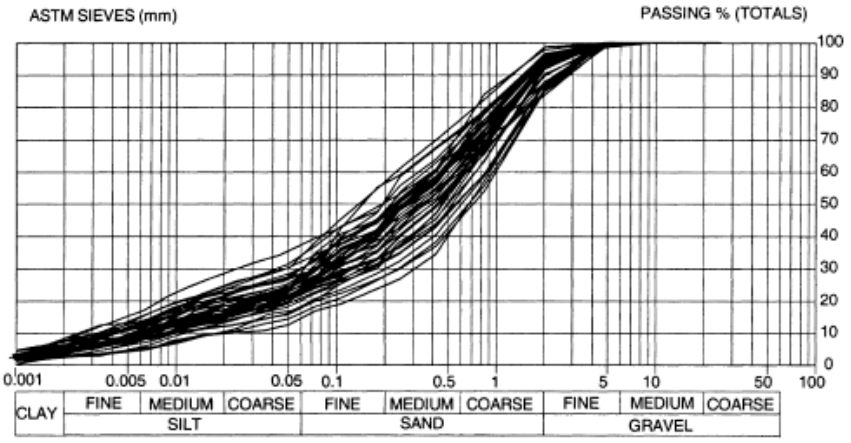

Figure 6.1. Grain size distribution curves of Porto silty sand (Viana da Fonseca, 2003)

In order to have a consistent research work and to have a grain size distribution of the soil that would fulfil the recommendations of the Portuguese and Spanish specifications described in Chapter 2 it was decided to correct the grain size distribution curve of the soil. As reported in Table 2.4, the Portuguese specification and the Spanish standard - PG3, 2004 - (for S-EST3 and SC20) agree that the fines content, defined as the % of particles passed in ASTM sieve nº200 (75 μm) or the % of particles lower than 63 μm, should be lower than 35%. For that reason it was decided that the corrected soil would have around 30% of fines. In Figure 6.2 the grain size distribution curves of the natural soil before correction (with around 40% of fines) are plotted together with the ISC'2 curves and with some grain size distributions curves of the corrected soil (around 30% of fines).

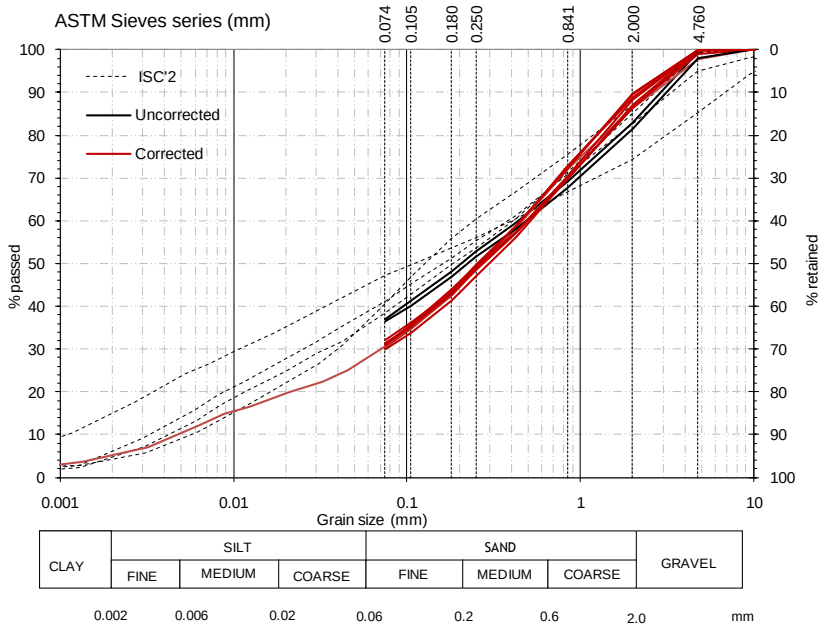

Figure 6.2 Grain size distribution curves of the soil before and after correction and their comparison with the curves presented in ISC'2 for the FEUP experimental site

This soil is classified as a silty sand (SM) according to the unified classification system (ASTM, 1998a) or a B5 (sables très silteux) according to GTR 2000 (AFNOR, 1992) being a very well graded soil. The Atterberg limits gave values of w_L =34% and w_P =31% thus I_P=3, which makes this soil non plastic. Table 6.1 summarizes some physical parameters of the soil.

Table 6.1 Physical parameters of the soil

γ_s	D_{50}	C_u	C_c	w_L	w_P
kN/m^2	mm			%	%
26.6	0.25	113	2.72	34	31

where,

- γ_s is the particles unit weight
- C_u is the uniformity coefficient
- D_{50} is the largest particle size in the smallest 50%
- C_C is the curvature coefficient

6.2.2 QicPic test

In this section some results will be presented on the particle size and shape obtained with the QicPic test whose equipment (from the Geotechnical Laboratory of Imperial College London) was described in Chapter 5. For this test, a representative small mass of around 10 g of the coarse part of Porto silty sand (> 0.075 mm - ASTM sieve nº200) was analysed.

An interesting point of this test is that the shape of the particles can be seen. In Figure 6.4 some particles are shown as example together with the EQPC number. The EQPC is the diameter of a circle that has the same area as the projection surface of the particle (Figure 6.3). Being this soil derived from a residual soil from granite their particles are very sharp and angular as they suffered no transport to smooth their edges. This is quite clear in Figure 6.4 where particles of several different shapes are shown. The shape of the particles is also a consequence of the mineralogy of the soil composed mainly by quartz, feldspars and mica grains. Some of the feldspars have been "transformed" into caulinite becoming part of the fines content but not all, as this residual soil is a saprolite (young residual soil) and, therefore, the weathering degree is not very high. The mica grains, essentially biotite and muscovite, have lamellar shape so they may correspond to the more elongate particles of Figure 6.4.

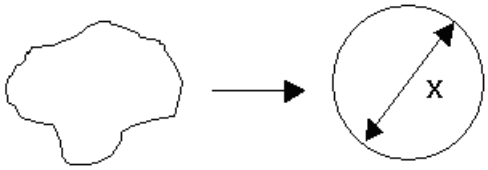

Figure 6.3 The equivalent circle to calculate the EQPC number

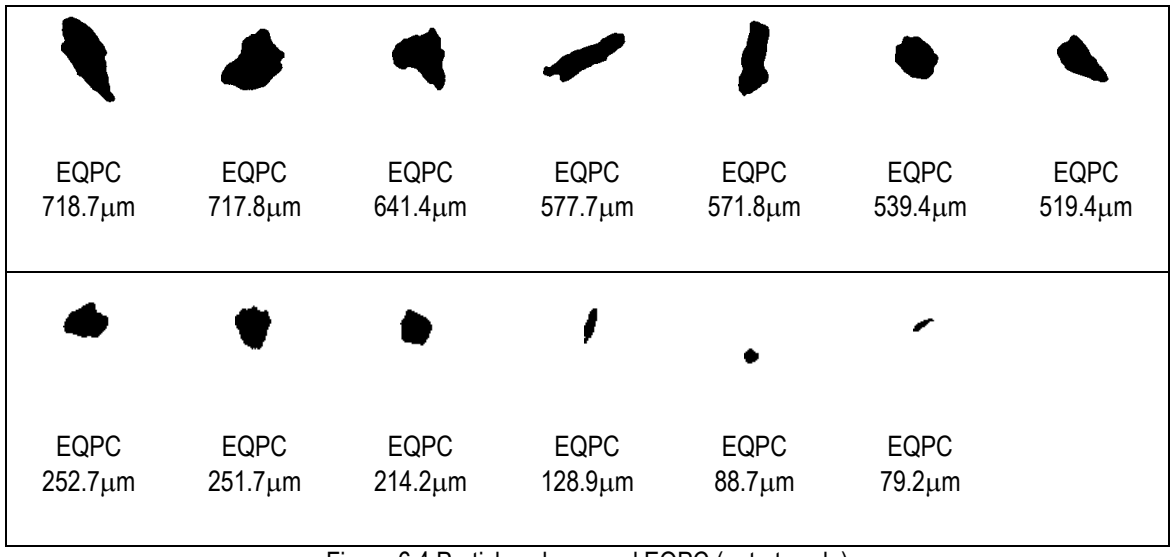

Figure 6.4 Particles shape and EQPC (not at scale)

There are some other parameters calculated automatically by the equipment software. One of the parameters based on the equivalent circle (Figure 6.3) is the sphericity, which is the ratio of the perimeter of the equivalent circle, P_{EQPC}, to the real perimeter, P_{real}, as equation (6.1):

$$sphericity = \frac{P_{EQPC}}{P_{real}} = \frac{2\sqrt{\pi A}}{P_{real}} \quad (6.1)$$

The result is a value between 0 and 1 (the smaller the value, the more irregular is the shape of the particle) being that most natural soils have sphericity values around 0.8 (Cho, G.C. et al., 2006, Cavarreta et al., 2010, Altuhafi and Baudet, 2011). This results from the fact that an irregular shape causes an increase of the perimeter. The ratio is always based on the perimeter of the equivalent circle because this is the smallest possible perimeter with a given area.

Along with the EQPC there is another way of giving the diameter of the particles: the Feret Diameter (Walton, 1948). This is not a diameter in its actual sense but the common basis of a group of diameters derived from the distance of two tangents to the contour of the particle in a well-defined orientation (Figure 6.5). In simpler words, the method corresponds to the measurement by a slide gauge (slide gauge principle). Maximal or minimal Feret diameters can be calculated after consideration of all possible orientations (0°...180°). If a particle has an irregular shape, the Feret diameter usually varies much more than with regularly shaped particles. The maximum can therefore be significantly larger, the minimum significantly smaller than the diameter of the equivalent circle.

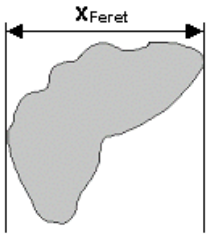

Figure 6.5 Illustration of the Feret diameter (orientation horizontal: 0°)

One of the shape parameters derived from the Feret diameter is the aspect ratio defined as the ratio of the minimal to the maximum Feret diameter. Figure 6.6 shows the evolution of sphericity and aspect ratio with the particles size. They both seem quite regular: sphericity within high values and aspect ratio with low values, meaning that in spite of sharp edges the particles are not so irregular.

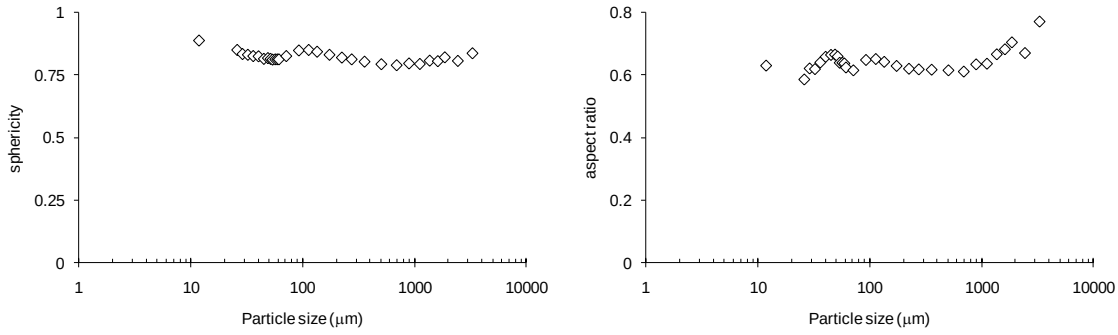

a) b)

Figure 6.6 Shape parameters against the particle size: a) sphericity and b) aspect ratio

Finally, it is presented in Figure 6.7 the grain size distribution curve obtained by the QicPic test for the coarse part of the soil (retained on ASTM sieve nº200) including sand and a small quantity of fine gravel. In the same graph one of the sieve analysis presented before in Figure 6.2 was also plotted taking into account that only the coarse part of the soil was used. This plot shows that the QicPic gives coarser particles than the sieve analysis. The soil for the QicPic was washed with water in order to take out the fines but no anti-flocculant was used, and therefore, it may be that some fine particles were aggregated indicating coarser particles.

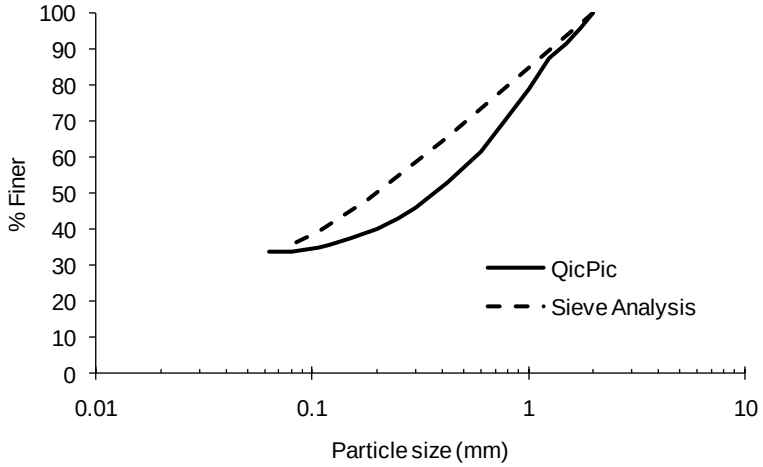

Figure 6.7 Grain size distribution curve of the coarse part of Porto silty sand

6.3 Specimen preparation

6.3.1 Introduction

The aim of this research work is to study different mixtures of soil and cement and their comparison with uncemented specimens compacted in the same way. For this reason, only

remoulded specimens were used, which always followed the preparation procedure described in this section.

6.3.2 Cement and curing period

For the cemented specimens, the soil described above was mixed with different quantities of high strength Portland cement (CEM I 52.5 R) with high initial strength, together with a certain amount of water. The moulding water was tap water as distilled water was only used in triaxial tests for cell and back pressure.

The idea of using such cement quality from Secil® (Portuguese Cement Company) was to improve the time of the experimental work. Unfortunately, the results revealed that the specimens strength was not stabilising at 7 days as it was first expected (Foppa, 2005; Consoli, 2007; Lopes, 2007). Figure 6.8 shows the results of late unconfined compression tests performed at 4, 7, 14, 28 and 56 days of curing period over specimens moulded with 5% and 7% of cement.

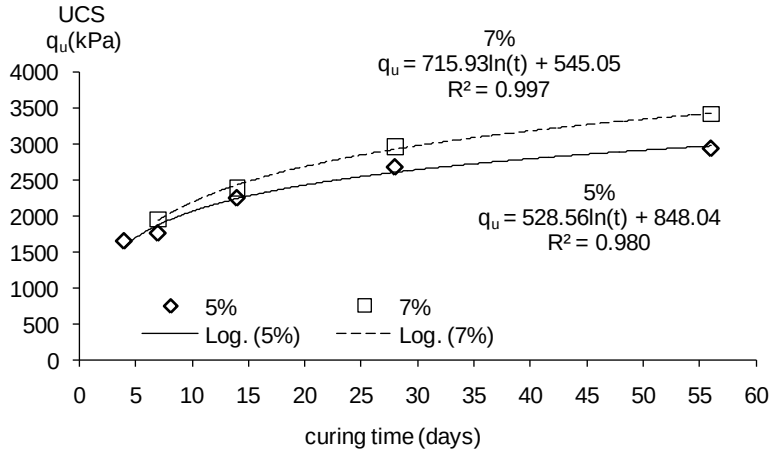

Figure 6.8 Evolution of the unconfined compression strength with curing time

Amaral (2009) has proposed some curves, relating the evolution of the dynamic Young modulus derived from seismic wave velocities with time, presented in Figure 6.9 for the 5% and 7% cement content specimens. These specimens have the same initial void ratio than the ones of Figure 6.8, however, conversely to the unconfined compression test performed in this work where the specimens were placed in water at 7 days of curing (except the 4 and 7 days curing that were submerged in the day before the test), these specimens were tested at their moulding state, i.e., without being submerged in water.

From this data, a logarithmical trend was observed, which means that the comparison of tests performed at different curing periods needs to be corrected by the equations shown in

Figure 6.8 and 6.9. In spite of the amount of days in water, Figure 6.8 and 6.9 show that the evolution laws that control the increase in strength and stiffness with time are different.

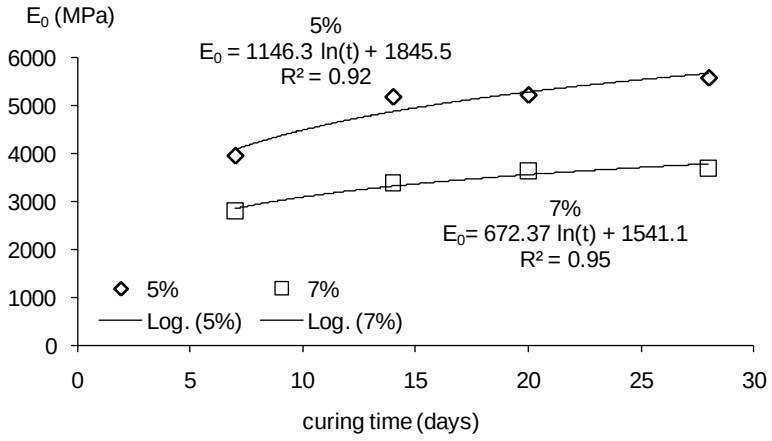

Figure 6.9 Evolution of the dynamic Young modulus with curing time (Amaral, 2009)

6.3.3 Soil grain size distribution curve

As expressed before, the grain size distribution of the soil was always corrected in order to have the same grading in all performed tests. However, adding cement changes the grain size distribution of the soil, as the quantity of fines will be greater. It is well known that the amount of fines has a significant influence on behaviour of soils, especially on the influence of the water content in their behaviour. In order to prevent the results from the influence of higher fines content, a quantity of fines equal to the amount of cement to be introduced was taken out from the soil before preparation of the mixture. This procedure also assures that the dry unit weight of the mixture will remain constant with increasing cement content so that mixtures with different cement contents and the same compaction degree will be comparable.

It became clear from the equipment description in the previous chapter that most of the specimens were moulded with 70 mm of diameter. However, some other specimens were 50 or 38 mm of diameter in order to fit some triaxial cells prepared for smaller specimens. In the 38 and 50 mm specimens, the larger particles retained on ASTM sieve No.10 were removed in order to avoid strain concentration in those particles with respect to the size of the specimen used in the mechanical tests.

6.3.4 Mixture preparation

After weighting the right quantities of the three components, the soil and cement were mixed until reaching uniform consistency. Water was then added while continuing mixing

until a homogeneous paste was created. The soil-cement mixture was then stored in a covered container to avoid moisture loss until it was subjected to static compaction in a stainless steel lubricated mould (the compaction procedure is described in detail in the next section where two different methods are compared). The specimen was left inside the mould at least 12 hours to prevent swelling and then it was stored in the humid chamber inside a plastic bag to avoid moisture loss. Therefore, the specimens cure was done without any stress. The procedures of mixing and compaction took less than 30 min as recomended in the Portuguese standard LNEC E-264 (1972a). Figure 6.10 illustrates the main procedures described above for the preparation of the specimens.

Figure 6.10 Sequence for the preparation of the specimens

6.3.5 Compaction

The European standards suggest four different methods for the manufacture of test specimens of hydraulically bound mixtures: using Proctor equipment or vibrating table (EN 13286-50), using vibrating hammer compaction (EN 13286-51); using vibrocompaction (EN 13286-52) or axial compression (EN 13286-53). From these methods, the last (EN 13286-53, CEN, 2004b) was considered to be the most appropriate.

On the other hand, the undercompaction method proposed by Ladd (1978) is also frequently used in similar works (e.g. Rotta, 2005; Cruz, 2008).

In order to select the best method for compaction, two specimens were compacted in different ways: the first followed EN 13286-53 (CEN, 2004b) and the other followed the

general idea of the undercompaction method proposed by Ladd (1978) where static compaction was applied in three layers.

The specimens were prepared with the same cement content (7%), water content (12%) and dry unit weight (16.4 kN/m^3) and then tested in unconfined compression after 6 days in the humid chamber and one day submerged in water. The European standard method was not very practical because the mixture had to be placed in the mould in one step, which was not easy since, when loose, the mixture did not fit in the mould. To avoid this problem some manual tapping was performed during this procedure. The three layer compaction following Ladd (1978) undercompaction method was performed dividing the mixture into three equal portions, and then, each portion was statically compacted until a certain fraction of the desired height was achieved. For the first layer a little bit more than 1/3 was used, for the second almost 1/3 was used and for the final layer the whole height had to be filled. This was calibrated by experience. The top of each layer was slightly scarified before the compaction of the next layer to improve their interpenetration.

After the unconfined compression tests, the specimen compacted in three layers showed a clear shear plane of failure characterized by localized deformation along a plane oriented at angles between 60° and 70° with respect to the horizontal direction (Figure 6.11a). Instead, the specimen compacted following the European standard presented a failure with vertical cracks at the base (Figure 6.11b and c).

a) b) c)

Figure 6.11 Specimens compacted in two methods tested in unconfined compression strength: a) three layer compaction; b) and c) european standard method

According to these results, the three layer compaction following Ladd (1978) undercompaction method was considered the most convenient because it seems to provide a much better homogeneity of the specimen by the evidence of a clear shear plane failure along the total height of the specimen as it is usually observed in triaxial tests. In

opposition, the mode of failure observed in the specimen compacted by the European standard method does not indicates a very homogeneous behaviour as most of the cracks were on the base of the specimen.

6.3.6 Quality control and calculations

Quality control of the moulding procedure was also checked by measuring the weight and dimensions of the specimen after being extracted from the mould. The specimens were considered suitable for testing if they met the following tolerances:

- Dry density (γ_d) within ±1% of target value;
- Moisture content (w) within ±0.5% of the target value;
- Diameter within ± 1 mm; and
- Height within ± 2 mm.

These criteria were used in spite of the specimen's size, but the tests were only rejected when the specimen's dimensions were far from their tolerances, as no significant difference was noticed in the results.

It is important to point out that the cement content was based on the quantity of dry soil and the water content was based on the quantity of dry soil and cement just like Zhu et al. (1995) have suggested. Finally, as the specific gravity of the cement grains (3.1) is greater than the specific gravity of the soil grains (2.71), for the calculation of void ratio and porosity, a composite specific gravity based on the soil and cement percentages in the specimen was used. In Appendix A the main expressions used in the calculations of the right quantities of soil, cement and water are presented.

6.4 Proctor tests

Standard and Modified Proctor tests were conducted in uncemented specimens and Modified Proctor tests were performed in cemented specimens with 3% of cement content. The testing procedure followed the Portuguese standard LNEC (1972b). Table 6.2 summarizes the optimum values obtained in the three Proctor tests and the corresponding curves are plotted in Figure 6.12.

The data show that the cement does not introduce a significant influence on the optimum dry unit weight or on the shape of the curve in the dry side. The cement seems to slightly decrease the optimum water content and to lift the wet side part of the curve as it would be expected due to the increase in the specific surface area by the fines of the cement. Lohani et al. (2004) also found compaction curves of uncemented and cemented compacted

gravel to be similar for the same compaction conditions as the fines contents do not have a significant effect in these materials.

Considering that all the specimens moulded in this experimental program have the same fines content (see section 6.3.3), it is expected that the Proctor curves for different cement contents will be similar. For this reason, these curves were used to identify the moulding conditions for the specimens tested in unconfined compression. Two lines were drawn (an horizontal line at 17.2 kN/m^3 and a vertical line at 12% of water content) and eight moulding points were defined in those lines as Figure 6.12 illustrates.

Table 6.2 Optimum values obtained in Normal and Modified Proctor tests

	Proctor			
	Normal		Modified	
	w_{opt} (%)	γ_d (kN/m^3)	w_{opt} (%)	γ_d (kN/m^3)
soil	17.5	16.9	13	18.6
soil-cement	-	-	12	18.7

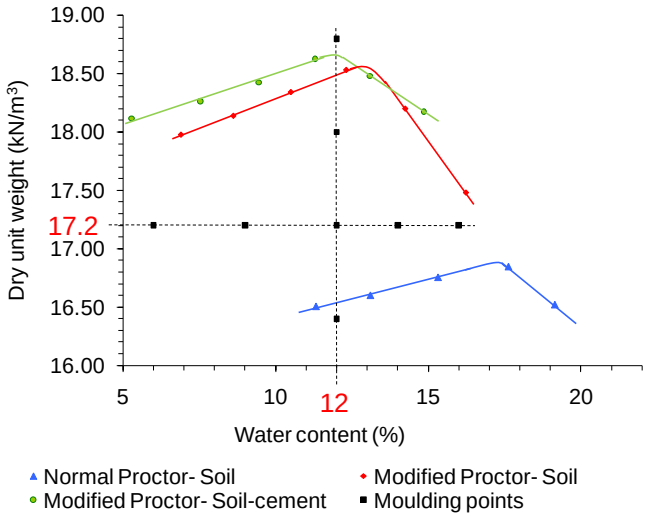

Figure 6.12 Normal and Modified Proctor curves for soil and soil-cement specimens

6.5 Unconfined compression tests

6.5.1 Tested specimens

Unconfined compression tests were performed over specimens moulded in the conditions expressed above. In the vertical line the water content remained constant (12%), four dry unit weights were established (16.4, 17.2, 18.0 and 18.8 kN/m^3) and four cement contents were used (2%, 3%, 5% and 7%) comprising 16 tests. From these tests the influence of the dry unit weight and cement content on the unconfined compression strength (UCS) could be analysed. In the horizontal line the aim was to study the influence of the water content

on the unconfined compression strength and the profile of that variation for each cement content. In this case the dry unit weight was kept constant and equal to 17.2 kN/m^3 and four water contents were considered (6%, 9%, 14% and 16%) which totalises more 16 tests taking the four cement contents expressed before.

Each test was repeated at least 4 times in order to confirm the results, and the values deviating more than 10% from the average value were rejected.

The specimen preparation followed the procedure described in section 6.3 and then after 6 days in the humid chamber the specimens were placed under water during 24 h to improve saturation and decrease suction. The specimen was then taken out of water dried superficially with an absorbent cloth and then immediately tested in the load frame described in the previous chapter following the standard EN 13286-41 (CEN, 2003b). The tests were performed with local measurement of deformation using Local Deformation Transducers (LDT's) as illustrated in Figure 6.13a) and so, the results will be analysed in terms of unconfined compression strength and initial tangent stiffness as well.

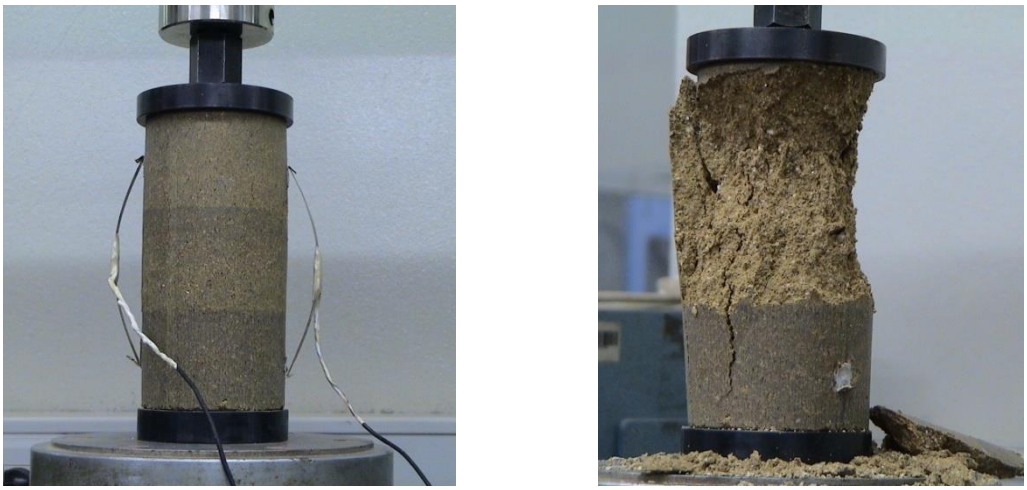

a) b)

Figure 6.13 Photographs of the specimen: a) before the test; b) after the test

6.5.2 Strength Results

Vertical line results

The results obtained in the tests executed in the vertical line are plotted in Figure 6.14. First, the relation between the unconfined compression strength (UCS) and cement content is presented for each dry unit weight, and then, the relation between the UCS and the dry unit weight is showed for each cement content. In both graphs the power law was the trendline that showed the best correlation to adjust the data.

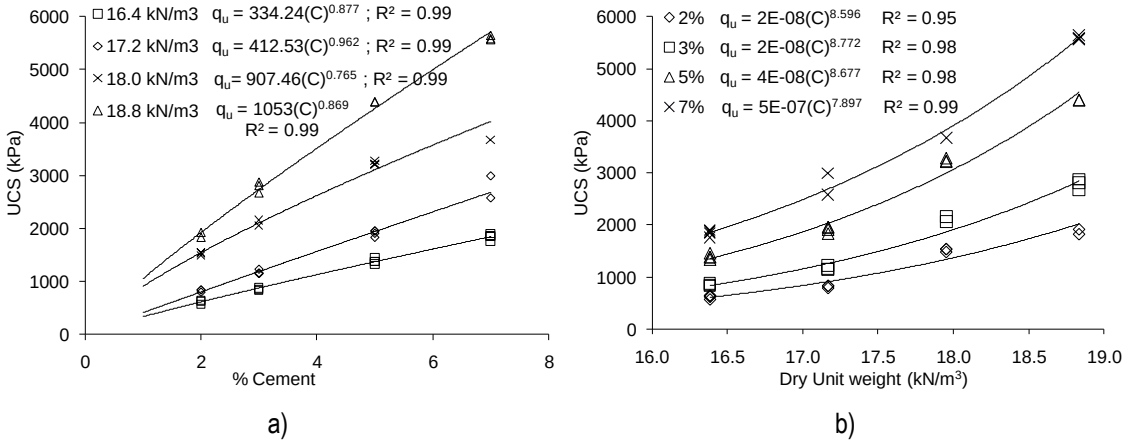

a) b)

Figure 6.14 Relationship between cement content and unconfined compression strength for each dry unit weight (a); Relationship between dry unit weight and unconfined compression strength for each cement content (b)

From these results, it is clear that the cement content has a significant influence on the unconfined compression strength as small amounts of cement can highly increase the strength of the soil. This increase in strength appears to be more important in denser specimens where there are more contact points between particles and, thus, the effectiveness of cementation is improved as reported in chapter 4.

Another way of looking to these results is to plot the UCS in terms of porosity or in terms of the inverse of cement volume, for each cement content. As Figure 6.15 shows there is a very good adjustment when power laws are applied but there is a great difference between the trendlines of each cement contents.

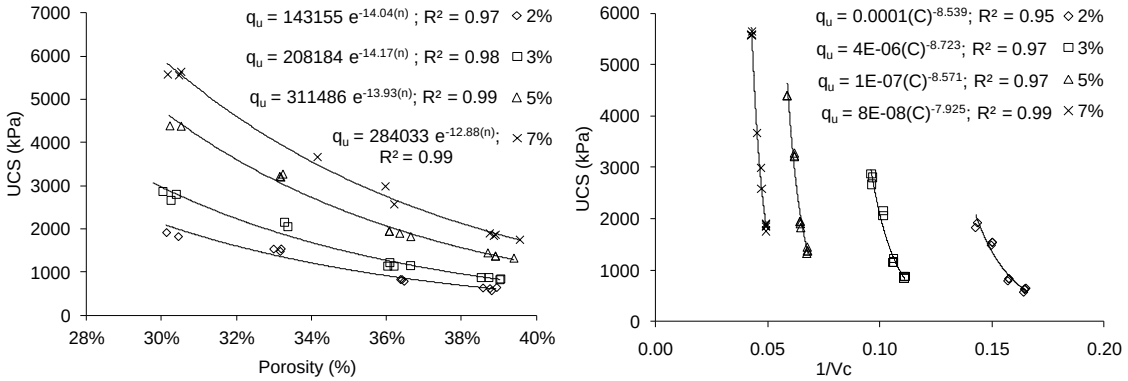

a) b)

Figure 6.15 Relationship between the unconfined compression strength and porosity (a) and inverse of cement volume (b).

In order to find an index ratio that would characterise the behaviour of soil-cement mixtures reproducing the influence of both cement content and void ratio, Consoli et al. (2007) have

proposed a parameter that is the ratio of porosity to the volumetric cement content (n/C_{iv}) as described in chapter 3 (section 3.2.6). This ratio is equivalent to the ratio of the volume of voids to the volume of cement (V_v/V_c), however, the former has the advantage of being almost independent of the specimen size and thus more convenient to compare specimens of different sizes. From Figure 6.16a), it is clear that this ratio does not reproduce the influence of both parameters as several correlations have to be established for each cement content. However, applying an exponent to the volumetric cement content changes the plot (Figure 6.16b) and a unique trend (equation (6.2)) can be observed with a high correlation coefficient.

$$UCS\ (kPa) = 4E+09\ (n/C_{iv}^{0.21})^{-4.296} \quad (6.2)$$

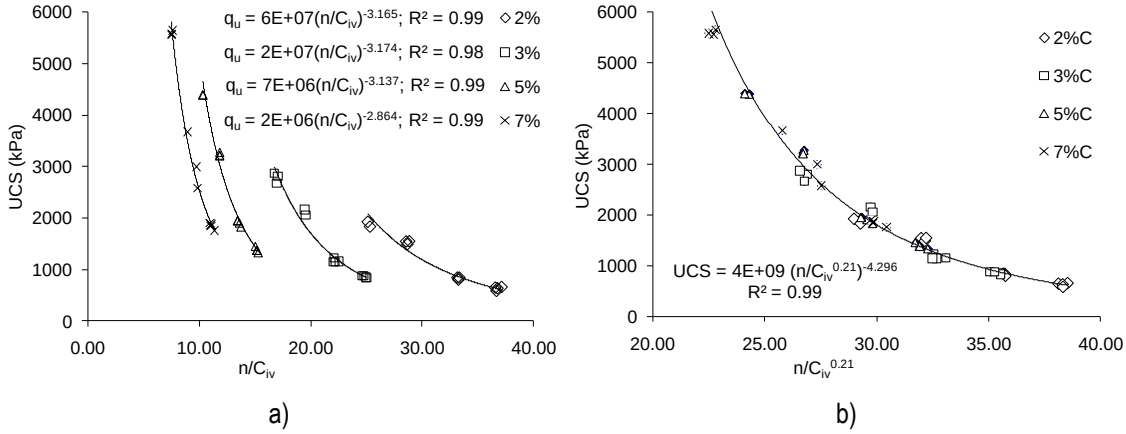

Figure 6.16 Relationship between the unconfined compression strength and the index proposed by Consoli et al. (2007)

This exponent is defined as the value that allows the best correlation coefficient in the data, which, for this material, was found to be 0.21. Apparently this exponent seems to depend on the type of soil as other authors have found different coefficients when working with different soils (Consoli et al., 2007, 2009): an exponent of 0.28 was found in a residual soil from sandstone (Botucatu soil), while a value of 1.0 was found in an uniform sand (Osorio sand). More results will be necessary with different types of soils, but it seems that the wider the grain size distribution curve the lower is the value of the exponent. From now on this ratio will be used extensively in this work to analyse and compare different data and it will be referred as adjusted porosity/cement ratio ($n/C_{iv}^{0.21}$).

Horizontal Line results

The horizontal line results follow: in Figure 6.17a) the plot of UCS against moulding water content is presented to each cement content and in Figure 6.17b) there is the plot of UCS

against the cement content to each water content. It should be pointed out that the fitted curves of Figure 6.17a) are not really trendlines with specific equation. There are just splines linking the average value obtained for each condition to give an idea of the variation of the strength with the water content. As expressed before, some fines were taken out of the soil when the cement was introduced meaning that the influence of the water content is not related to the presence of fines, at least significantly, since a small influence may be admitted due to the different nature of the soil fines and the cement fines.

Figure 6.17 shows that for all cement contents, the 6% water content specimens are the weakest and the 14% water content specimens are the strongest. Also, there is no significant difference in strength between 9 and 12% of water content, except for 7% of cement content.

Comparing the optimum water content (12%) and the water content that achieved higher strengths (14%), it is clear that different values were obtained due to the lower density of the horizontal line. If we look at the Normal Proctor curve (with lower energy) of the uncemented soil the optimum water content is much higher around 18%, and it is well known that the optimum water content decreases when the compaction degree increases.

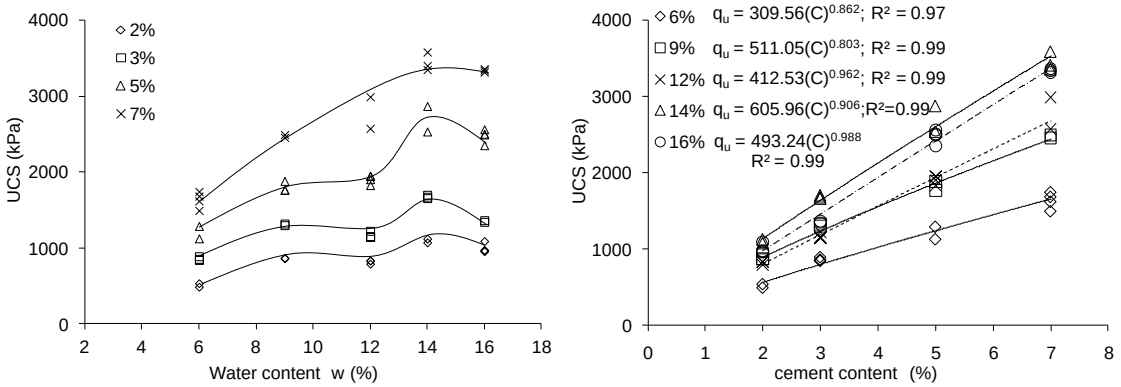

Figure 6.17 Relationship between water content and unconfined compression strength for each cement content (a); Relationship between cement content and unconfined compression strength for each water content (b)

Finally, in Figure 6.18 the horizontal line results are plotted in terms of the UCS against the adjusted porosity/cement ratio where a greater dispersion is observed in relation to the vertical line results. In the same way as Figure 6.16, in Figure 6.18 the different cement contents are distinguished for a better analysis putting in evidence that specimens with the same cement contents and different water contents have different strength values but similar $n/C_{iv}^{0.21}$.

The French GTS (2000) considers that the absorption of water by the cement is around 0.3 to 0.5% of water content per percentage of cement, which means that the higher the cement content the higher the amount of water absorbed by cement. Therefore, the quantity of water introduced in the mixtures seemed to be more than enough to hydrate the cement even with 6% of water content and 7% of cement content. However, there is still a great difference between specimens with equal cement content but moulded with different water contents, which may be explained considering the higher amount of fines of this soil (30%). Perhaps, the fines are taking a significant part of the water that should be hydrating the cement and therefore, lower water content means a reduced number of bonds between particles, and thus, lower strength.

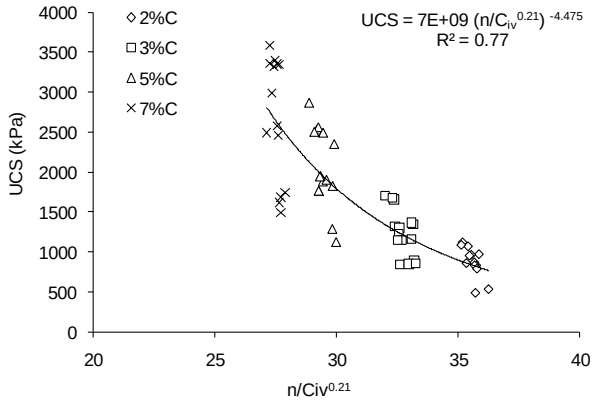

Figure 6.18 Plot of the unconfined compression strength against the index ratio $n/C_{iv}^{0.21}$ for the horizontal line results

6.5.3 Stiffness Results

The unconfined compression tests were performed with local measurement of deformation using LDT's and so the stiffness modulus could be evaluated. An initial tangent modulus (E_{ti}) was then calculated based on the linear part of the stress-strain curve as illustrated in the example of Figure 6.19a). Plotting this modulus against the ratio defined above for the vertical line results, as Figure 6.19b) shows, it can be concluded that the general adjustment of the data is quite reasonable. As expected, stiffness parameters are more scattered than strength parameters because strain measurements are always more sensitive to non-homogeneities of the specimen and anchors are introduced in the specimen in single reference points. On the contrary, strength measurements capture more easily an average value of the whole specimen. Figure 6.19c) shows the same modulus against the adjusted void cement ratio for the horizontal line results showing the same scatter observed in strength in Figure 6.18, probably due to the same explanation.

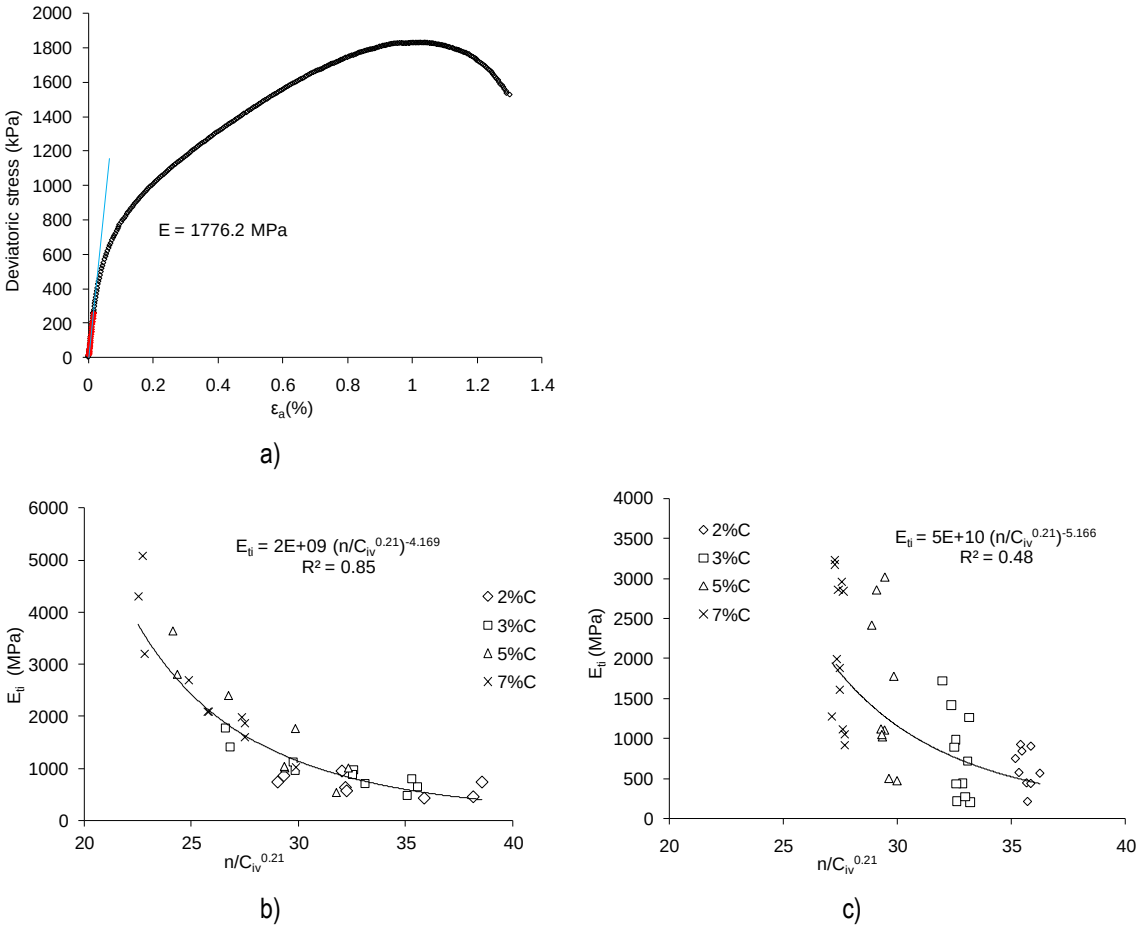

Figure 6.19: a) E_{ti} on a stress-strain curve (5% cement content and 17.2 kN/m^3); b) Initial tangent modulus (E_{ti}) from unconfined compression tests performed on the vertical line; c) Initial tangent modulus (E_{ti}) from unconfined compression tests performed on the horizontal line

6.6 Suction measurements

6.6.1 Filter paper method

The filter paper method is a simple and cheap way to estimate the soil suction (Marinho, 1994). It assumes that when a wet soil is placed in contact with a drier filter paper inside a sealed container, the paper absorbs water from the soil until both materials reach equilibrium of suction. Following Marinho and Oliveira (2006), the migration of water can occur in two ways: i) by capillary flow, when filter paper and soil are in contact, which allows the evaluation of matric suction; ii) by vapour flow, when not in contact, where total suction (osmotic and matric suction) is instead measured. The equilibrium is characterised by equal suction in both filter paper and soil, although their water contents may be different. The calibration curve of the filter paper (that is the soil water retention curve for this material) relates suction with filter paper water content and therefore, the suction of the soil can be estimated by this means. According to Sibley and Williams (1990) who analysed five

different absorbing materials, the Whatman No.42 is the most adequate filter paper for the measurement of suctions between 0 and 200 kPa. Considering the low range of suctions measured in this work the Whatman No.42 was the selected filter paper for which the calibration curves from Chandler et al. (1992) were used:

If the filter paper water content is higher than 47% (w > 47%):

$$\text{Suction (kPa)} = 10^{(6.05-2.48 \log w)} \quad (6.3)$$

If the filter paper water content is lower than 47% (w < 47%):

$$\text{Suction (kPa)} = 10^{(4.84-0.0622 w)} \quad (6.4)$$

In spite of being a simple method, some testing details need careful attention in order to obtain reliable data. Feurharmel et al. (2006) summarise as follows the most important issues in the matric suction evaluation:

- contact between filter paper and soil;
- the time allowed for reaching equilibrium of suction;
- the hysteresis between drying and wetting paths;
- the measurement of filter paper water content;
- the number of papers used;
- the temperature fluctuation.

6.6.2 Procedures and specimens tested

The filter paper method was used in the unconfined compression tested specimens to evaluate the matric suction and hence the effectiveness of the 24h in water procedure for specimens saturation. The filter paper was used air-dry directly from the box (and not oven dried as it is suggested in the standard - ASTM, 1998b), following Marinho and Oliveira (2006) who advocate that the standard procedure may affect the absorption characteristics of the paper requiring appropriate calibration. The suction measurement was made in a piece of the specimen tested in unconfined compression test with approximately 2.5 cm high and 70 mm of diameter taken from the middle part. A piece of Whatman No.42 filter paper is placed over and below the soil and wrapped with cling film so as to assure a good contact between soil and filter paper. Each piece of filter paper was carefully handled with a tweezer to avoid changing its original characteristics (Figure 6.20a). The wrapped specimens were then inserted in a plastic bag and finally sealed with sticky tape. During the equilibrium time the specimens remained in a Styrofoam box to avoid the effect of temperature fluctuations (Figure 6.20b). Although the minimum time suggested by the

ASTM (1998b) is seven days regardless the type and magnitude of suction being measured, Feuerharmel et al. (2006) considered that four days is an adequate equilibrium time for matric suctions below 10000 kPa, being seven days the required time for higher suction values. Based on this information seven days were conservatively considered for the equilibrium time. After the equilibrium time the paper filter was carefully removed and the water content was measured in a high precision balance (accuracy of 0.001 g). This procedure was done as fast as possible to avoid loss of humidity in the filter paper. To weight the filter paper pieces, special glass recipients were used, which were very thin and light to improve the measurement accuracy (Figure 6.21). From the remaining part of the specimen tested in unconfined compression test a representative portion was used to evaluate the water content from which the saturation degree (S) was obtained.

a) b)

Figure 6.20 Procedure for the filter paper method: a) specimens, paper filter and tweezer before the test); b) specimen during equilibrium time (wrapped specimens placed in a styrofoam box)

a) b)

Figure 6.21 Procedure to evaluate the filter paper water content after the equilibrium time: a) Removal of the filter paper; b) weight of the filter paper in a high precision balance

6.6.3 Filter paper method results

The results obtained in these tests are summarized in Table 6.3 in terms of the limit and average values. The filter paper results have indicated an average suction of 19 kPa with a maximum value of 65 kPa corresponding to filter paper water contents in the range of 50 to 220%. The water contents of the remaining soil were between 10 and 20% which indicated saturation degrees of around 80%. It should be pointed out that these results were taken after the unconfined compression tests which mean that at the moment of the test the specimen could be slightly more saturated and thus with lower suction values.

Table 6.3 Filter paper method results

	Soil		Filter paper		Suction/UCS
	water content	saturation degree	water content	suction	
	%	%	%	kPa	%
Range	[11.54; 19.16]	[63.31; 90.77]	[51.13; 216.74]	[1.81; 64.92]	[0.16; 3.58]
Average	16.01	78.49	95.40	18.80	1.19

From this data, it can be concluded that the levels of suction obtained by this method are insignificant in terms of the unconfined compression strengths (UCS∈ [550-6000 kPa]) of these materials representing around 1% of the UCS, and therefore, the unconfined compression strength is almost exclusively due to soil strength and not due to suction. This is even clearer when dealing with cemented soils, where the confining pressures has such a low influence in the mechanical behaviour of these specimens.

6.7 Bender elements and compression transducers

6.7.1 Procedures

A great number of seismic wave velocity measurements were performed in soil-cement specimens using Bender Elements (BE) and Compression Transducers (CT) from ISMES described in the previous chapter. The aim of these tests was to define a relationship between the maximum shear modulus (G_0) and the adjusted porosity/cement ratio ($n/C_{iv}^{0.21}$) as it has been done in unconfined compression strength in the previous section.

The tests were executed over specimens especially moulded for that purpose in the four moulding points of the vertical line of Figure 6.12 in the same conditions of the specimens prepared for unconfined compression tests described in the previous section, comprising 16 tests. After 24h in water the specimens were superficially cleaned with an absorbent cloth and tested immediately. The only difference to the unconfined compression tests specimens is the size of the specimens, as these were 70 mm of diameter and 70 mm high.

A small hole approximately with the bender size and shape was made in the specimens before curing and to improve coupling between the piezoelectric transducers and the specimen, a small quantity of gypsum was used. To avoid Bender Elements damaging, a special care was considered by using a small quantity of vaseline placed on the BE before gypsum introduction to facilitate their removal after the test when the gypsum is dry and stiff.

The BE calibration was performed with the transducers in contact to evaluate which was the polarity of the received wave: normal polarity means that the received wave has the same shape as the transmitted wave; inverted polarity means that the shape of the received wave is symmetric (on the xx axes) to the transmitted wave. This is very important for shear (S) wave interpretation because the user must know if the received wave will start with increasing amplitude (normal polarity) or decreasing amplitude (inverted polarity). In this case, inverted polarity was obtained.

The S waves BE measurements were analysed in terms of Time and Frequency domain (TD, and FD, respectively). For TD the travel time is obtained by the difference between arrivals of the transmitted wave and the received wave. For S wave measurements, frequencies were used in the range of 1 and 15 kHz, while for compressional (P) wave measurements, frequencies between 25 and 100 kHz were applied. For FD an application created and embedded onto a Microsoft Excel spreadsheet ABETS (Automatic Bender Element Testing System) available in the Laboratory of Geotechnics at FEUP was used. The solution for wave measurement and acquisition in frequency domain was inspired in the original work of Greening et al. (2003) and Greening and Nash (2004) and consists in an algorithm, based on Fast Fourier Transforms (FFT). A continuous sine-sweep input wave is preset at the function generator and the acquisition is carried out via the spectrum analyzer-oscilloscope using ABETS which computes the travel time, wave velocity and shear modulus. Initially a sweep sine input signal with 0.1-20 kHz bandwidth was used but later a broader range was used (0.1-50 kHz) due to the high stiffness of cemented materials. Narrower frequency ranges should be selected for computing travel time, mainly based on the results of the coherence function. Further details about this application can be found in Ferreira (2008) and Viana da Fonseca et al. (2009).

The P waves obtained through CT measurements were analysed in time domain only. The signal obtained by this mean is very sharp and clear, as illustrated in the example of Figure 6.22, allowing a reliable interpretation.

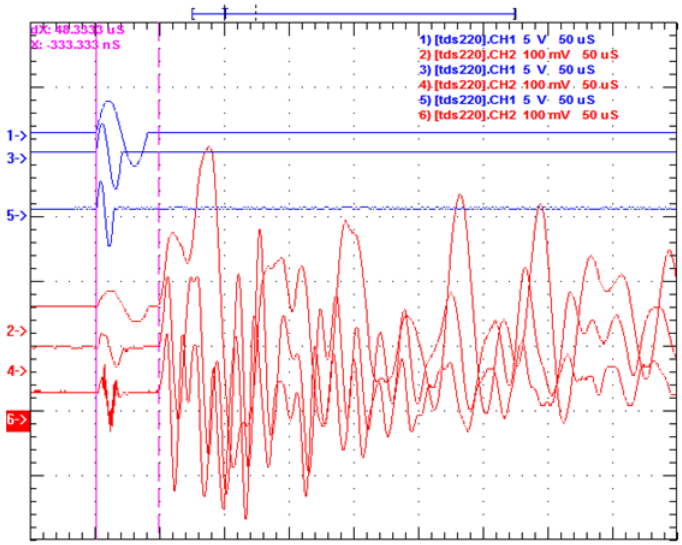

Figure 6.22 P waves obtained by compression transducers with time domain interpretation (frequencies of 25, 50 and 75 kHz) for the specimen with 7% cement content and 16.4kN/m³ of dry unit weight: t_P = 48.3 us; v_P = 1511 m/s

6.7.2 Maximum shear modulus results

Three methods

Three different values of the maximum shear modulus were used whose results are expressed Figure 6.23:

G_0^{TD} - the maximum shear modulus obtained by equation (6.5) from results of S wave velocities (V_S) obtained in the TD method;

G_0^{FD} - the maximum shear modulus obtained by equation (6.5) from results of S wave velocities (V_S) obtained in the FD method;

G_0^{VP} - the maximum shear modulus obtained by equations (6.6), (6.7) and (6.8) from results of P wave velocities (V_P) assuming a Poisson ratio of 0.37 for the reasons explained below.

$$G = \rho V_s^2 \quad (6.5)$$

$$M = \rho V_P^2 \quad (6.6)$$

$$E = \frac{(1+\upsilon)(1-2\upsilon)M}{(1-\upsilon)} \quad (6.7)$$

$$G = \frac{E}{2(1+\upsilon)} \tag{6.8}$$

The Poisson ratio of 0.37 is the average value obtained by the TD method using S and P waves velocities (V_S and V_P) through the following expression:

$$\upsilon = \frac{\left(\frac{V_P}{V_S}\right)^2 - 2}{2\left(\frac{V_P}{V_S}\right)^2 - 2} \tag{6.9}$$

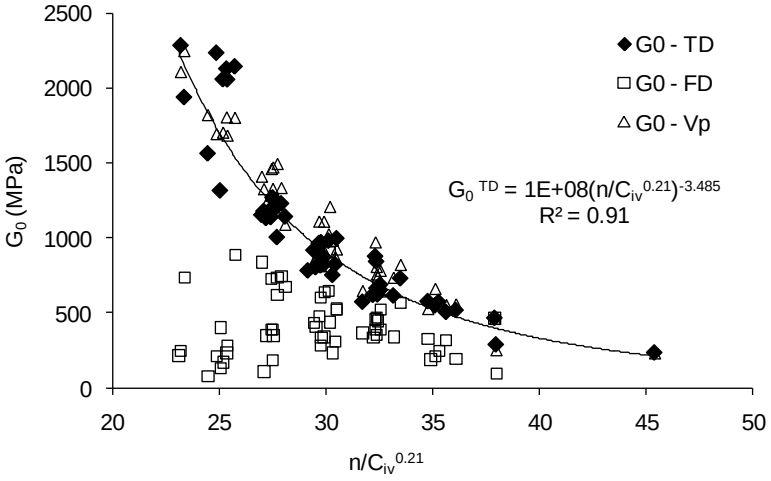

Figure 6.23 Maximum shear modulus (G_0) obtained by time and frequency domain S wave velocities (G_0^{TD} and G_0^{FD} respectively) and from P wave velocities (G_0^{VP})

Figure 6.24 shows for clarity, the maximum shear modulus obtained in time domain from S and P wave velocities showing that the trends are quite similar giving consistency to the interpretation analysis.

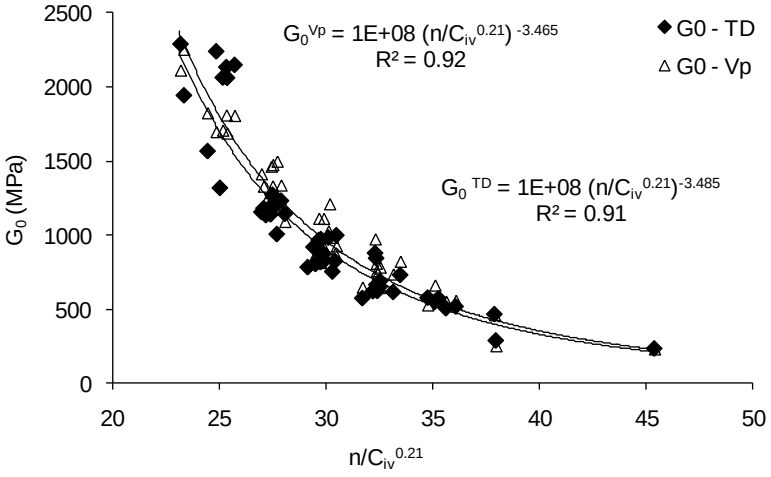

Figure 6.24 Maximum shear modulus (G_0) obtained by time domain from S wave velocities (G_0^{TD}) and from P wave velocities (G_0^{VP})

S wave interpretation

It is clear from Figure 6.23 that the frequency domain results do not show any consistent trend, which may indicate that, even with a broader range of frequencies, this method cannot be applied to these materials in the same way that has been successfully used in other cases (Ferreira, 2008).

Bender elements are designed to generate S waves but it is impossible to avoid some P wave generation at the same time. These very stiff materials involve high S wave velocities, which become closer to P wave velocities preventing a good separation between both waves. This problem may be in the origin of the frequency domain problems and it has also been detected in time domain measurements bringing some difficulties in their interpretation. The analysis of a single S wave time domain arrival was therefore extremely difficult. Consequently, the values of G_0^{TD} presented in Figure 6.23 were obtained in an attempt to perform a consistent and global analysis of the full range of data that has resulted in the publication of Carvalho et al. (2011). In Figure 6.25 the time domain results obtained for S waves are presented for one case with 7% cement content, so as to express the criteria used in the interpretation analysis.

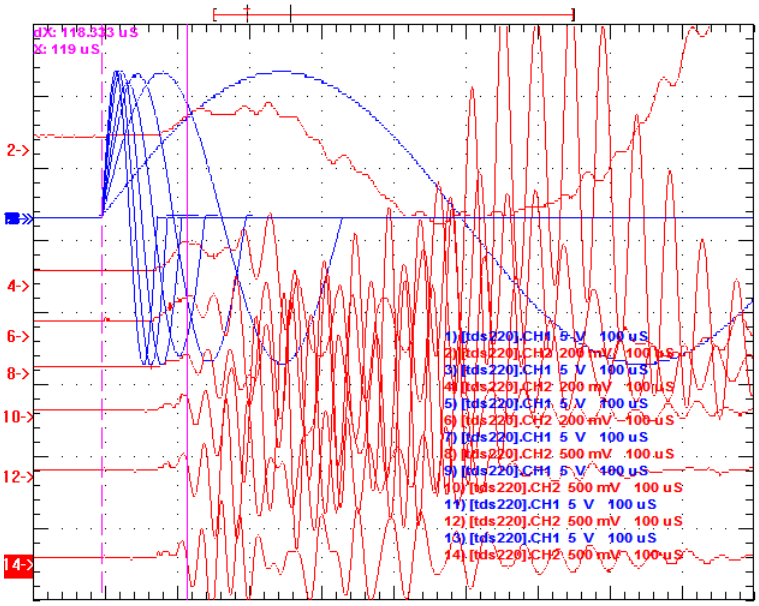

Figure 6.25 BE "S" waves time domain interpretation for the specimen with 7% cement and 16.4 kN/m^3 of dry unit weight: t_S= 118.3 us; V_S = 581 m/s (preset frequencies: 1, 3, 5, 7, 9, 11, 13 kHz; outputs in reversed polarity)

In Figure 6.26 the graphs of the maximum Young modulus (E_0) obtained from shear wave velocities in time domain and the initial tangent modulus (E_{ti}) determined in unconfined

compression tests (UCT) are plotted together, where it is evident that the first is higher than the second due to the different level of strain involved in both types of tests.

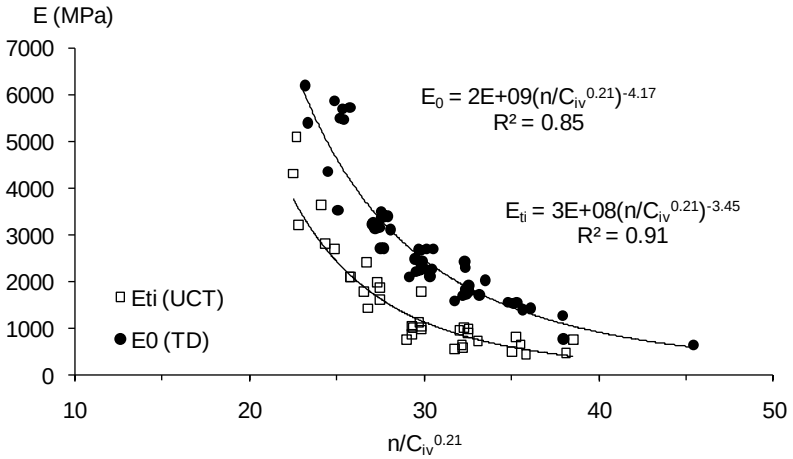

Figure 6.26 Comparison between maximum Young modulus (E_0) obtained from shear wave velocities in time domain and initial tangent modulus (E_{ti}) determined in unconfined compression tests (UCT)

P wave interpretation

In contrast, P wave arrival times derived from compression transducers allow a separate analysis of this type of wave as no S wave is generated at the same time. Consequently, a clear and marked response is obtained and thus a confident P wave velocity was achieved. Assuming that P wave velocities are correctly determined, the maximum shear modulus computed by this mean is only affected by the Poisson ratio. The effect of the Poisson ratio on the maximum shear modulus is expressed in Figure 6.27 where two additional Poisson ratios were considered (ν = 0.25 and 0.30) as well as the value of 0.37 reported before. It seems that the Poisson ratio generates an increase or decrease of the absolute values but the trend in not significantly changed.

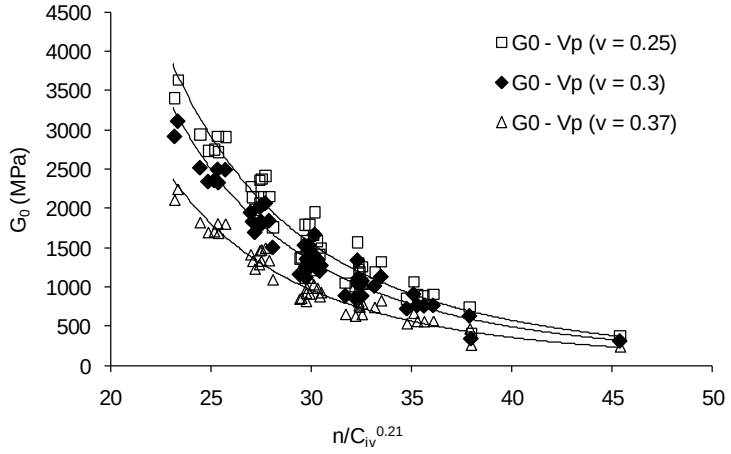

Figure 6.27 Comparison between the maximum shear modulus obtained through P wave velocities assuming different Poisson ratios (ν = 0.25, 0.30 and 0.37)

Consequently, it can be concluded that the trend found in Figure 6.23 for the maximum shear modulus determined by the time domain procedure (G_0^{TD}), and very similar to the trend obtained by the P wave velocities, is in agreement to the trend obtained for the unconfined compression strength in Figure 6.16b). This is quite important as it validates the adjusted porosity/cement ratio as an important index to evaluate both stiffness and strength.

Comparison to other works

In spite of the very broad range of obtained values of the maximum shear modulus [100-2200 MPa] due to the several mixtures studied and, the large number of parameters involved (type and cement content, curing conditions, void ratios, type of soil among the parameters reported in chapter 3) an attempt was made to identify reference works from the literature, where BE were used to evaluate maximum shear modulus in cemented materials, in order to allow a comparison with the results herein presented. From the literature data, tests in soils artificially cemented with Portland cement were selected and are summarized in Table 6.4. Although most of the works involve clean sands that are not directly comparable with a very well graded soil with around 30% of fines, as the soil used in this study, the values of the maximum shear modulus from the literature are in the range of those presented above.

Table 6.4 Maximum shear modulus of some artificially cemented sands

Reference	Type of soil	G_0 (MPa)
Baig et al. (1997)	Ottawa sand	300-2000
Ismail et al. (2004)	carbonate sand	700
Kuwano and Boon (2007)	sand	up to 800
Consoli et al. (2009)	Osorio sand	500-2000

6.8 Ultrasonic tests

6.8.1 Introduction

The initial aim of these tests was to evaluate the bonding degradation due to cyclic triaxial testing (as it will be expressed in chapter 8) by performing these non destructive tests before and after cycling. Unfortunately, this goal was not achieved as the increase in stiffness due to the cement hydration (in saturated conditions) during all process of preparation and different phases of the static triaxial tests, appears to be more significant than the cyclic degradation. However, it is still interesting to analyse the results as they can provide an idea of the compression wave velocities that these materials can achieve.

6.8.2 Calibration

The system was calibrated by Amaral (2009) measuring the travel time in 5 steel specimens with different sizes. The 5 specimens were all cut from a unique specimen piece so they are all from the same material (Figure 6.28). The procedure used for the calibration (zero-time adjustment) is the following: a coupling agent (high vacuum grease) is applied to the end of the reference bar, and the transducers are firmly pressed against the ends of the bar until a stable travel time is reached. The different lengths of the specimens were measured and the corresponding travel times obtained after the generation of a 50 kHz sinusoidal wave were registered. From the results that are plotted in Figure 6.29, a 1.36 μs time delay was found, which was used afterwards to correct the direct measured values.

a) b)

Figure 6.28 Steel specimens: a) different sizes; b) calibration setup (Amaral, 2009)

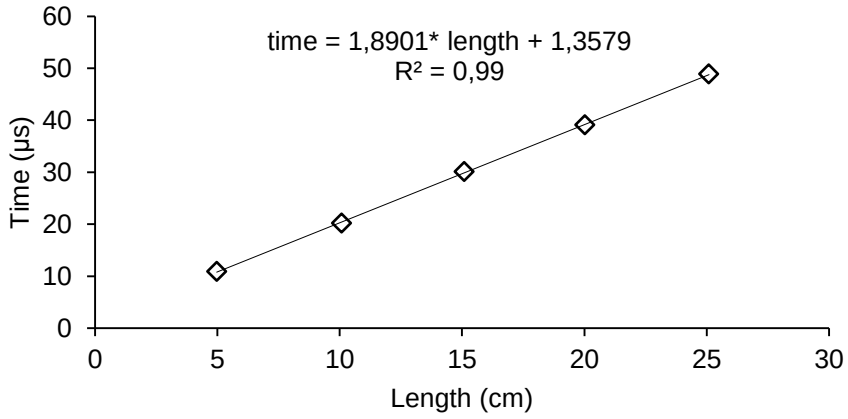

Figure 6.29 Linear regression of the time versus length in order to obtained the desired delay (Amaral, 2009)

6.8.3 Procedure

The typical outputs of this test are plotted in Figure 6.30 respectively for square wave (Figure 6.30a) and sine waves (Figure 6.30b). For sinusoidal waves, frequencies of 25, 50

and 75 kHz were used, while for the square wave a single frequency of 50 kHz was used as suggested by Amaral (2009). Very close results of the travel time were obtained with both types of waves being the square wave results slightly smaller than the sinusoidal wave results. The travel time is measured by the difference of arrivals between transmitted and received waves.

It should be noted that specimens to be used in triaxial tests cannot be tested with grease (as reported in chapter 5) during ultrasonic tests, since grease could fill the voids of the specimen faces and this should have a negative influence on the drainage conditions through the faces of the specimen during the cyclic triaxial test, performed afterwards. In these conditions, some manual pressure had to be applied during the test to improve coupling between specimen and transducer and to enable a good output response.

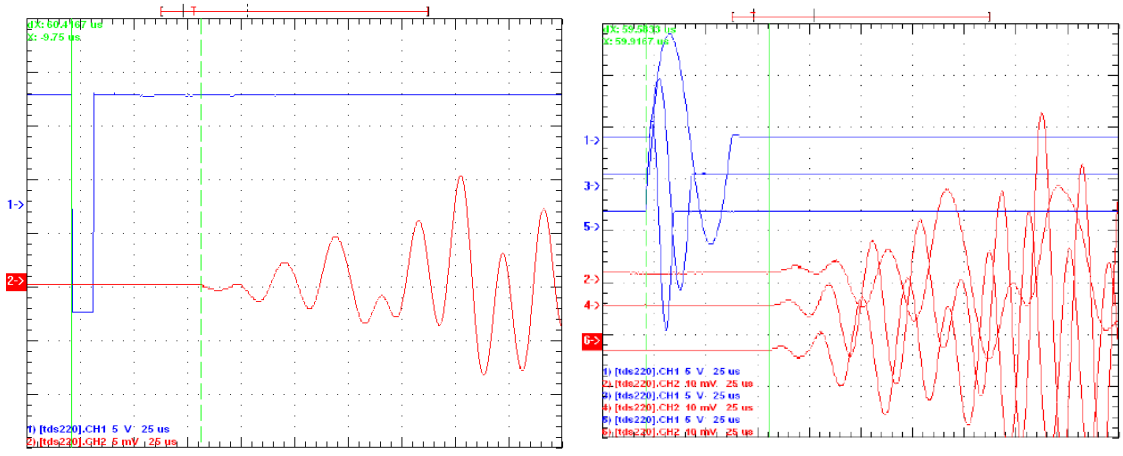

a) b)

Figure 6.30 Outputs of an ultrasonic wave measurement: a) emitted square wave (blue line); received signal (red line) b) emitted sine waves (blue lines); received signal (red lines).

6.8.4 Results

Khan et al. (2006) have proved that compression waves propagate at different velocities in an infinite medium when compared with the same material with the geometry of a rod. When the wave-length (λ) is equal to or greater than the diameter (D) of the rod (λ≥D), the velocity of the compression wave can be called the longitudinal wave velocity (V_L) and is given as a function of the Young Modulus (E) and the mass density of the rod (ρ),

$$E = \rho V_L^2 \tag{6.10}$$

It is assumed that at the moment of the wave arrival all the specimen is already excited due to the small diameter compared to the wave length. In opposition, in a infinite medium the lateral deformation of the specimen is constrained and so the velocity of the compression

wave (now called V_P as usual) depends on the Constrained Modulus (M) - equation (6.6). For this reason, the ASTM standard where this method is described for concrete (ASTM, 2002), suggests that the least dimension of the specimen should be higher than the wavelength, to assure that P waves are being transmitted through the specimen.

In this study all the specimens had 70 mm of diameter, which means that for the range of velocities obtained [500-2500 m/s] and for a frequency of 50 kHz, it can be assumed that an infinite medium is established and therefore the derived velocities depend on the constrained modulus instead of the Young modulus. Unfortunately, only one test allows a direct comparison between these results and the values presented before in section 6.7 since the test conditions are different. However, for this single test, marked in bold in Table 6.5, the results are in perfect agreement with the previous P wave velocities measurements.

Table 6.5 Moulding and testing conditions of the specimens and obtained compression wave velocities

Moulding conditions				Test conditions			Results
C	γ_d	w	$n/C_{iv}^{0,21}$	Saturation conditions	Curing days	Excitation wave	V_P
%	kN/m^3	%					(m/s)
Samples in their moulding state							
5	17	12	29.9	w = 12%	7	square	1450
5	17	12	29.9	w = 12%	7	sinusoidal	1413
7	16.4	12	30.2	w = 12%	0	square	532
7	16.4	12	30.2	w = 12%	0	sinusoidal	545
7	16.4	12	30.2	w = 12%	6	square	1160
7	16.4	12	30.2	w = 12%	6	sinusoidal	1160
7	16.4	12	29.8	w = 12%	1	square	1014
7	16.4	12	29.8	w = 12%	6	square	1435
7	16.4	12	29.8	w = 12%	6	sinusoidal	1398
7	16.4	12	30.0	w = 12%	6	square	1436
7	16.4	12	30.0	w = 12%	6	sinusoidal	1399
7	16.4	12	29.8	w = 12%	1	square	1016
7	16.4	12	29.8	w = 12%	1	sinusoidal	962
7	16.4	12	29.8	w = 12%	7	square	1437
7	16.4	12	29.8	w = 12%	7	sinusoidal	1400
7	16.4	12	30.0	w = 12%	6	square	1342
7	16.4	12	30.0	w = 12%	6	sinusoidal	1320
7	18	12	25.7	w = 12%	6	square	1604
7	18	12	25.7	w = 12%	6	sinusoidal	1620
Saturated samples after cyclic triaxial testing							
5	17	12	29.8	saturated	21	square	2121
5	17	12	29.8	saturated	21	sinusoidal	2108
7	**16.4**	**12**	**30.0**	**saturated**	**7**	**square**	**1442**
7	**16.4**	**12**	**30.0**	**saturated**	**7**	**sinusoidal**	**1442**
7	16.4	12	30.0	saturated	12	square	1842
7	16.4	12	30.0	saturated	12	sinusoidal	1762
7	16.4	12	29.8	saturated	13	square	1905
7	16.4	12	29.8	saturated	13	sinusoidal	1636
7	18	12	25.7	saturated	17	square	2316
7	18	12	25.7	saturated	17	sinusoidal	2350

As explained before, the initial idea of these tests was to have compression wave measurements before and after the cyclic triaxial tests. For this reason, Table 6.5 shows specimens in their moulding state within 7 days of curing time, together with specimens with much higher curing periods (between 12 and 21 days), saturated, after being subjected to a cyclic loading. An attempt was made to correct the stiffness values for different curing times assuming that the law of the normalised gain in strength ($q_u(t)/q_u(7\ days)$) would be the same in stiffness and in strength (this last presented in section 6.3.2). However, this was not considered reasonable as the stiffness values presented in Table 6.5 for 13 or 21 days are much higher than the values predicted by the normalised strength.

In spite of the heterogeneous conditions represented in Table 6.5 it is clear that the difference between square and sinusoidal wave velocities was not important (around 30 m/s).

For the reasons presented above this technique seems quite promising if the specimens curing time is much greater than the cyclic period.

6.9 Resonant column tests

6.9.1 Aims and procedures

Some specimens, moulded in FEUP in the same conditions as the others, were taken to the Technical University of Lisbon (IST) to perform some resonant column tests. These tests were performed under the supervision and technical assistance of Javier Camacho-Tauta who was responsible for the development of IST equipment under his PhD program.

Two types of tests were performed: the conventional resonant column test (called herein as RCCT) and, another test developed by Camacho-Tauta (2010) which is the analysis of the resonant column for a noise signal called Resonant Column Random Noise (RCRN). The difference between both methods is that the last involves the generation of a random signal instead of a sinusoidal excitation as in the conventional test (ASTM, 2000). Moreover, the random signal provides lower distortions than the sinusoidal excitation making the tests complementary to each other.

It is not certain that resonant column tests provide good results on these soil-cement specimens due to their high stiffness. The conventional interpretation of the resonant column assumes a linear variation of the distortion through the length of the specimen: zero distortion on the base (fixed base) and maximum distortion on the top (active end). If the

specimen is so stiff that the bottom base cannot be completely fixed, a partial excitation of the specimen can be established (Khan et al., 2006). Lovelady and Picornell (1990) have reported that improper fixing conditions produce the underestimation of wave velocity in resonant column tests due to the flexibility of the interfaces. The test showed two modes of vibration around 150 and 450 Hz. Considering that the first mode corresponds to a quite low distortion modulus for these materials; this mode may be due to that partial excitation. However, the results for the second mode seem to be very interesting and therefore they will be presented herein.

Two different specimens were tested in the resonant column by the two reported methods and then bender elements measurements were performed in the same test stages. These measurements were performed without any confinement (σ'_c=0 kPa), and with three different confining pressures (30, 50 and 80 kPa). Table 6.6 presents the moulding conditions of the tested specimens. Another stiffer specimen was also tested unsuccessfully due to the high stiffness since the equipment had not enough energy to provide a good excitation. Therefore, only the results of these two specimens will be presented in the following graphs (Figure 6.31). The preparation of the specimens was done as described in section 6.3 and the specimens were tested at 7 days of curing period after 24h in water just like the others.

Table 6.6 Moulding conditions of the specimens tested in the resonant column

Sample name	C %	γ_d kN/m^3	e_0	w %	$n/C_{iv}^{0,21}$
RC(3)	3	17.8	0.51	12	30.4
RC(7)	7	16.4	0.65	12	30.4

6.9.2 Results

The comparison of shear wave velocities measured by the Bender Elements in both laboratories, IST and FEUP, presented in Table 6.7, is related to BE measurements executed without confinement in IST and FEUP, this latter as presented in section 6.7.

Table 6.7 Shear wave velocities from BE measurements at IST and FEUP in specimens without confinement

Sample name	S wave velocities (m/s) IST	FEUP
RC(3)	582	649
RC(7)	557	633

The BE data from IST obtained in the three confining pressures is plotted in Figure 6.31 together with resonant column results assuming a distortion value of $5*10^{-5}$ for bender elements measurements (Dyvik and Madshus, 1985).

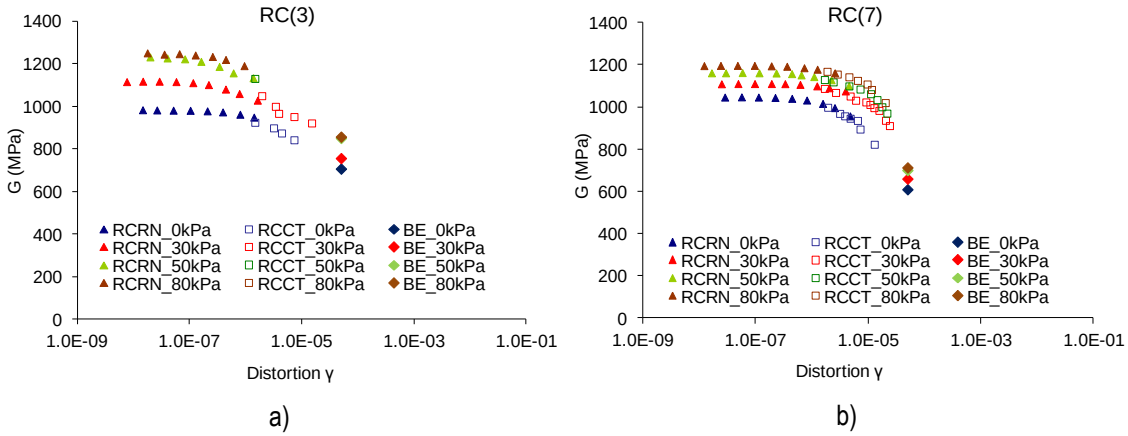

Figure 6.31 Resonant column conventional test (RCCT), resonant column random noise (RCRN) and bender elements (BE) results: a) RC(3) specimen; b) RC(7) specimen

From these results some interesting points can be observed:

- there is a small increase in stiffness with confining pressure in both specimens, but the difference is more marked in the less cemented specimen (RC(3)). This is reported by many authors, with the effect of confining pressure being less evident on the stiffness modulus when higher cement contents are used. This characteristic was briefly expressed in chapter 4 (Figure 4.30 and 4.31 from Fernandez and Santamarina, 2001 and Baig et al., 1997, respectively);
- the elastic plateau seems to be short and, apparently, there is a fragile loss at distortions around 10^{-6} for RC(3) and slightly after (around $5*10^{-6}$) for RC(7). In fact, it is expected that with increasing cement content the specimens would have an extended elastic plateau;
- assuming a distortion value of $5*10^{-5}$ for BE measurements they seem to be fairly convergent to the RC results, and all the three methods seem to be complementary showing a good agreement between them. RC(7) shows higher non-linearity in the degradation curve of the maximum shear modulus than RC(3) that may explain the higher distance between the BE and the RC measurements in RC(7);
- the shear wave velocities measured in FEUP showed slightly higher values than the same results obtained in IST;
- two specimens are not enough to take appropriate conclusions about the performed tests, especially in terms of bender elements results. Moreover, the resonant column procedure is not considered very appropriate to tests very stiff materials like cemented mixtures. In some cases, it was not possible at all to take results. However, the random noise procedure, using lower distortion values, may be less sensible to improper fixing conditions and thus, more useful to test very stiff

materials. Therefore, the data presented herein is considered a good indication as a starting point to some other investigation on the elastic stiffness of these materials.

6.10 Indirect tensile tests

6.10.1 Indirect tensile tests results and comparison with unconfined compressive strength

The same specimens tested with piezoelectric transducers, as described in section 6.7, were then subjected to indirect tensile tests following the standard EN 13286-42 (CEN, 2003a). A relationship similar to equation (6.2) obtained for the unconfined compression strength was defined for the indirect tensile strength,

$$R_{tb}\ (kPa) = 2E+09\ (n/C_{iv}^{0.21})^{-4.719} \quad (6.11)$$

The results showed that the indirect tensile strength was about 11% of the unconfined compression strength. In Figure 6.32 both indirect tensile strength (R_{tb}) and unconfined compression strength (UCS) are plotted against the adjusted porosity/cement ratio ($n/C_{iv}^{0.21}$) in different scales for comparison. It is clear that both trends are very similar (except for the absolute values) corroborating the convenience of the adjusted porosity/cement ratio.

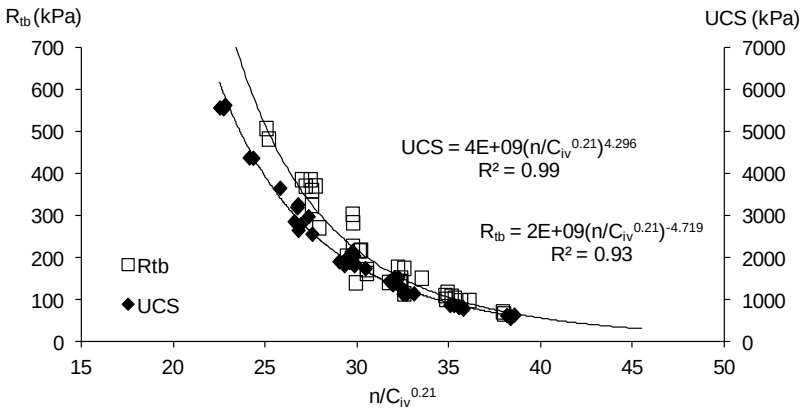

Figure 6.32 Indirect tensile strength (R_{tb}) and unconfined compression strength (UCS) with the adjusted porosity/cement ratio ($n/C_{iv}^{0.21}$)

In Consoli et al. (2011b), where the data from these tests is plotted together with data from other two soils, it is shown that for the three soils a decrease in porosity promotes an increase in the tensile strength as a consequence of the higher number of contact points between particles which improves the cementation. Also for the other two soils, a unique

correlation was found between the adjusted porosity/cement ratio and the indirect tensile strength, being the exponent of the ratio dependent of the soil.

6.10.2 Classifications based on specifications and standards

Two different specifications were introduced in Chapter 2, the European standard (CEN, 2006) and the French guide (GTS, 2000), which present classification systems for cement treated materials using the tensile strength and the stiffness modulus. As reported in section 2.6.4 these two classifications seem quite similar but in fact they assume different configurations. The same graph presented before (Figure 2.11) comparing the two specifications, is plotted again in Figure 6.33 together with the results presented in this chapter. The data refers to the 16 different specimens tested in indirect tensile tests, seismic wave measurements and unconfined compression tests, being the tensile strength obtained by the indirect tensile test and the stiffness modulus from the unconfined compression tests as explained in section 2.6.4.

It is clear from Figure 6.33 that most of the points are not included in the classification chart. These specimens were tested at 7 days of curing time as an early strength Portland cement was used, instead of the 90 days suggested in the standards. However, the GTS (2000) short term criteria for 7 days were achieved by most specimens.

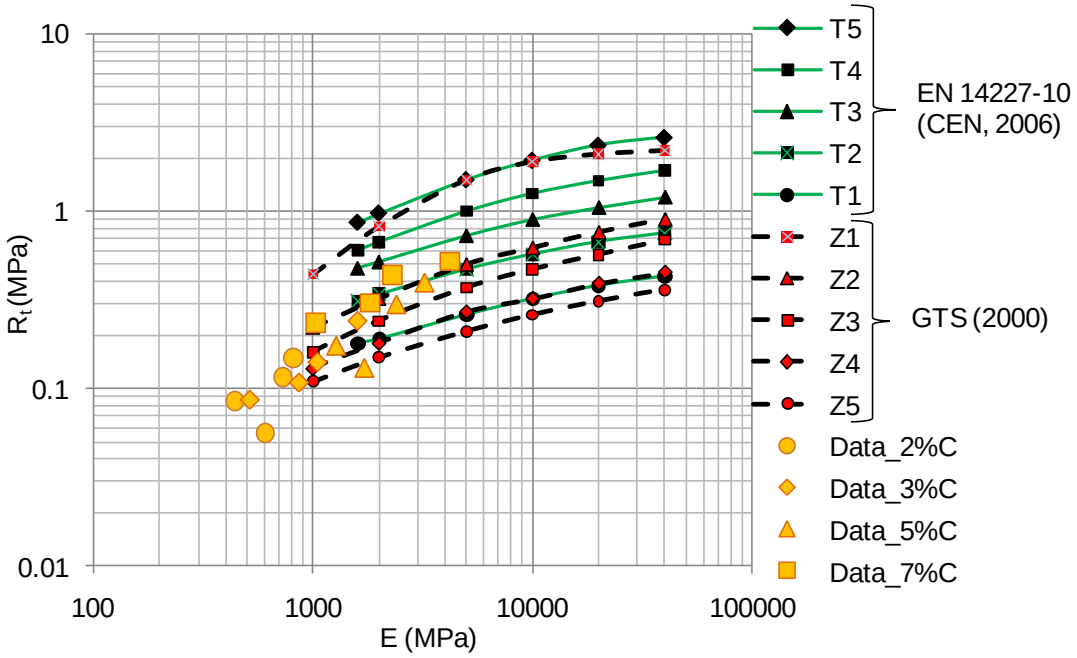

Figure 6.33 Classification of soil-cement mixtures through CEN (2006) and GTS (2000) based on the tensile strength (R_t) and on the stiffness modulus (E).

6.11 Oedometric constant rate deformation tests

6.11.1 Tested specimens

One-dimension compression tests in oedometric cells with constant rate of deformation (CRD) were performed over soil-cement specimens of different mixtures and uncemented specimens in different void ratios. Table 6.8 summarizes the moulding conditions of the specimens expressing for each one the cement content (%C), the dry unit weight (γ_d), the initial void ratio (e_0), the moulding water content (w%), the index ratio ($n/C_{iv}^{0.21}$) and finally, the percentage of the correspondent Modified Proctor optimum dry unit weight (%MP). For the calculation of this last parameter, it was considered the optimum dry unit weights indicated in Table 6.2 for the soil-cement (18.7 kN/m^3) and for the soil (18.6 kN/m^3). The tests name includes the cement content and the moulding dry unit weight.

The preparation of the different mixtures for these tests followed the same procedure of the other tests. Due to the size of the mould the static compaction was performed in one layer, although the soil was placed in several stages followed by tapping. The mould with the compacted mixture inside was placed in a plastic bag and stored in the humid chamber for 7 days. On the test day, the specimen (inside the mould) was placed in water for 1 h in a big container being tested immediately after, keeping the specimen submerged within the oedometer cell full of water.

Table 6.8 Moulding conditions of constant rate deformation tests

Test name	%C	γ_d (kN/m^3)	e_0	w (%)	$(n/C_{iv})^{0.21}$	% MP
CRD_2_16.7	2%	16.7	0.61	12.0	36	89%
CRD_3_15.9	3%	15.9	0.70	12.0	36	85%
CRD_4_15.4	4%	15.4	0.76	12.0	36	83%
CRD_4_16.4	4%	16.4	0.63	12.0	33	88%
CRD_4_17.3	4%	17.3	0.54	12.0	29	93%
CRD_5_17.0	5%	17.0	0.58	12.0	29	91%
CRD_5_14.9	5%	14.9	0.80	12.0	36	80%
CRD_6_16.7	6%	16.7	0.63	12.0	29	90%
CRD_7_16.4	7%	16.4	0.64	12.0	29	88%
CRD_7_17.0	7%	17.0	0.58	12.0	28	91%
CRD_0_15.4	0%	15.4	0.73	12.0	-	83%
CRD_0_16.4	0%	16.4	0.64	12.0	-	88%
CRD_0_9.8	0%	9.8	1.72	18.0	-	53%

Some cemented specimens were moulded to have two different adjusted porosity/cement ratio ($n/C_{iv}^{0.21}$ = 36 and $n/C_{iv}^{0.21}$ = 29), which correspond to UCS of 800 and 2000 kPa according to the equation (6.2). These two ratios were used extensively on the preparation of the specimens for the triaxial tests that will be described in the next chapter. On the other

hand, there are also tests where the cement content was fixed and the void ratio was reduced or increased so that the effect of the void ratio could be understood.

For the calculation of the mean effective stress (p') in each test the value of the coefficient of earth pressure at rest (K_0) was considered equal to 1 due to the high compaction degree that the specimens were subjected during the moulding procedure (>80% of MP). The only exception is the third uncemented test (CRD_0_9.8) executed in different conditions, as the soil was moulded very very loose and then the load was applied very slowly (0.01 mm/min) while the settlement was being read by the system. Thus, the calculation of the mean effective stress (p') assumed in this case a coefficient of earth pressure at rest (K_0) calculated by Jaky's equation ($K_0=1-\sin\phi'_{cv}$) being ϕ'_{cv} = 34º from chapter 7.

The aims of the experimental program of the constant rate deformation tests were the following:

Cemented conditions:

- to analyse the behaviour of the oedometric curve with the same adjusted porosity/cement ratio;
- to observe the behaviour of the oedometric curve with the same cement content but different void ratios;

Uncemented conditions:

- to analyse the behaviour of oedometric curves for the specimens with different void ratios;
- to compare the very loose uncemented test with the isotropic compression tests.

6.11.2 Results

The results presented in Figure 6.34 and Figure 6.35 show that the curves void ratio against p' seem to join together when three groups are considered separately: uncemented specimens; cemented specimens with an index ratio $n/C_{iv}^{0.21}$ = 29 and cemented specimens with an index ratio $n/C_{iv}^{0.21}$ = 36.

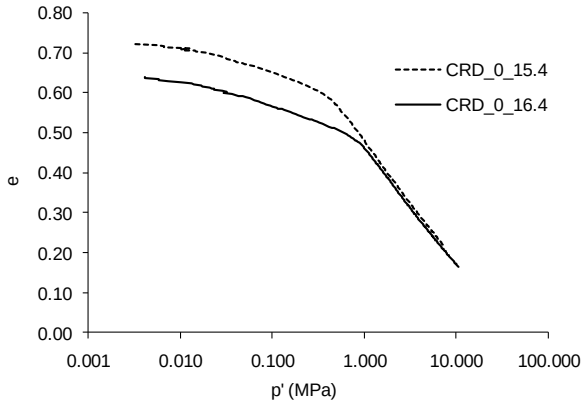

Figure 6.34 Void ratio against mean effective stress p' in uncemented specimens with two different void ratios

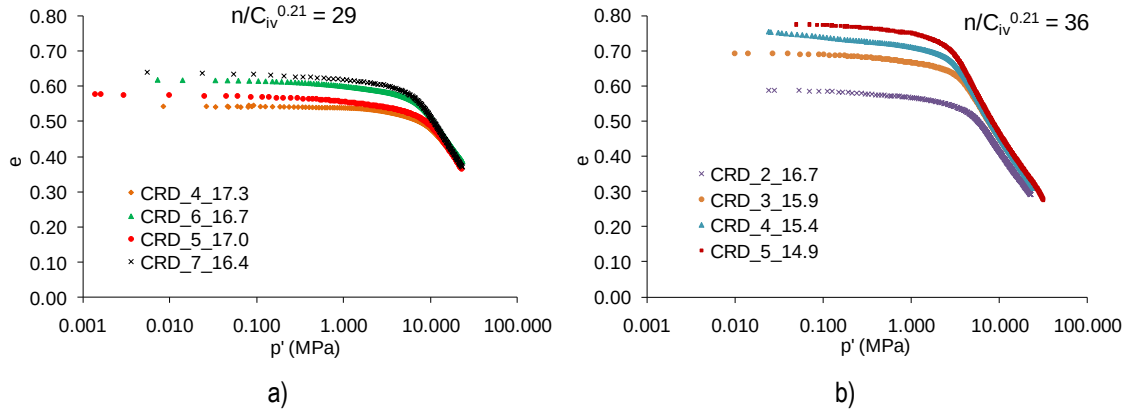

Figure 6.35 Void ratio against mean effective stress p' in cemented specimens with two different porosity/cement ratios: a) $n/C_{iv}^{0.21} = 29$; b) $n/C_{iv}^{0.21} = 36$.

It should be noted that, in Figure 6.34, only two tests were presented. Due to specificity of the third test it cannot be compared with the others CRD tests and so the results will be presented in chapter 7 together with isotropic triaxial tests results.

Concerning the cemented specimens data it is interesting to note that only the 2% cement content specimen has a slightly different behaviour than the others. After some experience in the laboratory with these materials this is not really surprising as the 2% specimens always have a slightly different behaviour that may be related to a very low state of cementation. For example, 1% cemented specimens were also performed at the beginning of this experimental program but they felt apart when submerged in water after 7 days of curing period as the cementation was not enough. This was not observed in the 2% specimens but it was clear that they are much more fragile than the others. Cruz (2010) has also found a different type of behaviour between less than 3% specimens and more cemented specimens.

Figure 6.36 shows the results of specimens with the same cement content and different void ratios as well as data from specimens with different cement contents but with the same initial void ratio. It is observed that the curves do not really converge together in such a perfect way as in Figure 6.35. These results give an indication that the adjusted porosity/cement ratio can better reproduce the behaviour in one-dimensional compression than the cement content or initial void ratio alone.

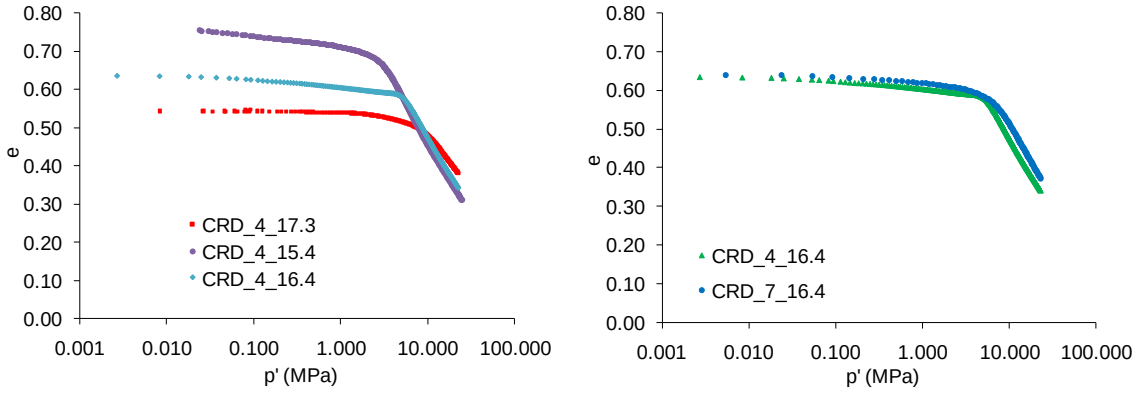

a) b)

Figure 6.36 Void ratio against mean effective stress p' in cemented specimens: a) 4% of cement content and different void ratios; b) 16.4 kN/m^3 of dry unit weight and different cement contents

6.12 Synopsis of chapter 6

This chapter presented a great number of data from different tests. Together, they allowed a better understanding of the artificially cemented soil used in this work. Compressive and tensile strength, dynamic and static stiffness and one-dimensional behaviour were some of the most important issues studied.

In terms of unconfined compression strength, the effect of porosity, cement and water content were fully investigated, becoming clear that the increase in strength due to cementation is more significant in denser specimens where there are more contact points between particles improving the effectiveness of cementation. The relationship between compressive and tensile strength was also obtained, considered around 11%.

Seismic wave measurements were performed by means of bender elements, compression transducers, ultrasonic transducers and resonant column devices. Some of them were considered more useful by providing an easier interpretation, like P wave velocity measurements from compression transducers. The resonant column tests, although with questionable fixing conditions that may lead to wrong interpretations in very stiff materials, gave quite reasonable results which might indicate that the random noise procedure may be interesting to test these materials, due to the reduced distortion level.

Most of these tests were analysed by mean of the adjusted porosity/cement ratio ($n/C_{iv}^{0.21}$) which has proved to be a very interesting parameter for normalizing these materials behaviour. In fact, artificially cemented mixtures with different cement contents or void ratios, but the same adjusted porosity/cement ratio, have shown similar behaviour not only in terms of strength, but also in static and dynamic stiffness, indirect tensile strength and one-dimensional compression.

Chapter 7.
STATIC TRIAXIAL TESTS

7.1 Introduction

This Chapter is related to static triaxial tests performed in this work over uncemented and cemented specimens. It includes isotropic compression and triaxial compression tests performed at low and high pressure in drained and undrained conditions. After a brief description of the experimental program the results of the tests are presented. The first analysis will be focusing in the stress-strain-volumetric/pore pressure curves or v vs p' curves (in the case of isotropic tests) considered as the starting point for the understanding of the tests results. The triaxial tests are then analysed focusing in specific characteristics like stiffness, stress-paths, strength envelopes, stress-dilatancy, or final void ratio. Normalized results are also presented in an attempt to define the yield and state boundary surfaces. The aim is to present a general framework for the behaviour of an artificially cemented well graded soil in static conditions within the context of critical state soil mechanics.

7.2 Static triaxial tests experimental program

7.2.1 Drained and undrained low pressure triaxial tests in uncemented specimens

Drained and undrained conventional compression triaxial tests were performed in uncemented specimens with two different void ratios. The specimens were moulded as described in chapter 6 (section 6.3) with no addition of cement, and no fines removal.

Table 7.1 summarizes the moulding and test conditions of the specimens, prepared to have two different compaction degrees and void ratios corresponding to 15.4 and 17 kN/m^3. However, due to the specimens swelling the moulding void ratios (e_0) are slightly higher than expected.

The water content was kept constant during all the tests, and a value of 12% was considered, obtained as the optimum water content for a mixture of 3% of cement content (see chapter 6). The percentage of the correspondent Modified Proctor optimum dry unit weight (%MP) is also shown and it is mainly around 82 and 90% for the two void ratios considered. The effective isotropic confining pressure (σ'_c) ranged between 30 and 250 kPa and remained constant during shearing. The lowest confining pressure was defined by the reasonable pressure that soil-cement layers are generally subjected in the field. For the others, higher values were set in order to have a large range of confining pressures. The low pressure isotropic test went up to 1200 kPa.

The name of the specimens has the following meaning:

- CV - drained conventional compression test (CV90 means the denser specimens);
- CIU - undrained conventional compression test (CIU90 means the denser specimens);
- ISO - isotropic test (LP means low pressure);
- (0) - cement content;
- _30 - effective confining pressure.

Table 7.1 Test conditions for uncemented specimens tested in low pressure triaxial

Name	%C	γ_d (kN/m^3)	e_0	w (%)	% MP	σ'_c (kPa)	Draining Conditions	Equipment
ISO(0)_LP	0	15.2	0.75	12	82%	1200	Drained	CT_BE
CV(0)_30	0	15.3	0.75	12	82%	30	Drained	CT
CV(0)_80	0	15.1	0.77	12	81%	80	Drained	CT_BE
CIU(0)_30	0	15.3	0.74	12	82%	30	Undrained	CT
CIU(0)_250	0	15.3	0.75	12	82%	250	Undrained	CT
CV90(0)_30	0	16.7	0.60	12	90%	30	Drained	CT_BE
CV90(0)_100	0	16.6	0.61	12	89%	100	Drained	CT_BE
CV90(0)_250	0	16.6	0.60	12	89%	250	Drained	CT_BE
CIU90(0)_30	0	16.7	0.60	12	90%	30	Undrained	CT_BE
CIU90(0)_250	0	16.6	0.61	12	89%	250	Undrained	CT_BE

CT - convential triaxial cell (description in section 5.6.5)

CT_BE - conventional triaxial cell with bender elements (description in section 5.6.4)

7.2.2 Drained and undrained low pressure triaxial tests in cemented specimens

The same type of tests described above was carried out over cemented specimens, moulded as described on chapter 6. To define the moulding conditions two adjusted porosity/cement ratios were chosen ($n/C_{iv}^{0.21}$ = 36 and 29), which correspond to UCS of 800 and 2000 kPa according to the equation (6.2). The same approach has been used for the CRD tests described in chapter 6. In all triaxial tests each of this adjusted

porosity/cement ratio was subdivided in two moulding points characterized by cement content and dry unit weight, while the water content remained constant and equal to 12%. For the first ratio ($n/C_{iv}^{0.21}$= 36), 2 and 4% cement contents were considered which lead to dry unit weights of 16.7 and 15.4 kN/m^3, respectively. For the second ratio ($n/C_{iv}^{0.21}$ = 29) higher strength was needed, so 5 and 7% of cement contents were assumed with 17.0 and 16.4 kN/m^3 of dry unit weight. Obviously, when the cement content was increased the dry unit weight had to decrease in order to keep the same adjusted porosity/cement ratio. In Table 7.2 this information is summarized presenting the test conditions for each specimen. The test name follows the rules presented above. As explained on chapter 6, the specimens were left in the humid chamber to cure for 7 days, after which they would be placed on the triaxial cell following the test procedures described in chapter 5.

Table 7.2 Test conditions for cemented specimens tested in low pressure triaxial

Test name	%C	γ_d (kN/m^3)	e_0	w (%)	$n/C_{iv}^{0.21}$	q_u (kPa)	σ'_c (kPa)	Draining Conditions	Equipment
CV(2)_30	2	16.6	0.61	12	36	800	30	Drained	ISMES
CV(2)_80	2	16.5	0.62	12	36	800	80	Drained	ISMES
CV(2)_250	2	16.7	0.60	12	36	800	250	Drained	ISMES
CV(4)_30	4	15.4	0.74	12	36	800	30	Drained	ISMES
CV(4)_80	4	15.7	0.71	12	36	800	80	Drained	ISMES
CV(4)_250	4	15.5	0.73	12	36	800	250	Drained	ISMES
CV(5)_30	5	16.9	0.59	12	29	2000	30	Drained	ISMES
CV(5)_80	5	17.0	0.58	12	29	2000	80	Drained	ISMES
CV(5)_250	5	17.0	0.58	12	29	2000	250	Drained	stress-path
CV(7)_30	7	16.3	0.66	12	29	2000	30	Drained	stress-path
CV(7)_80	7	16.5	0.63	12	29	2000	80	Drained	CT
CV(7)_250	7	16.7	0.61	12	29	2000	250	Drained	ISMES
CIU(2)_80	2	16.6	0.61	12	36	800	80	Undrained	CT
CIU(2)_250	2	16.7	0.60	12	36	800	250	Undrained	CT
CIU(4)_80	4	15.3	0.75	12	36	800	80	Undrained	CT
CIU(4)_250	4	15.5	0.73	12	36	800	250	Undrained	CT
CIU(5)_80	5	16.9	0.59	12	29	2000	80	Undrained	CT
CIU(5)_250	5	17.0	0.58	12	29	2000	250	Undrained	CT
CIU(7)_80	7	16.4	0.63	12	29	2000	80	Undrained	CT
CIU(7)_250	7	16.3	0.65	12	29	2000	250	Undrained	CT

ISMES - Enel.Hydro system cell (description in section 5.6.2)
stress-path - Bishop-Wesley stress-path cell (description in section 5.6.3)
CT - conventional triaxial cell (description in section 5.6.5)

7.2.3 High pressure triaxial tests in uncemented and cemented specimens

The cemented specimens tested in high pressure triaxial tests were moulded in the same four moulding points expressed in section 7.2.2, for the two referred adjusted porosity/cement ratios. In the same way, the uncemented specimens were moulded to have the two void ratios of section 7.2.1. The initial void ratio was slightly higher than expected due to some expansion of the specimens.

As reported in chapter 5, isotropic compression tests were performed at Imperial College, London (IC) and undrained triaxial compression tests were carried out at the University College of London (UCL). All specimens were moulded at FEUP according to the procedure described in chapter 6 and then sent by mail to London to be tested, except one loose uncemented specimen (CIU(0)_10000) that was moulded in place. In this specimen (CIU(0)_10000) the dry soil was mixed with water and moulded in place at UCL by the use of a splitting mould where the membrane has been previously stretched by the application of vacuum to the mould.

The pre-moulded specimens had the following dimensions: the tests executed at IC had 50 mm of diameter and 100 mm high and the specimens tested at UCL laboratory had 38 mm of diameter and 79 mm of height. Some tests have already been previously performed at FEUP to analyse the effect of the specimen size in the stress-strain behaviour, which was considered irrelevant.

Table 7.3 summarizes the test conditions of each specimen. The test name follows the same rules indicated in section 7.2.1, except for the first two isotropic uncemented specimens where the dry unit weight is indicated to distinguish between the two. The effective confining pressure presented in the table refers to the maximum effective confining pressure achieved in the isotropic compression tests and to the effective confining pressure kept constant during shearing in the undrained triaxial compression tests.

Table 7.3 Test conditions of high pressure tests

Test name	%C	γ_d (kN/m^3)	e_0	w (%)	$n/C_{iv}^{0.21}$	q_u (kPa)	σ'_c (kPa)	Draining Conditions	Equipment
ISO(0)_14.7	0	14.7	0.81	12	-	-	24000	Drained	IC
ISO(0)_16.1	0	16.1	0.66	12	-	-	32000	Drained	IC
ISO(2)	2	16.0	0.75	12	36	800	41000	Drained	IC
ISO(4)	4	15.1	0.78	12	36	800	32000	Drained	IC
ISO(5)	5	16.4	0.64	12	29	2000	43000	Drained	IC
ISO(7)	7	15.8	0.70	12	29	2000	43000	Drained	IC
CIU(0)_10000	0	12.2	1.21	21.6	-	-	10000	Undrained	UCL
CIU(5)_10000	5	16.8	0.60	12	29	2000	10000	Undrained	UCL
CIU(5)_20000	5	16.8	0.60	12	29	2000	10000	Undrained	UCL
CIU(7)_10000	7	16.4	0.65	12	29	2000	20000	Undrained	UCL
CIU(7)_20000	7	16.4	0.65	12	29	2000	20000	Undrained	UCL

IC - high pressure apparatus of Imperial College Geotechnical laboratory (description in section 5.8.2)
UCL - high pressure apparatus of the Sediment Deformation laboratory at UCL (description in section 5.8.3)

7.3 Calculations and corrections in triaxial tests

7.3.1 Area correction

The section area of the specimen changes during the test and therefore a correction to the initial value has to be made. It is assumed that during saturation and consolidation the strains involved are quite small and therefore the shape of the cross-section remains constant. During the first part of shearing the specimen tends to barrel and so the following equation can be applied to evaluate the area at each stage (Head, 1982):

$$A = A_0 \left[\frac{1 - \varepsilon_V}{1 - \varepsilon_a}\right] \tag{7.1}$$

where,

- A_0 is the initial area in the beginning of shearing;
- ε_v is the volumetric strain
- ε_a is the axial strain.

If a shear plane failure starts to develop another type of correction is applied, in this case, to the deviatoric stress ($q=\sigma_v-\sigma_H$) which is calculated as usual by the ratio between the axial force P acting on the piston and the area (A) (Head, 1982):

$$q_{corr.} = f_s \frac{P}{A} \tag{7.2}$$

$$f_s = 1 + 0.06 * \theta * \frac{\varepsilon_s}{100} \tag{7.3}$$

where,

- θ is the angle of failure measured from the vertical plane in degrees;
- ε_s is the axial strain measured from the start of slip (%);
- A is the area of the specimen when the failure plane starts to develop considered at peak and derived from equation (7.1) so that barrelling is taken into account before the failure plane.

This simplification is acceptable if ε_s <15% and if 27º< θ < 35º. In this case, the measured angle of the shear plane failure with vertical was 25º and, so equation (7.2) could be applied.

7.3.2 Membrane correction

The membrane acts on the specimen by pushing it inside with a force which depends on the membrane stiffness (which changes with thickness) and on the specimen deformation itself. Henkel and Gilbert (1952) came to the following expression for deviator stress correction due to the membrane effect during the specimen barrelling:

$$q_{corr.} = q - C_M \tag{7.4}$$

$$C_M = \frac{0.4\ M\ \varepsilon_a\ (100 - \varepsilon_a)}{d_0} \tag{7.5}$$

being,

- M the membrane stiffness modulus in N/mm;
- d_0 the diameter of the specimen in the beginning of shearing in mm;
- ε_a the axial strain (%).

According to Head (1982) this correction is in some cases unnecessary and insignificant. In this work this procedure was only applied in the uncemented specimens, which have clearly exhibited barrelling, having a slight effect at higher strains.

Another correction is available to account for the membrane effect in case of a shear plane failure. The proposal of La Rochelle et al., (1988) for the deviatoric stress is evidenced in the next expressions:

$$q_{corr.} = q - f_c \tag{7.6}$$

$$f_c = \frac{1.5\ \pi\ d_0 \sqrt{(M f\ d_0 \delta)}}{A} \tag{7.7}$$

where,

- $f = \sigma'_3 \tan \phi'$, being ϕ' the angle of shearing resistance of the soil considered 40º;
- δ was considered to be the difference between the axial strain at a given stage and the axial strain at peak, considering the soil as a perfectly rigid dummy;
- M is the membrane stiffness modulus in N/mm;
- d_0 is the diameter of the specimen in the beginning of shearing in mm; and,
- A has the meaning expressed above.

The membrane stiffness modulus was taken from Topa Gomes (2009) who has performed tensile tests in the same type of latex membranes used in this work. For a 70 mm diameter

membrane (with 0.33 mm of thickness) a stiffness modulus of 0.55 N/mm was obtained. The high pressure tests used two neoprene membranes whose stiffness modulus was not possible to evaluate so this correction was not applied in this case.

7.3.3 Volumetric strains calculation

The volumetric strain (ε_v) often presented in the test results was calculated from the flow of water in and out of the specimen. Even being an external measure with some errors associated with it, namely bedding errors and compliance of tubing and chambers, it was the only possibility in most cases and it has the advantage of being read until the very end of the test. In this section comparisons with other methods to calculate the volumetric strain will be compared and discussed.

In uncemented specimens, some low pressure tests were executed with axial and radial instrumentation and thus the volumetric strain was also calculated by the well known equation:

$$\varepsilon_v = \varepsilon_a - 2\,\varepsilon_r \tag{7.8}$$

being,

ε_a the axial deformation and ε_r the radial deformation

A comparison between the two methods is illustrated in Figure 7.1 where tests are presented as an example. In these graphs the volumetric strain is plotted against the external axial strain. In the very beginning there is some agreement between both methods but soon a clear divergence is observed.

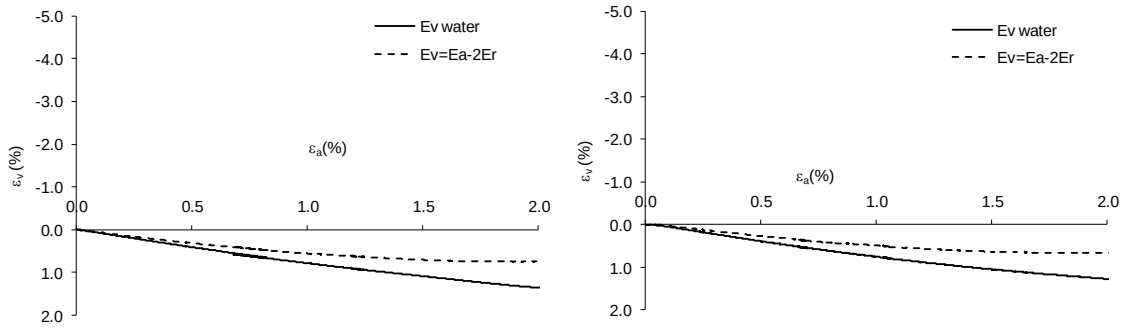

Figure 7.1 Comparison between volume strain calculated by the flow of water or by the local instrumentation: a)CV90_100; b)CV90_250

In most cemented specimens only axial deformation was available and thus, the volumetric strain was calculated by the axial strain and assuming a Poisson ratio of ν=0.3 close to the value obtained in the previous chapter for dynamic conditions (0.37),

$$\varepsilon_v = \varepsilon_a (1+ 2\ \nu) \tag{7.9}$$

which is, obviously, only accepted in elastic ranges.

The single cemented specimen that had radial instrumentation allowed a comparison between the three methods that is represented in Figure 7.2b). In the others, the volumetric strain by the flow of water was compared to the volumetric strain calculated by equation (7.9).

Figure 7.2 evidences that, up to the point of volumetric inversion, the flow of water gives similar strains to the local instrumentation. After this point, close to peak, already over the elastic and pseudo-elastic locus (where ν may be considered constant), the shear plane failure starts to develop and, thus, the differences between the methods are much higher. Figure 7.2b), where the three methods are presented, indicates that the volumetric strains from equations (7.8) and (7.9) are quite similar which gives validity to the Poisson ratio assumed before (ν=0.3).

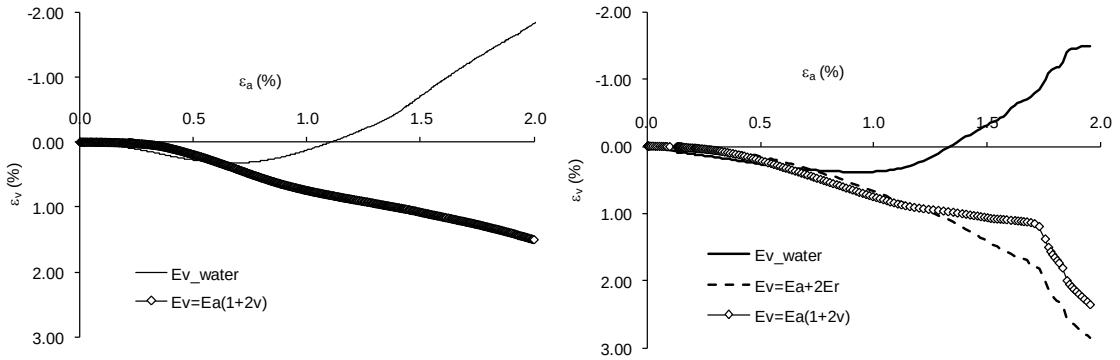

Figure 7.2 Comparison between volume strain calculated by the flow of water or by the local instrumentation: a)CV4_30; b)CV7_30

7.3.4 Void ratio calculation

Void ratio is quite an important parameter, especially when analysing triaxial test results. In isotropic tests, for instance, a good reliability on the initial void ratio is of crucial importance as the relative position of some curves with respect to the others is controlled by the initial void ratio. On the other hand, being a parameter that can be obtained from different test measurements, it can be treated as a control variable. Shipton (2010) reports that the void

ratio is a very sensitive parameter, so, it is extremely important to have a high level of accuracy in all measurements. For that reason, a comparison between different void ratios obtained in a given test is presented in the next sections using the four independent methods given by equations (7.10) to (7.13) further below.

The void ratio at the beginning of consolidation is the most relevant value and also the most difficult to know when the volume change is measured by the flow of water as it is not possible to know the volume change during saturation. Shipton (2010) has proposed an iterative procedure to calculate the initial void ratio by correcting the flow of water during saturation assuming that all the air in the voids will be replaced by water during this process. Unfortunately, this important contribution was only published in the very end of the work herein presented and therefore, the flow of water was not measured during the saturation of the specimens tested in this experimental work. Consequently, the void ratio control was done by the final void ratio, comparing the values obtained by four methods described subsequently taking into account that at the end of saturation the soil should be completely saturated and therefore, the saturation degree can be considered 1 in equation (7.10).

Method 1: $Gw = Se$ (7.10)

Method 2: $\gamma_d = \frac{\gamma_s}{1+e}$ (7.11)

Method 3: $\gamma = \gamma_s \frac{1+w}{1+e}$ (7.12)

Method 4: $\frac{\Delta V}{V_0} = \frac{\Delta e}{1+e_0}$ (7.13)

being,

- G the specific gravity, taken as the weighted average between the specific gravity of the soil and cement in function of their dry weights;
- γ_s the particles unit weight defined as $G^*\gamma_w$ where γ_w is the water unit weight taken as 9.81 kN/m^3;
- γ_d the dry unit weight calculated as ratio between the weight of dry soil and the final volume of the specimen. The dry weight is the quantity of dry mixture inserted in the mould for the specimen preparation, which was compared to the dry weight of the specimen measured after the test;
- γ the unit weight calculated by the ratio between the humid weight at the end of test and the volume of the specimen at the end of test;

- w the final water content of the soil measured according to the European standard CEN ISO/TS 17892-1 (CEN, 2004c);
- V_0 the volume of the specimen before consolidation;
- ΔV the volume change during consolidation and shearing measured by the flow of water;
- e_0 the void ratio at the start of consolidation.

In the first procedure referring to equation (7.10), the soil is considered completely saturated (S=1), while the other procedures admit different saturation degrees. However, only method 1 and 3 rely on the final water content. Comparing method 2 and 3 the only difference concerns the way of calculating the dry weight: in method 2 the moulding dry weight is considered while method 3 relies on the final dry weight. If the soil is too soft or if it has too much water at the end of the test, the final dry weight can be difficult to obtain as the soil is not totally collected from the triaxial apparatus. In this case, the final dry weight is smaller than the initial dry weight. On the other hand, the initial moulding dry weight can also have some errors as it was calculated from the quantity of humid soil introduced in the mould and the moulding water content taken from two different pieces of soil. Finally, method 4 depends on the volume change during the test, measured from the flow of water, and on the initial void ratio, which means that any problem in the calculation of the initial void ratio will be reflected in this value. The initial void ratio is calculated from moulding conditions using method 3, when w is the moulding water content and γ is calculated from the weight of soil introduced in the mould divided by the volume of the mould.

7.3.5 Dilatancy calculation

Stress-dilatancy analysis was performed over the test results obtained in this work as it will be shown in section 7.13. The following well know expression was used in those analyses for dilatancy (ψ) calculation:

$$\psi = \frac{\delta \varepsilon_v}{\delta \varepsilon_s} \tag{7.14}$$

where,

- ε_v is the volumetric strain measured by the flow of water in and out of the specimen as explained in section 7.3.3;
- ε_s is the shear strain given by,

$$\varepsilon_s = \frac{2(\varepsilon_1 - \varepsilon_3)}{3} \quad (7.15)$$

In triaxial conditions $\varepsilon_v = \varepsilon_1 + 2\,\varepsilon_3$ and $\varepsilon_a = \varepsilon_1$ thus, equation (7.15) can be rewritten as following,

$$\varepsilon_s = \varepsilon_a - \frac{\varepsilon_v}{3} \quad (7.16)$$

where,

ε_a is the axial strain given by the external instrumentation to be compatible to the water volumetric strain

7.4 Isotropic tests results

7.4.1 Uncemented tests

The results from all the isotropic tests at low and high pressures together with the results from one oedometer test will be presented in this section. First, uncemented test results will be shown, followed by the cemented tests allowing the comparison between both types of specimens.

The uncemented data included two high pressure isotropic tests (ISO(0)_14.7 and ISO(0)_16.1 - see Table 7.3) performed at Imperial College, as well as one low pressure isotropic test (ISO(0)_LP - see Table 7.1) and one oedometer test executed at FEUP (CRD(0)_9.8 - see Table 6.8). These results will be plotted in Figure 7.3 together with two other isotropic tests performed at two different void ratios with the same material and in similar conditions as described by Amaral et al. (2011). The results are expressed in terms of specific volume (v=1+e) against the mean effective stress ($p'=(\sigma'_v+2\sigma'_H)/3$) as it is conventional in critical state soil mechanics. According to Amaral et al. (2011) the yield pressure obtained in those tests was around 800 and 300 kPa respectively for the highly and less compacted.

It is clear from the graph that all the tests tend to a unique alignment. The only exception is the looser specimen tested at Imperial College (ISO(0)_14.7). It should be remembered, as stated in chapter 5, that this test had a problem during setup because no split mould was placed around the specimen during the vacuum percolation and therefore the initial void ratio could be incorrect. The alignment given by this test seems parallel to the other tests which corroborates the idea that it should be a problem in the initial void ratio.

The isotropic curves convergence at higher pressures is typical of most soils from clays to clean sands due to simple compression in the first case (Burland, 1990) and particle breakage in the second (Coop and Airey, 2003). The exception to this behaviour characterizes the so-called Transitional Soils carefully studied by Shipton (2010).

It is not possible to know exactly if there was any particle breakage during isotropic compression of the silty sand as no grain size distribution curve was done with the tested material. However, it is supposed that although some weaker grains may have experienced some breakage, the strong quartz grains should have remained intact as it was observed in the SEM analysis presented in the next section 7.5.

From these results a unique normal compression line (NCL) of the silty sand could be obtained whose parameters are the following: N = 2.352 and λ = 0.112; where N is the specific volume for p'=1kPa and λ is the gradient of the NCL, which completes the following equation,

$$v = 2.352 - 0.112 \ln(p') \tag{7.17}$$

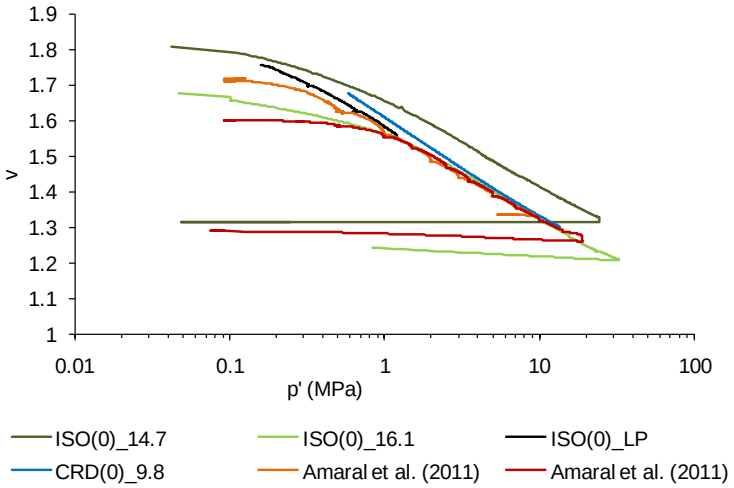

Figure 7.3 Uncemented isotropic tests

7.4.2 Cemented tests

The cemented tests comprise 4 high pressure isotropic compression tests at two different adjusted porosity/cement ratios ($n/C_{iv}^{0.21}$ = 36 and 29). The tests ISO(2) and ISO(4) have a $n/C_{iv}^{0.21}$ equal to 36 and tests ISO(5) and ISO(7) have a $n/C_{iv}^{0.21}$ equal to 29. The results of these tests are plotted in Figure 7.4 where the uncemented NCL from the previous section is also shown for comparison. The following comments can be addressed about these results:

- as expected, the cemented NCL plots to the right of the uncemented NCL, filling the structured permitted space as explained in Chapter 4 (section 4.4.1) which is a sign of cementation;
- the isotropic curves of the specimens with the same adjusted porosity/cement ratio ($n/C_{iv}^{0.21}$) tend to converge to an unique NCL;
- at the stress levels achieved in these tests a convergence between all the cemented tests was not possible;
- even extending the uncemented NCL it is not possible to observe a unique NCL between cemented and uncemented specimens.

The non convergence between cemented and uncemented specimens may indicate that the two materials are different even after 40 MPa of confining pressure. It should be noted that to have a unique line for cemented and uncemented specimens, the clusters of soil mixed with cement had to be completely destroyed, which apparently was not possible for the range of pressures involved in these tests.

The NCL parameters of the two cemented NCL are presented in Table 7.4 together with the uncemented NCL values.

Table 7.4 NCL parameters for uncemented and cemented specimens

	N	λ
Uncemented	2.352	0.112
$n/C_{iv}^{0.21}$ = 36	2.893	0.154
$n/C_{iv}^{0.21}$ = 29	2.797	0.138

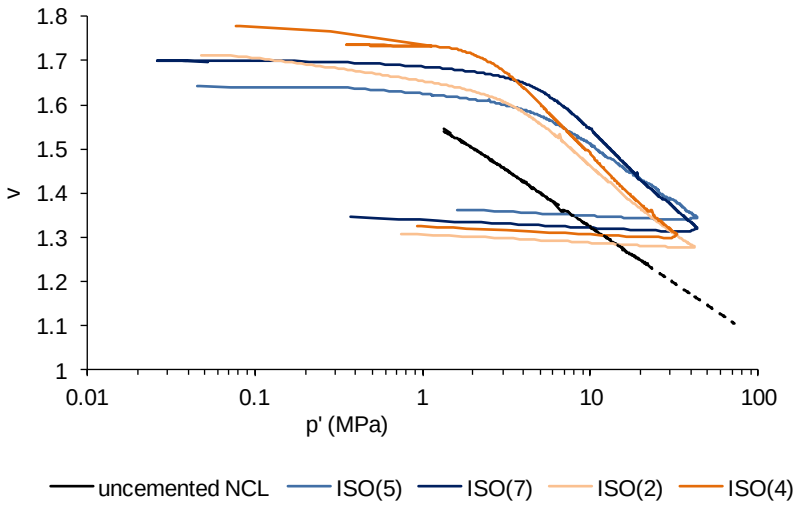

Figure 7.4 Cemented isotropic tests

7.5 Scanning electron microscope analysis

7.5.1 Uncemented specimen

The following micrographs (Figures 7.5 to 7.7) were taken on an uncemented specimen tested in isotropic compression up to 30 MPa. The procedure was essentially performed in two steps: first, less zoomed pictures were taken to have an idea of the specimen (e.g. Figures 7.5 and 7.6) and then, some other pictures with more zoom were picked in restricted areas (e.g. Figure 7.7). By picking singular points, the equipment software gives a spectra of the chemical composition from which the mineralogical composition is derived. The particles of potassium feldspar and micas are difficult to distinguish by chemical composition as they both have silica, aluminium and potassium. For that reason, these particles are generally distinguished by their shape.

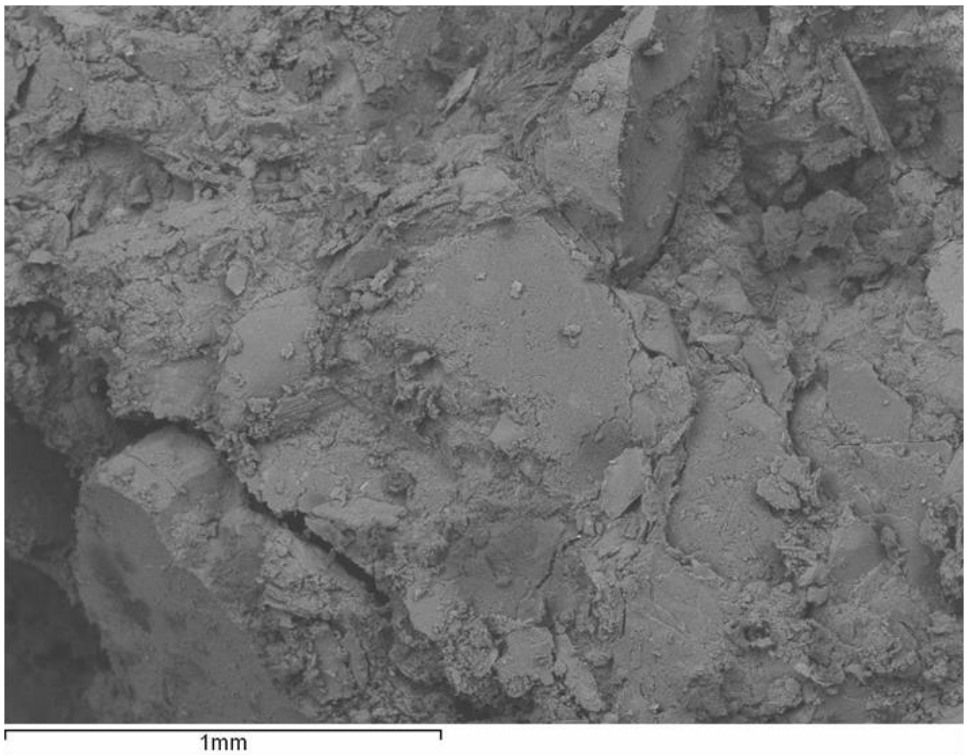

Figure 7.5 SEM micrographs of the uncemented specimen showing bigger grains mostly covered with fines as a result of being a very well graded soil

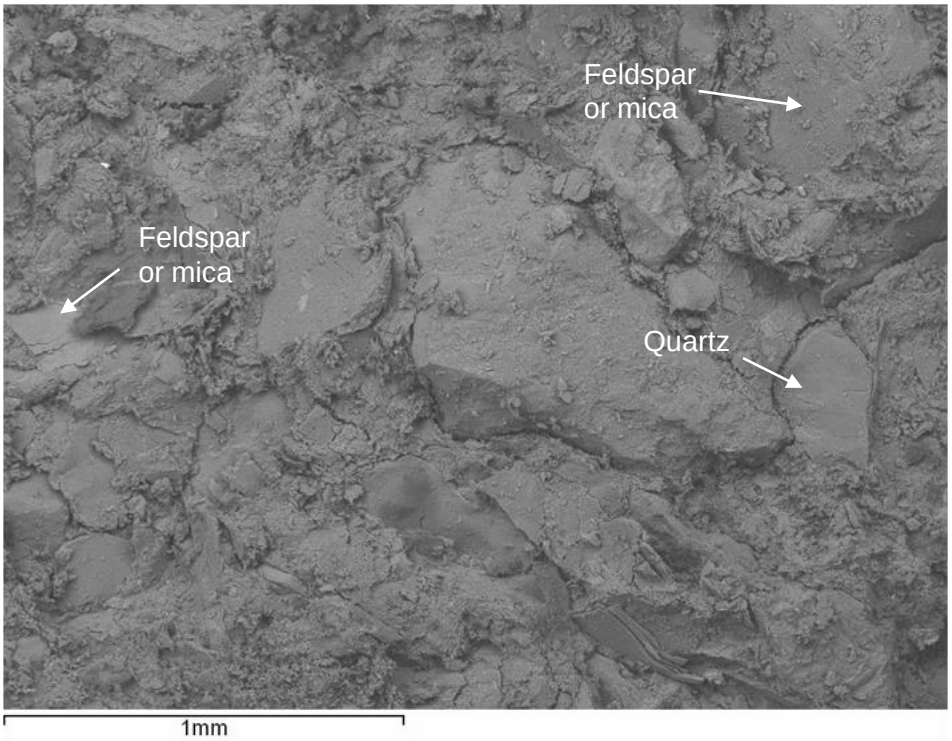

Figure 7.6 SEM micrograph of the uncemented specimens for particle identification

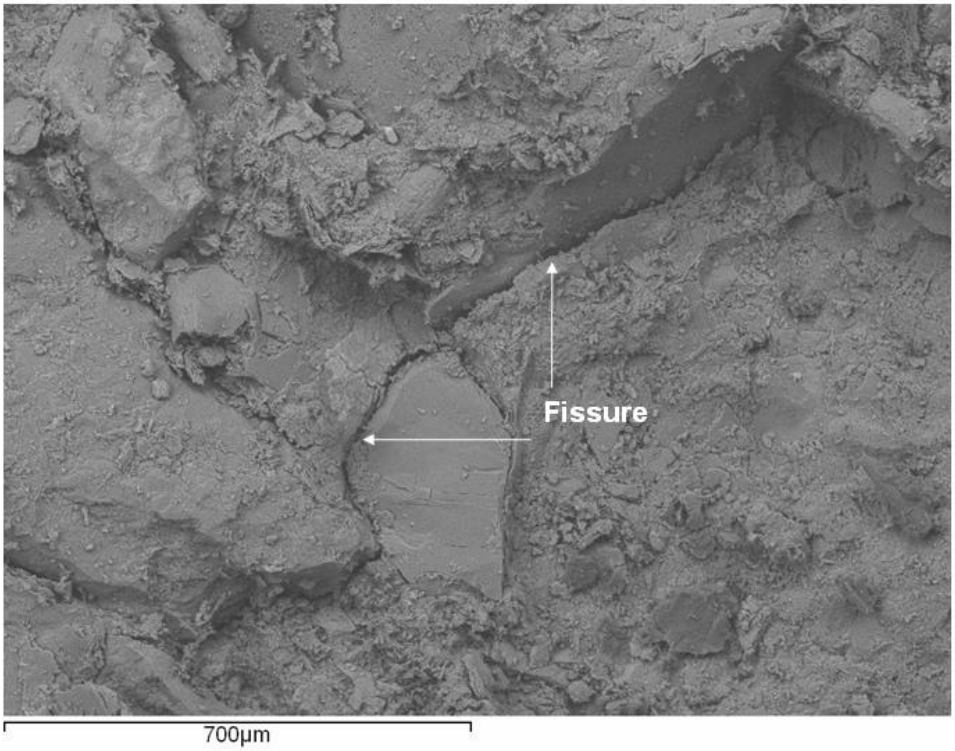

Figure 7.7 SEM micrograph of the uncemented specimen at a higher magnification highlighting one of the fissures observed on the previous figure

From the previous figures the following comments can be addressed:

- even after very high pressures of confinement is not clear from these micrographs the evidence of particle breakage (at least the strong quartz grains, although micas and feldspars may be reduced which cannot be verified in these micrographs);
- instead, some joints are visible around the grains as a proof of the great compression (Figure 7.7);
- most particles are covered with clay (being a problem to particle identification) which is in agreement to the high percentage of fines of this soil (≈30% of fines from which 8% of clayey fraction);
- in spite of the presence of clay (kaolinite) cover, it was possible to identify particles of quartz, feldspar, and micas (Figure 7.6);
- there were also small amounts of iron, which may have been derived from old fractures on the mother rock where water minerals were deposited during percolation.

7.5.2 Cemented specimen

The same technique was applied to a cemented specimen tested in isotropic compression up to 40 MPa, giving rise to Figure 7.8 and 7.9.

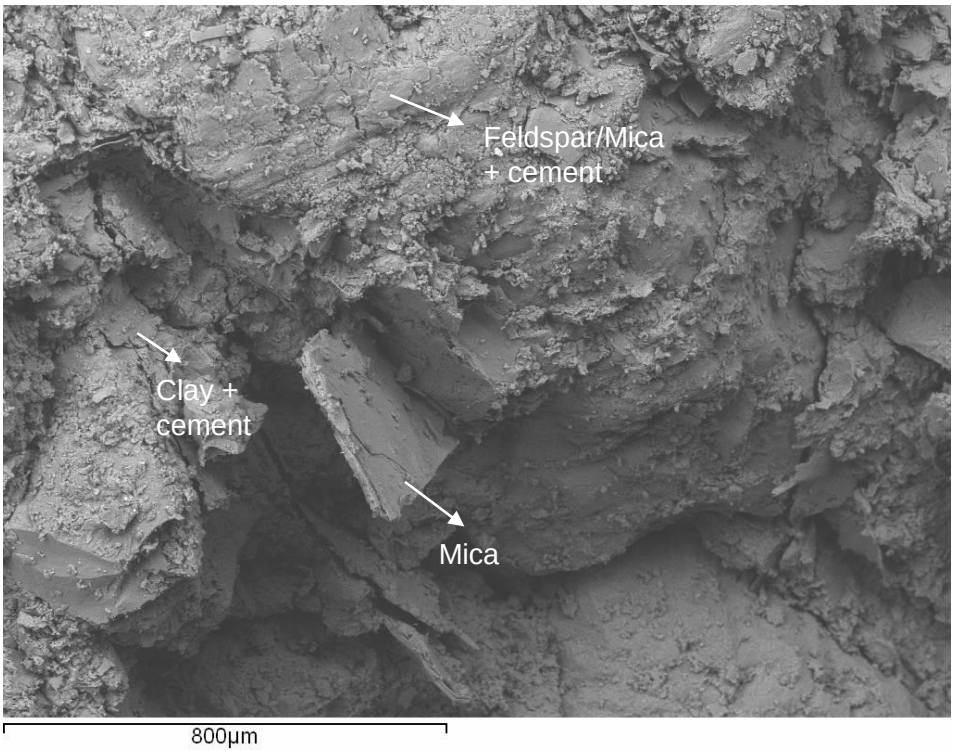

Figure 7.8 SEM micrograph of a cemented specimen for particle identification

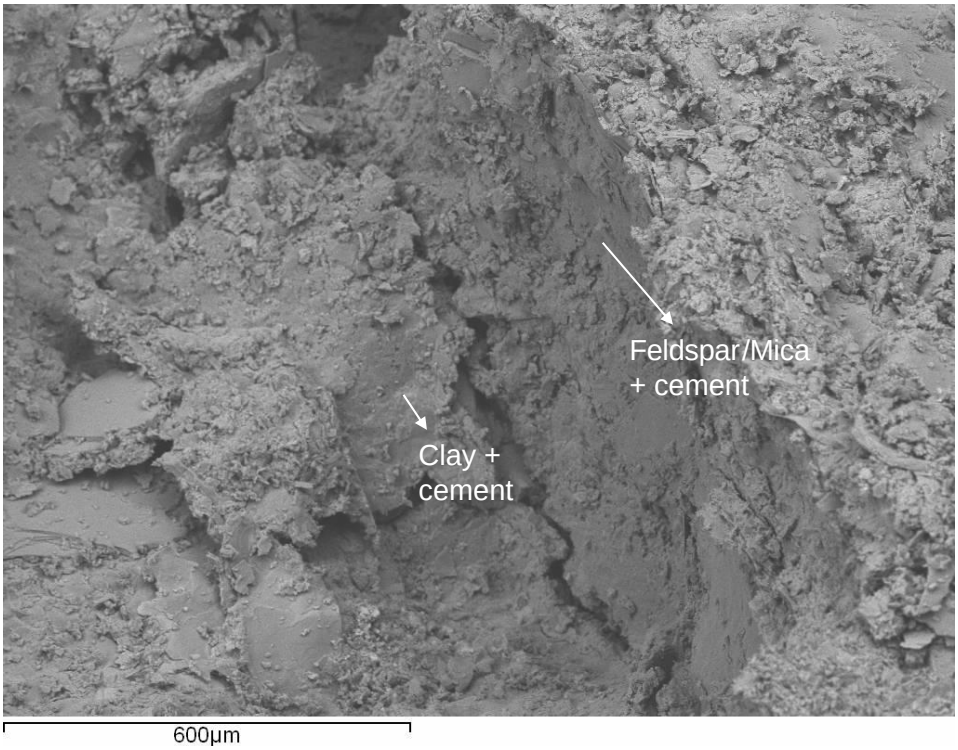

Figure 7.9 SEM micrograph showing the texture of the bonding material

The comparison between uncemented and cemented micrographs shows a different texture when cement is present. It seems that the bonds between the bigger grains are mostly a mixture of fines and cement, indicating that the cement has aggregated most of the fine particles. No particle breakage if visible in these micrographs, instead there are some joints derived probably from cement breakage.

In Figure 7.8, a mica particle is clearly seen, coming out from the mass of soil and cement. Some joints on the cemented bonds are also seen. In Figure 7.9 the texture of the cemented specimen is observed, which is clearly different from the uncemented texture exhibited in Figure 7.5. The small sharp points on the microtexture indicate the presence of cement.

7.6 Uncemented specimens triaxial tests results

7.6.1 Drained triaxial tests

The results of five drained low pressure triaxial tests performed over uncemented specimens moulded with two different void ratios, presented in Table 7.1, are discussed herein. In Figure 7.10 the stress-strain-volumetric behaviour observed in each of these tests is plotted together. The results are expressed in terms of the deviator stress ($q=\sigma_V-\sigma_H$)

and the axial strain (ε_a) measured by the external transducer to be comparable with the volumetric strain (ε_v) measured by the flow of water in and out of the specimen.

In the fourth Chapter some basic principles of critical state soil mechanics were introduced, where compressive and dilatant behaviour were associated to the initial state of the soil with respect to the critical state line (soils at the dry side of critical show dilation and soils at the wet side of critical exhibit compression). The state depends on the initial void ratio and initial mean effective stress with respect to the critical state line so, without knowing the position of this line, it is not possible to predict which specimens would compress or dilate.

From the data presented in Figure 7.10 the relationship between confining pressure and initial density and their effect on the compressive and dilatant behaviour of the specimens is clearly illustrated. The specimens moulded with the higher initial void ratio and consolidated to an effective confining pressure of 80 kPa, or moulded with the lower void ratio but consolidated to effective confining pressures of 250 kPa show compressive behaviour associated to strain hardening. Conversely, the specimens confined to the lower pressure (30kPa) and the specimen with the lower void ratio and 100 kPa of confining pressure show dilatant behaviour and strain softening, being clear a well defined peak.

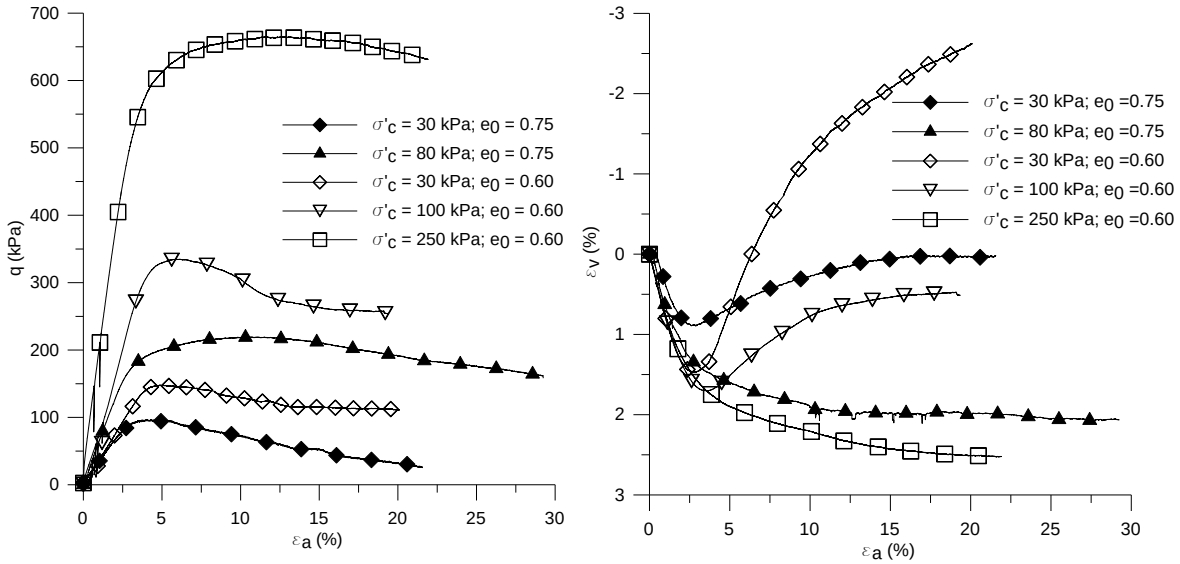

a) b)

Figure 7.10 Stress-strain-volumetric response of the silty sand at low pressures (a) stress-strain behaviour (b) volumetric behaviour

7.6.2 Undrained triaxial tests

In this section, four undrained low pressure triaxial tests over uncemented specimens with two different void ratios are presented according to the moulding conditions expressed on

Table 7.1. The results plotted in Figure 7.11 show the stress-strain curve as well as the pore pressure (u) against the axial strain. Undrained shearing of the uncemented sand was accompanied by an increase in pore water pressure and strain hardening in the looser specimens, while in the denser specimens the pore pressure reached a peak before reducing to a stable value.

Additionally, one undrained high pressure triaxial test was performed at 10 MPa of effective confining pressure, named CIU(0)_10000 in Table 7.3, whose results are plotted in Figure 7.12. Although this specimen was moulded very loose, the graphs show typical contractant behaviour with strain hardening and pore pressure generation due to the very high pressures of confinement.

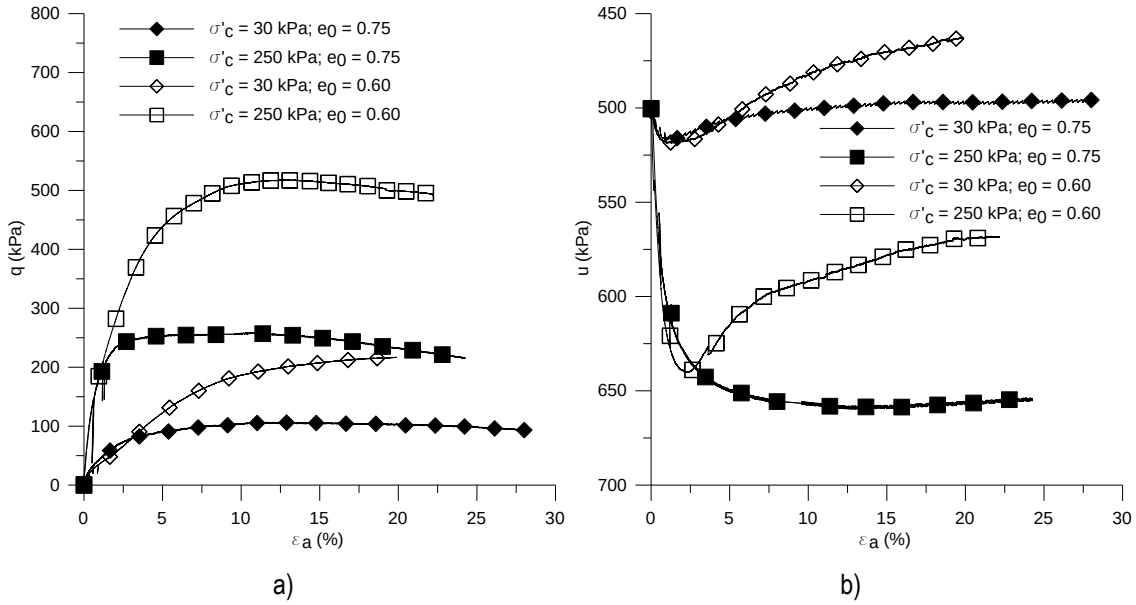

Figure 7.11 Stress-strain-pore water pressure response of the silty sand at low pressures: (a) stress-strain behaviour (b) pore pressure behaviour

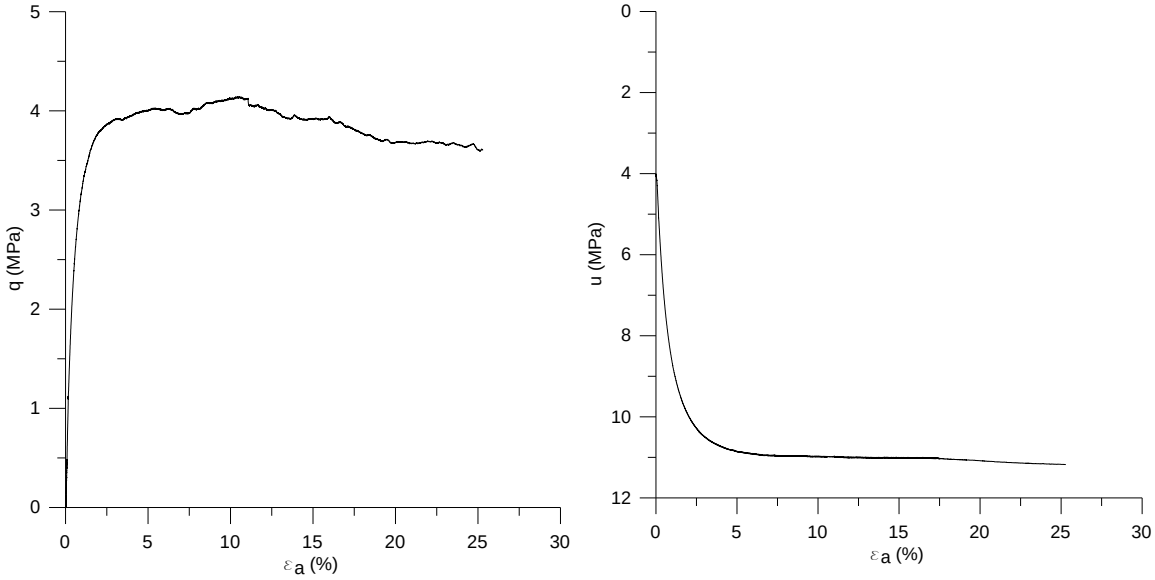

Figure 7.12 Stress-strain-pore water pressure response of the silty sand at 10 MPa of confining pressure (a) stress-strain behaviour (b) pore pressure behaviour

7.7 Cemented specimens triaxial tests results

7.7.1 Drained triaxial tests

Drained triaxial tests at low pressures (with 30, 80 and 250 kPa of effective confining pressure) were executed over four types of specimens (with four different cement contents) corresponding to two adjusted porosity/cement ratios ($n/C_{iv}^{0.21}$=36 and 29), comprising 12 tests. The results of these tests presented in Figure 7.13 refer to stress-strain curves, plotting the deviator stress (q) against the axial strain (ε_a), and strain-volume curves that is the axial strain against the volumetric strain (ε_v).

The purpose of presenting a graph for each confining pressure is to show that two different types of behaviour are found depending on the adjusted porosity/cement ratio, highlighting that the dosage, quantified by the adjusted porosity/cement ratio, plays the most significant role in the cemented soil behaviour. The stress-strain curves of Figure 7.13 clearly evidence that the specimens with $n/C_{iv}^{0.21}$=29 have higher peak deviator stresses than the specimens with $n/C_{iv}^{0.21}$=36 independently of the cement content, while in contrast, this difference is not observed in the volumetric curves. Adding cement to the sand had the effect of increasing the shear strength by up to five times for the adjusted porosity/cement ratio of 36 and by tenfold for the adjusted porosity/cement ratio of 29.

All specimens initially compressed, followed by significant dilation, which was associated to a peak strength, before strain softening. This is typical of cemented soils, with the maximum rate of dilation taking place right after the peak strength (Viana da Fonseca, 1996, 1998, Schnaid et al., 2001). The peak strength corresponds to the onset of significant breakage in the cement, while dilation involves particle rearrangement that is only possible after bonding breakage. Assuming only compressive volumetric deformations up to the point of zero dilation, beyond this point yielding exists, which indicates that the onset of cement breakage is progressive starting even before peak. However, being the peak strength not frictional but controlled by the cement yielding, then most destructuration may take place only at peak.

7.7.2 Undrained triaxial tests

Tests at low pressures

Undrained triaxial compression tests in specimens in the same four moulding conditions of the previous section, were performed at 80 kPa and 250 kPa, comprising eight tests. The results, presented in Figure 7.14, were again plotted for each confining pressure in function of the adjusted porosity/cement ratio, showing that the pore pressure rose sharply up to a peak after which it decreased to a stable value less than half the peak. The same considerations stated before for the drained tests with respect to the different behaviour for each $n/C_{iv}^{0.21}$ could be done for the undrained tests. Moreover, another interesting feature can be observed. Most specimens with higher initial stiffness have lower peak deviator stress. This is more clear in the undrained tests with 80 kPa plot (Figure 7.14a) but the same has been detected in the drained specimens as well.

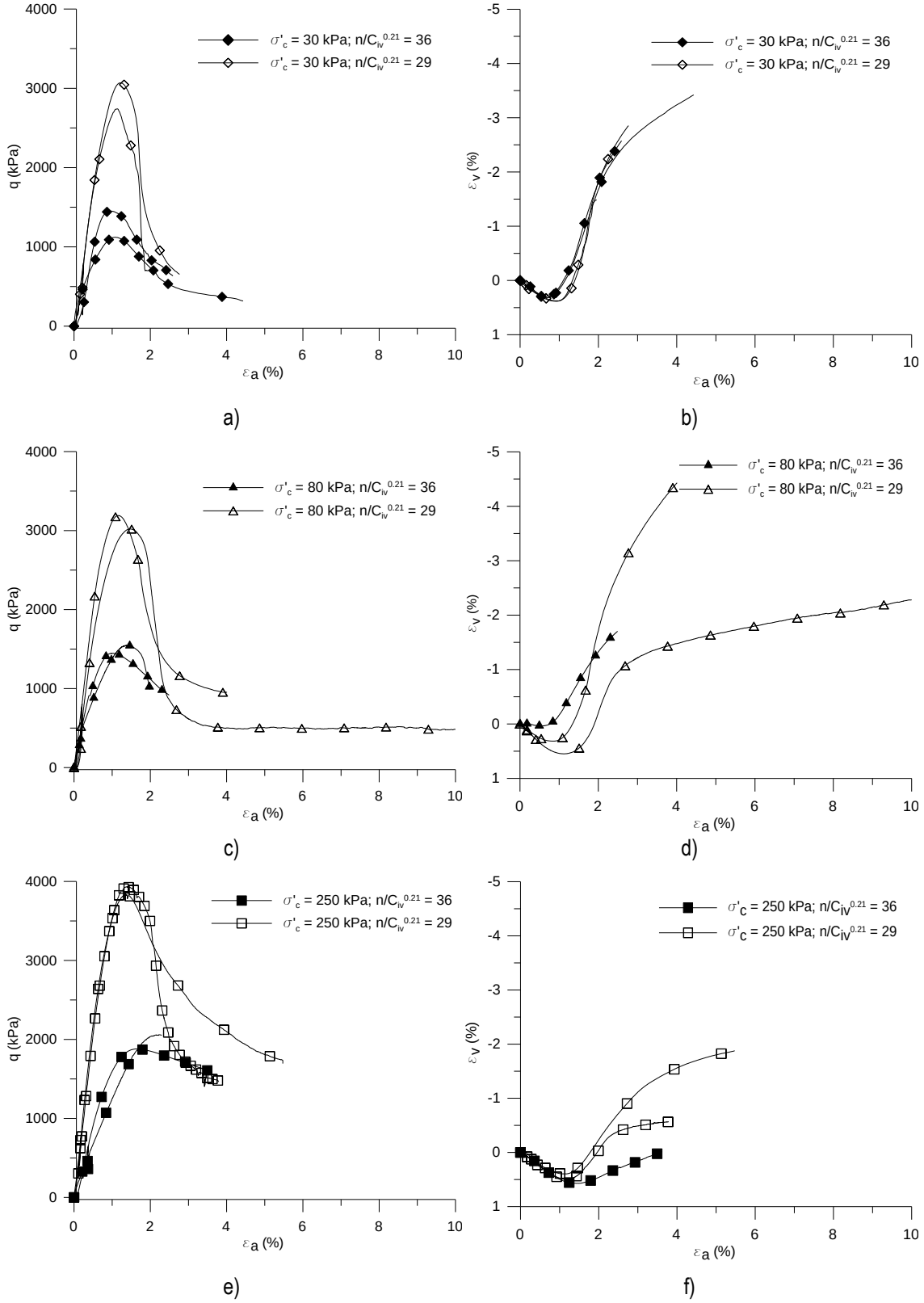

Figure 7.13 Stress-strain and strain-volume curves for cemented specimens: a), c) and e) stress-strain curves for 30 kPa, 80 kPa and 250 kPa of confining pressure respectively; b), d) and f) strain-volume curves for 30 kPa, 80 kPa and 250 kPa of confining pressure respectively

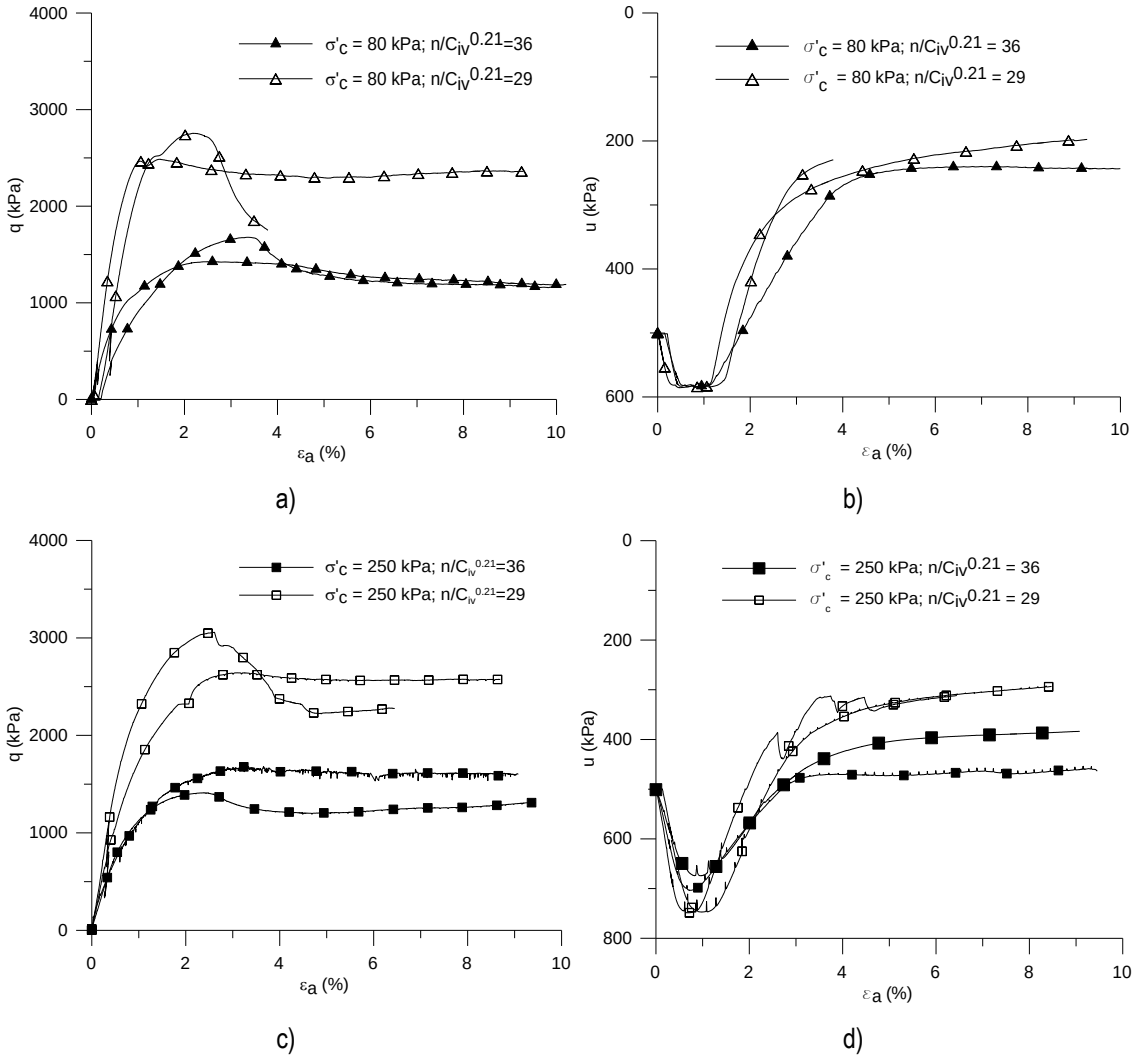

Figure 7.14 Stress-strain-pore pressure curves of the undrained triaxial tests: a) and b) stress-strain curves for 80 kPa and 250 kPa; c) and d) strain-pore pressure curves for 80 kPa and 250 kPa

Tests at high pressure

Another four tests at two different moulding conditions (Table 7.3) but the same adjusted porosity/cement ratio ($n/C_{iv}^{0.21}=29$) were performed at very high pressures (10 and 20 MPa). The results are plotted in Figure 7.15 where it is clear that for each confining pressure the behaviour is very similar. Specimens with lower confining pressures have higher peak deviator stresses and lower pore pressure generation. The discrepancy of the curves after peak may be due to strain localisation.

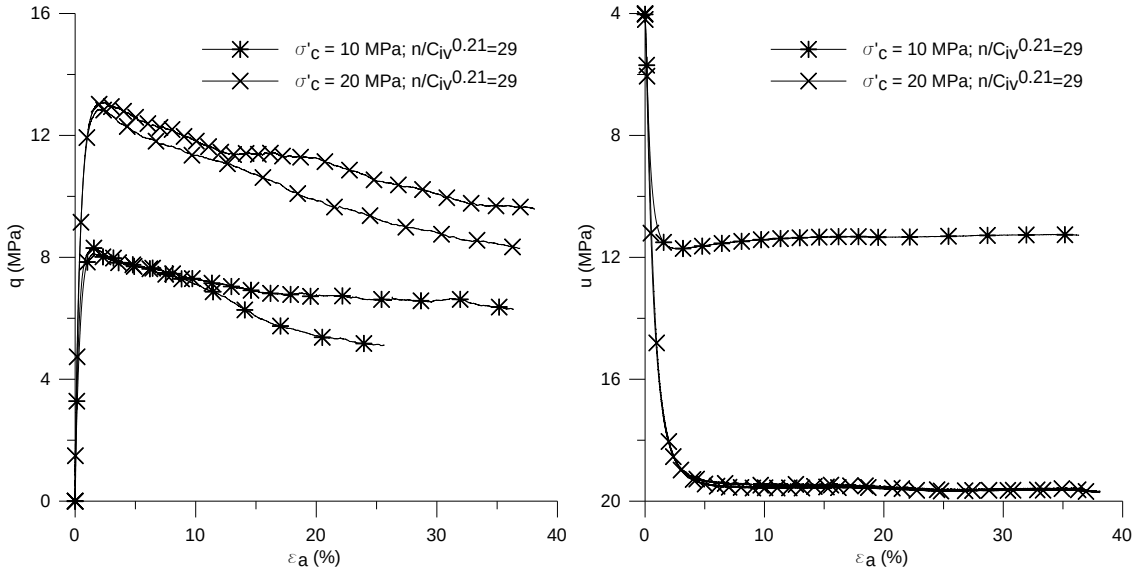

Figure 7.15 Results of the high pressure tests executed at cemented specimens with $n/C_{iv}^{0.21}=29$

7.8 Final void ratio evaluation

7.8.1 Uncemented specimens

The four different procedures presented in section 7.3.4 for the final void ratio calculation will be now analyzed starting in this section by the uncemented specimens tested in low pressure triaxial tests.

A judicious analysis of the data comprised by drained and undrained uncemented triaxial tests allows some preliminary conclusions. The comparison between the moulding dry weight and the final dry weight reveals that the initial dry weight is slightly higher although the differences are not significant (the maximum discrepancy of 0.8% has an impact in the void ratio of around 0.01). The saturation degree calculated through equation (7.10) from the final void ratio (obtained by method 3) and from the final water content stays around 100% (always a little bit higher) but in one test it went up to 127%, indicating that there might be some error perhaps in the final water content.

The results of the final void ratios are summarized in Table 7.5. It is interesting to observe that methods 2 and 4 give similar values although derived from different tests measurements indicating that there is some agreement in the data. On the other hand, the results from method 1 are always different from the others, sometimes very different, demonstrating that there might be some problem in the final water content. The difference seems to be higher in the specimens consolidated to 250 kPa where the volume change is more significant meaning that apparently this method does not seem to be so sensible, as

the final water contents are always similar irrespective of the consolidation stress. Method 3 also depends on the final water content but this test measurement is compensated by the unit weight calculated from the final humid weight.

The low reliability on the final water content may be related to some problems in their measurements. As the porous stones were usually stuck to the soil at the end of the test, in some cases, the wet soil together with the filter papers, membrane and porous stones were weighted before and then using some distilled water the porous stones and filter papers were cleaned and weighted separately, so that the wet weight could be the difference between the first measure and the weight of the porous stones and filter papers. The problem of this procedure is to know if the porous stones and filter papers were exactly with the same moisture during the first and the second measurement. The procedure was established because it was assumed that at the end of the test soil, filter papers and porous stones would be completely saturated and therefore, cleaning them from the soil grains would not make them heavier. However, this assumption may be wrong if soil absorbs water from the porous stones.

Considering the reliability of method 2, this procedure was chosen for the subsequent analysis namely for the calculation of the void ratio during the test.

Table 7.5 Comparison between four different methods of calculating the final void ratio

	Test name	$e^{\text{Method 1}}$	$e^{\text{Method 2}}$	$e^{\text{Method 3}}$	$e^{\text{Method 4}}$
Drained tests	CV0_30	0.759	0.728	0.732	0.729
	CV0_80	0.706	0.708	0.704	0.708
	CV90_0_30	0.685	0.619	0.634	0.619
	CV90_0_100	0.608	0.546	0.554	0.548
	CV90_0_250	0.602	0.485	0.493	0.485
Undrained	CIU_0_30	0.744	0.733	0.740	0.735
	CIU_0_250	0.696	0.671	0.679	0.674
	CIU90_0_30	0.666	0.587	0.594	0.588
	CIU90_0_250	0.637	0.494	0.502	0.495

7.8.2 Cemented specimens

In complement to the procedure presented before for uncemented tests, the comparison between the four different methods of calculating the final void ratio will be shown for cemented triaxial tests.

The comparison between initial and final dry weight as a means for test measurements control will be expressed in the same way as for uncemented specimens. In the cemented specimens the difference between the initial and final dry weight is a little bit higher, especially in the low pressure drained tests, but is mostly below 0.8% of the initial dry weight except in three tests. However, it is interesting to notice that, conversely to

uncemented tests, in these tests the final dry weight is higher than the initial value, which cannot be explained by loss of particles during the specimen recovery at the end of the test. Being a consistent observation in all cemented tests (drained and undrained at low and high pressures) it is hardly to believe that it is related to a less rigorous evaluation of the moulding dry weight as stated in section 7.3.4. This anomalous observation may be related to the cement hydration during the curing process. In the first place, the weight of soil and cement were measured, but in the final measurement clusters of soil-cement hydrated with water were weighted. Moreover, the differences seem to increase with the cement content as it is expressed in Figure 7.16 for the low pressure results. The high pressure tests are not included for simplicity and due to their limited number of tests in several cement contents, although the same trend was also observed in these tests.

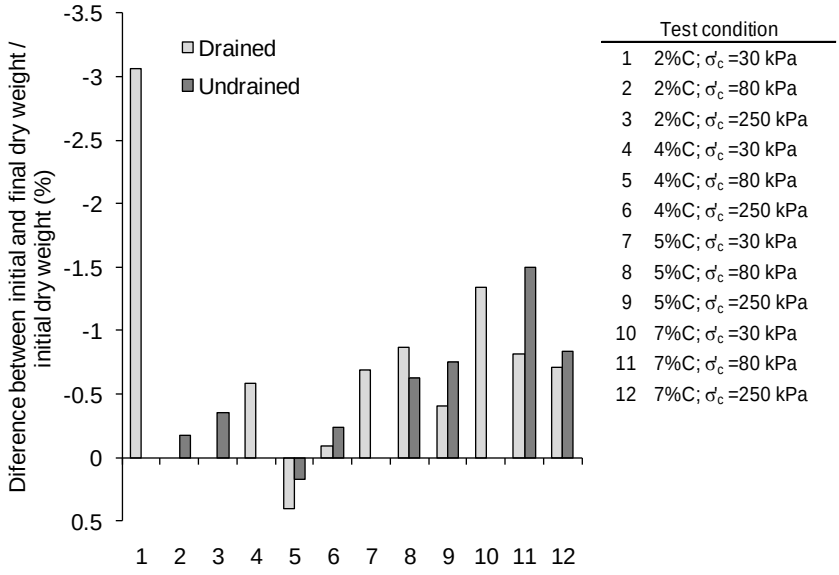

Figure 7.16 Percentage of the difference between initial and final dry weight divided by the initial dry weight in function of test conditions (negative values correspond to an increase in the dry weight)

In terms of the saturation degree calculated by the final void ratio obtained through method 1 and by the final water content, the values are lower than in uncemented specimens. In drained low pressure tests it ranges between 82 and 94%, while in undrained low pressure tests the saturation degree is higher floating around 100%. In the isotropic high pressure tests the saturation degree ranges between 86 and 123% while the undrained shear triaxial tests results are more constant varying between 95 and 97%.

Table 7.6 evidences the comparison of the four methods to compute the final void ratio where it is also clear a good agreement between methods 2 and 3. The differences between the void ratios derived from method 1 and the others are higher where the

reported saturation degree is lower, namely in the low pressure drained tests. This divergence may be a consequence of a wrong final water content measurement, as explained in detail on the previous section. For this reason, method 2 was, once again, considered to be the most reliable method and was used subsequently for the following calculations.

Table 7.6 Comparison between four different methods of calculating the final void ratio

	Test name	$e^{Method\ 1}$	$e^{Method\ 2}$	$e^{Method\ 3}$	$e^{Method\ 4}$
Low pressure drained tests	CV2_30	0.507	0.667	0.617	0.667
	CV4_30	0.655	0.780	0.769	0.785
	CV4_80	0.660	0.737	0.744	0.741
	CV4_250	0.620	0.723	0.722	0.731
	CV5_30	0.509	0.607	0.595	0.625
	CV5_80	0.518	0.643	0.626	0.643
	CV5_250	0.540	0.592	0.586	0.604
	CV7_30	0.586	0.691	0.669	0.693
	CV7_80	0.622	0.673	0.660	0.670
	CV7_250	0.539	0.615	0.604	0.616
Low pressure undrained tests	CIU2_80	0.614	0.596	0.605	0.605
	CIU2_250	0.583	0.597	0.592	0.597
	CIU4_80	0.701	0.741	0.745	0.750
	CIU4_250	0.700	0.714	0.716	0.726
	CIU5_80	0.612	0.583	0.574	0.585
	CIU5_250	0.585	0.566	0.554	0.566
	CIU7_80	0.613	0.629	0.605	0.642
	CIU7_250	0.785	0.633	0.622	0.640
Isotropic high pressure tests	ISO(2)	0.288	0.308	0.310	0.308
	ISO(4)	0.399	0.324	0.323	0.324
	ISO(5)	0.310	0.368	0.358	0.368
	ISO(7)	0.324	0.346	0.335	0.346
Undrained high pressure tests	CIU(5)_10000	0.537	0.526	0.516	0.526
	CIU(5)_20000	0.432	0.435	0.421	0.435
	CIU(7)_10000	0.617	0.567	0.570	0.567
	CIU(7)_20000	0.475	0.463	0.450	0.463

7.9 Stiffness evaluation

7.9.1 Uncemented specimens

In the uncemented low-pressure tests, two small static cycles were performed during shearing. The first was executed between 15% and 5% of the expected peak deviator stress (q_f) and the second was performed between 30% and 15% of the same value (q_f). These loads were selected to avoid soil yielding before the cycles so the modulus could be assumed elastic (Figure 7.17a), but in some cases (mostly at the lowest confining pressure) the stress-strain plot seems to be curved right from the beginning indicating a progressive yielding (Figure 7.18a).

To have a more reliable evaluation of the stiffness modulus in these cycles local instrumentation was used, with the average value of the two axial transducers being taken (except when there was any problem with one of them). The stiffness modulus (E_{ur}) corresponds to the gradient of the line that links both peaks of the hysteresis loop as shown by Figure 7.17b) and 7.18b).

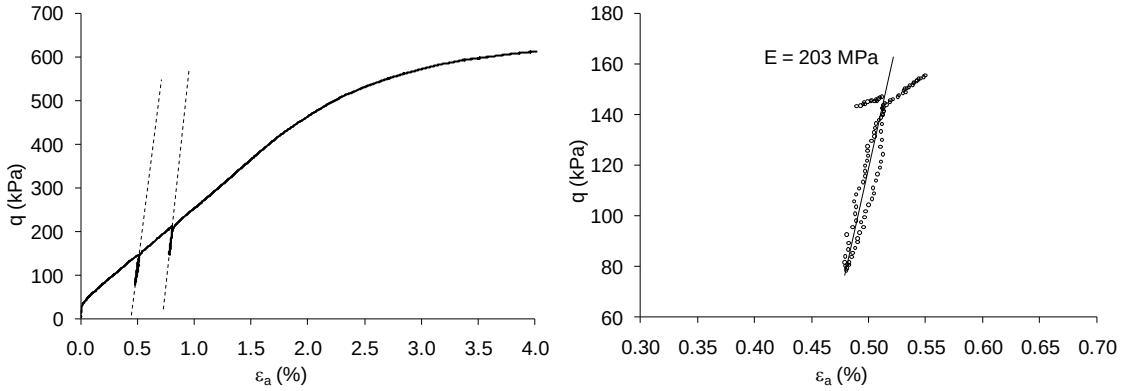

Figure 7.17 Part of the stress-strain curve of the test CV90(0)_250: a) stress-strain curve with the two load cycles; b) stiffness modulus obtained in the first cycle.

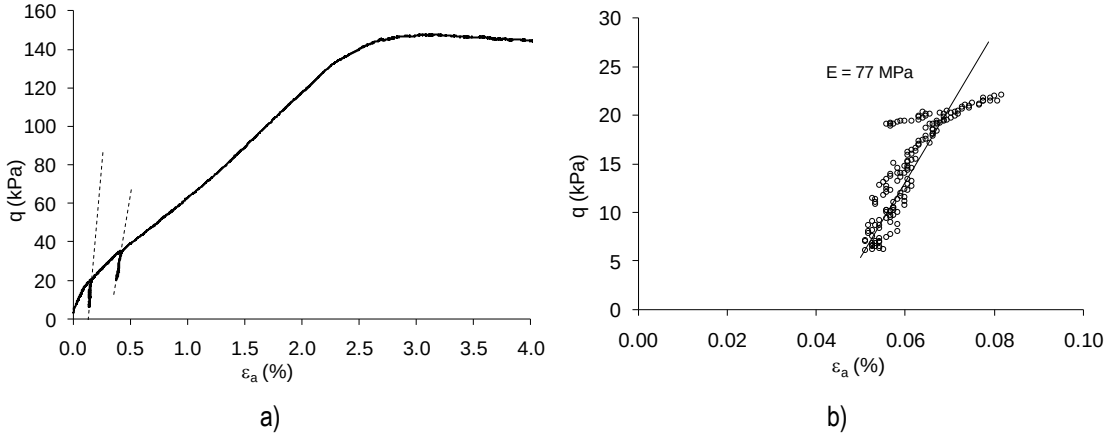

Figure 7.18 Part of the stress-strain curve of the test CV90(0)_30: a) stress-strain curve with the two load cycles; b) stiffness modulus obtained in the first cycle.

The results are plotted in Figure 7.19 for both cycles. It is interesting to observe that the second cycle has higher stiffness than the first cycle except when the confining pressure was 30 kPa which corresponds to an early yielding (Figure 7.18). The stiffness modulus tends to increase with the confining pressure.

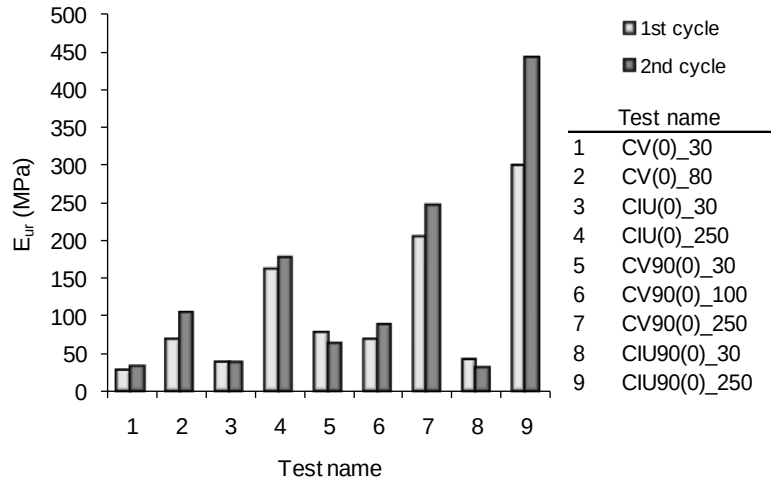

Figure 7.19 Stiffness modulus obtained in each one of the load cycles

In order to remove the effect of the confining pressure from the previous results, the stiffness moduli were divided by the average mean effective stress obtained in unloading and reloading (p'_{ur}). However, this created a different behaviour between drained and undrained tests, as the effective stress increases on the first and decreases on the second type of tests. In the normalisation, plotted in Figure 7.20, the second cycle also exhibited a higher ratio E_{ur}/p'_{ur} than the first cycle (except for some specimens confined to 30 kPa), in opposition to what should be expected from a progressive degradation of the elastic stiffness. In the drained test this could be due to the reduction in the void ratio during the first part of the test where these cycles were performed, but in undrained tests this is not expected, indicating that there may be some problems of measurement.

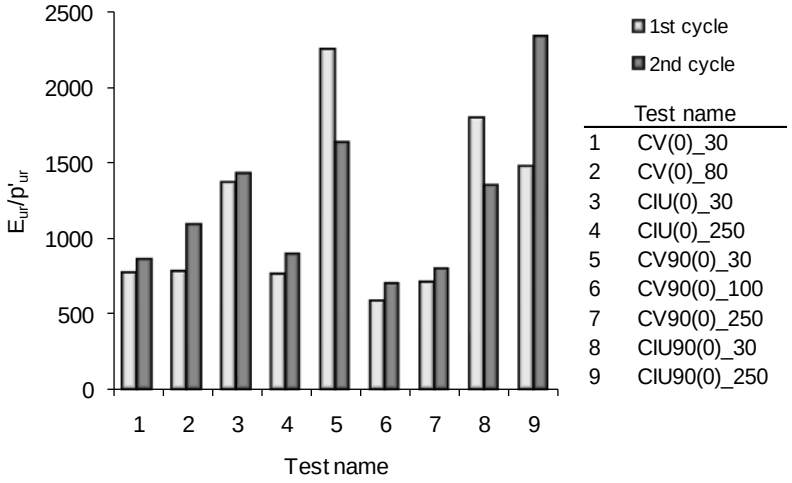

Figure 7.20 Normalised stiffness modulus obtained in each one of the load cycles

The evolution of the secant modulus was also analysed so that a better understanding of stiffness behaviour in this soil could be investigated. For that purpose, the ratio of the secant stiffness modulus (E_{sec}) by the mean effective stress (p') was plotted against the deviator stress (q) normalised by the peak value (q_f). A different pattern of behaviour was observed on drained and undrained tests and, for that reason, they are shown separately in Figure 7.21, although with the same scales in the xx and yy axes. The rate of degradation of the secant stiffness modulus seems faster in the drained tests, while in the undrained tests the stiffness presents higher values for most of the tests. This fact might be related to the dilation that occurs in most of drained tests at higher strain levels, in the sense that it reduces the number of contacts between particles and therefore, the stiffness decreases. Moreover, undrained tests reach the yield surface much faster than drained tests due to their stress-paths.

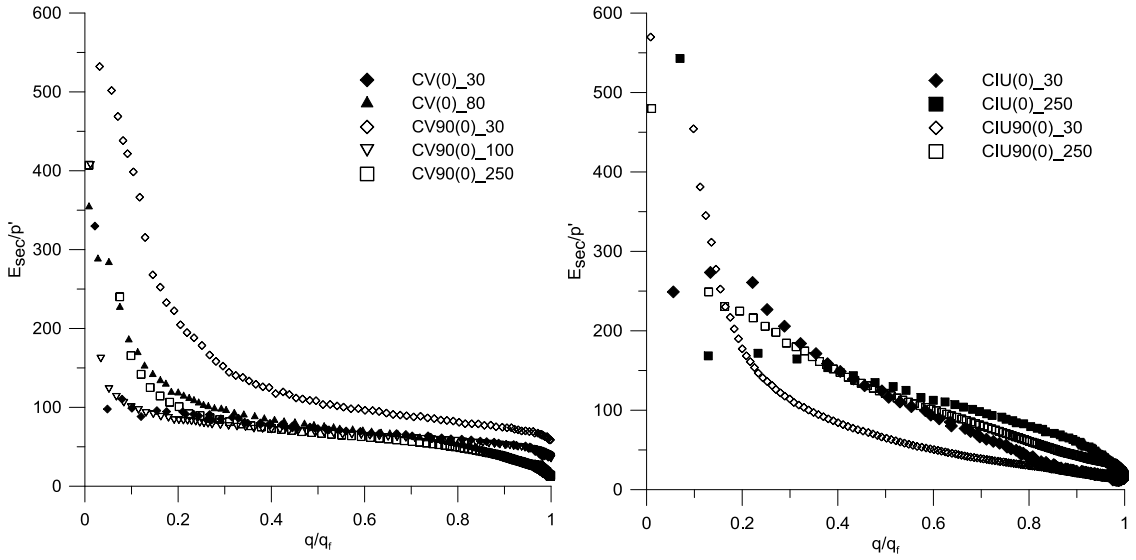

Figure 7.21 Normalised secant stiffness modulus: a) drained triaxial tests; b) undrained triaxial tests

It is also interesting to observe that most tests within the same group have similar ratio E_{sec}/p' in spite of their initial void ratio or confining pressure. The exception is the drained and undrained tests consolidated to 30 kPa and with initial void ratio of 0.6 indicating perhaps that the consolidation pressure was not enough to remove the effect of compaction.

Another interesting way to look at the secant modulus is to plot it against the axial deformation in logarithmic scales as in Figure 7.23 where drained and undrained tests are again distinguished. According to Malandraki and Toll (1996) this plot allows the identification of the "first" and "second yield" points (Figure 7.22).

The drained tests (Figure 7.23a) show a clear change in the slope of the stiffness degradation curve which should be associated with a second yield point. Unfortunately, it is not certain that this second yield point corresponds to Y2 in terms of Jardine's model (Jardine, 1992) described in chapter 4 (section 4.6), although it may be considered that it constitutes a gross yield approximately close to the end of the linear part of the stress-strain curve.

This can be easily checked looking at the stress-strain curve of CV90(0)_100 in Figure 7.17a) and comparing it with the secant stiffness degradation curve of the same test in Figure 7.23a). It is interesting to notice that the same cannot be deduced from undrained tests as most of the tests represented in Figure 7.23b) do not evidence a well defined change in the slope of the degradation curve.

Unfortunately, the Y1 yield point (Jardine, 1992) corresponding to the "first yield" of Malandraki and Toll (1996) was not possible to detect in these tests, possibly due to the low level of accuracy of strain transducers, or some limitation in the perfect pivoting of these instruments in the specimen.

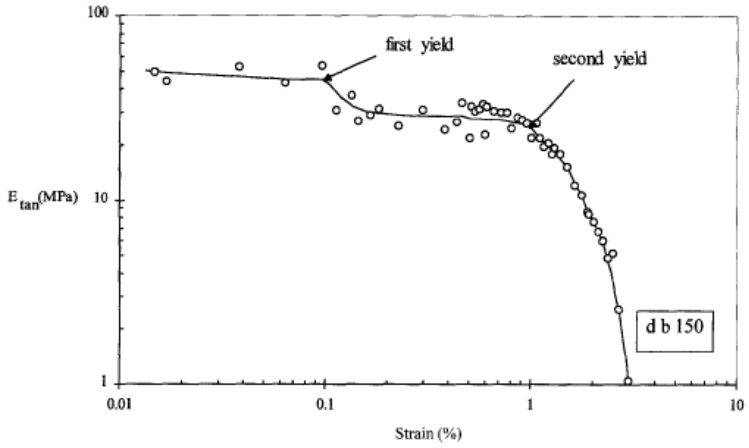

Figure 7.22 First and second yield defined from the tangential stiffness graph (Malandraki and Toll, 1996)

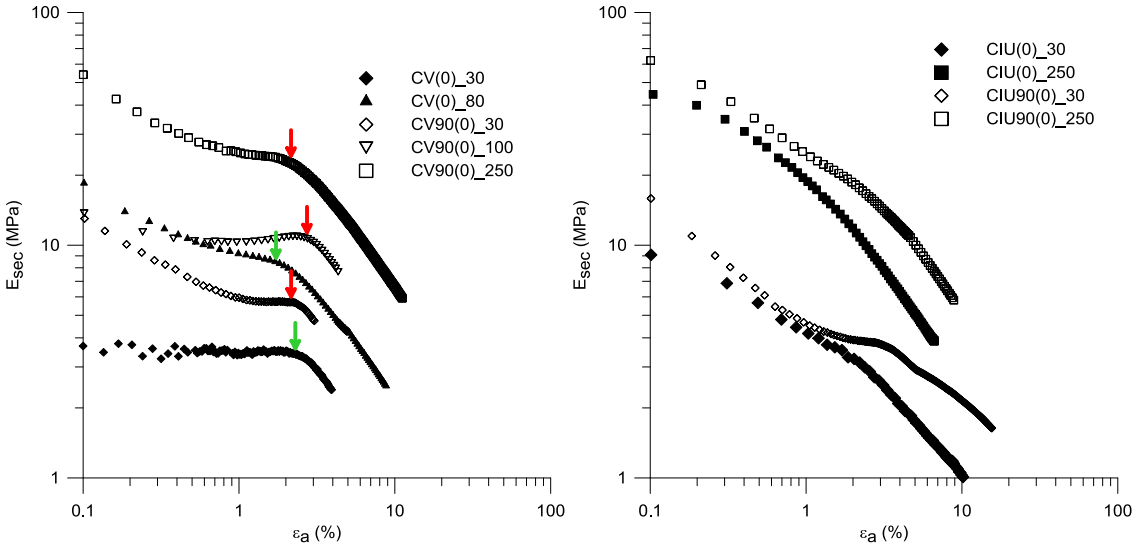

Figure 7.23 Secant stiffness modulus: a) drained triaxial tests; b) undrained triaxial tests (Note: the arrow points identify second yield points)

7.9.2 Cemented specimens

Just like the uncemented triaxial tests, load cycles were performed during shearing of the cemented specimens. However, in this case, only one cycle was executed between 30% and 15% of the expected maximum deviator stress. Figure 7.24 summarizes the results for drained and undrained triaxial tests.

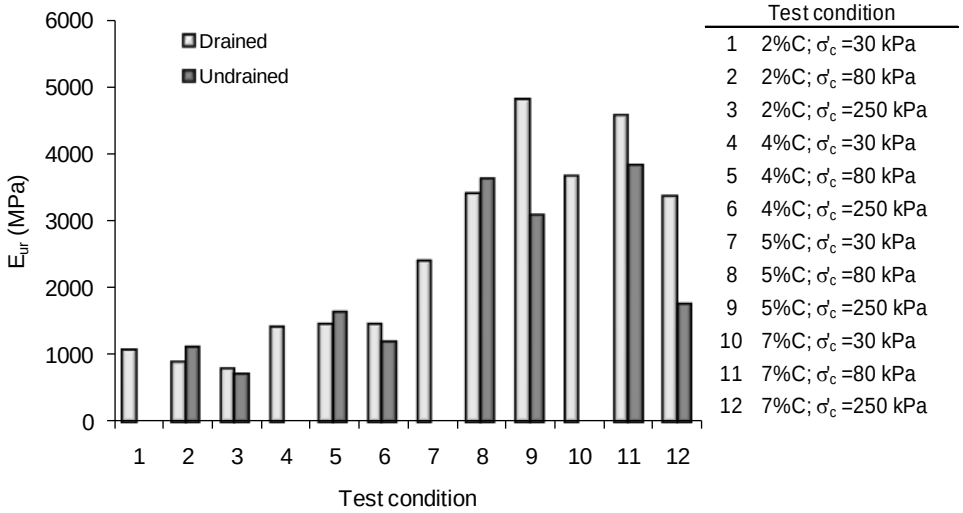

Figure 7.24 Stiffness modulus obtained in the load cycles

The values of the unload-reload modulus obtained from these triaxial tests are higher than the initial tangent modulus obtained in unconfined compression tests presented in Chapter 6 (section 6.5.3). This can be considered expected because an unload-reload modulus is

usually assumed to follow an elastic pattern, if performed at low ranges of cyclic stress, while in the initial monotonic loading path some compliance errors of strain gauges may be presented.

This graph also evidences a clear and almost discrete increase in the stiffness modulus values for the specimens with $n/C_{iv}^{0.21}$=29 (5% and 7% cement contents) in comparison with the specimens with distinct ratio $n/C_{iv}^{0.21}$=36 (2% and 4% cement contents). This could be even clearer if the instrumentation would perform completely satisfactory in the highest cemented mixtures (that is for 5% and 7% of cement content).

Following the same procedure applied in the uncemented specimens, the unload-reload modulus was normalised by the average mean effective stress in order to remove the effect of the confining pressure (Figure 7.25). The normalised results indicate a reduction of the normalised modulus when the confining pressure increases in most specimens. This is a sign of the induced interparticle bonding drop with the stress confinement increase. Additionally, the normalised modulus seems to be higher in undrained conditions for the less cemented specimens while for the higher cemented specimens an inverse behaviour is observed. This trend, which cannot be considered too much consistent, may be a sign of the low influence of the effective stress in such cemented mixtures, where bonding may prevail when comparing such values.

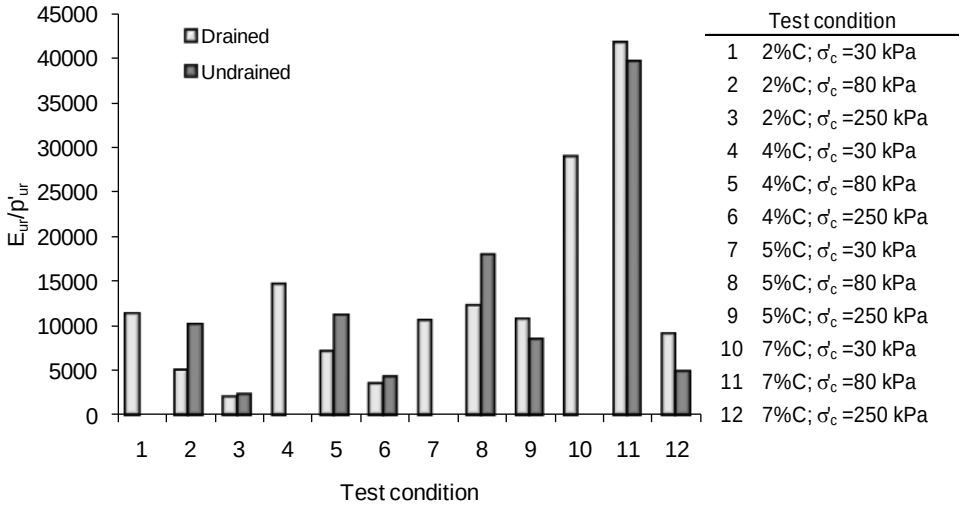

Figure 7.25 Normalised stiffness unload-reload modulus obtained in each test

The secant modulus was also analysed in the cemented specimens. The graphs of Figure 7.26 and 7.27 plotting the normalised modulus against the normalised deviator stress show a different pattern between the two adjusted porosity/cement ratios. As expected, the specimens with $n/C_{iv}^{0.21}$=36 show lower stiffness than the specimens with a lower ratio ($n/C_{iv}^{0.21}$=29). The higher difference of the pattern of degradation curves in the weaker ratio

($n/C_{iv}^{0.21}$=36) is a clear sign of the utmost sensitivity of these mixtures to the stress level including damaging, while in the strongest cement ratio the stability of the degradation pattern is clearly a sign of the prevailing bonding towards the stress level.

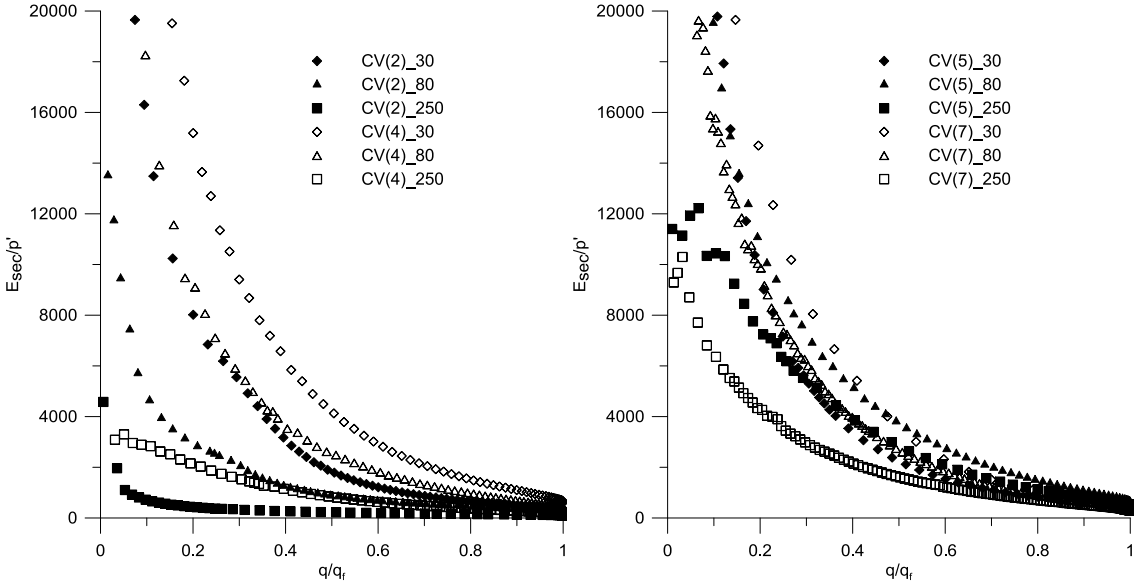

Figure 7.26 Normalised secant stiffness modulus in drained tests of cemented specimens: a) $n/C_{iv}^{0.21}$=36; b) $n/C_{iv}^{0.21}$=29

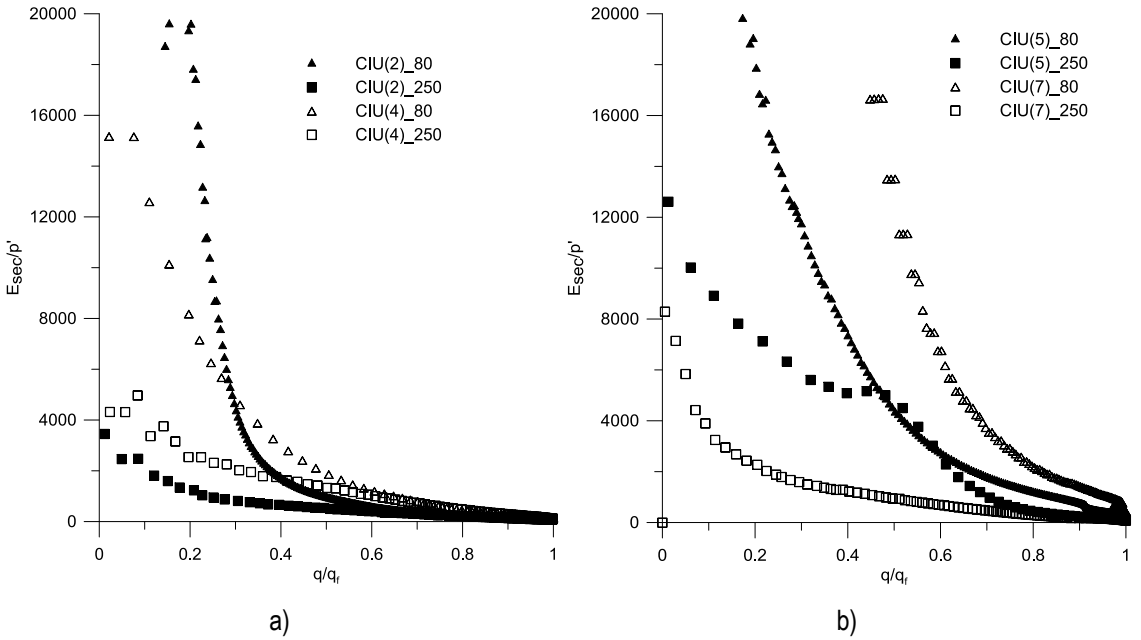

Figure 7.27 Normalised secant stiffness modulus in undrained tests of cemented specimens: a) $n/C_{iv}^{0.21}$=36; b) $n/C_{iv}^{0.21}$=29

The next set of graphs relating the secant modulus against the axial strain in Figure 7.28 and 7.29 also show the same patterns but it is not possible to identify the second yield point, as described for the uncemented specimens, except for some 2% specimens tested drained. In the same graphs a dashed line is drawn, indicating the strain (around 10^{-4}) where a clear and continuous reading starts to be observed. At that point, most of the tests evidence a sharp drop on the stiffness degradation curve indicating that the first yield point should be before or at that point. Before this point there is not enough accuracy to identify a yield point and thus, to distinguish between the yielding behaviour of more and less cemented specimens.

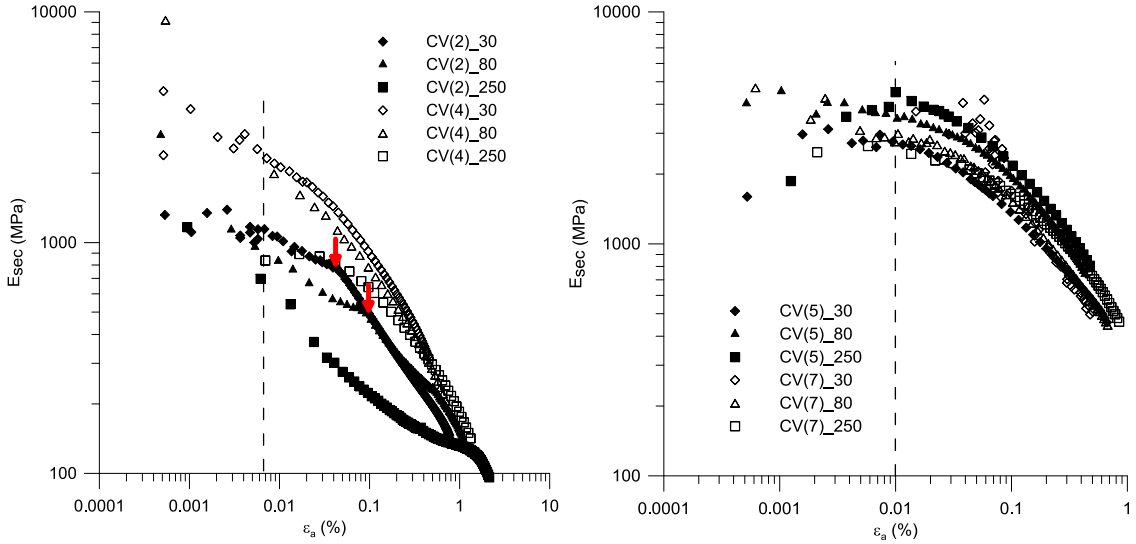

Figure 7.28 Secant stiffness modulus in drained tests of cemented specimens: a) $n/C_{iv}^{0.21}=36$; b) $n/C_{iv}^{0.21}=29$

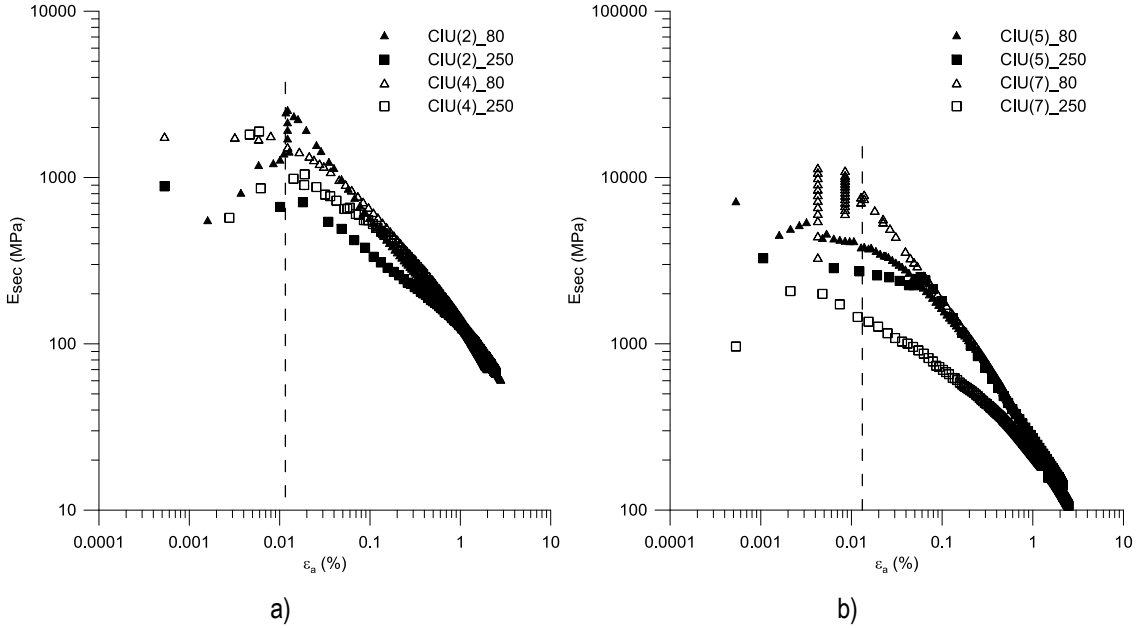

Figure 7.29 Secant stiffness modulus in undrained tests of cemented specimens: a) $n/C_{iv}^{0.21}=36$; b) $n/C_{iv}^{0.21}=29$

7.10 Stress-paths in q vs p' plot

7.10.1 Uncemented specimens

In Figure 7.30 all the tests presented in sections 7.6.1 and 7.6.2 are plotted together in terms of the stress-paths defined in the q vs p' plane, being q the deviator stress and p' the mean effective stress. All the tests were performed with constant confining pressure and increasing axial stress, thus, the drained tests show linear stress-paths which gradient q/p' is equal to 3. Looking at the undrained stress-paths it is possible to observe that one of the low pressures specimens consolidated to 250 kPa seems to be moulded on the wet side of critical as well as the high pressure one moulded to 10 MPa because the stress-path show a decrease on the mean effective stress.

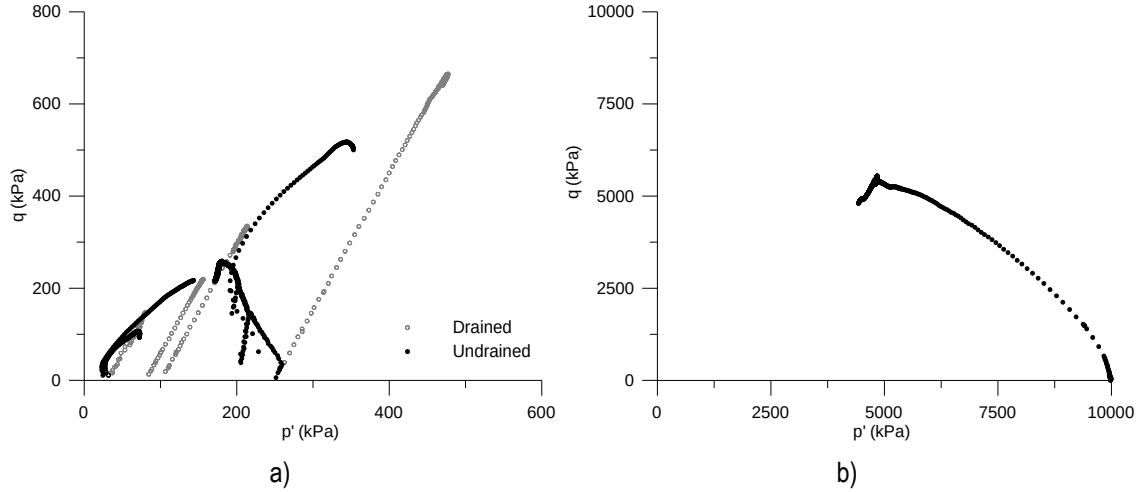

Figure 7.30 Drained and undrained stress-paths of triaxial compression tests over uncemented specimens: a) low pressures; b) high pressures

7.10.2 Cemented specimens

In this section the stress-paths for low and high pressures tests of cemented specimens will be presented. Drained and undrained stress-paths obtained in the low pressure triaxial tests, illustrated in Figure 7.31, are all dilatant with clear localisation and strain softening. The two adjusted porosity/cement ratios are distinguished as the peak strengths are completely different. The drained tests reach higher peaks than the undrained tests, as evidenced in Figure 7.31 but especially in Figure 7.31b), suggesting that they might have suffered less from localization. Hamidi and Haeri (2008) have also reported a similar behaviour stating that drained specimens are more brittle than undrained ones. In the graphs of Figure 7.31 it is also marked the peak points, considered at the maximum deviatoric stress.

It should be remembered that according to the elasticity theory, an isotropic soil subjected to an elastic undrained loading, which does not involve any volumetric strains, follows a vertical stress-path (Muir Wood, 2004). In the stress-paths of the cemented tests results only the more confined tests show some kind of vertical stress paths. The less confined tests have a curved stress-path right from the beginning indicating that they may have suffered shear plastic deformations at that stage. Also the load cycles performed at low deviatoric stresses can impose small plastic strains that can explain the stress-path. However, in the middle of all undrained tests the stress-path seems to follow the slope of the drained tests, as if there was some kind of drainage.

The stress paths started from high pressures are typical of normally consolidated soils with contractant behaviour associated to strain-softening (Figure 7.32). If there wasn't strain localisation they would probably converge, following the critical state line.

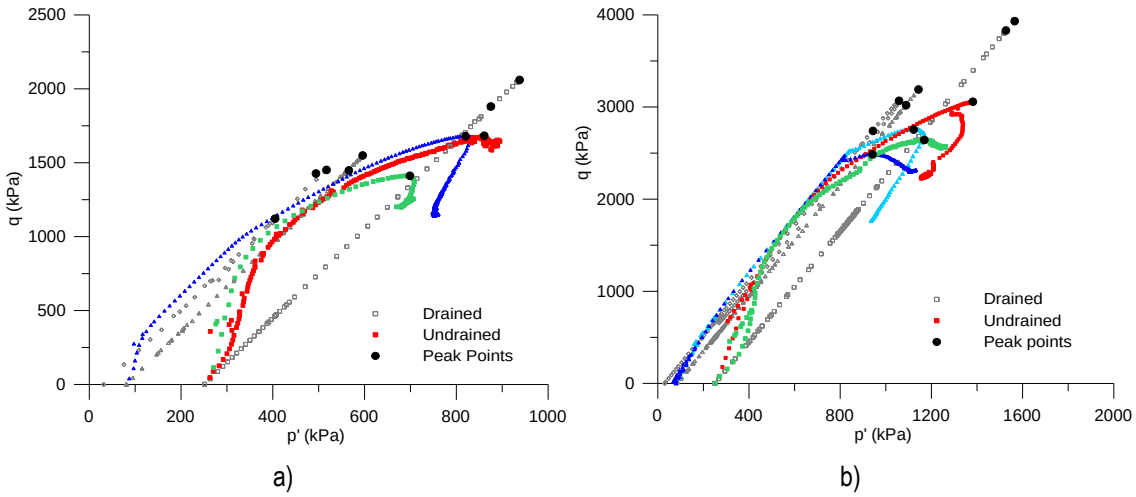

Figure 7.31 Drained and undrained stress-paths of triaxial compression tests over cemented specimens: a) $n/C_{iv}^{0.21}$ =36; b) $n/C_{iv}^{0.21}$=29 (the scale of xx and yy is different to allow a better zoom)

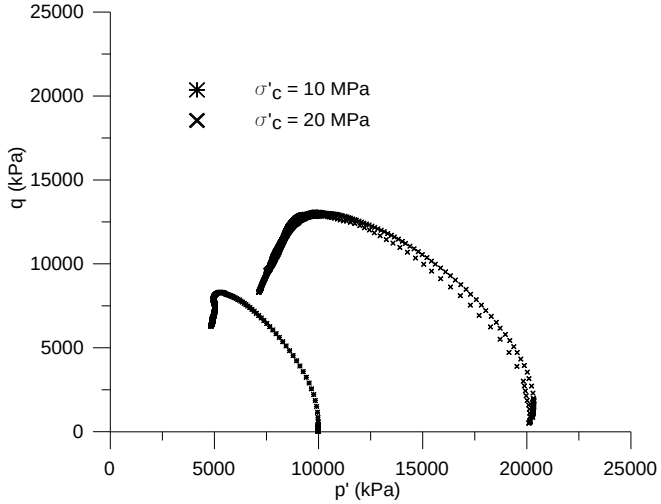

Figure 7.32 Undrained stress-paths of high pressure triaxial tests over cemented specimens ($n/C_{iv}^{0.21}$=29)

7.11 Strength envelopes and post rupture analysis through Mohr circles

7.11.1 Introduction

All the cemented specimens tested in triaxial tests suffered strain localisation. Therefore, it becomes difficult to rely on the local instrumentation at strain levels close and after the peak, but especially at ultimate conditions. For this reason, instead of plotting the strength envelopes in the q versus p' plot a different approach based on the Mohr circles was developed which will be described below.

In the uncemented specimens this problem is not present so the conventional strength envelope on the q versus p' plot will be compared to the Mohr circle methodology.

7.11.2 Post rupture analysis

Burland (1990) has first presented the concept of post rupture strength in specimens that show shear strain localization. As it is shown on Figure 7.33, the author has demonstrated that after the development of the slip surface, usually at peak, the overall strains are not the same as the local strains, and the stress state at this failure surface is not represented by the principal stresses monitored by the radial and axial stresses in the specimen. Thus, the post rupture deformation consists on a near-rigid body sliding on the failure plane.

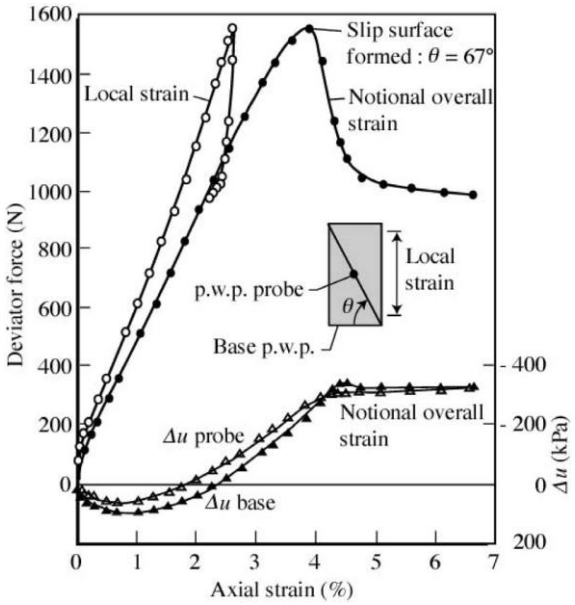

Figure 7.33 Unconsolidated undrained triaxial test with pore pressure measurement in Tody clay showing post-rupture behaviour (Burland, 1990)

In general, the interpretation of triaxial tests results takes into account that the global stress-strain measurements are representative of the conditions throughout the

deformation process and at all points within the specimen. If strains incur in localization during the deformation process, then, clearly, global behaviour obtained by boundary measurements of force and displacements would not be representative of the stress-strain behaviour within the deforming mass after localization. Consequently, the strength can no longer be analysed in terms of axisymmetric stress invariants, but the stresses acting on the shear plane can be determined. This is especially important in the evaluation of steady-state conditions.

7.11.3 Cemented specimens

The procedure based on the Mohr's circles analysis used by Gasparre (2005) was applied to calculate the stresses acting on the shear plane by measuring the angle of the shear plane of the specimens after testing. This angle can be represented in a Mohr circle plot, as the angle that the line drawn from the pole does with the horizontal axes (α in Figure 7.34). Finally, the stresses on the shear plane failure are those that result from the intersection of the Mohr circle with the line representing the shear plane as indicated on Figure 7.34 by point A. As the figure demonstrates the tangent to the strength envelope (point B in the Figure) does not coincide with point A and therefore, the stresses on the planes (σ',τ) cannot be determined by the tangent but by point A. In Appendix B, the Mohr circle equation is presented and the intersection with the failure plane is explained in detail.

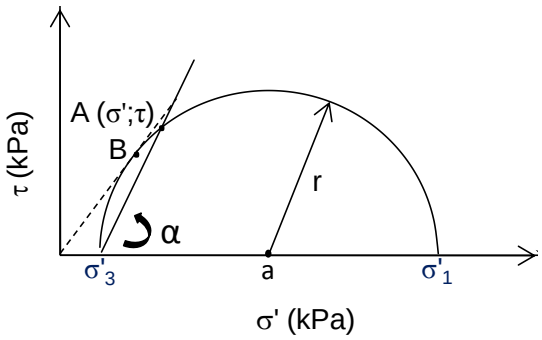

Figure 7.34 Mohr circle analysis

The angle of the shear plane failure observed in the cemented specimens was around 65º degrees. In Figure 7.35 the stresses acting on the plane for low pressure tests are plotted on a (σ', τ) graph for peak and ultimate condition (with no clear correspondence with critical state) from which the correspondent strength parameters were obtained. The points are assigned to each adjusted porosity/cement ratio ($n/C_{iv}^{0.21}$) expressed before.

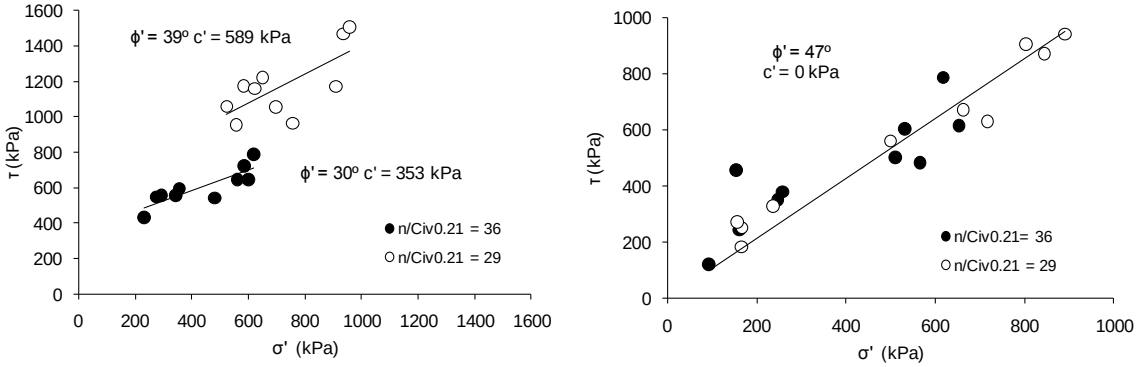

Figure 7.35 Stresses at the failure plane τ and σ' for: a) peak and b) ultimate conditions

It is interesting to notice that for peak conditions two strength envelopes were obtained depending on the index ratio, while for ultimate conditions a unique failure envelope was defined irrespective of their porosity/cement index. The adjusted porosity/cement ratio influences the peak angle of friction and cohesion intercept, with the peak envelope for the index $n/C_{iv}^{0.21}$=29 higher than that for the index equal to 36. This could have been predicted from moulding characteristics as each ratio corresponds to different unconfined compression strengths. Consoli et al. (2009) have also presented different peak strength envelopes depending on the porosity/cement ratio.

Considering that the specimen is constituted by a cemented material these high angles of shearing resistance are not surprising. Table 7.7 presents some data reported in the literature about the ultimate angle of shearing resistance found in cemented specimens. Clough et al. (1981) found values in the range of 33-35° while Coop and Atkinson (1993) reported 37° for artificially cemented carbonate sands. Schnaid et al. (2001) have found angles of shearing resistance of 44° when testing artificially cemented silty sand. Observing this data, it seems that the higher values correspond to the better graded soil, as it is the case of the silty sand tested by Schnaid et al. (2001), which is actually a sandstone residual soil (Botucatu residual soil). As the soil studied in this work has a wider grain size distribution curve than Botucatu residual soil, it is expected that the strength parameters are even higher.

Table 7.7 Angles of shearing resistance obtained in the literature for cemented soils

Reference	Type of mixture	Ultimate angle of shearing resistance
Clough et al. (1981)	naturally cemented sands and uniform sand mixed with Portland cement	33-35º
Coop and Atkinson (1993)	artificially carbonate sand	37º
Schnaid et al. (2001)	artificially cemented silty sand	44º

However, when the high pressure tests are plotted together, the angles of shearing resistance are lower (ϕ' = 29.5°) as Figure 7.36 demonstrates. It should be noted that the specimens tested at pressures higher than the isotropic yield stress were sheared from stress states on their normal compression line, and it is expected that they lost some of their initial bonding during the initial compression stage and may develop high particle breakage. Conversely, the specimens tested at confining pressures less than the isotropic yield stress would have retained most of their initial structure before the start of shearing, and thus both sets of specimens should be regarded as different soils at the start of shearing, i.e, with different degrees of destructuration and crushing from the initial state.

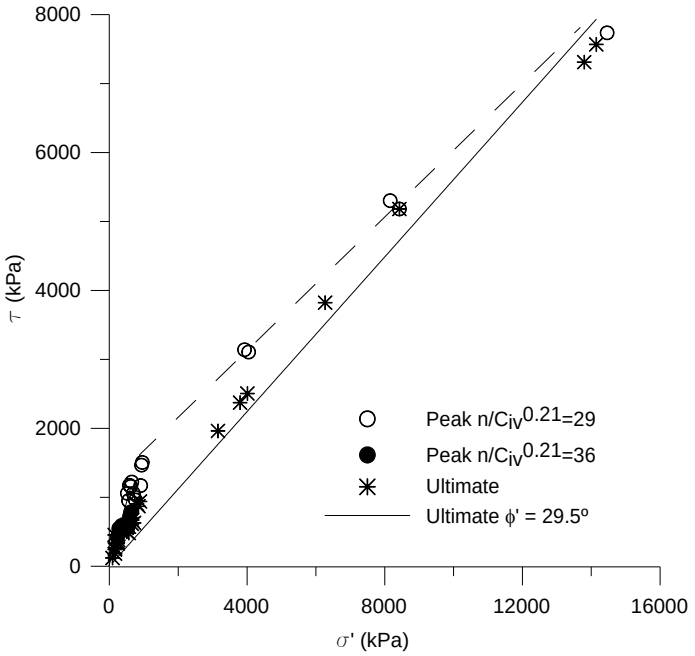

Figure 7.36 Peak and ultimate strength envelopes for low and high pressure triaxial tests in cemented specimens

7.11.4 Uncemented specimens

The uncemented specimens showed a typical barrelling effect when compressed in triaxial conditions as will be illustrated in Figure 7.42b), so the stress invariants remain acceptable to evaluate the strength parameters of the clean silty sand, providing that the appropriate corrections are performed as expressed in section Figure 7.3.

The drained and undrained stress paths at low to medium pressures shown before define a steady state line corresponding to a value of M, defined as the gradient of the critical state line in the q versus p' plot, equal to 1.36 which corresponds to ϕ' =34°, according to equation (7.18) whose deduction is presented in Appendix C for triaxial compression conditions.

$$M = \frac{6\sin\phi'}{3-\sin\phi'} \tag{7.18}$$

However, it is also clear from Figure 7.37b) that the low pressure envelope does not fit exactly with the high pressure stress-path.

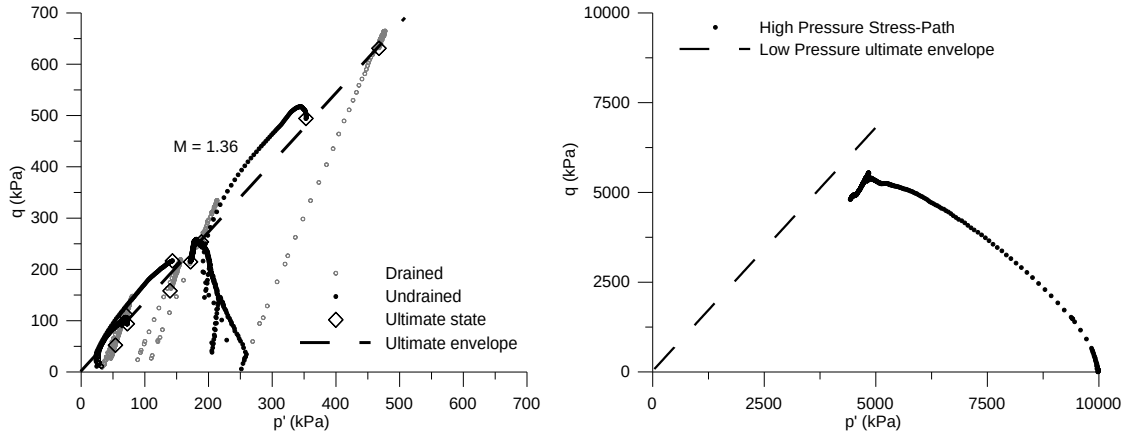

Figure 7.37 Drained and undrained stress-paths of triaxial compression tests over uncemented specimens together with the ultimate envelope: a) low pressures tests; b) high pressure test

The strength envelopes will be now plotted for peak and ultimate envelope for the calculation of the angle of shearing resistance. The first set of graphs shown in Figure 7.38 includes drained and undrained triaxial tests performed at low pressures only (up to 250 kPa). Peak and ultimate conditions were distinguished although a similar envelope was found with an angle of shearing resistance of 34° in agreement with the value of 1.36 presented before. In Figure 7.39 the same strength envelopes are presented including also the undrained high pressure triaxial test. The angle of shearing resistance tends to decrease slightly at higher pressures, indicating that the strength envelope tends to curve at higher pressures as illustrated in the same figure. However, although the reason may be associated to the increase of fines, just one test at higher pressures does not allow further conclusions.

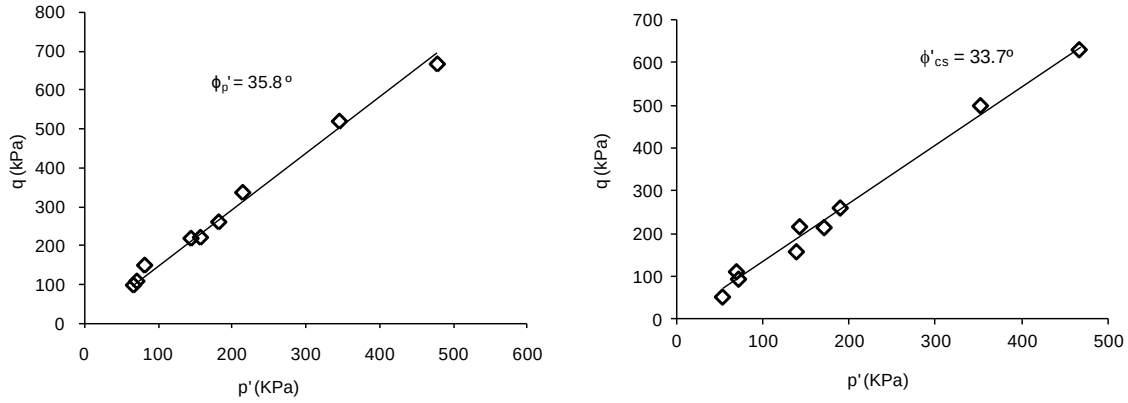

Figure 7.38 Strength envelopes for the low pressure tests of uncemented specimens: a) Peak strength envelope; b) Critical state strength envelope

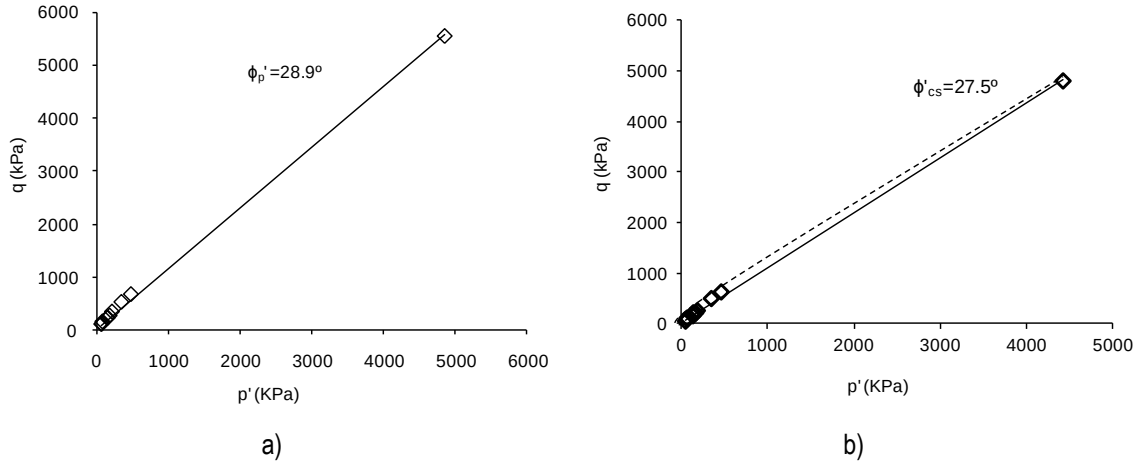

Figure 7.39 Strength envelopes for the low and high pressure tests of uncemented specimens: a) Peak strength envelope; b) Critical state strength envelope

Although uncemented specimens did not suffer from localisation, the strength envelope in terms of (σ', τ) was also calculated for comparison with the cemented envelope. Those stresses were obtained by the intersection of the Mohr circle with the tangent line (like point B in Figure 7.34), as there is no shear plane failure.

The results were similar to Figure 7.38 and 7.39 giving rise to similar angles of shearing resistance as expected (Figure 7.40).

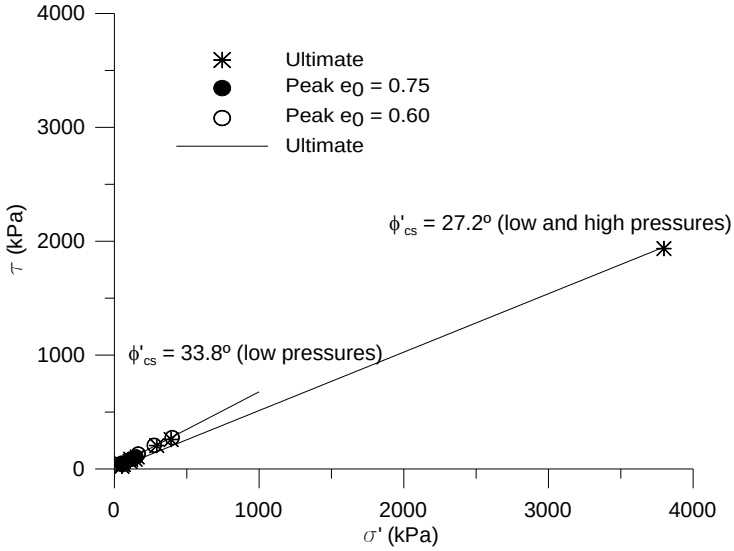

Figure 7.40 Peak and ultimate envelopes for low and high pressure triaxial tests in uncemented specimens

These values were analysed, once again, in the scope of what has been found in the literature which is summarized on Table 7.8. The carbonate sand studied by Coop and Atkinson (1993) has higher angles of shearing resistance but taking the other two soils, both residual soils from granite, 34° seems to be quite reasonable. Although the soil presented by Viana da Fonseca (2003) is from the same region of the soil studied herein, the grain size is slightly different being coarser than the one here analysed.

Table 7.8 Angles of shearing resistance obtained in the literature for uncemented soils

Reference	Type of soil	Ultimate angle of shearing resistance
Coop and Atkinson (1993)	carbonate sand (Dogs bay, Ireland)	40º
Lee and Coop (1995)	decomposed granite soil (Korea)	39º
Viana da Fonseca (2003)	residual soil from granite (Portugal)	31.6º
Ventouras and Coop (2009)	Thanet sand (London, UK)	32º

7.11.5 Comparison of results

In Figure 7.41 there are the strength envelopes at low pressures for cemented and uncemented specimens obtained through the Mohr circle analysis for peak and ultimate conditions. It seems that the angles of shearing resistance are lower in uncemented specimens but the major difference is observed in the cohesion intercept. In fact, some authors have reported (Dupas and Pecker, 1979; Clough et al., 1981; Allman and Poulos, 1988) that the increase in cementation only affects the cohesion intercept and not the angle of shearing resistance. Nevertheless, there are some published works in the literature (Lade and Overton, 1989) which have found that cementation increases both the cohesion

intercept and the angle of shearing resistance (at least for low pressures). This may be, however, a simple consequence of the genesis of groups or aggregations of particles (under cementation), that sustain even in ultimate conditions.

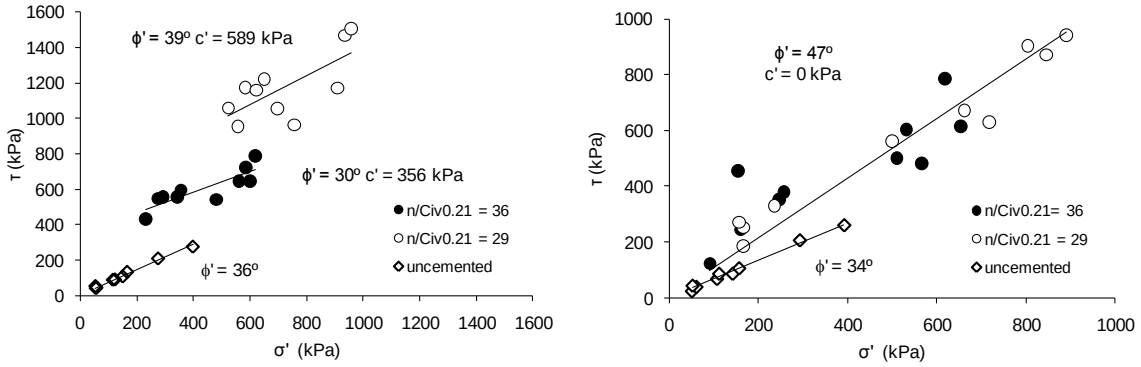

a) b)

Figure 7.41 Stresses obtained by the Mohr circles on uncemented and cemented specimens: a) peak; b) ultimate conditions (not critical conditions)

In fact, it could be expected that in ultimate conditions, both soil-cement and soil specimens would have a similar behaviour (Coop and Atkinson, 1993). However, it seems that the breakage of cementation leaves clusters of soil and cement providing high interlocking that explains the higher angles of shearing resistance. On the other hand it should be noticed that, in opposition to cemented specimens, in the soil specimens there is no shear plane failure, i.e, no shear strain localisation (Figure 7.42).

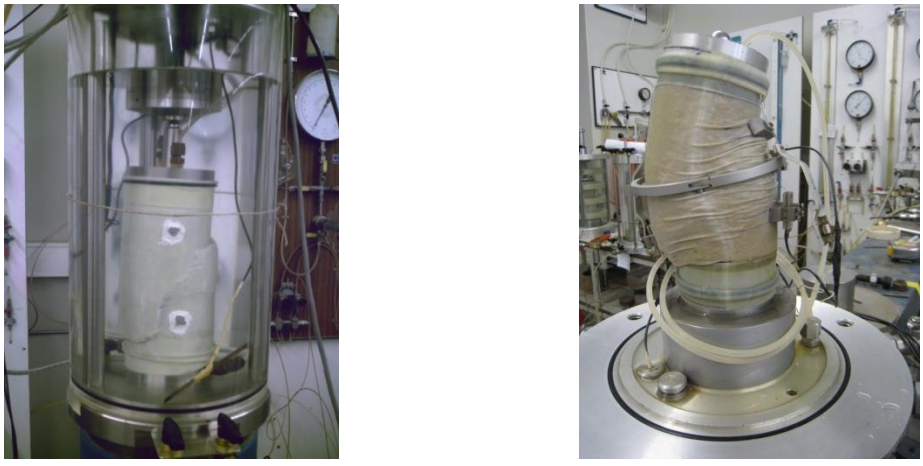

a) b)

Figure 7.42 Photographs of the specimen after the test: a) cemented specimen; b) uncemented specimen

The strength envelopes presented herein were all linear Mohr-Coulomb envelopes. However, some authors (Acar and El-Tahir, 1986) have reported the strength envelope to be non-linear for low stresses. Lade and Overton (1989) have reported that the curvature of

the strength envelope increases with cement content, following similar pattern as in rock masses. From the data concerned by this work, there is an indication of a curvature of the Mohr-Coulomb envelope but only at higher stress levels.

7.12 Failure envelope and stress-paths in v against p' plot

Following a similar approach to critical state soil mechanics, as described in Chapter 4, the failure envelope (CSL) was also determined in terms of specific volume (v) against mean effective stress (p'). This is based on the assumption that the mean effective stress is representative of the stress state of the specimen after failure.

In Figure 7.43 to 7.45 the stress paths described by uncemented and cemented specimens in drained and undrained tests are shown separately for the pure silty sand and the two adjusted porosity/cement ratios.

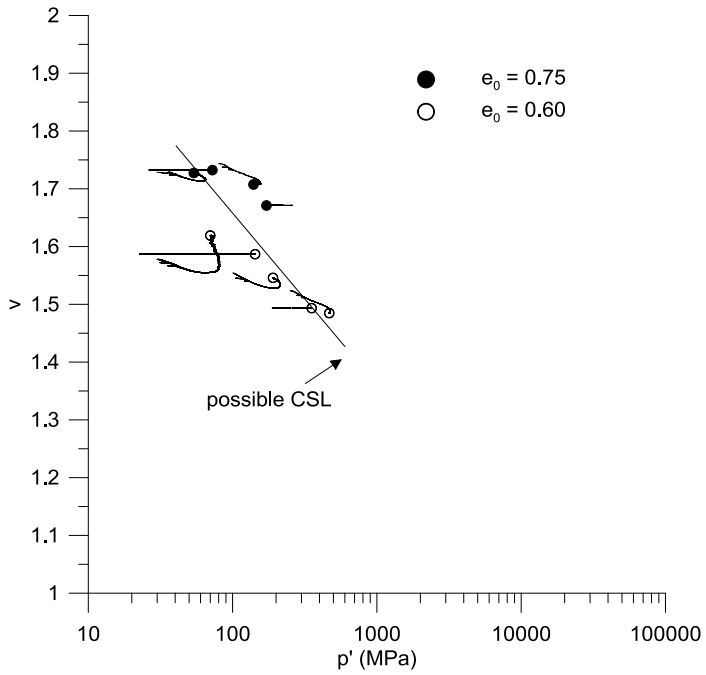

Figure 7.43 Failure envelopes in v - ln p' for the pure silty sand

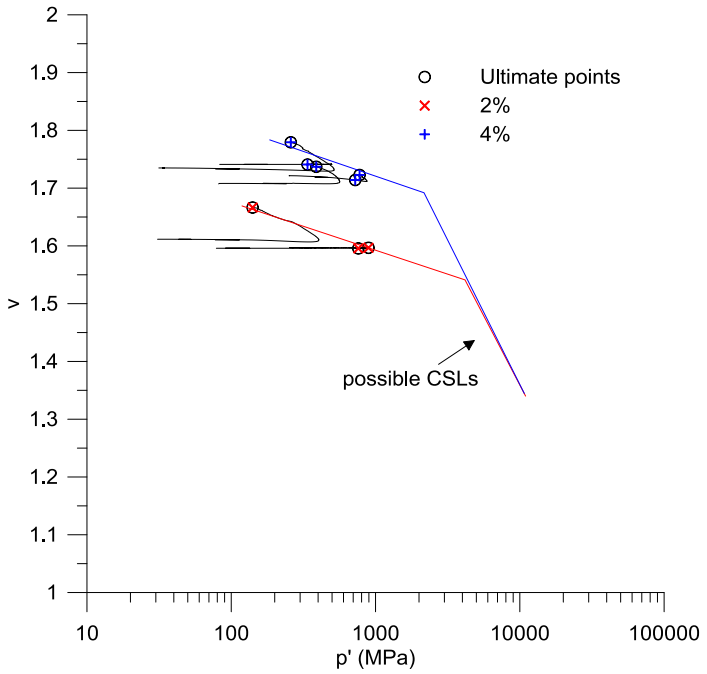

Figure 7.44 Failure envelopes in v - ln p' for the cemented sand ($n/C_{iv}^{0.21}$= 36)

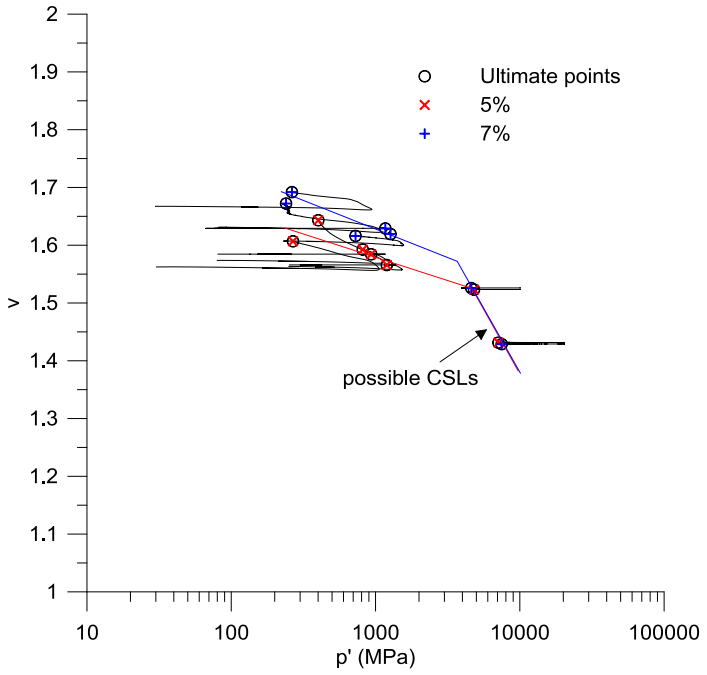

Figure 7.45 Failure envelopes in v - ln p' for the cemented sand ($n/C_{iv}^{0.21}$= 29)

In Figure 7.43 the CSL for the pure silty sand is reasonably well defined by the final points of the tests. To decide whether the points were on the dry or wet side of critical state locus, the behaviour observed in each test was analysed in terms of stress-paths or stress-strain curves as presented before.

A bi-linear CSL is proposed for the cemented failure line as it has been suggested by several authors (e.g. Klotz and Coop, 2002, Carrera et al., 2011). According to the data presented in Figure 7.44 and 7.45 it seems that each cement content corresponds to a specific failure line, although they may converge to a unique line at higher pressures for each adjusted porosity/cement ratio. In fact, in Figure 7.44, the ultimate plots points for 5% and 7% of the ratio ($n/C_{iv}^{0.21}$=29) consolidated to 10 MPa are almost coincident as well as the points consolidated to 20 MPa, indicating a unique CSL at high pressures for this ratio.

Figure 7.46 plots together uncemented and cemented tests results so that their relative position could be identified, namely the CSL for the pure silty sand which seems quite parallel to the NCL_{sand}. A global CSL for the cemented specimens was proposed although the scatter is much higher than in Figure 7.45. It should be noted that some tests were not conducted until very large strains and all of them exhibited strain localisation which may have prevented the test to reach critical state. For that reason, in each test that did not reach a constant volume at the end of shearing, the direction of the stress path is indicated by an arrow. The low to medium pressure plotted points are considered as the upper bound of the stress-path that was behaving dilatant before failure where shear localization occurred, for what the CSL was drawn in this bonder line.

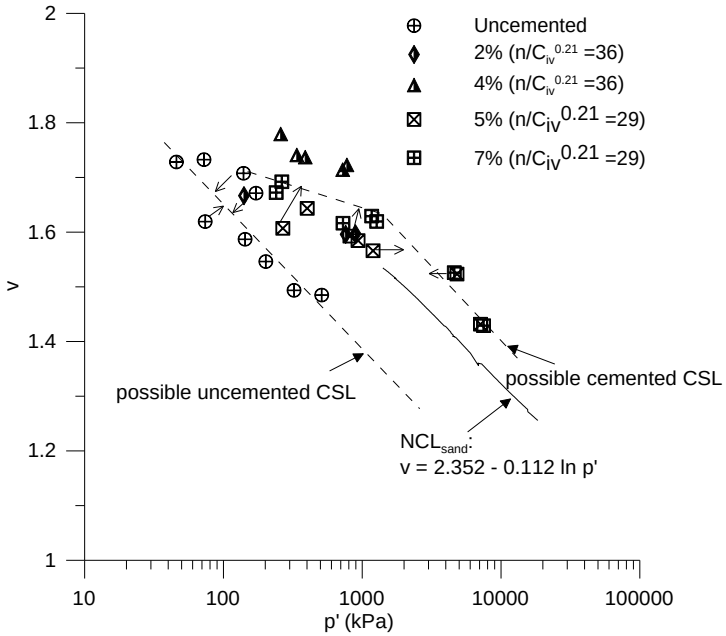

Figure 7.46 Failure envelopes in v - ln p' for pure silty sand and cemented sand

7.13 Stress-dilatancy analysis

In section 4.5.4 some considerations were made about stress-dilatancy and the convenience of this analysis in terms of critical state evaluation was highlighted. This issue

was thus explored in the results of static triaxial tests over uncemented and cemented specimens giving rise to interesting conclusions.

Figure 7.47 illustrates the comparison between the stress-dilatancy behaviour observed in drained tests of uncemented and cemented specimens. In uncemented tests a linear trend was obtained while the stress-dilatancy plots of the cemented specimens show a completely different behaviour.

The results of the stress ratio given by q/p' against dilatancy ($d\varepsilon_v/d\varepsilon_s$) for uncemented specimens (Figure 7.47a) demonstrates that all the tests tend to a stress ratio close to 1.4 ($\phi' \approx 35°$), which is accordingly to the strength envelope results. The exception is the last test consolidated to 250 kPa with e_0 =0.6 that reveals a slightly higher value indicating that this test may have been affected by a small leakage that lead to an excessive measured dilatancy.

In the cemented tests, the shape of the stress-dilatancy plot is explained as follows: in the initial part of the test the inter-particle bonding is preventing the soil from dilation and, thus, there is no volumetric deformation (the plot shows a vertical line). When the cementation starts to break and yield of the soil is taking place, dilation occurs demonstrated by the change in direction of the plot. After a peak rate of dilation, dilation reduces together with the stress ratio. Zero volumetric deformation was not reached in the experiments but, by extrapolation, a stress ratio of 1.8 ($\phi' \approx 44°$) would have been reached, which is slightly above the value of M for the uncemented sand.

Ideally, both uncemented and cemented specimens should arrive at the same value of M, however, as stated previously in Chapter 4 reporting the work of Coop and Wilson (2003), due to localisation dilation reduces more rapidly than the stress-ratio, bringing the path "inside" the frictional relationship. On the other hand, to have the same value of M at critical states in both uncemented and cemented specimens, all cemented clusters had to be destructured in order to have the same grain size distribution curve. In fact, at the end of the test a very different material is obtained when compared with the original soil (uncemented), as revealed in the normal compression line. Taking the value of the angle of shear resistance obtained by the Mohr circle analysis for the ultimate condition (ϕ'= 47°), M assumed the value of 1.9, which is similar to the value obtained by stress-dilatancy analysis reading directly on Figure 7.47b), or by extrapolation up to zero dilation (M value of 1.8, as previously states).

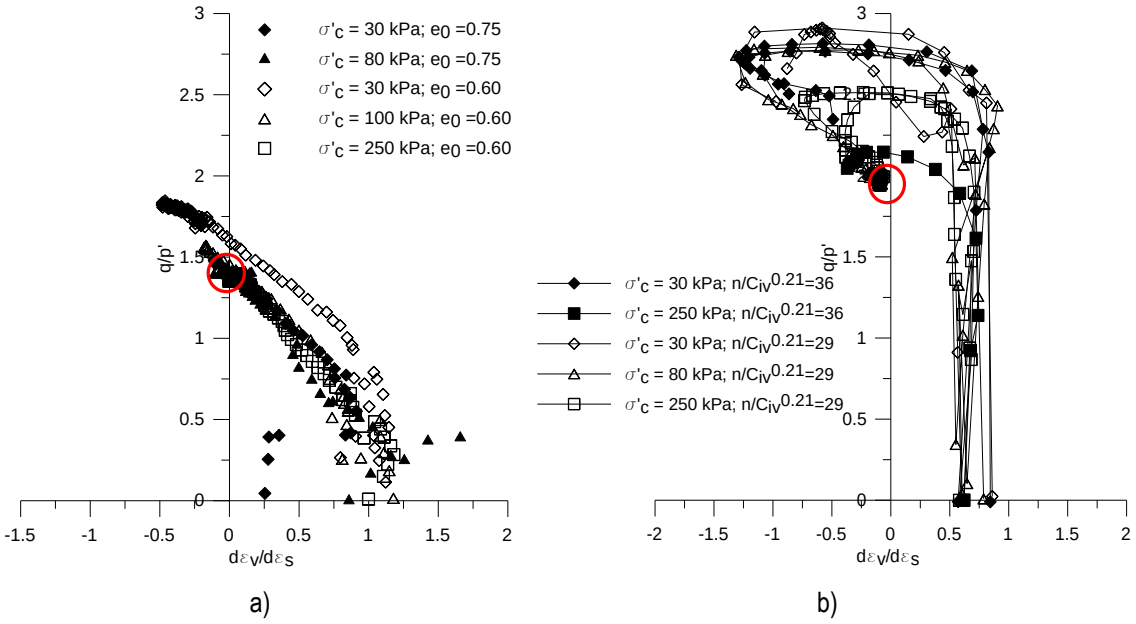

a) b)

Figure 7.47 Stress-dilatancy response in drained tests: a) pure silty sand; b) cemented sand

The same concept of "stress-dilatancy" was adopted for undrained tests using the correspondent in terms of the ratio between pore pressure and the axial strain, which is expressed in Figure 7.48. Taking the fact that all high pressure tests were undrained they were also included in the same plot. However, this was only possible by normalising the data by the initial effective consolidation pressure (p'_0). The results are more scattered than drained tests but, even though, they are in clear agreement with the drained results.

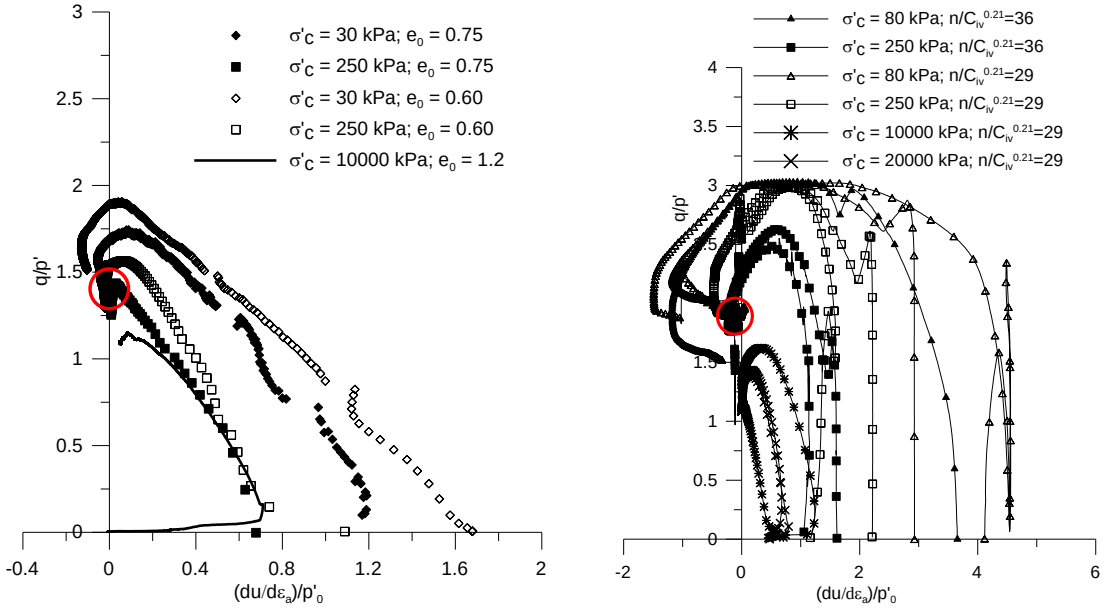

a) b)

Figure 7.48 Stress-dilatancy response in undrained tests: a) pure silty sand; b) cemented sand

7.14 Normalized triaxial tests: Yield surface and State boundary surface

In this section, the results previously presented for uncemented and cemented specimens with $n/C_{iv}^{0.21}$=29, will be now normalized for the effect of volume. The cemented specimens with the other porosity/cement ratio ($n/C_{iv}^{0.21}$=36) are not included in this analysis as there are no high pressure tests moulded on this ratio.

First, the normalization was performed by taking an equivalent pressure, p'_e, on the isotropic normal compression line of the uncemented soil, NCL_{sand} (Figure 7.49). The normalized stress paths for the tests carried out at low pressures all plot fairly close to each other, with the drained and undrained stress paths following similar directions. The normalized stress paths for the tests carried out at 10 MPa and 20 MPa plot well outside the uncemented state boundary surface called herein intrinsic state boundary surface (intrinsic SBS), which should be of size equal to unity. The stress paths bend to the left and reach a peak strength, before strain-softening towards the intrinsic states. The stress path for the test performed at 20 MPa plots closer to the intrinsic state boundary surface than the stress path for that performed at 10 MPa, and displays a lower stiffness and lower strength. This should be due to the fact that the specimens compressed to 20 MPa before shearing suffered more destructuration than the specimens compressed to 10 MPa, and thus their bonding was more damaged. Since these specimens were sheared from normally consolidated states the normalized stress paths should be a representation of the collapse of the state boundary surface towards intrinsic states, similarly to the results found on a variety of structured soft and stiff soils (e.g. Smith et al. (1992) for Bothkennar clay).

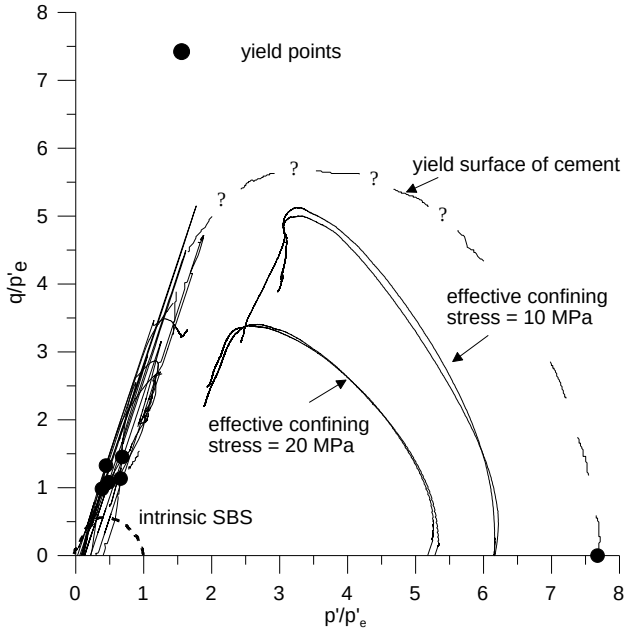

Figure 7.49 Normalized results for the yield surface with respect to the NCL_{sand}

For each test performed at low or high pressure, the yield stress was defined as the point where the stress-strain curve departs the linear range, as performed before for the initial tangent modulus shown in Chapter 6 in Figure 6.19a). The yield points determined following that method are represented in Figure 7.49. Following Coop and Airey's (2003) suggestion, reported in Chapter 4 (Figure 4.21), that the yield points define the yield surface of the cement aggregation, a tentative yield surface has been drawn. It passes through the yield points defined from the shearing tests at low pressures. For the specimens tested at high pressure, the cement yielded during the compression stage and thus the isotropic yield point was taken. According to Coop and Airey (2003), the stress paths at high pressures plot inside the yield surface as a sign of the collapse of the state boundary surface towards intrinsic states.

The state boundary surface was determined by normalizing the stress path data using an equivalent pressure on the appropriate normal compression line. For the pure sand, the NCL_{sand} was used as reference line. For the cemented sand specimens, a single reference was used for a given adjusted porosity/cement index, in this case $n/C_{iv}^{0.21}=29$, and that was the $NCL_{cement(29)}$ defined in Table 7.4.

The normalised stress paths of the uncemented soil, plotted in Figure 7.50a), determine a unique state boundary surface as might have been expected for a sandy soil, called intrinsic SBS in Figure 7.49. More tests with an initial normalized effective stress p'/p'_e around 0.3 would be of great interest in order to confirm the state boundary surface in that area and, to identify if there was any error in the stress path of the test with σ'_c = 80 kPa and e_0=0.75.

The normalized stress paths for the cemented specimens moulded with $n/C_{iv}^{0.21}=29$ are shown in Figure 7.50b). The stress paths for the tests carried out from states on the normal compression line (confining stresses 10MPa and 20MPa) define a unique boundary surface on what is traditionally called the "wet side of critical", starting from the $NCL_{cement(29)}$ despite the different cement contents used in the tests. The higher the effective consolidation pressure the lower is the plot of the normalized stress-path indicating the evolution of the cemented soil towards a progressively destructured material, as explained before. The stress paths carried out at low stresses, which dilated during shearing, all plot to the left and also define a boundary surface on the so called "dry side of critical". Again, the interest in other triaxial tests at intermediate pressure is highlighted as it would allow the closing of the state boundary surface.

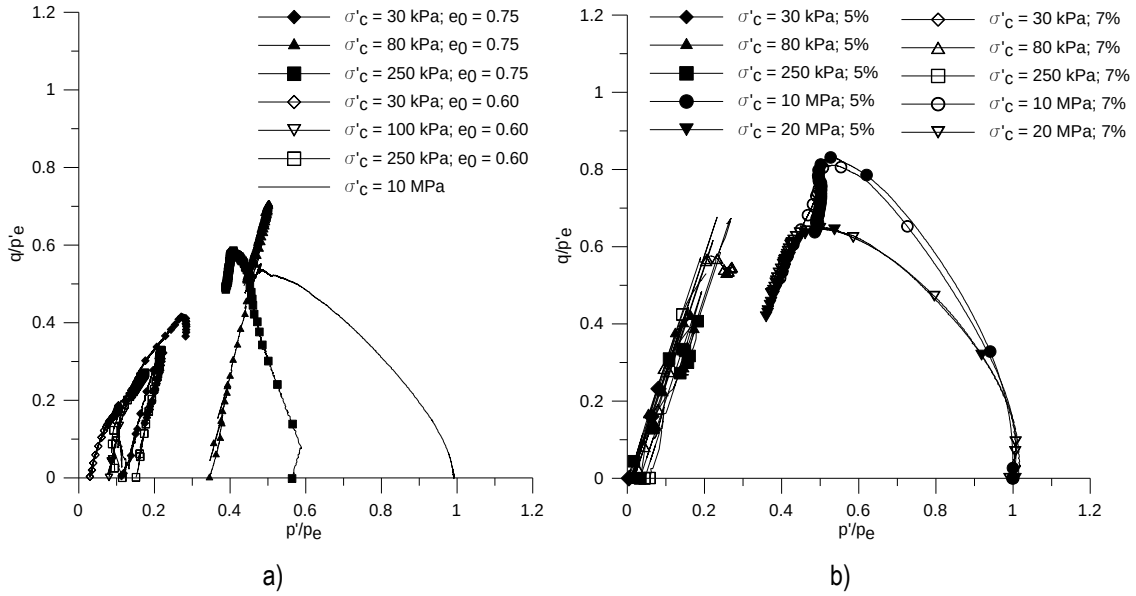

Figure 7.50 Normalized results for the state boundary surface: a) normalization with respect to the NCL_{sand}; b) normalization with respect to the $NCL_{cement(29)}$

7.15 Conclusions

This chapter focused on the static triaxial tests performed at low and high pressures giving rise to important contributions on the understanding of the mechanical behaviour of soil-cement mixtures. After a brief presentation of the tests involved in this experimental program the stress-strain-volumetric/pore pressure curves were presented considered as the individual basic result of the tests. After this, several types of analysis were presented where these tests were compared and discussed in terms of final void ratio, stiffness, stress-paths, strength envelope and, stress dilatancy. Finally, an attempt was made to obtain a possible yield and state boundary surfaces.

This large amount of data, allowed some interesting comments. It was observed that uncemented and cemented tests could not be directly compared in the sense that even with high pressures the cementation was not totally destroyed and the uncemented behaviour could not be recovered. This was clear not only in the isotropic compression tests where different NCL were obtained for uncemented and cemented conditions but also in the strength envelopes. In the latter peak and ultimate conditions should be distinguished: while in peak strength envelopes each porosity/cement ratio presented a different envelope, in ultimate conditions all cemented points seemed to align in the same trend. The stress-dilatancy results also showed different M values for uncemented and cemented specimens.

Having well defined the NCL for the sand and for each adjusted porosity/cement ratio, the evaluation of the CSL was pursed. In uncemented conditions, the CSL was well defined at low pressures in both q vs p' and v against p' planes. However, the high pressure test did not fit exactly within this envelope which can be either because the test is not totally reliable or the strength envelope tends to curve at higher pressures, which may be associated to the increase of fines. More tests over uncemented specimens at high pressures were necessary to know the real cause. The CSL of the cemented specimens was much more difficult to obtain because of incomplete testing in some cases and strain localisation. All the tests were quite stiff and so, strain localisation, generally close to the peak, was unavoidable. For that reason, a post rupture analysis based on the Mohr circles was developed in order to know the stresses acting on the shear plane. Again a curved strength envelope in the q vs p' plane was found, which was quite expected in this case, as the high pressure tests were sheared from their normal compression line, i.e., after yielding, with a significant damage in their cemented structure. The CSL in the v against p' plane was not so well defined due to a great scatter which may indicate a curved CSL for each cement content that eventually can join together (for similar adjusted porosity/cement ratios) at higher stresses. However, the results were not completely certain in this point which should be verified with a greater number of tests.

Finally, possible yield and state boundary surfaces were defined by the normalization of the test data for the effect of volume. Some more tests would highly improve the definition and the reliability of these surfaces, providing other points at intermediate stresses.

Chapter 8.
CYCLIC TRIAXIAL TESTS

8.1 Introduction

The experimental program included in this research work comprised also cyclic triaxial tests performed over cemented specimens similar to the ones tested in static conditions. One of the main purposes of these tests was to evaluate the validity of the European standard for cyclic triaxial tests developed for unbound granular materials (CEN, 2004a), in these cemented materials. This standard comprises resilient and permanent deformation analyses, which are very important to understand the cyclic behaviour of soils including cemented mixtures. Additionally, the fatigue phenomenon was also pursed because the durability of soil-cement layers subjected to cyclic loads is often questioned.

8.2 Moulding conditions and procedures

The same conditions of preparation and moulding described in chapter 6 and applied to the specimens of the tests described in the previous chapters were used for the cyclic triaxial tests. Table 8.1 summarises the moulding conditions of the specimens tested in cyclic conditions expressing as before the dry unit weight, the void ratio, the water content, as well as the adjusted porosity/cement ratio and the corresponding unconfined compression strength. All the specimens were cemented and they were left to cure in the humid chamber for 7 days as previously reported for the low pressure triaxial tests. The percolation, saturation and consolidation stages were similar to those tests as described in chapter 5.

Table 8.1 Moulding conditions of the specimens tested in cyclic triaxial tests

Sample name	C	γ_d	e_0	w	$n/C_{Iv}^{0,21}$	q_u
	%	kN/m^3		%		kPa
TC(2)	2	16.7	0.60	12	36	800
TC(5)	5	17.0	0.58	12	29	2000
TC(5*)	5	18.0	0.50	12	27	2837
TC(7)	7	16.4	0.64	12	29	2000
TC(7*)	7	18.0	0.50	12	24	4335

After the consolidation stage the cyclic loading took place. A sinusoidal type of loading was applied as expressed by Figure 8.1. The load amplitude corresponds to the difference between the maximum and minimum deviatoric stress ($q=\sigma_V-\sigma_H$) and a specific cyclic frequency was adopted.

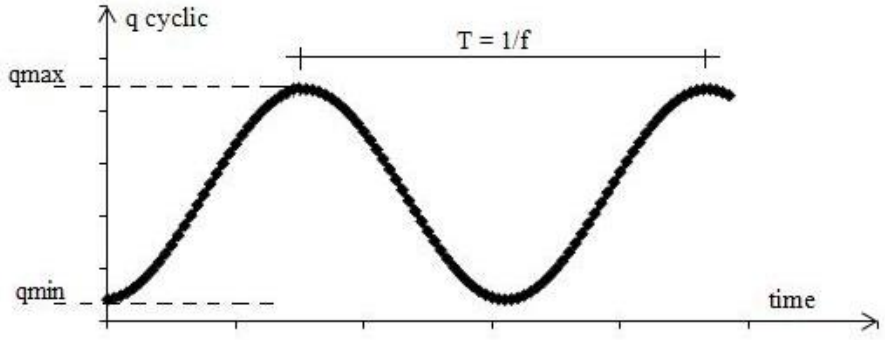

Figure 8.1 Cyclic sinusoidal loading

The tests presented here were all carried out at 1 Hz, which is within the range of frequencies suggested in the European standard (0.1-10Hz). Some unsuccessful attempts were made at higher frequencies, since with the desired load amplitudes the equipment was not fast enough to perform the cycles and the piston lost contact with the top of the specimen which was being literally knocked at each cycle. This was more notorious in the stiffer materials. It should be noted that the equipment where these tests were performed was only able to apply vertical cyclic stresses and for that reason the confining pressure was kept constant within each cyclic stage (Method B in the European standard).

In order to obtain a good definition of the sinusoid described by the cyclic loading, 20 measurements per second (with f =1Hz, it means 20 points per sinusoid) were registered automatically by the software. Therefore, a great amount of data was available at the end of the test, which had to be used selectively as it will be explained further below.

The tests were performed in undrained and drained conditions, both methods presenting advantages and disadvantages. In drained cyclic triaxial tests there were some difficulties in having accurate volume changes measurements because of the fast loading and the

compliance caused mainly by the small diameter of the drainage system (holes) as well as some flexibility of the tube lines. On the contrary, pressure measurements performed in undrained tests were easier and more reliable. However, undrained tests showed a large generation of pore pressures decreasing the effective pressure to almost zero which inhibited the evaluation of the effect of confining pressure.

8.3 Testing program

8.3.1 Introduction

Three types of tests were performed in cyclic conditions. The first two were based on the European standard for cyclic triaxial tests (CEN, 2004a), Type 1 tests comprising the procedure for the study of the resilient behaviour while Type 2 tests refer to a procedure for the study of permanent deformations. Type 3 tests were performed at a great number of cycles and low range of loads in order to study the fatigue phenomenon.

8.3.2 Range of loads

At this moment, the European standard is only available for unbound granular materials, and therefore an adaptation of the suggested loads was introduced for type 1 and type 2 tests. The load level was defined as a compromise between reality and laboratory possibilities within the limitations imposed by such high stiffness materials. For the lower stress levels, the loads were defined based on the typical range of loads applied to hydraulic bounded materials in railways platforms of medium and high speed; for the higher stress levels, higher loads had to be selected to have a clear response from the internal LVDT's.

In the first procedure (Type 1) the aim is to define values of the material resilient modulus for different stress levels. For that purpose, a cyclic conditioning is first applied to stabilise the material permanent deformations due to equipment compliance and subsequently attain the resilient behaviour. This conditioning is performed by applying a large number of cycles at a significant stress level. The load levels were adapted from tables 4 and 5 of the European standard considering the part of the table related to the "high stress level". The number of cycles suggested in the standard for evaluation of the resilient modulus with stress level after conditioning is 100 cycles, however, 5000 cycles were performed at each stress level considering the fact that cemented material might be sensitive to extra cycling.

Type 2 tests were proposed in the European standard to evaluate the maximum stress levels which should not be exceeded to avoid the development of excessive permanent deformations. This procedure consists in applying a large number of load cycles of a stress

combination without prior conditioning to evaluate permanent deformations of the material for a particular stress level. The load levels for the permanent deformations procedure were adapted from table 6 of the same standard.

Finally, a different type of test (Type 3), not comprised in the standard, was pursed to evaluate the fatigue phenomenon. For that purpose, long tests with high number of load cycles and low stress levels were performed. The low level of stress was again a compromise between typical conditions that these materials should be subjected when applied in subgrades, but sufficiently significant to induce permanent deformations in the readability range of the measuring devices.

The equipment was not prepared to support tensile or zero stresses, and therefore, a minimum deviatoric stress of 5 kPa was always applied in all tests. Table 8.2 includes the effective confining pressure (σ'_c) and the maximum and minimum deviatoric loads applied in all stages of each type of tests. For an easier understanding the stress levels are summarised on Table 8.3.

Table 8.2 Load stresses applied in each type of test

Type 1				Type 2				Type 3			
σ'_c (kPa)	q_{cyclic}(kPa)		No. cycles	σ'_c (kPa)	q_{cyclic}(kPa)		No. cycles	σ'_c (kPa)	q_{cyclic}(kPa)		No. cycles
	min	max			min	max			min	max	
70	5	340	20 000	40	5	100	10 000	40	5	150	250 000 [2]
50	5	80	5000	40	5	240	10 000	40	5	200	250 000 [2]
50	5	115	5000	40	5	360	10 000				
50	5	150	5000	80	5	200	10 000				
50	5	200	5000	80	5	400	10 000				
50	5	280	5000	80	5	600	10 000				
100	5	150	5000	150	5	400 [1]	10 000				
100	5	200	5000	150	5	500 [1]	10 000				
100	5	280	5000	150	5	600 [1]	10 000				
100	5	340	5000								
100	5	400	5000								
150	5	200	5000								
150	5	280	5000								
150	5	340	5000								
150	5	400	5000								
150	5	475	5000								

[1] These loads were higher in the 7% cement content specimens

[2] In the drained tests, each stage comprised 500 000 cycles instead of only 250 000.

Table 8.3 Load levels for each type of test

Type 1			Type 2			Type 3		
σ'_c kPa	stress ratio q_{max}/σ'_c	No. cycles	σ'_c kPa	stress ratio q_{max}/σ'_c	No. cycles	σ'_c kPa	stress ratio q_{max}/σ'_c	No. cycles
70	4.9	20000	40	2.5; 6; 9	10000/each	40	3.8	250 000 (2)
50	1.6; 2.3; 3.0; 4.0; 5.6	5000/each	80	2.5; 5; 7.5	10000/each	40	5.0	250 000 (2)
100	1.5; 2.0; 2.8; 3.4; 4.0	5000/each	150	2.7; 3.3; 4 (1)	10000/each			
150	1.3; 1.9; 2.3; 2.7; 3.2	5000/each						

(1) These stress ratios were higher in the 7% cement content specimens

(2) In the drained test, each stage comprised 500 000 cycles instead of only 250 000.

8.3.3 Specimens and draining conditions

Type 1 and 2 tests were first applied to two different types of specimens with two different adjusted porosity/cement ratio named TC(2) and TC(5) according to Table 8.1.

The specimens with 7% of cement content also followed Type 2 procedure, until the end of the stress stages with 80 kPa of confining pressure described in Table 8.2. After that, due to the lack of strain answer of the internal LVDT's it was decided to impose higher loads. The specimen TC(7) was tested with maximum deviatoric stress of 400, 600 and 900 kPa in the last effective confining pressure of 150 kPa, respectively for the three stress stages. In the specimen TC(7*) six stress stages more were added. The first three, keeping 80 kPa of confining pressure, had maximum deviatoric stresses of 400, 600 and 900 kPa. The last three, with 150 kPa of confining pressure, were performed with maximum deviatoric stresses of 800, 900 and 1400 kPa. Although these stress levels are not indicated in the standard, it was decided to induce such loads in order to have a wider comprehension of this material behaviour subjected to higher loads.

In the type 3 tests only specimens with 5% of cement content (TC(5) according to Table 8.1) were tested. Unfortunately, being very long tests it was not possible to perform on time, more tests in other moulding conditions.

The summary of the performed tests in terms of type of test applied to each type of specimen and draining conditions is presented in Table 8.4.

Table 8.4 Type of test and draining conditions applied to each type of specimen

Type of sample	Type of test	Draining conditions
TC(2)	Type 1	Undrained
TC(5)	Type 1	Undrained
TC(2)	Type 2	Undrained
TC(5)	Type 2	Undrained
TC(7)	Type 2	Undrained
TC(7)	Type 2	Drained
TC(7*)	Type 2	Drained
TC(5)	Type 3	Undrained
TC(5)	Type 3	Drained
TC(5*)	Type 3	Drained

8.3.4 Analysed cycles

Due to the great number of data, not all the cycles were analysed. The European standard suggests a range of selected cycles where the readings should be recorded for 10 consecutive cycles around a specific already attained number of cycles. Considering this procedure quite reasonable, type 1 and type 2 tests followed the suggested cycles, while for type 3 test an adaptation of such recommendation was used, by extrapoling to a higher number of cycles.

Resilient behaviour (Type 1):

- Conditioning: [1 to 20; 50; 100; 200; 400; 1000; 2500; 5000; 7500; 10000; 12500; 15000; 20000]
- Stress stages: [1 to 20; 50; 100; 200; 400; 1000; 2500; 5000]

Permanent deformation (Type 2):

- Stress stages: [1 to 20; 50; 100; 200; 400; 1000; 2500; 5000; 7500; 10000]

Fatigue (Type 3):

[1 to 20; 50; 100; 200; 400; 1000; 2500; 5000; 7500; 10000; 12500; 15000; 20000; 30000; 40000; 50000; 60000; 70000; 80000; 90000; 100000; 120000; 140000; 160000; 180000; 200000; 220000; 250000; 260000; 280000; 300000; 320000; 340000; 360000; 380000; 400000; 420000; 440000; 460000; 480000; 500000]

8.3.5 Aims and work procedure

The experimental program of the cyclic triaxial tests comprised three different types of analysis:

- the first two types of specimens indicated in Table 8.1, respectively with the two adjusted porosity/cement ratios (TC(2) and TC(5)), were tested undrained and analysed in terms of the European standard within type 1 and type 2 tests, to evaluate the resilient and permanent deformation behaviour;
- the 7% specimens allowed the investigation of several issues: the behaviour at higher loads; the comparison of draining conditions (TC(7)); contrast of two different curing void ratio (TC(7) and TC(7*)); comparison between specimens of different cement contents but the same adjusted porosity/cement ratio;
- finally, specimens with 5% of cement content were tested at a higher number of cycles to evaluate the fatigue phenomenon in these materials.

8.4 Preliminary results

Before going into the results associated to the main aims of these tests, some preliminary results are introduced showing the type of stress-strain cycles obtained, on order to explain how the data was analysed. Afterwards, the following sections will address the topics previously reported.

The results will be presented in several ways: in some cases a summary of the whole test in a specific specimen is described, but in some other cases only one cycle of a certain stress stage is shown. For that reason, the following reference name was created so that each cycle from a given stress stage can be localised within the whole test, and within the reported experimental program:

TC(C)_Tx_σ'_c_q_{min}_q_{max}

where,

- TC(C) identifies the type of specimen;
- Tx indicates the type of test: T1, T2 or T3;
- σ'_c corresponds to the effective confining pressure of that stress stage;
- q_{min} and q_{max} are the minimum and maximum deviatoric stresses of that stress stage in kPa, being q_{min} always 5 (kPa)

As an example, TC(5)_T2_150_5_600 refers to a TC(5) specimen according to Table 8.1 tested in a type 2 test at 150 kPa of effective confining pressure being the maximum deviatoric stress 600 kPa that corresponds to the last stage of type 2 test, according to Table 8.2.

Resilient and permanent deformations were introduced in Chapter 3. Considering the great amount of data that a cyclic triaxial test represents, some simplifications had to be introduced to enable the automatic treatment of such large volume of information. Before going into details of these simplifications, some preliminary comments should be addressed about the results.

In the lower stress levels applied to stiffer specimens it was sometimes difficult to have a good response from the internal LVDT's due to the very small deformations that were observed. However, even being similar instruments, the second LVDT (LVDT2) showed better resolution than the first (LVDT1), as it is clear from the following graphs. Figure 8.2 shows the stress-strain cycle obtained with both local axial LVDTs in a specific specimen at the same stress stage: while LVDT2 shows a clear hysteresis loop, LVDT1 seems to have an unstable behaviour. This is even more obvious in the graph of Figure 8.3 where the cyclic response of both LVDTs during the whole test stage is plotted. When this happened, typically at low stress levels, only the second LVDT was considered instead of the average value. Even admitting that this option may be criticised, it was considered that the error of using measurements under the readability of the device would be worse option.

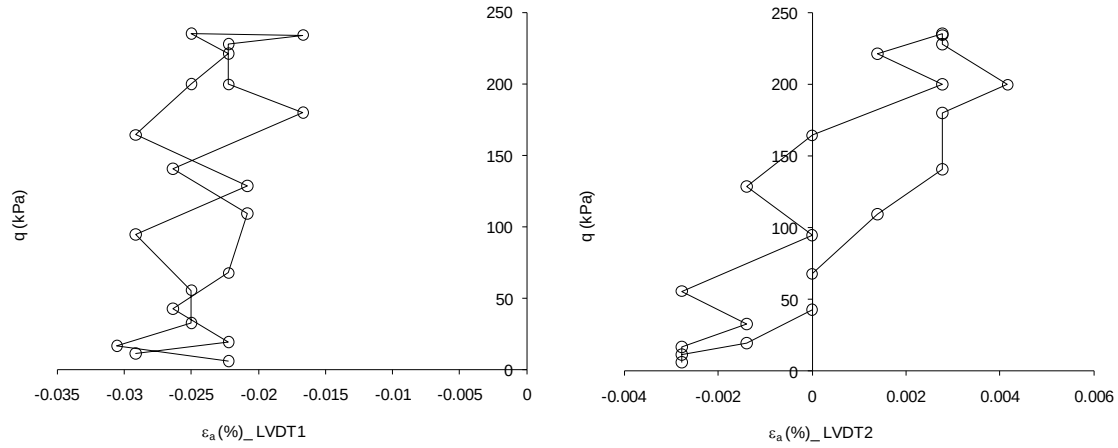

Figure 8.2 Stress-strain curves obtained with different LVDTs for the same test stage (TC(5)_T2_40_5_240): a) LVDT1; b) LVDT2

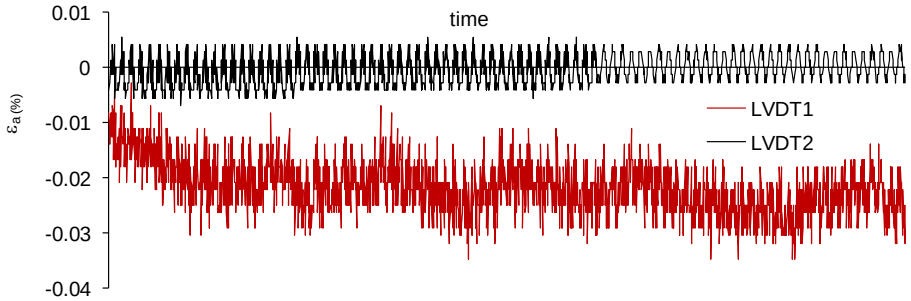

Figure 8.3 Axial strain with time during the test stage for both LVDTs (TC(5)_T2_40_5_240)

Another surprising characteristic of these cycles is the direction of the hysteresis loop. In contrast to what is commonly presented in the literature (Johnson, 1986, Werkmeister et al., 2001, 2005, Konrad and Nguyen, 2006), all the tests analysed in this work have exhibited the behaviour expressed in Figure 8.4. It seems that the stiffness increases during the load cycle, so that when the load increases in the beginning of the load cycle, the stiffness is lower than in the subsequent increments of load intervals. For this reason, the cycle has an anticlockwise loop which, in a first tentative explanation, may be due to some discrepancy on the dynamics of those two types of transducers involved. It seems that the load cell has a lower response rate than the LVDT's. However, that may be due to some flexibility of the interface on the extremes of the specimen (bedding compliance) which may delay for milliseconds the overall action in force. Still, the results are quite reliable in the global cycle since the vertices of the hysteresis are well defined.

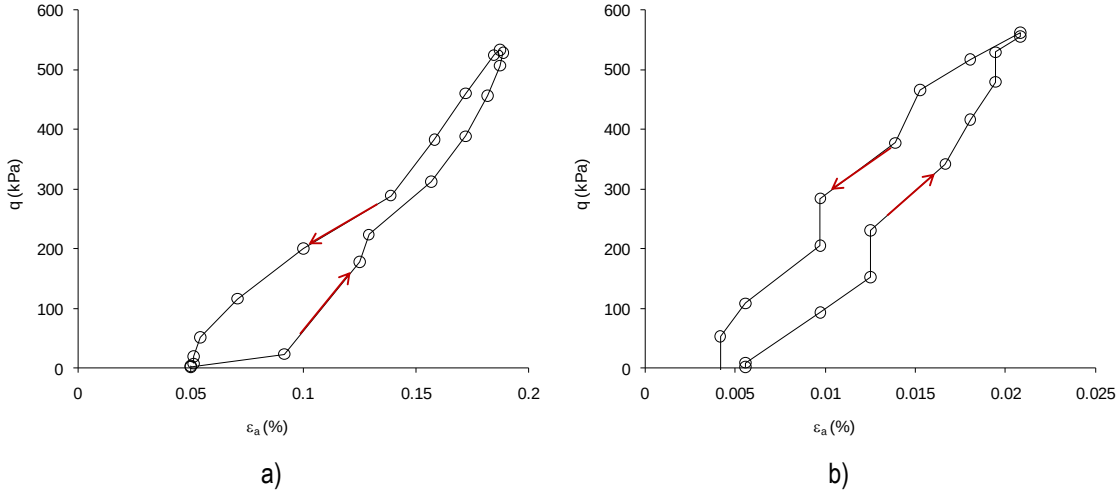

Figure 8.4 Stress-strain hysteresis loops of the first cycle of two different specimens at the same test stage: a) TC(2)_T2_150_5_600; b) TC(5)_T2_150_5_600

From these graphs, it is also possible to see that the plastic strain at the end of the cycle is almost zero. In fact, the permanent strain can only be measured accurately after a large number of cycles, as reported in Chapter 3, and the values are even quite reduced. This is clear in Figure 8.5 where several cycles of one test stage are presented (not all cycles are plotted for clarity) from the first until the tenth thousand. It should be noted that this figure refers to the less cemented specimen at the high level of stress. Therefore, it is possible to see at first sight that there is a clear evolution of the permanent deformation but, even though, the permanent deformation at the end of 10 000 cycles is not more than 0.01%. For that reason, the permanent deformation (ε_p) reported herein will always be considered the accumulated permanent deformation after a certain number of cycles.

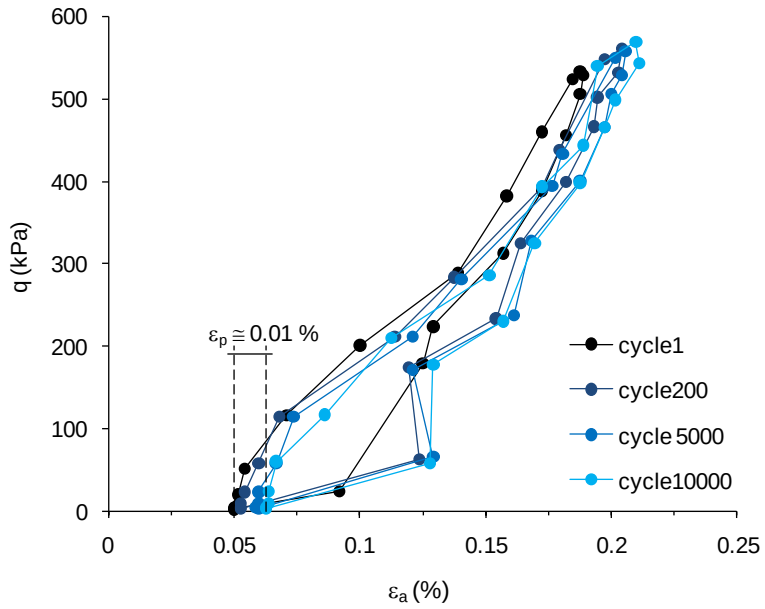

Figure 8.5 Evolution of the load cycles with the number of cycles in one test stage (TC(2)_T2_150_5_600)

Considering almost zero permanent deformations in each load cycle, some simplifications were introduced. The resilient modulus (E_r) was calculated by the slope of the hysteresis edge points instead of taking only the unloading part of the curve as stated in Chapter 3, following the equation,

$$E_r = \frac{q_{max} - q_{min}}{\varepsilon_a^{(associated\ to q_{max})} - \varepsilon_a^{(associated\ to q_{min})}} \tag{8.1}$$

In the same way, the resilient strain (ε_r) was calculated by the difference between the maximum and minimum axial strain of the cycle, instead of the maximum and last axial strain of the cycle.

Although low values of permanent deformations were obtained in each cycle, the hysteresis loops usually observed (such as Figure 8.4 and 8.5) are the evidence of plastic work. On the other hand, undrained tests also showed “hysteresis” in the q against p’ stress-path due to the generation of pore pressure. In Figure 8.6 an example is given illustrating the q versus p’ loop side by side with the q versus ε_a cycle. In the first, the ideal drained stress path is also shown for comparison so that the evolution of the excess pore pressures can be analysed. It is clear that the pore pressures are generated during loading associated to an increase of the axial strain, and are dissipated during unloading when the axial strains are recovered. Therefore, it can be concluded that the pore pressure generation should be related to the the specimen deformation and thus, bigger loops in the q vs p’ plot should also mean higher plastic work.

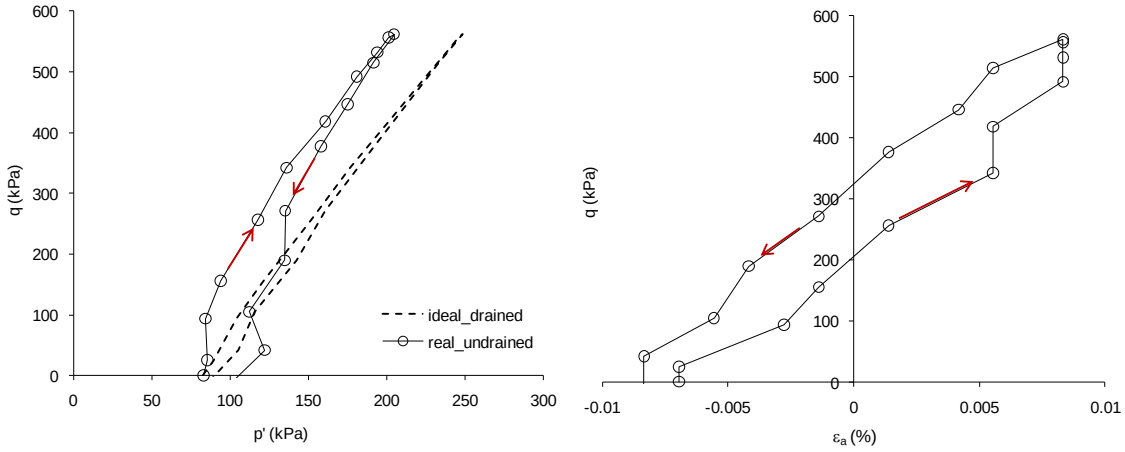

Figure 8.6 First cycle of TC(5)_T2_80_5_600: a) q against p'; b) q against axial strain

8.5 Type 1 tests results

Type 1 tests are tests based on the European standard (CEN, 2004a) for resilient behaviour evaluation. After an initial conditioning of 20000 cycles, several test stages of 5000 cycles are applied with different stress levels for which the average resilient modulus of the last 10 cycles is obtained. This type of test was performed over two different types of specimens moulded to have two different adjusted porosity/cement ratios, designated TC(2) and TC(5) in the terms reported before.

8.5.1 Effectiveness of initial conditioning

The initial stage of conditioning has the aim to subject the specimen to a large number of cycles with a significant load, expecting that the accumulated permanent deformation achieves a stable value in order to establish a resilient behaviour. In Figure 8.7 the plot of the accumulated permanent deformation against the number of cycles is presented for both types of specimens. It is clear from Figure 8.7 that only the less cemented specimen TC(2) allows a reasonable idea of the strain evolution since TC(5) strains are quite low. The permanent deformations in TC(2) highly decreases after 5000 cycles as the accumulated permanent deformation tends to stabilise giving validity to the conditioning suggested in the standard.

The resilient behaviour is expressed in Figure 8.8 where a stable resilient modulus was observed for both types of specimens. The scatter is more significant in TC(5) due to the low strain level. Figure 8.9 shows the evolution of the load cycles during conditioning to illustrate the accumulation of the permanent deformations in the first cycles of TC(2) and

the almost zero permanent deformation of TC(5). The cycles selected for this type of plots were based on the standard definitions, as explained in section 8.3.4.

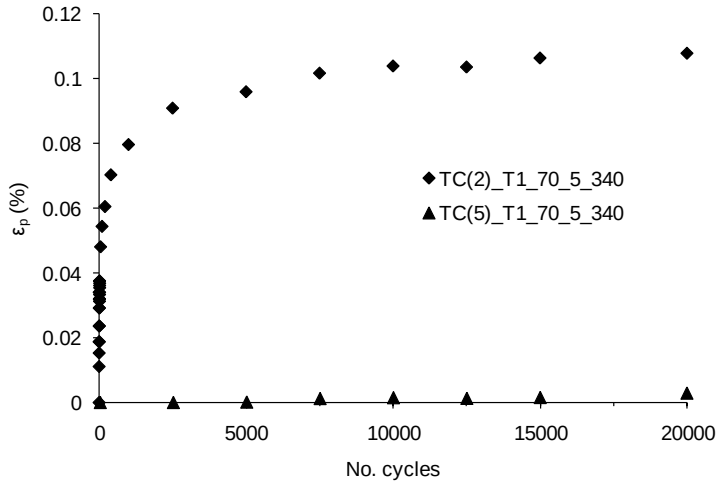

Figure 8.7 Evolution of the permanent strain during conditioning

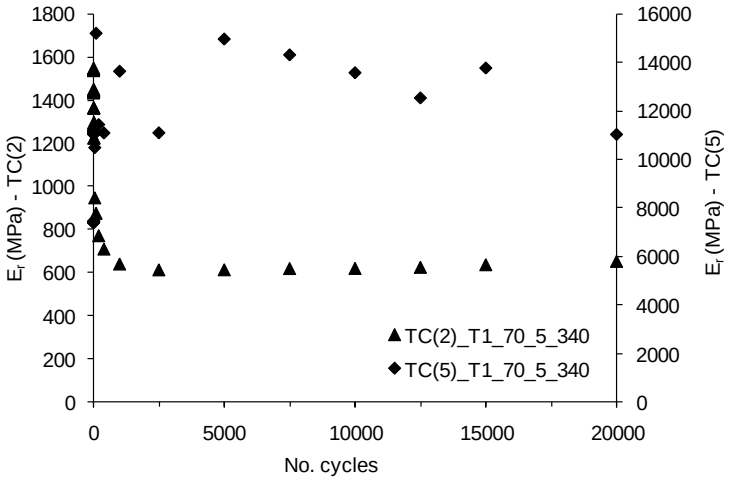

Figure 8.8 Evolution of the resilient modulus during conditioning

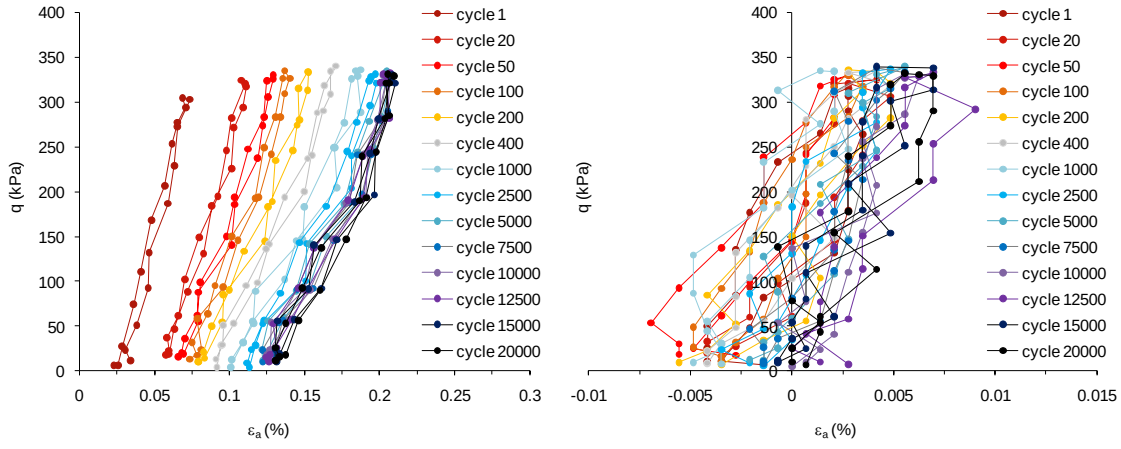

Figure 8.9 Stress-strain hysteretic cycles during the conditioning: a) TC(2)_T1_70_5_340; b) TC(5)_T1_70_5_340

8.5.2 Resilient modulus with stress level

To evaluate the resilient modulus, stress stages with 5000 cycles were applied to both types of specimens. All the tests showed quite constant resilient moduli along the cyclic period of each stress stage, especially in the last cycles, as illustrated in Figure 8.10 for TC(2)_T1 test. For that reason the representative resilient modulus of each stress level was considered the average value of the last 10 cycles, as suggested in the standard.

In Figure 8.11 the evolution of that characteristic resilient modulus with the stress level is analysed by plotting its value against the ratio of the maximum vertical stress ($\sigma'_v{}^{max}$) to the confining pressure (σ'_c). As there is a clear difference between the resilient modulus of both types of specimens, being the values of TC(5) almost tenfold of TC(2) for some stress levels, they are separated in different graphs. The stress stage associated to the first conditioning is also plotted for comparison.

The conditioning stage was performed at a significant stress level, as Figure 8.11 indicates, according to the standard suggestion, inducing a relevant damage in the specimens. While this conditioning is necessary and desirable in granular materials so that particles are better rearranged and can better support the following loads, in cemented materials the conditioning can induced bond breakage decreasing the benefits of cementations.

In TC(2), the low value of the conditioning resilient modulus is the evidence of a destructuration of the weak cementitous bonds and, thus, the behaviour became close to the one expected in a granular material. For that reason, in the following stages the resilient modulus decreased with increasing stress level for each confining pressure.

In the TC(5) the high conditioning resilient modulus indicates that the degradation induced by this stage was less important. However, it was still significant since the resilient moduli of the following stages exhibit lower values than the conditioning resilient modulus. Nevertheless, in the lower effective confining pressure (50 kPa) increasing stress levels correspond to an increase in the resilient modulus; while at the intermediate confining pressure, the resilient modulus only increased in the first increment of stress level, decreasing after that. Finally, at the higher confining pressure, the pattern is similar to TC(2) as the moduli decreased with increasing stress level.

This is understandable in the sense that the behaviour of a cemented soil is a compromise between cementation strength and destructuring induced by stress level. When the cementation is weak (as in TC(2)), even low levels of stress destroy the weak cementitous bonds and thus the resilient modulus decreased. When the cementation is stronger, low

levels of stress cannot destroy the structured material and so the modulus increased being more determinant the increasing value of the mean effective stress. As the stress level increased, the cemented bonds are progressively destroyed causing a decrease in the resilient modulus.

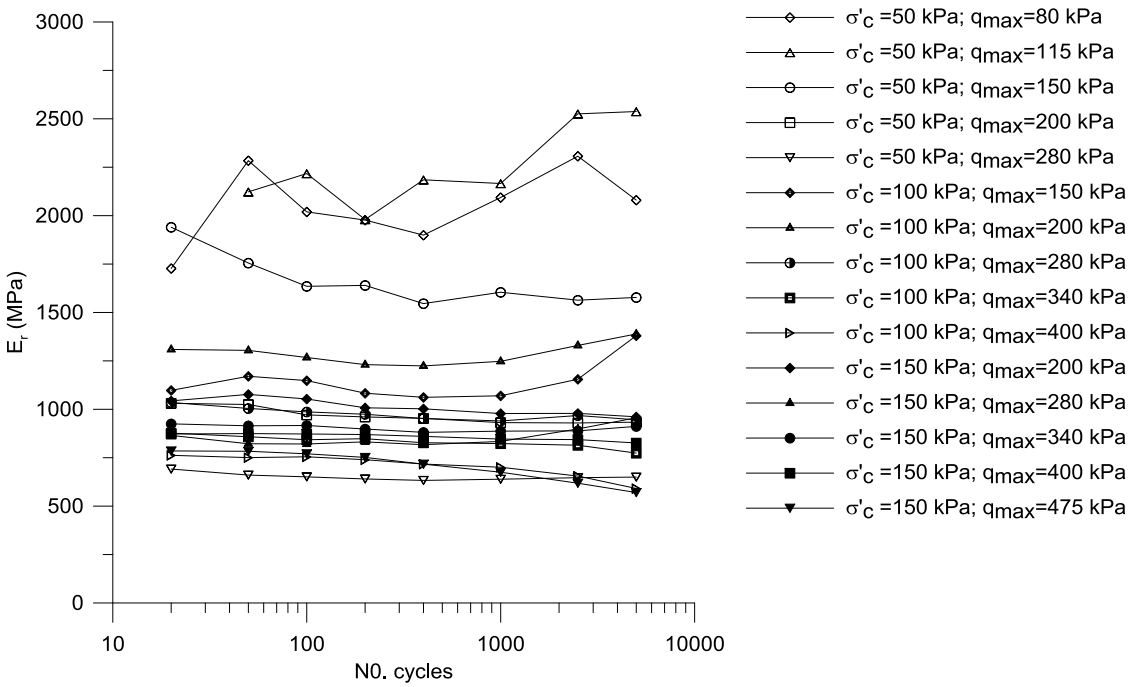

Figure 8.10 Evolution of the resilient modulus with the number of cycles for all the stress stages of TC(2)_T1 test

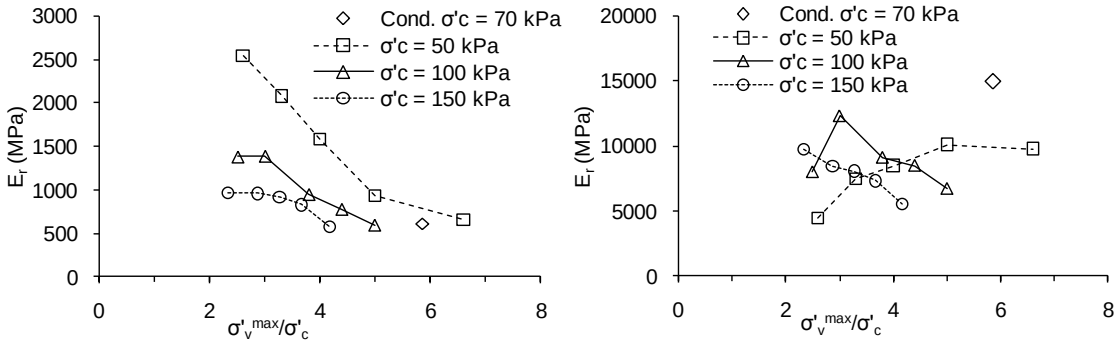

a) b)

Figure 8.11 Evolution of the resilient modulus with the stress level for each confining pressure: a) TC(2)_T1; b) TC(5)_T1

8.5.3 European Standard classification

Following the European standard (CEN, 2004a), unbound granular materials can be classified according to the permanent deformation obtained in the conditioning part ($\varepsilon_p{}^c$) and the resilient modulus for stress values of p'=250 kPa and q=500 kPa (E_c) according to Table 8.5.

Table 8.5 Classification based on the mechanical performance parameters E_c and $\varepsilon_p{}^c$ (CEN, 2004a)

Class	Characteristic elastic modulus, (E_c)	Characteristic permanent strain, ($\varepsilon_p{}^c$)
C1	500 MPa ≤ E_c	$\varepsilon_p{}^c \leq 2.5 \times 10^{-3}$
C2	500 MPa ≤ E_c	$2.5 \times 10^{-3} < \varepsilon_p{}^c \leq 6 \times 10^{-3}$
	250 MPa ≤ E_c < 500 MPa	$\varepsilon_p{}^c \leq 6 \times 10^{-3}$
C3	E_c < 250 MPa	$6 \times 10^{-3} < \varepsilon_p{}^c$

It can be seen that even the higher levels of stress suggested for the B method (constant confining pressure) do not achieve such high stress values. Therefore, the standard classification chart could not be applied correctly in this case. Nevertheless, it is clear that TC(5) stays highly above the upper class (C1) characterised by resilient modulus above 500 MPa and accumulated permanent deformation during conditioning below 0.25%. In the less cemented specimen (TC(2)) the accumulated permanent deformation is lower than 0.25% but the resilient modulus is slightly below 500 MPa, indicating that with a higher level of stress, a lower class (eventually “C2”) would be obtained.

8.6 Type 2 tests results

8.6.1 TC(2) and TC(5)

Type 2 tests, conducted for the permanent deformation evaluation, consist in the application of several stress levels in stages of 10 000 cycles, for which the accumulated permanent deformation is measured. First, the same two specimens tested before (TC(2) and TC(5)) were used according to the test program defined on section 8.3. For these two specimens, the standard procedure will be herein analysed.

The permanent deformation procedure can be interpreted by the shakedown theory explained in Chapter 3, which is the basis of the interpretation model suggested in the European Standard. Following Figure 3.15 similar graphs were plotted with the test data in order to see which type of behaviour was present.

Rate of accumulated permanent deformation

TC(2) results, plotted in Figure 8.12, show that the rate of the accumulated permanent deformation (ε_p rate), defined as equation (8.2), tended rapidly to zero, even in the most heavy stress stage (σ'_c = 80 kPa and q_{max} = 600 kPa). Figure 8.13, concerning TC(5) results, shows that the rate of permanent deformation are almost zero with some scatter due to the low level of strains. Considering these results, this material (even the least cemented) can be classified within Range A - Plastic Shakedown Range - characterised by

a plastic response for a finite number of cycles, while after the postcompaction period the response becomes entirely resilient without further permanent deformations.

$$\varepsilon_p\ rate\ (\%) = \frac{\varepsilon_p}{No.cycles} \tag{8.2}$$

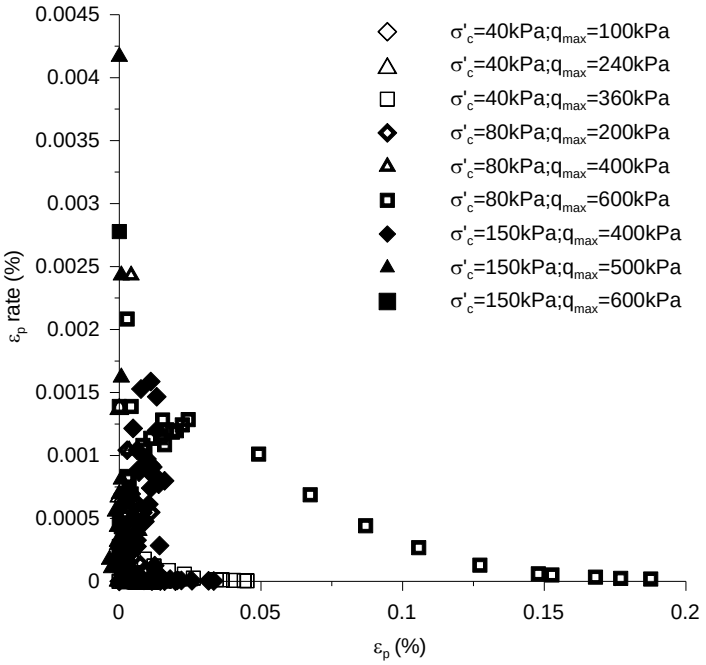

Figure 8.12 Plot of the vertical permanent strain rate against vertical permanent deformation in TC(2)_T2 following Werkmeister et al. (2004) to distinguish between different ranges of behaviour.

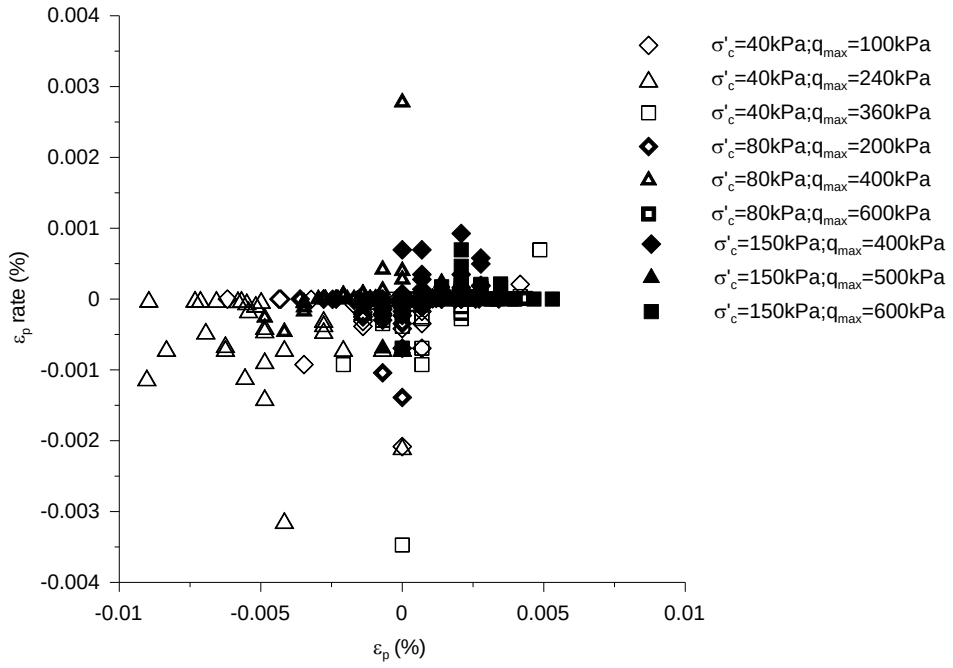

Figure 8.13 Plot of the vertical permanent strain rate against vertical permanent deformation in TC(5)_T2 following Werkmeister et al. (2004) to distinguish between different ranges of behaviour

Resilient strain

The results of the resilient strain presented in Figure 8.14 and 8.15 show a completely stabilised behaviour for both types of specimens after a few number of cycles, in agreement with the Range A classification reported before.

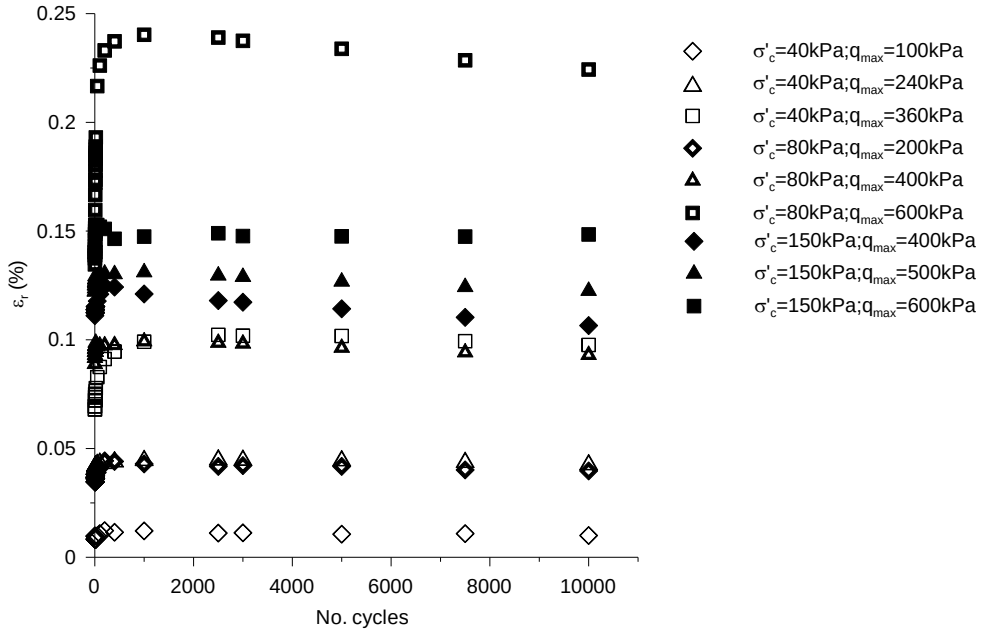

Figure 8.14 Plot of the vertical resilient strain against the number of cycles in TC(2)_T2 following Werkmeister et al. (2004) to distinguish between different ranges of behaviour.

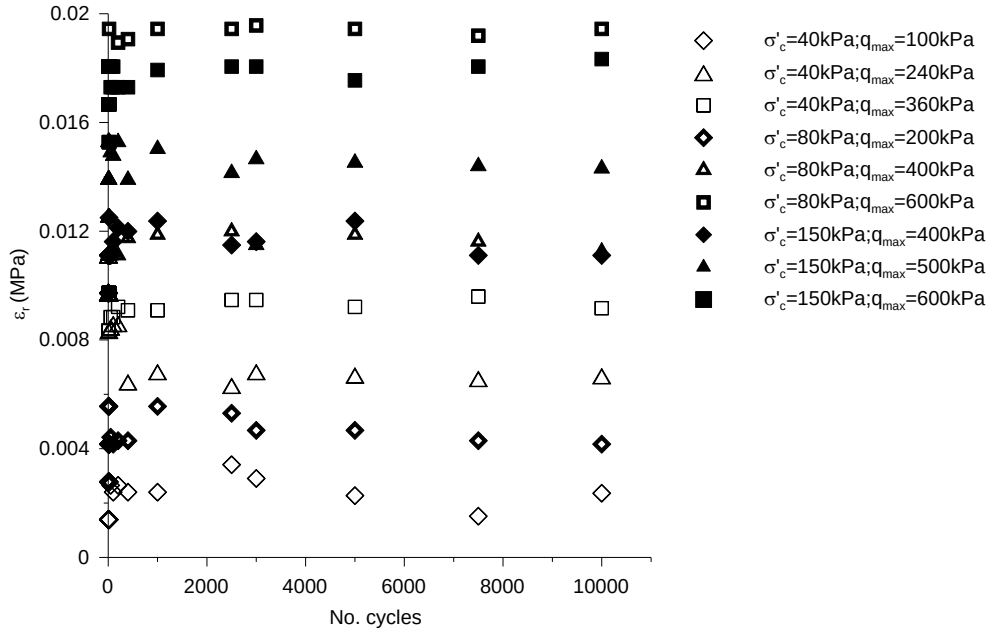

Figure 8.15 Plot of the vertical resilient strain against the number of cycles in TC(5)_T2 following Werkmeister et al. (2004) to distinguish between different ranges of behaviour

Permanent deformation

The evolution of the permanent deformation with the number of cycles in logarithmic scale was observed in the two specimens. In spite of the very low rate of permanent deformation in the TC(2) specimen (showed in Figure 8.12), the plot of the permanent deformation against the number of cycles in logarithmic scale shows a continuous increase even at 10 000 cycles (Figure 8.16), for the stress stage of σ'_c = 80 kPa and q_{max} = 600 kPa, indicating that at this stage the specimen shows Range B type of behaviour. In the TC(5) specimen the permanent deformation seems quite stable during the cycling period and within very small values (Figure 8.17), characteristic of Range A.

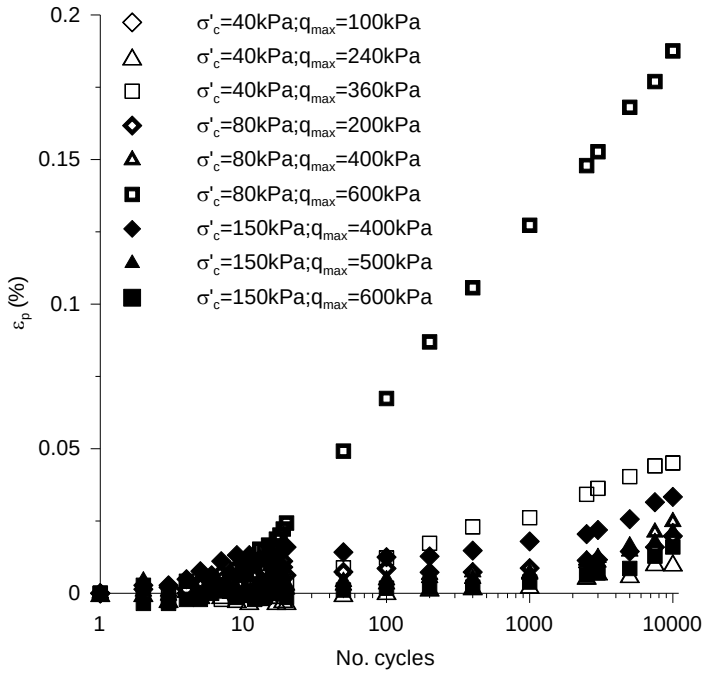

Figure 8.16 Plot of the vertical permanent strain against the number of cycles in TC(2)_T2

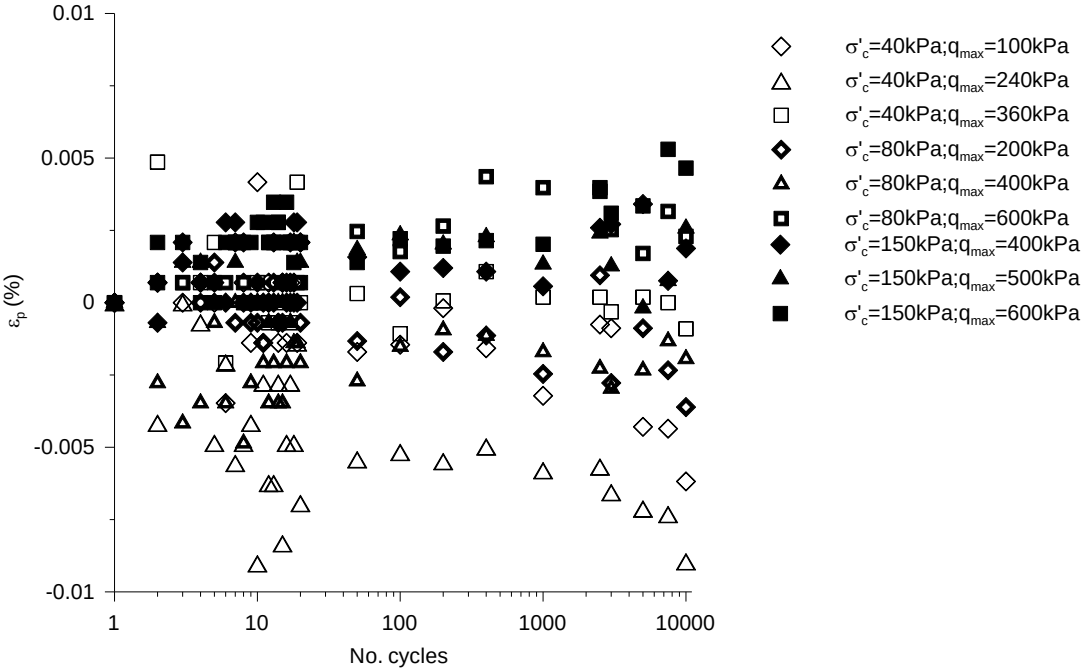

Figure 8.17 Plot of the vertical permanent strain against the number of cycles in TC(5)_T2

Standard model

In spite of the reduced number of tests a tentative was made to define a model for cemented materials, as proposed in the European standard described in Chapter 3, in which any material could be classified within the different ranges without performing more time consuming cyclic tests.

In order to define the model constants, it is necessary that for each confining pressure the specimen should be subjected to increasing deviator stress levels according to Table 3.4 until the following strain is reached: $\varepsilon_p 5000 - \varepsilon_p 3000 > 0.04\%$. Unfortunately, the levels of stress applied were not enough to obtain such strain values and therefore, the model could not be completed. Table 8.6 confirms that the accumulated permanent deformation between 5000 and 3000 cycles for each level of stress is always below 0.0045% for both types of tests with exception of just one stress level in TC(2). As reported in Chapter 3, the value of 0.0045% is the strain value suggested in the European standard (based on Werkmeister, 2003) for the definition of the Plastic Shakedown limit. The Plastic Creep limit would be then defined for accumulated permanent strains between 5000 and 3000 cycles of 0.04%.

It was observed that most stress stages show a Range A type of behaviour, except the one at σ'_c = 80 kPa and q_{max} = 600 kPa in TC(2). With just one point out of Range A it was not possible to define the curves of Figure 3.17. It is possible that these strain limits should be

revised for cemented materials. However, in this work not enough tests were performed to propose such values.

Table 8.6 Accumulated permanent deformation between 5000 and 3000 cycles for each stress level

σ'_c	q_{max}	$\sigma'_v{}^{max}/\sigma'_c$	ε_p (%) = ε_p(5000)-ε_p(3000)	
kPa	kPa		TC (2)	TC (5)
40	100	3.5	0.0004	0.0000
	240	7.0	0.0000	0.0000
	360	10.0	0.0040	0.0005
80	200	3.5	0.0028	0.0019
	400	6.0	0.0040	0.0006
	600	8.5	0.0153	0.0000
150	400	3.7	0.0037	0.0007
	500	4.3	0.0038	0.0000
	600	5.0	0.0015	0.0003

8.6.2 TC(7) and TC(7*)

Type 2 tests were also performed over three 7% cement content specimens with higher load levels in the last stages in drained and undrained conditions to pursue the following aims:

1 - analysis the behaviour at higher loads in terms of strains levels and the model proposed in the standard that could not be applied in the previous specimens;

2 - analysis the differences between drained and undrained behaviour (TC(7));

3 - compare two different void ratios keeping the same cement content (TC(7) and TC(7*));

4 - compare two different void ratios keeping the same adjusted porosity/cement ratio $n/C_{iv}{}^{0.21}$=29 (TC(5) and TC(7));

1) Higher loads

In these three specimens, tested at higher stress levels, the accumulated permanent deformation between 5000 and 3000 cycles was again always below 0.0045% which unabled once again the application of the European standard model indicating that these limit values should be adapted for cemented materials.

Taking into account that the standard procedure cannot be followed, the data comprised by these three tests was no longer analysed in the standard's point of view. The permanent deformation was analysed at the end of the cycling period, i.e., the accumulated permanent deformation at the end of the 10000 cycles and a reference resilient modulus taken in the

middle of the cycling period was selected, calculated as the average value of the resilient modulus between 4990 and 5000. These two variables will be used subsequently to fulfil the remaining aims pointed above.

2) Draining conditions

The effect of draining conditions during cycling has revealed to be quite significant when specimens of 7% of cement content were tested with the same stress levels but in different draining conditions. Note that even in undrained tests the drainage valve was opened each time the confining pressure was changed so consolidation was allowed to occur, meaning that at the beginning of a new consolidation stress the conditions were similar in drained and undrained tests.

As reported previously, drained and undrained conditions have several advantages and disadvantages. In drained tests the volume change was not measured accurately due to the fast loading and small diameter of the drainage system. On the contrary, undrained tests allow a reliable measure of pore pressure, but the large generation of high pore pressure reduces the effective confining pressure decreasing its effect.

Figure 8.18a) and Table 8.7 summarize the results of the resilient modulus at 5000 cycles obtained in each stress level, illustrating that undrained moduli are always higher than the same stiffness modulus obtained in drained conditions. The results of the accumulated permanent deformation for each stress level are plotted in Figure 8.18b) well in agreement to the resilient modulus results: higher permanent deformations in the drained test.

This fact, apparently unexpected, may be related to a higher yielding in the drained tests derived from the flow of water out of the specimen as a consequence of the specimen deformation. This seems to be more important than the increase of the stress level in undrained conditions due to the reduction of the effective confining pressure. On the other hand, the Young modulus is not a pure distortional modulus like the shear modulus (G) and it depends on the Poisson ratio (ν) according to equation (8.3),

$$E = 2G(1 + \nu) \tag{8.3}$$

Therefore, if the specimen has different Poisson ratios in drained and undrained conditions, then the Young Modulus can be different. Considering that undrained behaviour is characterized by no volume change, the Poisson ratio should be close to 0.5; while for draining conditions it is more difficult to know the exact value. However, whether the value of the Poisson ratio in drained conditions, the relationship between the undrained resilient

modulus and the drained resilient modulus has to be between 1 and 1.5 because the Poisson ratio only assumes values between 0 and 0.5,

$$\frac{E_r^{und}}{E_r^{dr}} = \frac{2G(1+0.5)}{2G(1+\upsilon_{dr})} = \frac{1.5}{1+\upsilon_{dr}} \tag{8.4}$$

The relationship between undrained and drained resilient modulus is also presented in Table 8.7. Most values are in the range [1-1.5] although there are also some exceptions which may be associated to yielding where the elastic Poisson ratio is no longer valid. For this reason, it is quite possible that the difference between drained and undrained modulus should be due to a distinct volumetric behaviour more than to the different value of the Poisson ratio. Measuring S wave velocities would allow the evaluation of the maximum shear modulus in both conditions, which could be compared without the volumetric effect. However, although being difficult to measure waves during a cyclic test due to interferences, in future works it is planned to allow for measurements of these velocities after each cycling phase.

Table 8.7 Effect of draining conditions in resilient modulus

σ'_c	q_{max}	q_{max}/σ'_c	E_r (MPa)		E_r^{und}/E_r^{dr}
kPa	kPa		Drained	Undrained	
40	100	2.5	3917	3799	1.0
	240	6.0	2609	3837	1.5
	360	9.0	2651	3527	1.3
80	200	2.5	2133	4460	2.1
	400	5.0	2494	3379	1.4
	600	7.5	1675	2989	1.8
150	400	2.7	1837	3147	1.7
	600	4.0	1810	2426	1.3
	900	6.0	1559	2022	1.3

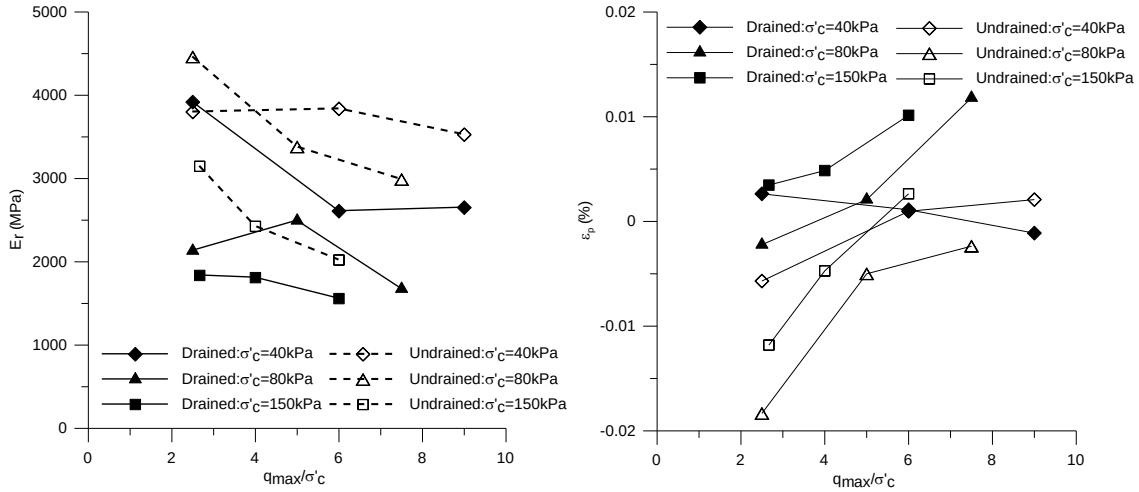

Figure 8.18 Comparison between drained and undrained cycling of specimens TC(7): a) resilient modulus at cycle 5000 against load level; b) accumulated permanent deformation during the cycling period for each stress stage

3) Initial void ratio

Two 7% cement content specimens, TC(7) and TC(7*), with the moulding conditions presented in Table 8.1, were moulded with different void ratios (respectively 0.64 and 0.50) so that the effect of the initial void ratio in the resilient modulus and permanent deformation could be analysed. The specimens were tested drained with the load sequence expressed before giving rise to the results expressed in Table 8.8 and Figure 8.19.

Table 8.8 Effect of void ratio on resilient modulus

σ'_c	TC(7*)			TC(7)		
	q_{max}	q_{max}/σ'_c	E_r	q_{max}	q_{max}/σ'_c	E_r
kPa	kPa	kPa	MPa	kPa	kPa	MPa
40	100	2.5	6091	100	2.5	3917
	240	6.0	7883	240	6.0	2609
	360	9.0	8461	360	9.0	2651
80	200	2.5	6265	200	2.5	2133
	400	5.0	9437	400	5.0	2494
	600	7.5	6820	600	7.5	1675
	400	5.0	5243			
	600	7.5	5038			
	900	11.3	4079			
150	800	5.3	3952	400	2.7	1837
	900	6.0	4428	600	4.0	1810
	1400	9.3	2956	900	6.0	1559

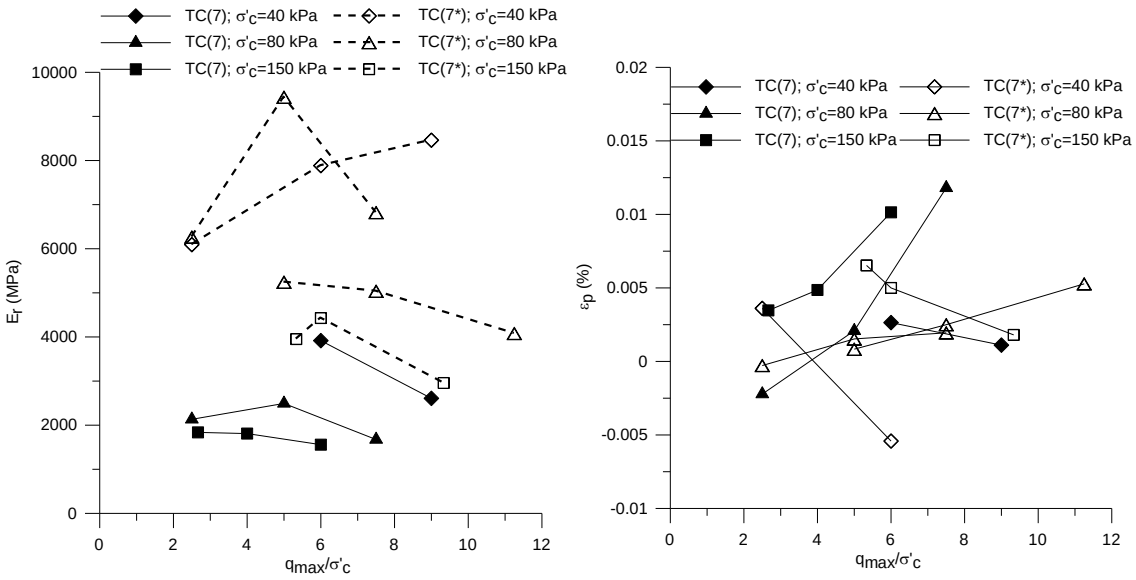

Figure 8.19 Different behaviour of specimens with the same cement content but different moulding void ratio (TC(7) with e_0=0.64 and $n/C_{iv}^{0.21}$=29; and TC(7*) with e_0=0.50 and $n/C_{iv}^{0.21}$=24): a) resilient modulus at cycle 5000 against load level; b) accumulated permanent deformation during cycling period for each stress stage

In spite of the stress levels of the first stages being the same in both specimens, the specimen with lower void ratio (TC(7*)) revealed much higher values for the resilient modulus (Figure 8.19a). In the last stages TC(7*) was tested with higher stress levels revealing a significant reduction in resilient moduli, which still remained above the TC(7) results tested at lower stress levels. From these results, it is clear that the initial void ratio has a significant effect on the resilient modulus.

The permanent deformation evolution is more difficult to interpret due to the scatter derived from the low strain level (Figure 8.19b).

3) Adjusted porosity/cement ratio

Finally, two specimens moulded with the same adjusted porosity/cement ratio ($n/C_{iv}^{0.21}$=29) but different cement contents (5% and 7%) were tested undrained in order to compare resilient moduli and permanent deformation results. In terms of resilience, the results are expressed in Table 8.9 and Figure 8.20a) while the permanent deformation results are presented in Figure 8.20b).

Apart of the usual scatter of permanent deformation results, it is still possible to recognize that TC(5) specimen shows higher resilient moduli. It is surprising that the higher permanent deformations are also from TC(5) but this may be the result of some scatter on the strain measurements. From the static results, where it was shown that the adjusted

porosity/cement ratio played an important role on the definition of strength and stiffness, it should be expected that resilient moduli would be similar for both specimens at similar stress levels. In fact, the difference between the moduli of both specimens is not as significant as it was observed in the previous item (TC(7) and TC(7*)), but there is still a slightly difference. More tests are to be performed in order to understand whether these results are due to the scatter of low strain measurements.

Table 8.9 Comparison of specimens with different cement content and same adjusted porosity/cement ratio

σ'_c	TC(5)			TC(7)		
	q_{max}	q_{max}/σ'_c	E_r	q_{max}	q_{max}/σ'_c	E_r
kPa	kPa	kPa	MPa	kPa	kPa	MPa
40	100	2.5	5620	100	2.5	3453
	240	6.0	4466	240	6.0	3837
	360	9.0	4260	360	9.0	3527
80	200	2.5	5328	200	2.5	4460
	400	5.0	3726	400	5.0	3379
	600	7.5	3129	600	7.5	2989
150	400	2.7	3717	400	2.7	3147
	500	3.3	3758	600	4.0	2426
	600	4.0	3668	900	6.0	2022

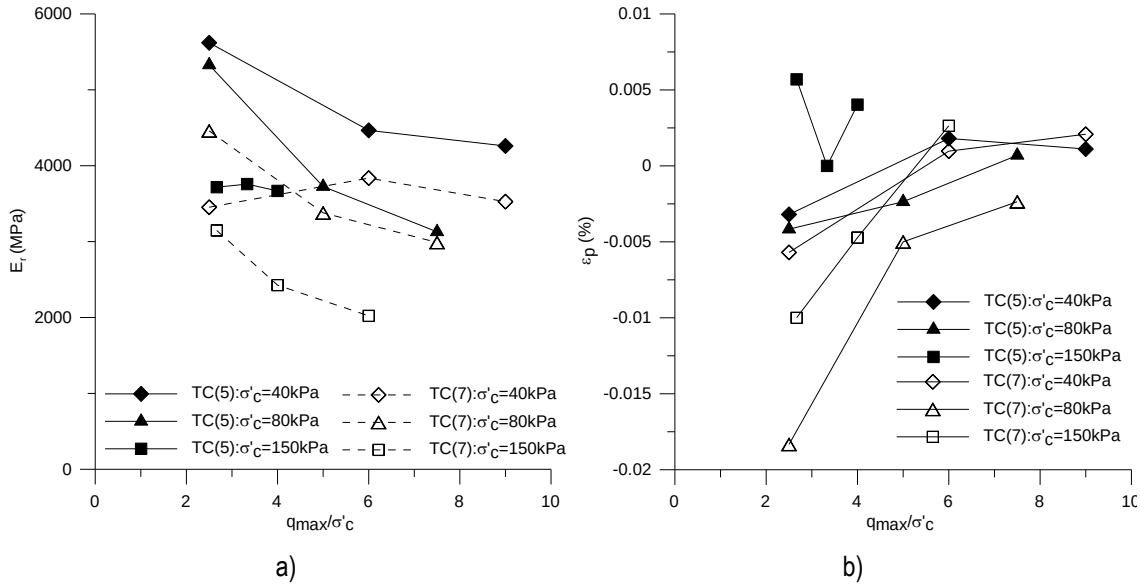

Figure 8.20 Different behaviour of specimens with the same adjusted porosity/cement ratio $n/C_{iv}^{0.21}$=29 but different cement contents: a) resilient modulus at cycle 5000 against load level; b) accumulated permanent deformation during the cycling period for each stress stage

8.7 Type 3 tests results

Type 3 tests are not stated in the European standard. The aim was to perform a great number of cycles at low stress level in order to analyse the fatigue response of very stiff

cemented soils. In fact, the behaviour of these mixtures in long term conditions is generally not very well know leading to some apprehension in their use in works with strict requirements.

In terms of the stress level, an attempt was made to use a low level of stress that would be representative of what is the expected load that soil-cemented mixtures are subjected in the foundation layers of the structural platforms in highway and railways lines (this including pavement or tracks and bases, sub-bases and ballast). The cyclic frequency of 1 Hz was kept constant throughout the work due to equipment limitations and therefore, performing tests with half million cycles was very time consuming. For that reason, only 5% cement content specimens were studied.

8.7.1 Undrained TC(5) test

The first test, performed on a TC(5) specimen, took place in two stages, both with 40 kPa of effective confining pressure, being the maximum deviatoric stress of 150 kPa in the first 250 000 cycles and 200 kPa in the next 250 000 cycles. The test was performed in undrained conditions in each load stage but between the two stages the drainage valve was opened and therefore the soil was allowed to consolidate.

The results for both load stages, in terms of resilient modulus and permanent deformation, are compared in Figure 8.21. The resilient modulus seems quite constant throughout the cyclic loading in agreement to the previous tests (Figure 8.21a). The accumulated permanent deformation against the number of cycles, plotted in linear scale (Figure 8.21b), shows some trend to stabilise, which is more precocious in the second and higher induced stress stage (q_{max} = 200 kPa) than in the first (q_{max} = 150 kPa). When plotting the same in logarithmic scale (Figure 8.21c) as presented before, no sign of any trend for stabilisation is observed. To help on a better interpretation of the trends, the rate of the permanent deformation was plotted against the load cycles (Figure 8.21d), being clear that it evolutes to very low values, although still not null.

It is interesting to notice that, even in a stiff specimen like TC(5) where negligible permanent deformations were observed in type 1 and 2 tests, there is a clear increase of the accumulated permanent deformations when higher number of cycles were imposed. Therefore, from the measured permanent deformations between 5000 and 3000 cycles, it cannot be concluded that the material has reached the plastic shakedown as the European standard suggests. It is likely that standard values should be revised when cemented mixtures are involved, not only in terms of permanent deformation limits but also in the number of cycles required for those analyses.

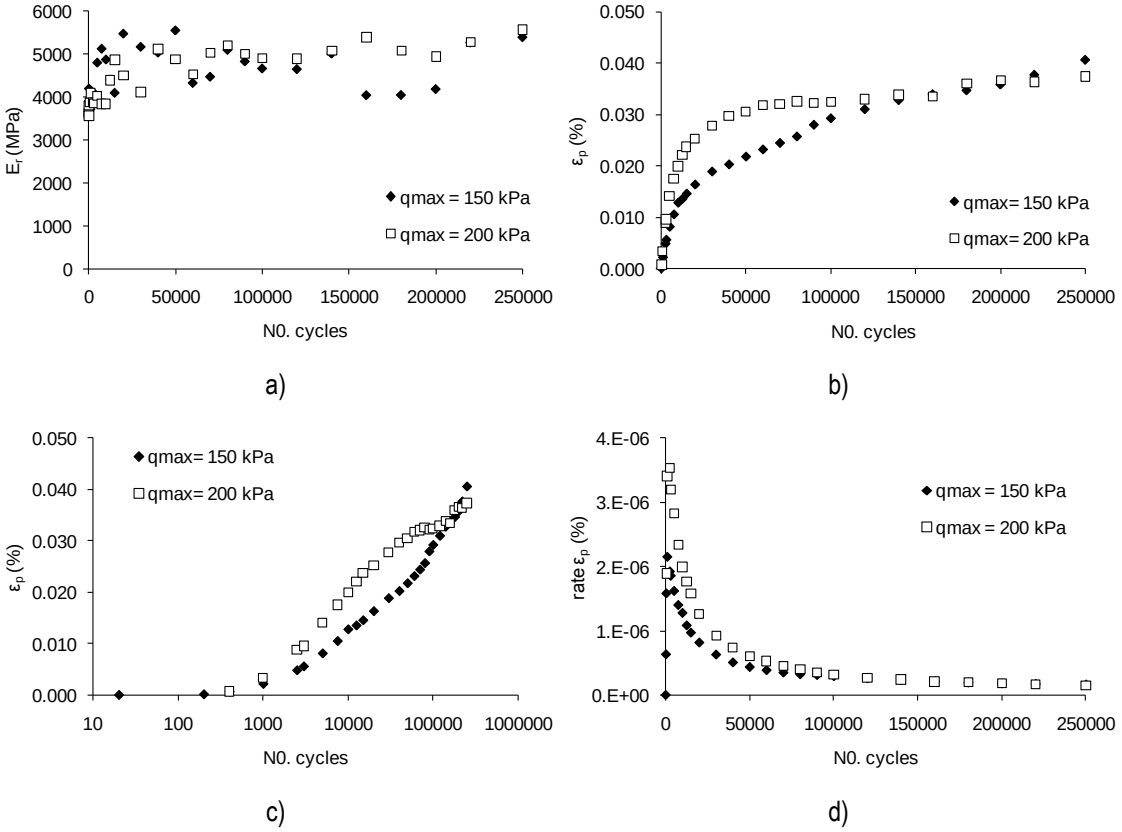

Figure 8.21 Results in TC(5) specimen tested in undrained conditions: a) evolution of the resilient modulus with the number of cycles; b) evolution of the permanent deformation in linear scale; c) and in logarithmic scale; d) rate of permanent deformation

8.7.2 Drained TC(5) test

The second test was similar to the first but in this case the test was totally drained and each load stage had half million cycles, which gives 1 million cycles at the end of the test. The resilient modulus evolution with the number of cycles, presented in Figure 8.22a), shows more scatter in the second stage with 200 kPa of maximum range of cyclic deviatoric stress, but, in general the modulus remains relatively constant during the test. The accumulated permanent deformation (Figure 8.22b and c) evolution was quite surprising, since in none of the stages it was observed any trend for stabilization, conversely to what happened in the previous test. The rate of permanent deformation seems to have achieved a constant value (Figure 8.22d), especially in the second stress stage (q_{max}=200 kPa).

This higher sensitivity to the accumulation of damage with the number of cycles in drained conditions is as important as determinant and so it should be checked in future works. Additionally, the behaviour before and after 10 000 cycles seems to be different (Figure 8.22c) indicating that the analyses of the first 10 000 cycles may be insufficient to evaluate this material behaviour.

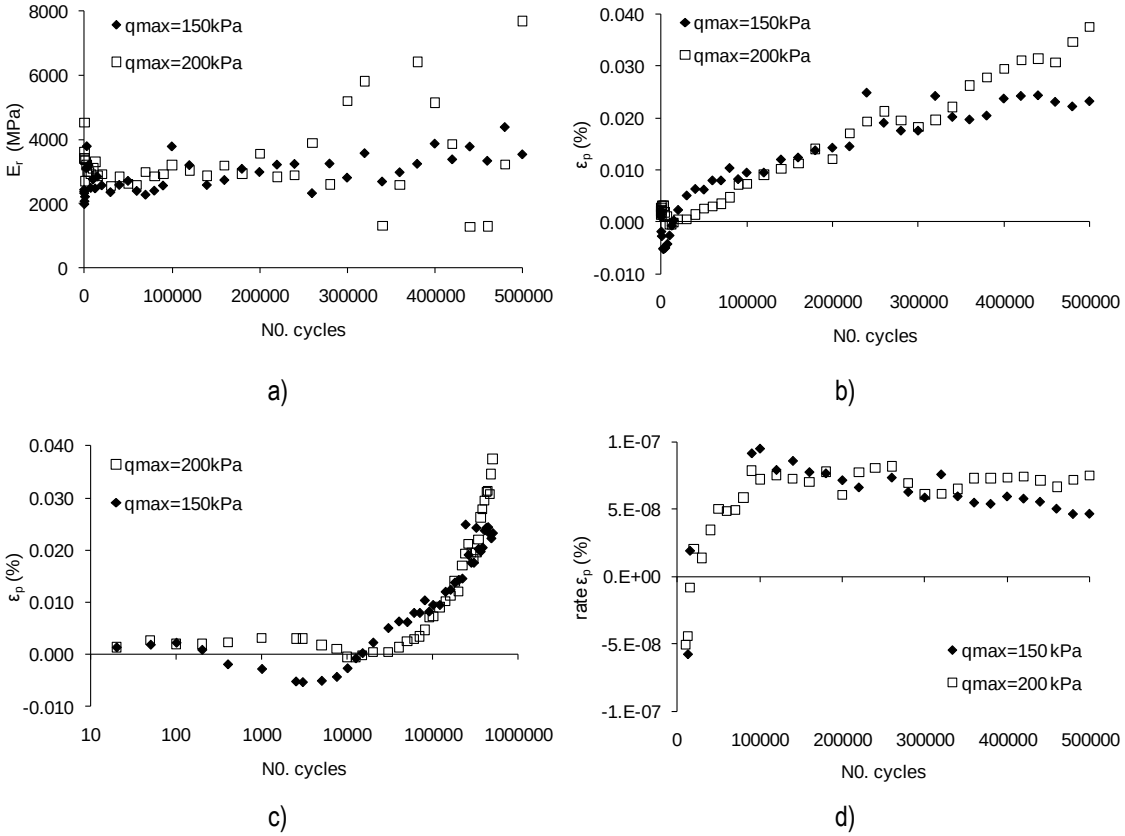

Figure 8.22 Results in TC(5) specimen tested in drained conditions: a) evolution of the resilient modulus with the number of cycles; b) evolution of the permanent deformation in linear scale; c) and in logarithmic scale; d) rate of permanent deformation

8.7.3 Drained TC(5*) test

A third test was performed over a more compacted specimen TC(5*) in order to evaluate if with a higher compaction level the permanent deformations were still increasing continuously as observed on the previous tests. This specimen was tested drained following the same procedure as the second test.

The results are presend in Figure 8.23 in the same way as before. In opposition to the previous two tests, the second stage loaded with 200 kPa showed higher resilient modulus than in the first stage with 150 kPa, although their value remained quite constant along the cyclic period (Figure 8.23a). The permanent deformations remained quite low during both load stages due to the high compaction level and no trend for increasing was noticed (Figure 8.23b and c) along with almost zero rate of permanent deformation (Figure 8.23d) conversely to the previous tests. Is it possible that an even higher number of cycles were needed to have enough accumulated permanent deformations in this very stiff specimen? Only more tests could answer this question.

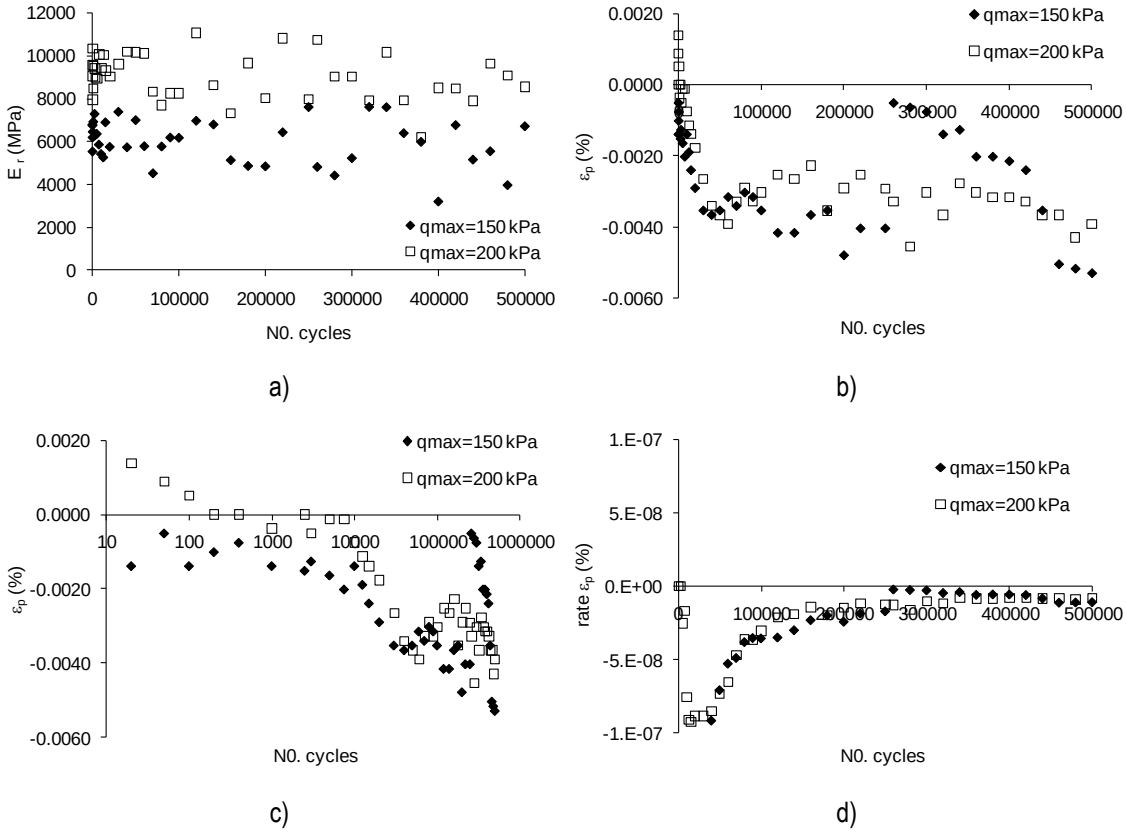

Figure 8.23 Results in TC(5*) specimen tested in drained conditions: a) evolution of the resilient modulus with the number of cycles; b) evolution of the permanent deformation in linear scale; c) and in logarithmic scale; d) rate of permanent deformation

8.7.4 Comparison between drained and undrained conditions

In the next graphs, the results obtained in the first two tests with TC(5) specimens, drained and undrained, are plotted for comparison, for each loading stage. On Figure 8.24 the resilient modulus is presented, being clear that the undrained moduli is always greater than the drained moduli, as concluded before in type 2 tests. In terms of permanent deformation, expressed in Figure 8.25, the difference between the values obtained in different draining conditions is significant: the undrained test revealed a strongly higher rate of increase of the permanent deformation than the drained tests. This fact is remarkable and it has not been previously observed when type 2 tests results were analysed. It seems that in undrained conditions the resilient deformation is smaller and the permanent deformation is higher while in drained tests the opposite is observed. Unfortunately, the small number of cycles applied in type 2 tests leading to the low level of accumulated permanent deformation was not enough to take consistent conclusions.

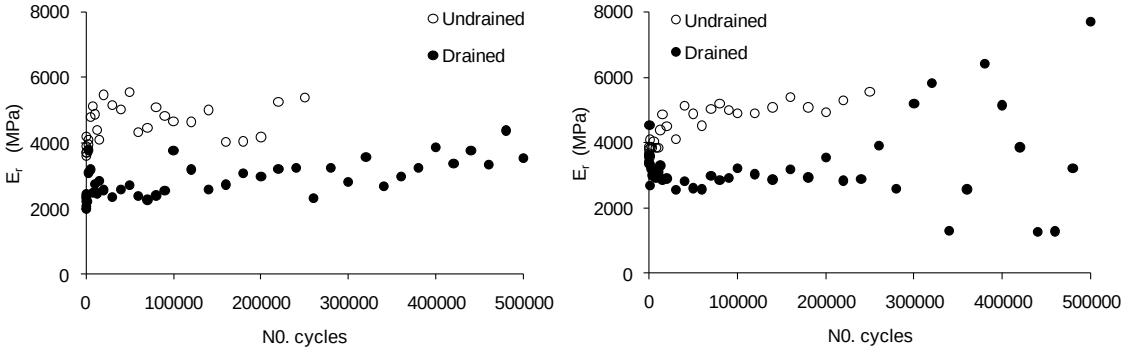

Figure 8.24 Comparison of the resilient modulus evolution in drained and undrained conditions: a) q_{max} = 150 kPa; b) q_{max} = 200 kPa.

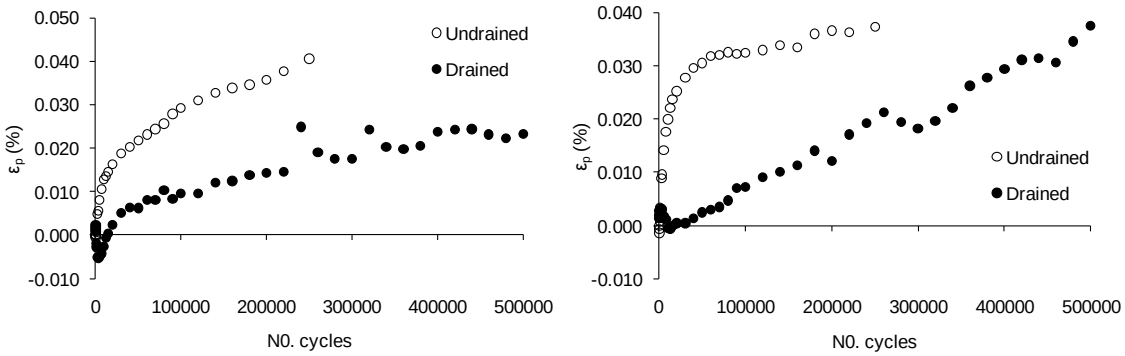

Figure 8.25 Comparison of the permanent deformation evolution in drained and undrained conditions: a) q_{max} = 150 kPa; b) q_{max} = 200 kPa.

8.7.5 Comparison between different initial void ratios

The following graphs will compare the second and third tests performed over 5% cement content specimens with different compaction levels (e_0= 0.58 and e_0=0.50) and tested drained. The results are very clear showing, as expected, that the higher compacted specimen has higher resilient modulus (Figure 8.26) and lower permanent deformations. In Figure 8.27 the different behaviour of both specimens in terms of permanent strain behaviour is obvious because the accumulated permanent deformation highly increases in TC(5) and remains constant in TC(5*).

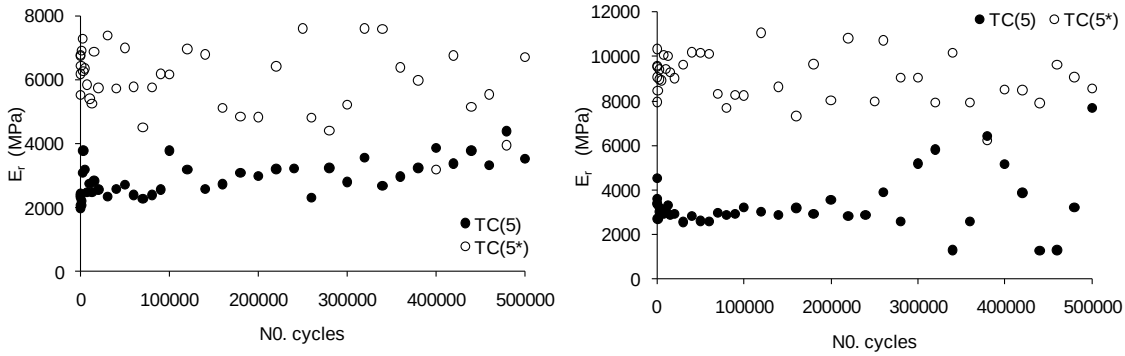

a) b)

Figure 8.26 Comparison of the resilient modulus evolution in TC(5) and TC(5*): a) q_{max} = 150 kPa; b) q_{max} = 200 kPa.

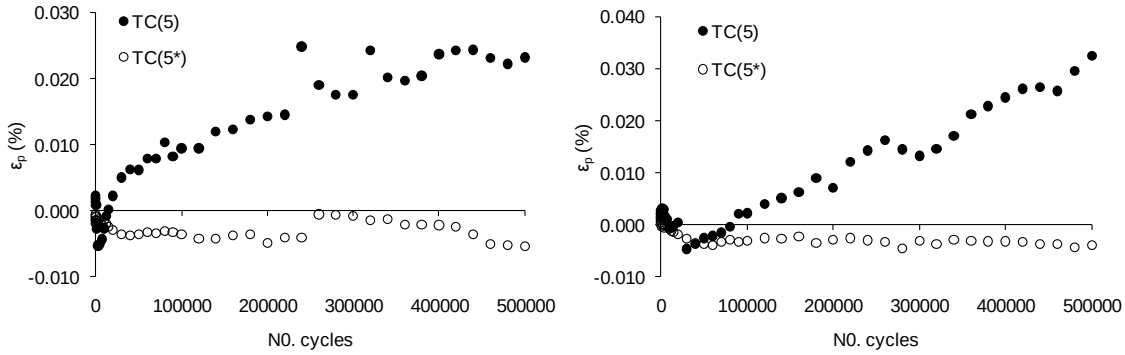

a) b)

Figure 8.27 Comparison of the permanent deformation evolution in TC(5) and TC(5*): a) q_{max} = 150 kPa; b) q_{max} = 200 kPa.

8.8 Conclusions

This chapter presented the results of 10 cyclic triaxial tests from which diverse and significant issues were analysed. The first tests focused mainly on the European standard procedures in order to evaluate the resilience and the permanent deformation accumulation. All the tests converged to a resilient behaviour after a few number of cycles, irrespectively of the cement content, stress level or initial void ratio. This was observed in the evolution of the resilient modulus or strain with the number of cycles. However, the resilient modulus takes different values depending, for example, on the stress level or cement content. The specimens moulded with 5% of cement content presented resilient modulus almost tenfold of the ones observed in the 2% cement content specimens. The evolution of the resilient modulus within the several stress stages revealed clearly the relationship between cementation and stress level in the sense that weak cemented bonds are easily destroyed by induced cyclic stresses. Therefore, the resilient modulus decreased

notoriously with higher stress levels. On the contrary, specimens with higher cement contents supported higher stresses until bonding breakage.

In terms of permanent deformation, according to the European standard procedure the studied soil-cement mixtures were all in the Range A named Plastic Shakedown Range, for most of the stress levels applied, characterised by a plastic response for a finite number of cycles, while after the postcompaction period the response becomes entirely resilient without further permanent deformations. However, the last tests performed in the stiff specimen (TC(5)) at a greater number of cycles, showed a continuous increase of the accumulated permanent deformations, while the previous “standard” tests performed on this specimen showed almost zero permanent deformations. For this reason, it is considered that a new standard adapted to cemented materials should be developed so that different loads, reference strain limits and classification charts can be adapted to these materials. It is not certain that the Shakedown theory, from which the actual European standard is based, can be directly applied to these materials, since cemented materials are progressively degradated (due to bonding breakage) with increasing stress level or number of cycles. To have a better understanding of this issue, tests with a great number of cycles like the last tests performed in this cyclic experimental program, can be very useful as the field situation is more accurately simulated, and long terms conditions are better understood.

The comparison between drained and undrained conditions also produced some interesting findings. Undrained conditions led to higher resilient modulus than drained conditions which might be related to the volumetric effect on the Young Modulus. In terms of plastic behaviour, the long tests revealed a much faster accumulation of the permanent deformation in the undrained tests that has not been detected before in the tests with a small number of cycles. It seems that in undrained conditions the resilient deformation is smaller and the permanent deformation is higher than in drained tests.

The initial void ratio introduced a significant effect on both the resilient or plastic behaviour, as it would be expected, while the adjusted porosity/cement ratio that was considered very much representative of strength and stiffness in static tests was not so efficient in cyclic conditions. However, this might be related to the greater scatter presented by these tests mainly due to the low level of strain involved.

Measuring strain and stiffness properties in very stiff materials is not an easy task, especially in cyclic conditions, however, some interesting issues were analysed and discussed, which might help other research works that are being developed.

Chapter 9.
CONSTITUTIVE MODEL CALIBRATION

9.1 Introduction

The aim of the work presented in this chapter was to take advantage of the great amount of laboratory data shown in the previous chapters to calibrate a constitutive soil model, in order to obtain the most representative parameters of the cemented soil studied in this research work. For that purpose, triaxial compression tests similar to the ones performed in the laboratory, were simulated by the numerical model taking into account diverse parameters.

9.2 Description of the constitutive model

9.2.1 The original CASM

The constitutive model selected for this calibration is based on the original Clay and Sand model (CASM) developed by Yu (1998), being a simple unified critical state constitutive model based on the state parameter defined as the vertical distance between current state (v, p') and the critical state line in v-ln p' space. One of its greatest advantages is that this model can be either applied to sands or clays.

CASM is an elastic-plastic strain hardening (or softening) model that postulates that a soil specimen can be considered as an isotropic continuum with an isotropic hardening law, that is, the isotropic volumetric plastic strain hardening follows a law like the one expressed in (9.1). It uses a non associated flow rule with a yield function presented in equation (9.2), while the plastic potential function depends on Rowe's stress-dilatancy relationship (Rowe, 1962), expressed in equation (9.3).

$$\frac{dp'_s}{p'_s} = \frac{v}{\lambda - k} d\varepsilon_v^p \tag{9.1}$$

$$f = \left(\frac{q}{M.p'}\right)^n \frac{1}{\ln r} ln \frac{p'}{p'_s} \tag{9.2}$$

$$\frac{d\varepsilon_v^p}{d\varepsilon_s^p} = \frac{9(M-\eta)}{9+3M-2M.\eta} \tag{9.3}$$

where η is the stress ratio (q/p'), and ε_v^p ; ε_s^p are the volumetric and shear plastic strains, respectively.

The plastic potential function can be obtained by the integration of equation (9.3), resulting:

$$g = 3M\ ln\frac{p'}{\zeta} + (3+2M)\ln\left(\frac{2q}{p'}+3\right) - (3-M)ln\left(3-\frac{q}{p'}\right) \tag{9.4}$$

where ξ is a size parameter

Table 9.1 summarizes the model constants concerning the parameters that control the elastic behaviour of the soil, the parameters that define the critical state line, the yield surface parameters, as well as a parameter for the initial condition of the soil.

Table 9.1 CASM constants

	Symbol	Description
Elastic constants	k	slope of the isotropic swelling line
	ν	Poisson ratio
Critical state constants	λ	slope of the critical state line
	Γ	specific volume of the critical state line at p'=1 kPa
	M	stress ratio (q/p') at critical state
Shape of yield surface	r	spacing ratio
	n	stress-state coefficient
Initial conditions	OCR	overconsolidation ratio

9.2.2 The cemented CASM

Description of the model

Constitutive models to simulate the behaviour of structured soils are frequently found in the literature of the last decade, not only for structured clays (e.g., Kavvadas and Amorosi, 2000; Baudet and Stallebrass, 2004; Yan and Li, 2011) but also for granular materials and soft rocks (e.g. Liyanapathirana et al., 2005; Pinyol et al., 2007; Jiang et al., 2007). However, most of them involve a great number of parameters which need time consuming in situ and laboratory tests for their calibration and sometimes reflecting exclusively particular conditions or specific materials.

The model applied in this work, called herein cemented CASM and described by Gonzalez et al. (2007, 2009), consists on the extension of CASM based on the cemented formulation proposed by Gens and Nova (1993). Presently, this model has already been applied with great success in clays, natural structured (Gonzalez et al., 2007, 2009), and artificially cemented (Arroyo et al, 2011 and Ciantia et al., 2011). However, it is the first time a granular soil is calibrated with this model.

It should be noted that another different model for cemented materials based on CASM has been published recently by Yu et al. (2007b), but it will not be applied hereby. Although some parameters herein presented might seem similar to the ones used in Yu et al. (2007b) proposal, their meaning is not always equivalent.

The main extension of this model related to CASM is the introduction of a new state variable, b, representing “bonding”, according to the definition of Gens and Nova (1993). The shape of the yield surface is assumed to be the same in uncemented and cemented conditions, while the bonding (b) controls the size of the yield surface, enlarging it with increasing amount of cementation.

Yield function

The way the yield surface is enlarged due to the effect of bonding (b) is defined by two different parameters related with b, p'_c and p'_t, which control respectively the isotropic compression yield and the tensile yield of the soil (Figure 9.1), according to the following expressions:

$$p'_c = p'_s(1 + b) \tag{9.5}$$

$$p'_t = p'_s(\alpha\, b) \tag{9.6}$$

where,

- p'_s is the equivalent pre-consolidation pressure of the corresponding uncemented material for each current state (see Figure 9.1);
- α is a parameter associated to tensile strength directly related to cementation.

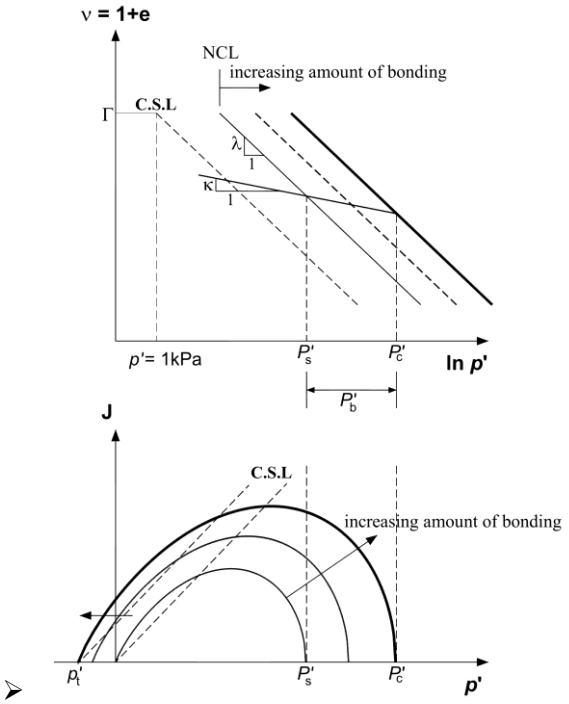

Figure 9.1 The normal isotropic consolidation lines (NCL), critical state lines (CSL) and yield surfaces for both unbonded and bonded materials (González et al., 2007).

The yield surface can, thus, be expressed by equation (9.7) similar to CASM yield function with some adjustments to account for the effect of bonding.

$$f = \left(\frac{q}{M(p' + p'_t)}\right)^n + \frac{1}{\ln r} ln\left(\frac{(p' + p'_t)}{p'_c}\right) \tag{9.7}$$

where M, n and r have the same meaning as in CASM, and p'_t and p'_c were described above.

Some of the cemented model parameters are from CASM, controlling the elastic behaviour (k and ν) and shape of the yield surface (r and n). The critical state line is not completely defined in this model as only the slopes in both v vs lnp' (λ) and q vs p' planes (M) are given. In opposition, a different approach is used to define the intrinsic normal compression line (NCL). Instead of introducing N as a parameter (the specific volume of the NCL at p'=1kPa), this value is automatically computed through equation (9.8) introducing the initial state values (e_0; p'_0) and p'_{s0} (it would not be necessary to introduce p'_{s0} if N was assumed as a material parameter). The detailed development necessary to obtain equation (9.8) is presented in Appendix D.

$$p'_{s0} = exp\left(\frac{N - (1 + e_0) - k \ln(p'_0)}{(\lambda - k)}\right) \tag{9.8}$$

where e_0 and p_0 are the current void ratio and mean effective stress of a point at a certain initial state.

The bonding degradation is defined by Gens and Nova (1993) according to the following exponential law,

$$b = b_0 \mathrm{e}^{-(h-h_0)} \tag{9.9}$$

$$dh = h_1 \left| \mathrm{d}\varepsilon_{\mathrm{v}}^{\mathrm{p}} \right| + \mathrm{h}_2 \left| \mathrm{d}\varepsilon_{\mathrm{s}}^{\mathrm{p}} \right| \tag{9.10}$$

where h_1 and h_2 are material parameters (greater than zero) defining the degradation rate derived from volumetric and shear strains, respectively; h_0 represents the initial degradation, usually null; and b_0 is the initial bonding. From equation (9.10), it becomes clear that the degradation increases monotonically independently of the sign of the plastic strains.

Flow rule and hardening parameter

In the version of the model that was available for this calibration the user can select one of three types of flow rules, allowing either the recovering of CASM (Flow rule 1) or its simplification. The yield function of the model is always provided by equation (9.7), being the three available types of flow rules as following:

Flow rule 1 - a non associated flow rule as in the original CASM; the plastic potential function (G) is based on Rowe's stress-dilatancy relation (equation (9.3)) and therefore, totally different from the yield function;

Flow rule 2 - a non associated flow rule where the plastic potential function (G) is related to the yield function (F) by a parameter "m" as G=m·F;

This last value, m, can be computed by equation (9.11) if a one-dimensional consolidation stress path (K_0) is followed, being K_0 obtained by Jaky's relation. Therefore, it becomes:

$$m = \frac{2}{3} \frac{[M(6-M)]^n - (3M)^n}{(6-M)(3M)^{n-1}} \frac{\lambda}{\lambda - \kappa} \tag{9.11}$$

In any case, whatever the value of m, the stress-dilatancy relation can be defined as follows,

$$\frac{d\varepsilon_v^p}{d\varepsilon_s^p} = \frac{M^n - n \cdot \ln r \cdot m^n \cdot \eta^n}{n \cdot \ln r \cdot m^n \cdot \eta^{n-1}} \tag{9.12}$$

Flow rule 3 - an associated flow rule where the plastic potential function (G) is equal to the yield function, as in Cam-Clay models.

The stress-dilatancy relation in this case, is similar to (9.13) when considering m=1, becoming,

$$\frac{d\varepsilon_v^p}{d\varepsilon_s^p} = \frac{M^n - n \cdot \ln r \cdot \eta^n}{n \cdot \ln r \cdot \eta^{n-1}} \tag{9.13}$$

In order to generalise these expressions - equations (9.12) and (9.13) - for cemented conditions the stress ratio is defined as,

$$\eta = \frac{q}{p' + p'_t} \tag{9.14}$$

The model comprises not only the reported parameters but also state variables (as the name indicates, they change during the test) that need to be initialised by certain initial values. The hardening law, used to update the p'_s value, assumes the expression proposed by Gens and Nova (1993), different from CASM hardening rule, including a combined volumetric and shear hardening - equation (9.15):

$$\frac{dp'_s}{p'_s} = \frac{v}{\lambda - k}\left[d\varepsilon_v^p + \Omega \cdot d\varepsilon_s^p\right] \tag{9.15}$$

where, Ω is a model parameter and $d\varepsilon_v^p$ and $d\varepsilon_s^p$ are the plastic volumetric strain increment and plastic deviatoric strain increment, respectively. Of course, if Ω=0 the hardening law of CASM (9.1) is recovered.

In conclusion, the original CASM can be easily recovered if Flow rule 1 is selected and if $b_0=h_1=h_2=\alpha=\Omega=0$. On Table 9.2 the constitutive model parameters and state variables are summarized.

Table 9.2 Constitutive model parameters and state values

	Symbol	Description
Model parameters related to:		
Elastic behaviour	k	slope of the isotropic swelling line
	ν	Poisson ratio
Critical state	λ	slope of the critical state line
	M	stress ratio (q/p') at critical state
	ϕ'_c	angle of shearing resistance at critical state(*)
Shape of yield surface	r	spacing ratio
	n	stress-state coeficient
Bonding degradation rate	h_0	initial degradation (considered zero in this work)
	h_1	degradation rate related to plastic volumetric strains
	h_2	degradation rate related to plastic shear strains
Tensile strength	α	constant
Hardening law	Ω	constant (assumed zero)
Flow rule 2	m	constant
Model initial values:		
	e_0	initial void ratio
	p'_{s0}	initial pre-consolidation pressure in the intrinsic NCL
	b_0	Initial bonding
Model state variables:		
	p'_s	updated by the hardening law (eq. 9.15)
	b	updated by the degradation law (eq. 9.9)
	among others	

(*) in triaxial conditions this happens to be related to M, therefore, it is not needed

9.3 Numerical model

The numerical implementation of the constitutive model described before, the cemented CASM, was defined by Gonzalez (2011) as a “User defined model” of the finite element code Plaxis® (version 8), user friendly commercial software widely known in geotechnics. This allowed a much easier calibration procedure consisting in the simulation of the low pressure triaxial tests presented in chapter 7, in order to know the values of the constitutive model parameters.

Taking advantage of the symmetrical axe and the revolution axe of the triaxial test specimen, the simulation was performed on ¼ of the specimen (1 x 1 m size) assuming the remaining part to be symmetrical and using appropriate boundary conditions (Figure 9.2). All calculations were performed in axisymmetric conditions to reproduce cylindrical specimens.

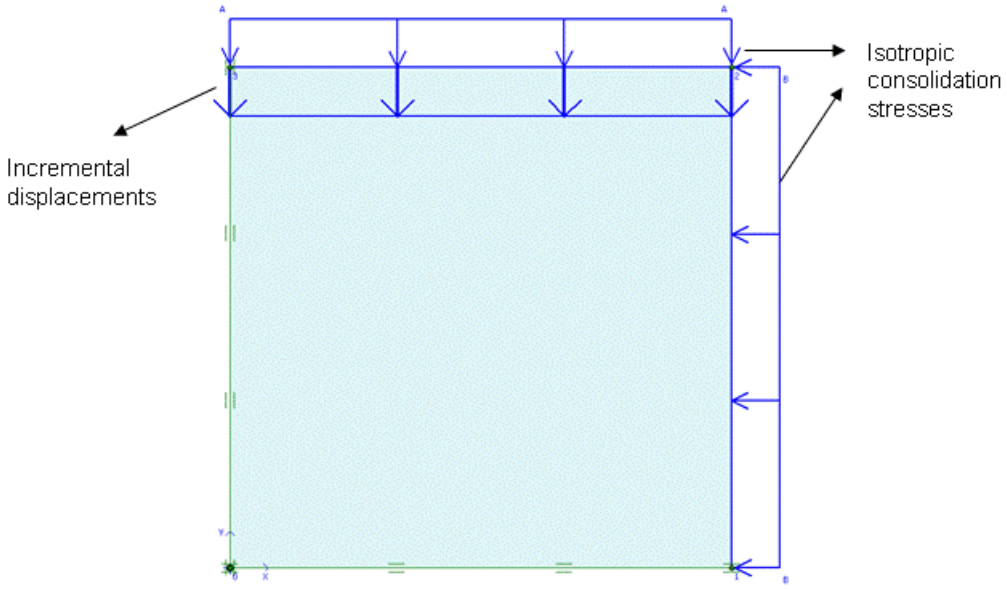

Figure 9.2 Numerical model of ¼ of the test specimen

Triangular 15-nodes elements were always employed. In this geometry, with perfect elements and ideal border conditions, the number of elements is irrelevant since the constitutive model is accomplished in similar way on all integration points. The unit weight of the soil is not important when compared to the stresses involved in both the confinement and the shearing phase, and so, it is assumed zero.

From the described conditions and since the simulation will be concentrated on the answer from confinement stage towards failure by shearing, the applied loads are effective stresses. In the case of undrained tests, excess pore pressures are generated as the water is not allowed to flow out of the specimen. In order to assure that during undrained loading there are no volumetric strains, excess pore pressures are computed internally assuming a water bulk modulus much higher than the soil skeleton stiffness.

The consolidation of the specimen was performed by the so called “staged construction” where the effective confining pressures were isotropically applied to the sample, thus load controlled. The shearing of the specimen was performed applying “total multipliers” of displacements, performing a displacement controlled loading in the top of the sample (Figure 9.2). Care was taken to have enough increments of displacements in order to reach critical state which was easily checked on the final results by seeing if the M value introduced in the parameters was recovered at the end of the simulated test.

In the simulation of triaxial tests of cemented samples with very low confinement (30 kPa) a numerical problem has arisen due to the highly brittle response of the soil, generated by the

combination of the use of a low confining stress and a high initial bonded state. To solve this problem, the arc-length control option of the "manual settings" for the iterative procedure was deactivated, which allowed the calculation convergence. The reference manual of Plaxis® indicates that “the arc-length control procedure should be used for load-controlled calculations, but it may be deactivated, if desired, for displacement controlled calculations. When using incremental multipliers as input, arc-length control will influence the resulting load increments. As a result, the load increments applied during the calculation will generally be smaller than prescribed at the start of the analysis”. In fact, having more increments at the beginning proved to be an advantage, as more points could be obtained in that part and consequently a better-defined stress-strain curve.

There are six state variables that can be assessed during the several stages of the load process, in the output of the software by this order: 1) p'_s; 2) p'_c; 3) p'_t; 4) b; 5) h; 6) F (numerical tolerance to give indications about the calculation convergence).

9.4 Calibration procedure

The triaxial tests from chapter 7 involved in this calibration were only the low pressure triaxial tests, for simplicity, as a first attempt to understand the performance of the model in this cemented silty sand.

The moulding and test conditions of the specimens can be found in Table 7.1 and 7.2, respectively for uncemented and cemented tests.

The calibration procedure comprised two main tasks:

- calibration of the six CASM parameters related to the elastic behaviour (ν and k), critical state (λ and M) and shape of yield surface (r and n) by running the simulations of the uncemented tests;
- calibration of the remaining parameters related to the bonded model by running the simulations of cemented tests. In this step the best adjustment of the six parameters obtained in the previous task was kept constant.

9.5 Calibration based on the uncemented tests results

9.5.1 Definition of the parameters directly from laboratory data

Most of CASM parameters were defined from the laboratory data. In this section their values will be presented following, as much as possible, the order presented on Table 9.2.

In terms of the elastic parameters, the slope of the swelling line (k) was obtained in the uncemented isotropic test ISO(0)_16.1 described in chapter 7. This test results were according to other data presented in Figure 7.3 validating the use of this test. Also, the results presented in the same figure, indicate that k value does not change significantly with the initial void ratio of the specimen. The test ISO(0)_16.1 is presented in Figure 9.3 illustrating a k value of 0.0097.

The other elastic parameter is the Poisson ratio (ν), for which there is not much information in this research work. The dynamic Poisson ratio obtained on Chapter 6 was 0.37, and on Chapter 7 a value of 0.3 was used to compare different methods for volume strain calculation which was considered quite suitable. For these reason, the value of 0.3 used in static conditions was assumed for this simulation.

As reported previously the critical state line in sands is very difficult to define clearly and this work was no exception; therefore, the critical state parameters were obtained by other means. The slope of the CSL in the v against ln p' plane (λ) is supposed to be similar to the slope of the NCL and so, the same value of Figure 9.3 was used: λ=0.112.

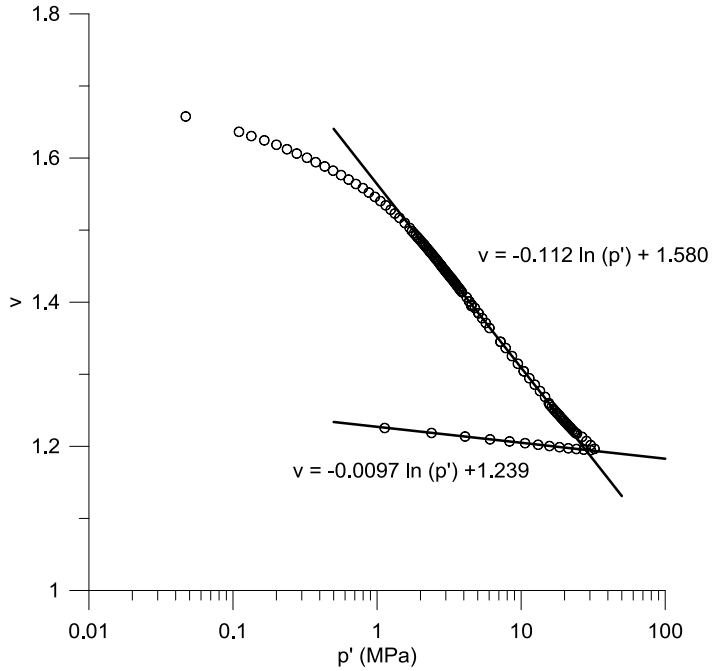

Figure 9.3 Isotropic compression line results in ISO(0)_16.1 test

The slope of CSL in the q versus p' plane (M) was obtained by the stress-dilatancy analysis presented in section 7.13, where Figure 7.47a) showed a value of M=1.4. This value was also corroborated by the strength envelope presented in section 7.11.4The r and n

parameters are specific of this model and thus it is not possible to derive them from laboratory data, so they have to be calibrated by tests results.

The constant Ω of the hardening rule was considered zero as a first approach and so, an isotropic volumetric hardening rule, as defined in CASM, was used.

9.5.2 Definition of yield surface parameters and flow rule

Flow rule

The definition of the flow rule (FR) was calibrated from the stress-dilatancy results taking into account equations (9.3), (9.12) and (9.13), presented previously. The data from the drained uncemented tests was plotted together with these relationships in order to see which suited better. The m value for FR 2, was calibrated for each set of yield surface parameters (r and n) in order to have a stress ratio (η) equal to M at zero dilatancy. In the results presented herein the following yield surface parameters were considered r = 2 and n =1.5 and so, in that case, m becomes 0.975. The results are presented in Figure 9.4 and 9.5 showing clearly that Rowe's stress-dilatancy relationship implemented in CASM and in FR 1 of cemented CASM is the one that best adjusts most results. The results of the second and third flow rule are quite similar because the m parameter was close to 1. When other yield surface parameters are considered the flow rules are not similar but Rowe's stress-dilatancy still seems the most convenient. Therefore, Flow Rule 1 was used in the forecoming calculations.

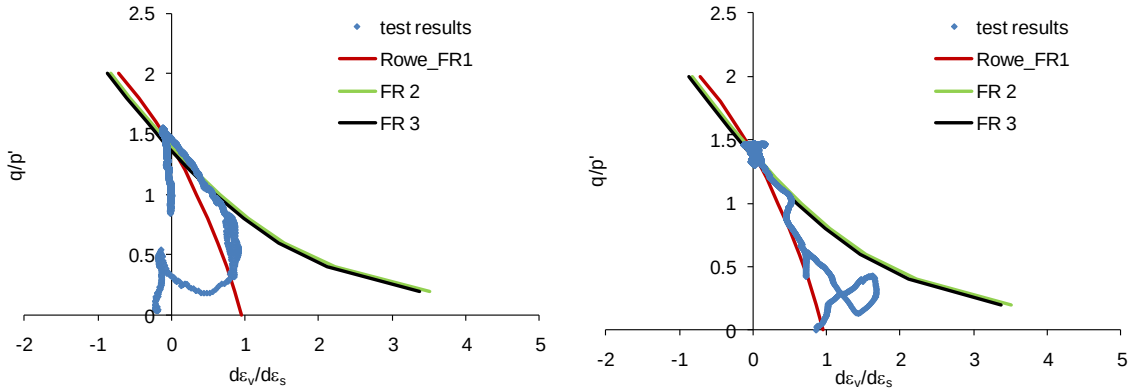

Figure 9.4 Stress-dilatancy curves of the looser uncemented tests: a) CV_30; b) CV_80

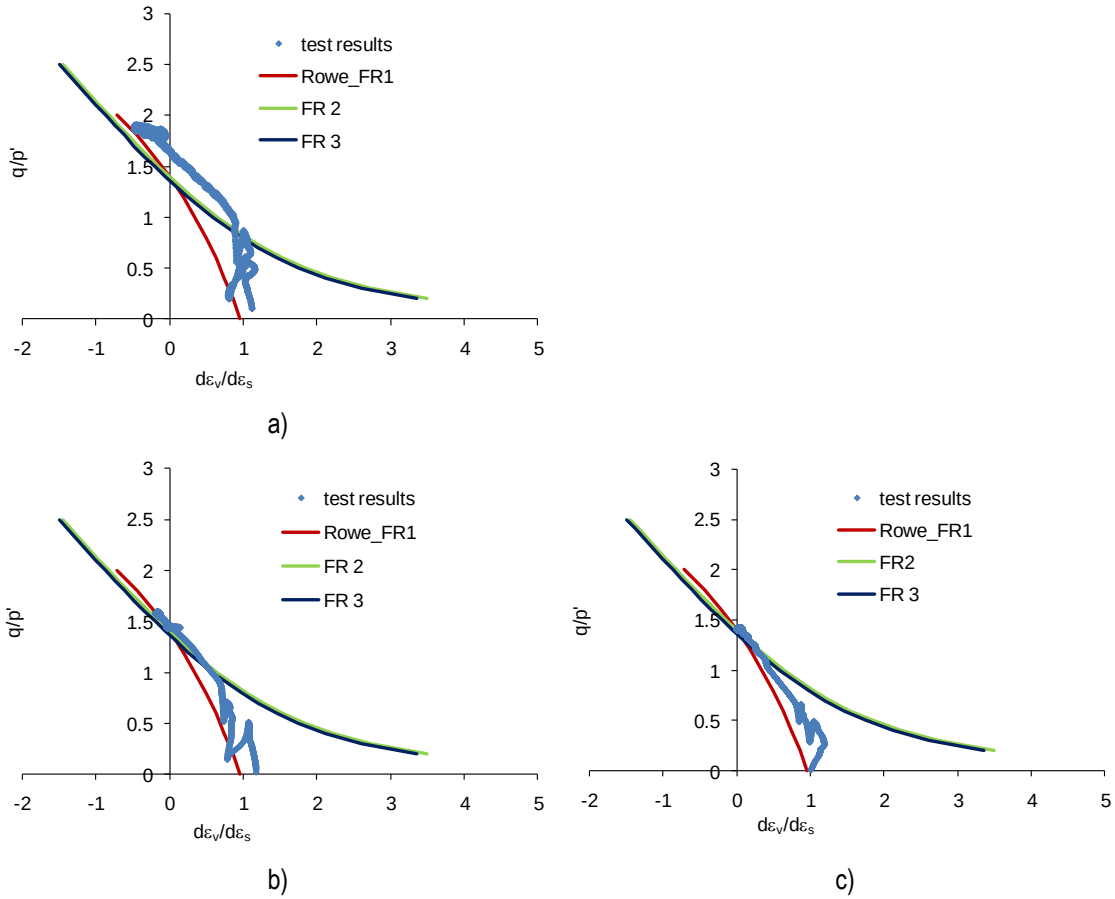

Figure 9.5 Stress-dilatancy curves of the denser uncemented tests: a) CV90_30; b) CV90_100; c) CV90_250

Initial values

Before evaluating the yield surface parameters the initial values corresponding to each triaxial test should be known. As explained before, the initial void ratio is related to p'_{s0} through equation (9.8), and so the two different densities of the specimens tested lead to two different p'_{s0}. Taking the value of N (the specific volume at p'=1kPa) from the same isotropic compression curve presented in Figure 9.3, the parameters λ and k described above, and the initial conditions given by the initial void ratio (e_0) and mean effective stress before consolidation (p'_0), the following p'_{s0} values were obtained,

$k = 0.0097; \quad \lambda = 0.112; \quad N = 2.352$

$e_0 = 0.6$
$p'_0 = 20$ kPa $\Rightarrow$ $p'_{s0} = 1172$ kPa

equation (9.8)

$e_0 = 0.75$
$p'_0 = 20$ kPa $\Rightarrow$ $p'_{s0} = 271$ kPa

As a result, the initial values of the tests performed with denser specimens will be: e_0=0.6 and p'_{s0}=1172 kPa. In the tests with the looser samples, the initial values will be: e_0=0.75 and p'_{s0}=271 kPa.

Yield surface

The yield surface parameters were calibrated plotting together the yield surface and the stress-path results of drained and undrained tests. This plot also allows a better understanding of the influence of r and n separately. In terms of n, when it is equal to 1.5, the yield surface is symmetrical; increasing this value the yield surface tends to shift the maximum deviatoric stress to the right aligning the symmetry to an axis with K<1; decreasing this value that peak shifts to the left (Figure 9.6). The r value is more related to the shape of the yield surface in deviatoric axis, in the sense that higher r values increase the peak of the surface while lower r values tend to decrease the peak leading to flatter surfaces (Figure 9.7).

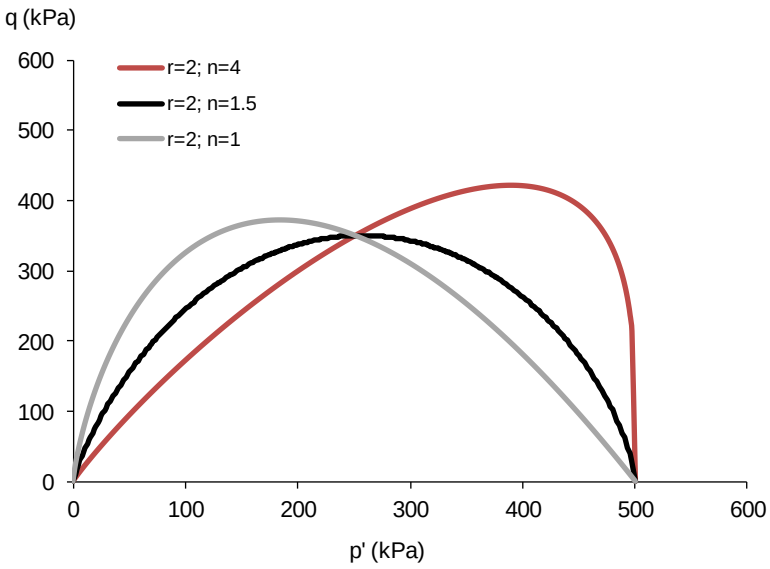

Figure 9.6 Shape of the yield surface for different n values

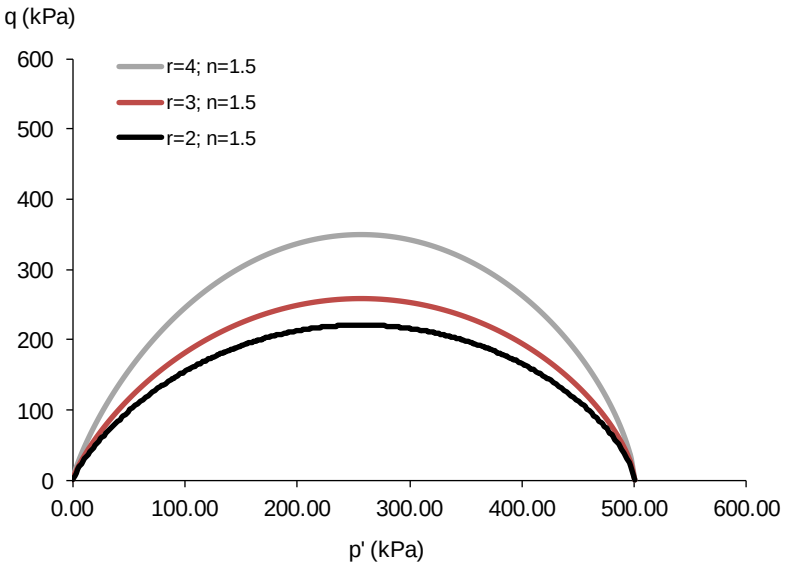

Figure 9.7 Shape of the yield surface for different r values

Bearing in mind the effect of r and n on the shape and size of the yield surface, the stress-paths of each group of tests with the same initial parameters were compared to the yield surface. The purpose of this exercise was to evaluate the convergence of the peak values of the tests stress-paths with the yield surface, and as a consequence calibrate r and n. Even having different values of e_0 and p'_{s0} both groups of tests should have the same yield surface parameters.

Looking at the stress paths it is clear that they follow the critical state line M=1.4, so it became clear that a yield surface bending to right would give better results. Several possibilities were tested, and the values r=2 and n=10 seemed to give the best fit as illustrated in Figure 9.8 and 9.9, respectively for the dense uncemented specimens (e_0=0.6) and the loose uncemented specimens (e_0=0.75).

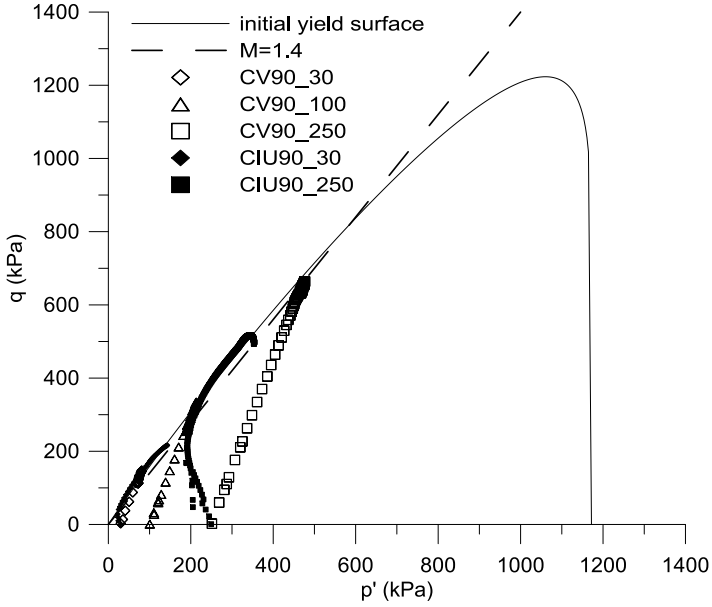

Figure 9.8 Yield surface for dense uncemented specimens (e_0=0.60)

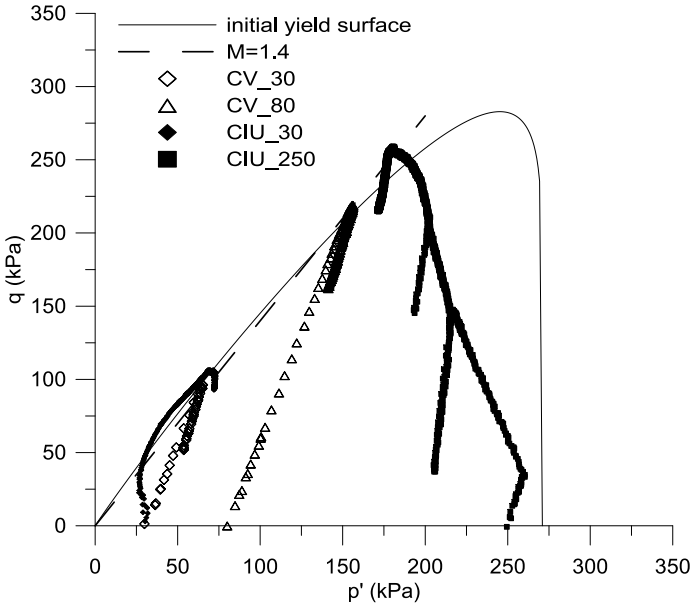

Figure 9.9 Yield surface for loose uncemented specimens (e_0=0.75)

9.5.3 Calibration results

After the definition of the most convenient parameters summarized in Table 9.3, each test was simulated in the numerical model described above.

Table 9.3 Constitutive model parameters - UC1

Model parameters							
k =	0.0097	M =	1.4	h_1 =	0	Ω =	0
ν =	0.3	r =	2	h_2 =	0	m =	0
λ =	0.112	n =	10	α =	0		
Initial values							
e_0 =	0.6	e_0 =	0.75				
p'_{s0} =	1172	p'_{s0} =	271				
b_0 =	0	b_0 =	0				

First, the drained tests are presented in Figure 9.10, plotting the stress-strain-volumetric curves of the tests and the model results. In general, the model adjusted reasonably to the test results although some features like strain-softening and dilation are not so well represented. It is interesting to notice that other yield surface parameters (e.g., r=3 and n=6) that did not show a good adjustment in the yield surface plots analogous to Figure 9.8 and 9.9, show quite a similar adjustment to Figure 9.10 when the stress-strain-volumetric curves are plotted together with the model.

Unfortunately, the undrained tests do not evidence such interesting results. The model assumes that there are no plastic strains until the yield surface is achieved and that there are no volumetric strains during undrained loading, consequently, the stress-path is vertical (with constant p') up to peak. However, the test results show a different behaviour. This discrepancy is eventually due to the development of plastic strains since the very beginning being this a consequence of some inhomogeneous stress distribution in the specimen. In Figure 9.11 the stress-strain curves are plotted comparing the model and the test results, being clear that the peak point was not well simulated. In order to have a better idea of the behaviour of the model, the q vs p' stress paths were plotted as well, presented in Figure 9.12 for the model and tests results. After yielding, the stress-paths seem to follow the yield surface (in both, test and model, as expected). However, test results show a stress-path much limited in development towards the ultimate condition. Considering that these tests were conducted until 20% of axial strain, this may be due to strain localization that prevented the increase of both deviatoric and mean effective stress, although a shear plane failure was not so clearly observed as in cemented specimens (Figure 7.42). This type of inhomogeneous stress distribution and strain localizations, the model cannot simulate and appear to be more relevant in undrained conditions.

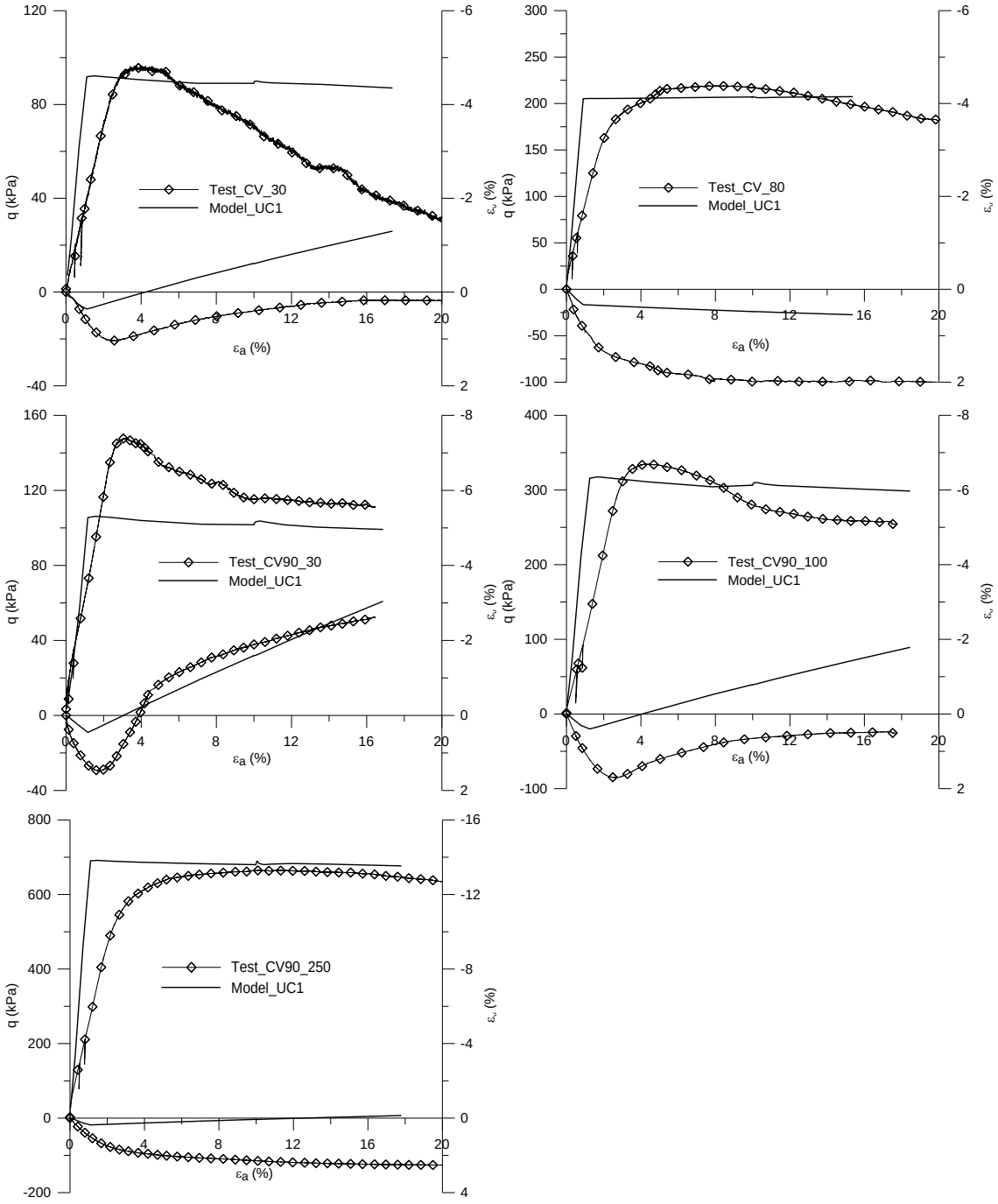

Figure 9.10 Calibration results with UC 1 in stress-strain-volumetric curves of drained tests

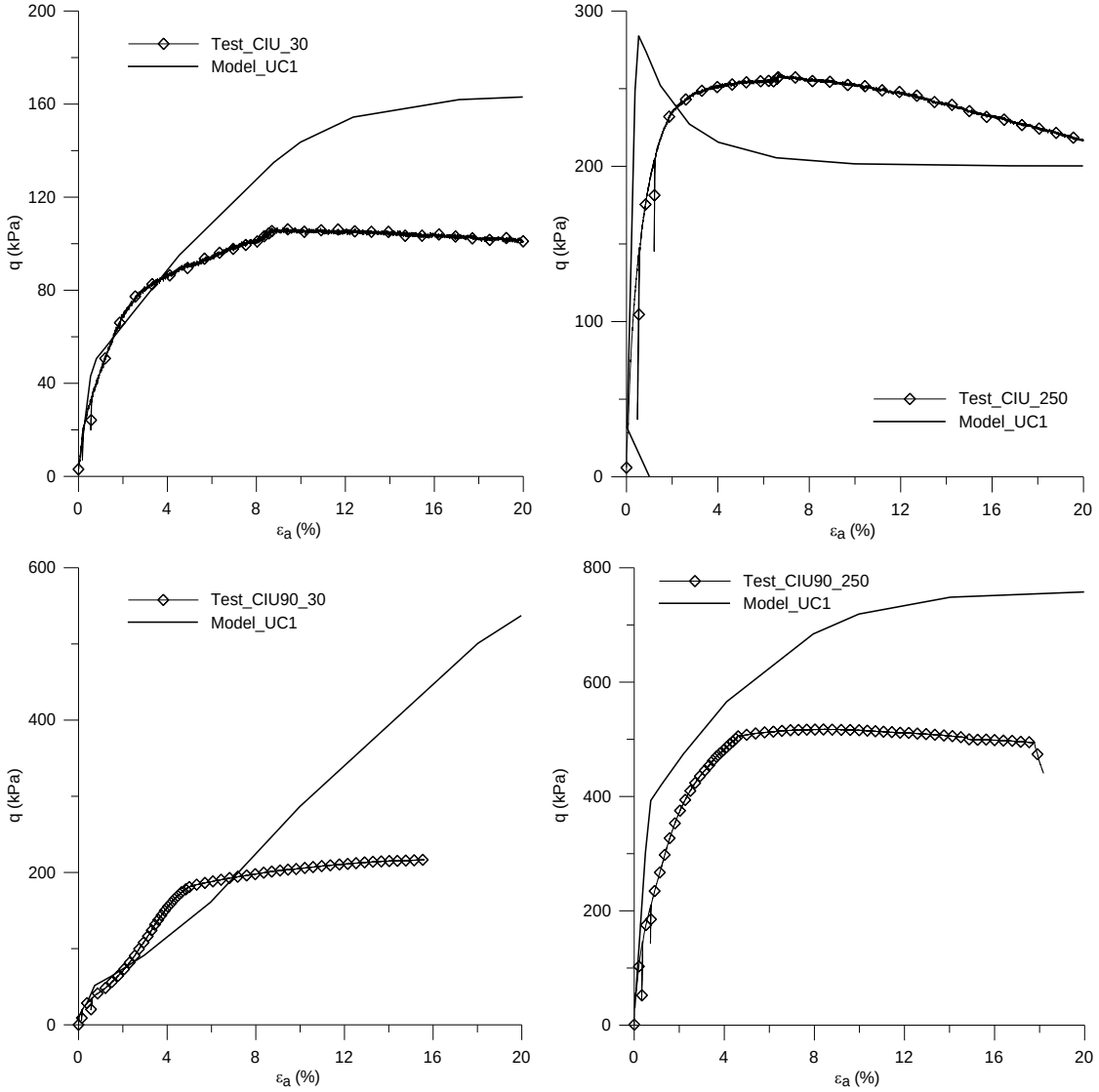

Figure 9.11 Calibration results with UC 1 in undrained stress-strain curves

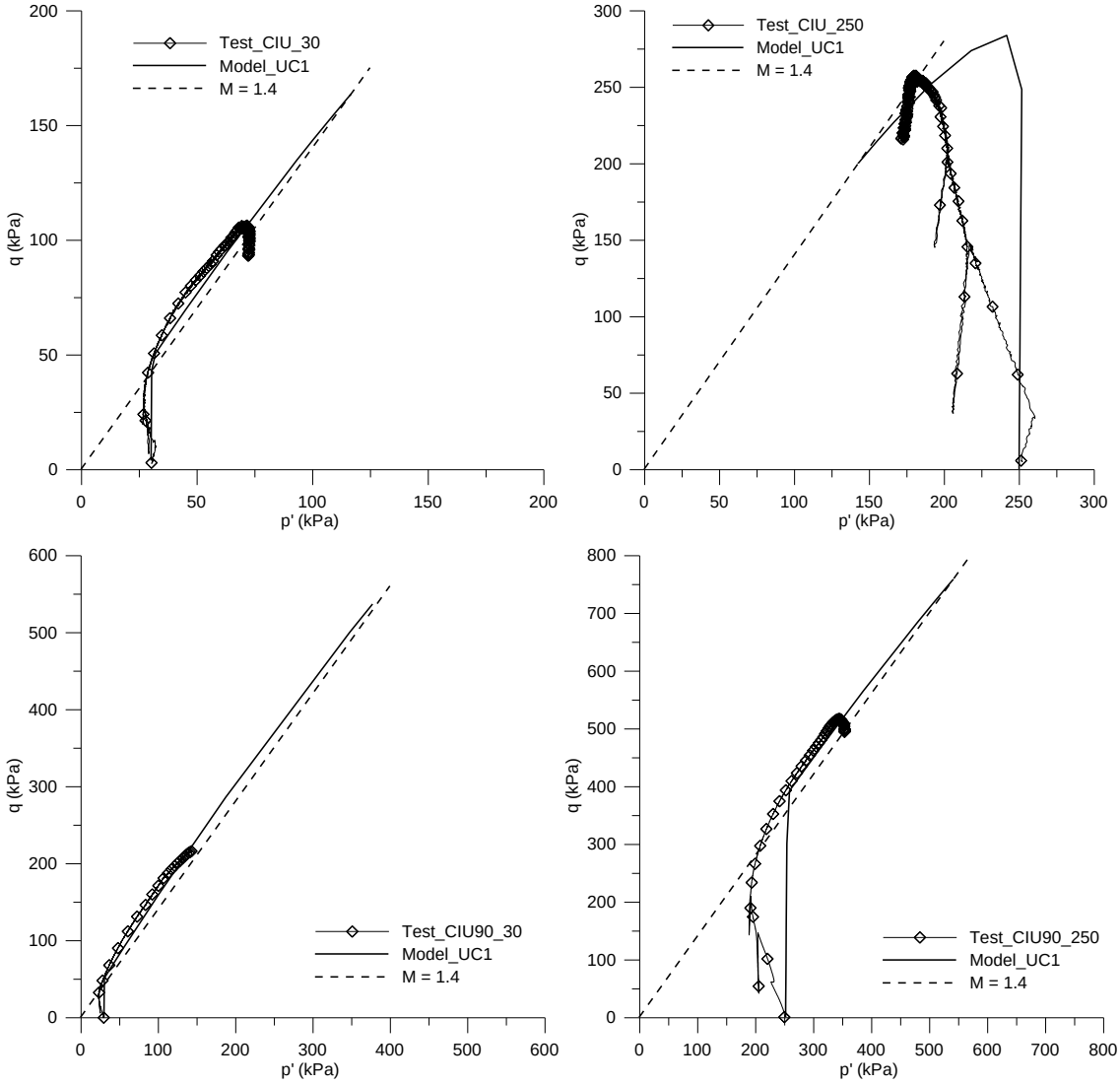

Figure 9.12 Calibration results with UC 1 in undrained stress-paths

9.6 Calibration based on the cemented tests results

9.6.1 Definition of α and initial values

For the remaining calibration of the model, the cemented tests will provide the definition of the parameters related to cementation like h_1, h_2 and α and also the initial value of bonding (b_0). The parameter α is calibrated by the yield surfaces taking into account the initial values corresponding to each test. The parameters h_1 and h_2 controlling the degradation of cementation will only influence the behaviour after peak, i.e., the rate to which the critical state is achieved.

The initial values of p'_{s0} related to each test are obtained in the same way as before, where for each initial void ratio (e_0) a value of p'_{s0} is found through equation (9.8).

k = 0.0097; λ = 0.112; N = 2.352

equation (9.8)

2% C e_0 = 0.61, p'_0 = 20 kPa ⇨ p'_{s0} =1063 kPa

4% C e_0 = 0.73, p'_0 = 20 kPa ⇨ p'_{s0} =329 kPa

5% C e_0 = 0.58, p'_0 = 20 kPa ⇨ p'_{s0} =1426 kPa

7% C e_0 = 0.65, p'_0 = 20 kPa ⇨ p'_{s0} =719 kPa

The initial value of b_0 which represents the amount of bonding in the model, was calibrated together with the parameter α, looking at the yield surfaces. For that purpose, the yield surface corresponding to the tests with a given cement content (which have the same initial void ratio and thus, the same p'_{s0}) was plotted together with the q vs p' stress-paths of the tests. The procedure consisted in changing the b_0 value and looking at the yield surface, to see which value suited better this set of tests. Of course, this has to be done for a specific value of parameter α, which will be the same for all the tests. Therefore, all four sets of tests had to be analysed simultaneously in order to identify the best adjustment.

As reported before in section 7.10.2 drained tests have achieved higher peak points than undrained tests possible due to a higher sensitivity to strain localization of the undrained tests. For this reason, and considering the uncemented test results (section 9.5.3), the drained tests were considered more reliable for the identification of the yield surface, and thus, b_0 and α values were defined for these tests. In Figure 9.13 the graphs of the yield surface for each cement content are shown for the best adjustment corresponding to an α value of 0.15 and b_0 values for each cement content as indicated in Table 9.4 (next paragraph).

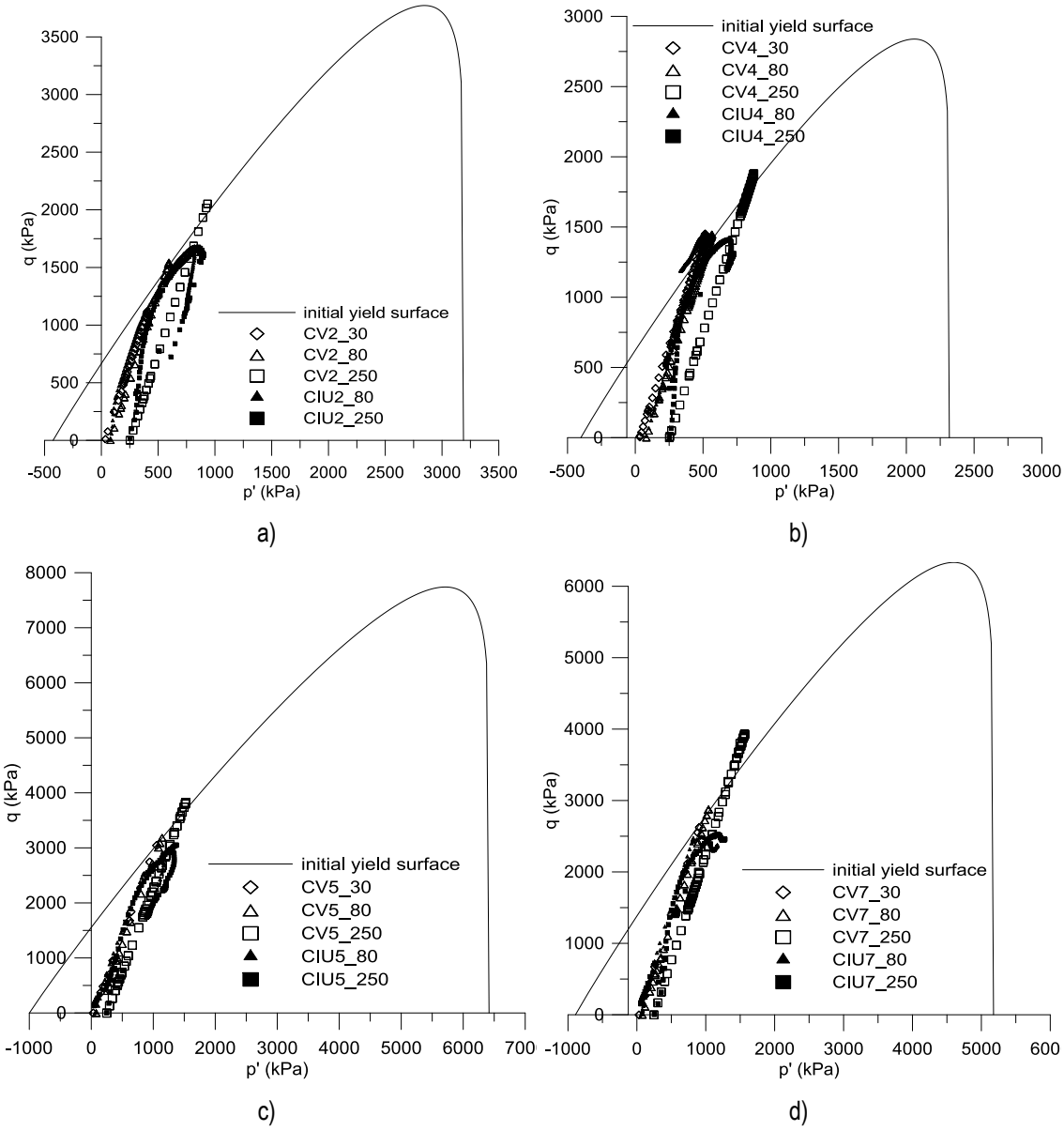

Figure 9.13 Yield surface: a) 2% cement content tests; b) 4% cement content tests; c) 5% cement content tests; 7% cement content tests

9.6.2 Calibration results

The results of the α and b_0 values obtained in the previous section will be joined with the other parameters obtained in the uncemented calibration composing CEM 1 set of parameters included in Table 9.3. The bonding degradation parameters were considered zero in a first approach because they will be calibrated by the stress-strain-volumetric curves. Each test was subsequently simulated by the numerical model using those parameters. **Error! Reference source not found.** shows the model and test results for ach one of the drained tests while Figure 9.15 presents the undrained tests.

Table 9.4 Constitutive model parameters - CEM1

Model parameters							
k =	0.0097	M =	1.4	h_1 =	0	Ω =	0
ν =	0.3	r =	2	h_2 =	0	m =	0
λ =	0.112	n =	10	α =	0.15		

Initial values							
2% C		4% C		5% C		7% C	
e_0 =	0.61	e_0 =	0.73	e_0 =	0.58	e_0 =	0.65
p'_{s0} =	1063	p'_{s0} =	329	p'_{s0} =	1426	p'_{s0} =	719
b_0 =	2.5	b_0 =	8	b_0 =	4.5	b_0 =	8.5

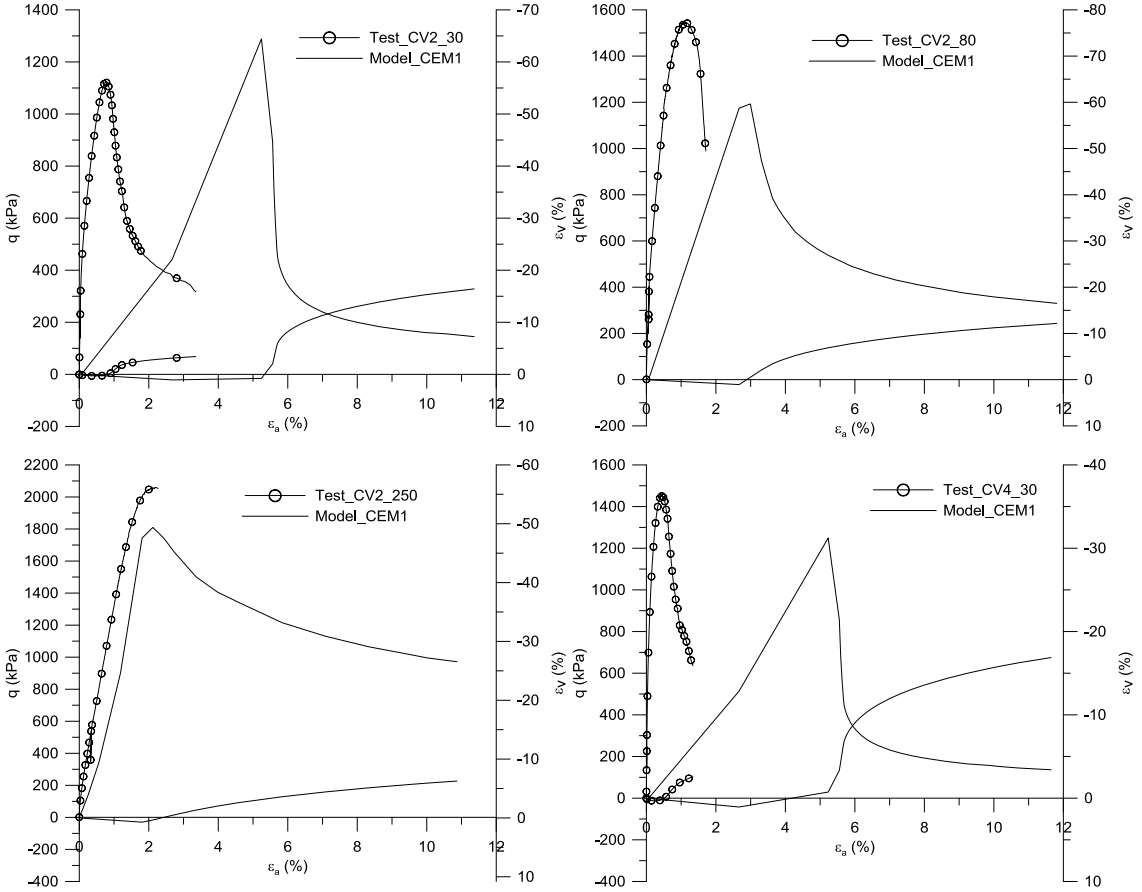

Figure 9.14 Calibration results with CEM 1 in drained tests

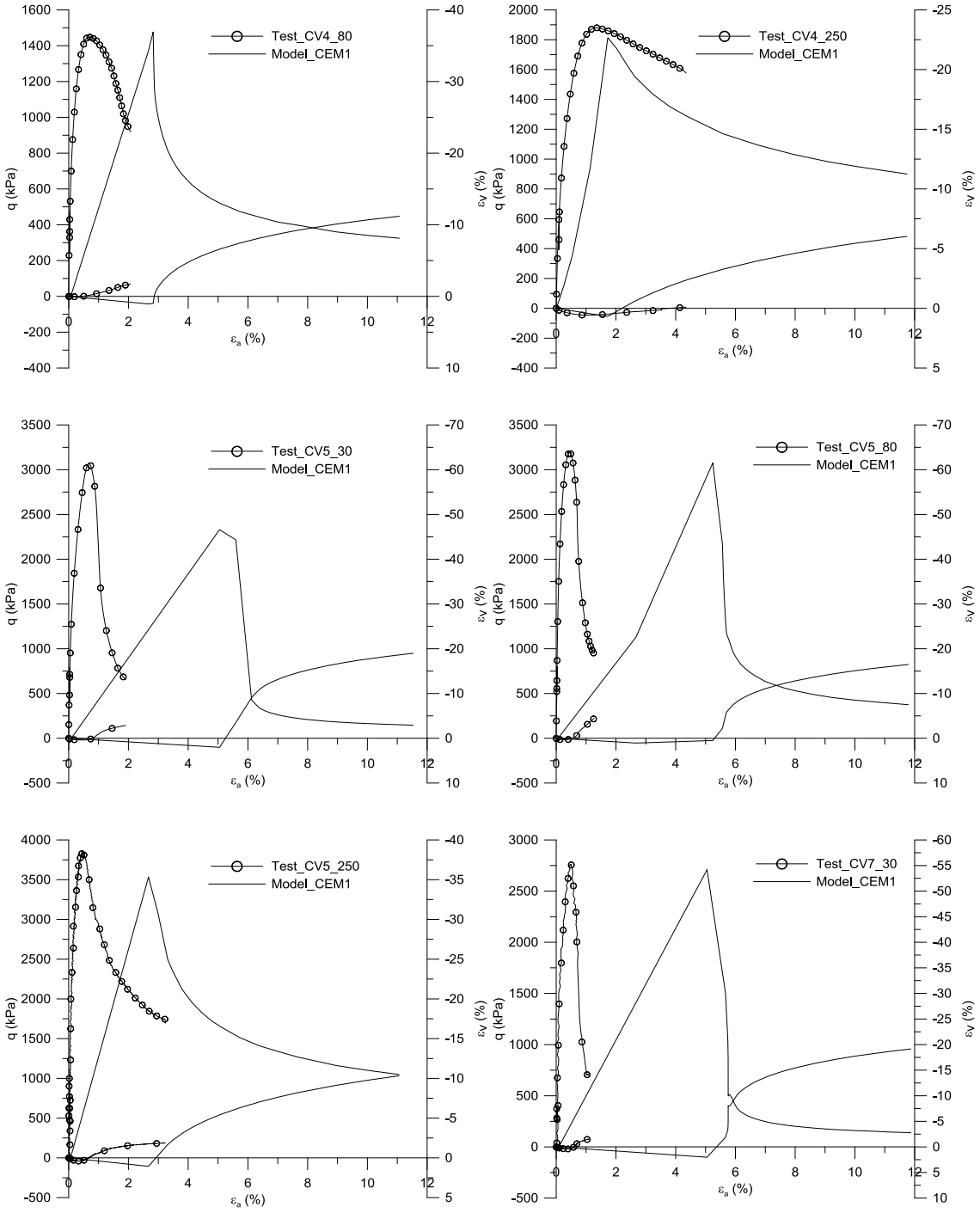

Figure 9.14 Calibration results with CEM 1 in drained tests (cont.)

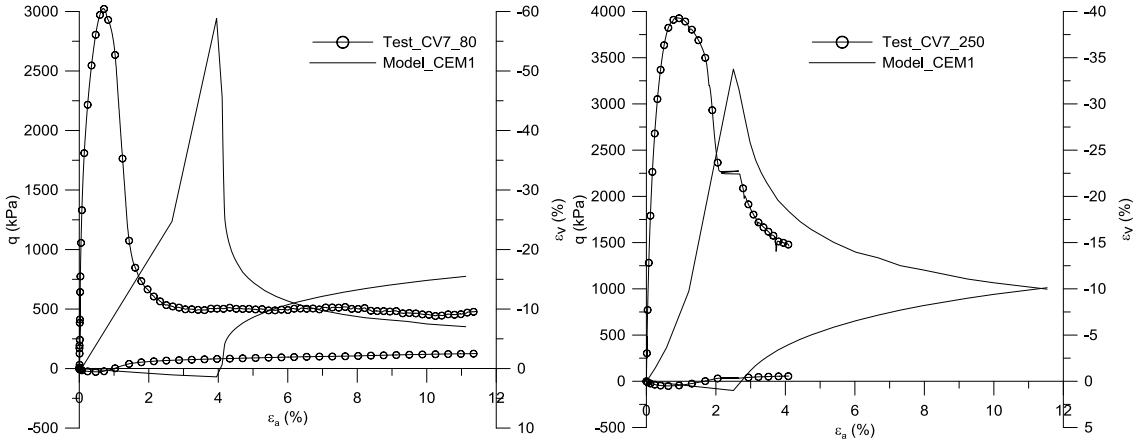

Figure 9.14 Calibration results with CEM 1 in drained tests (cont)

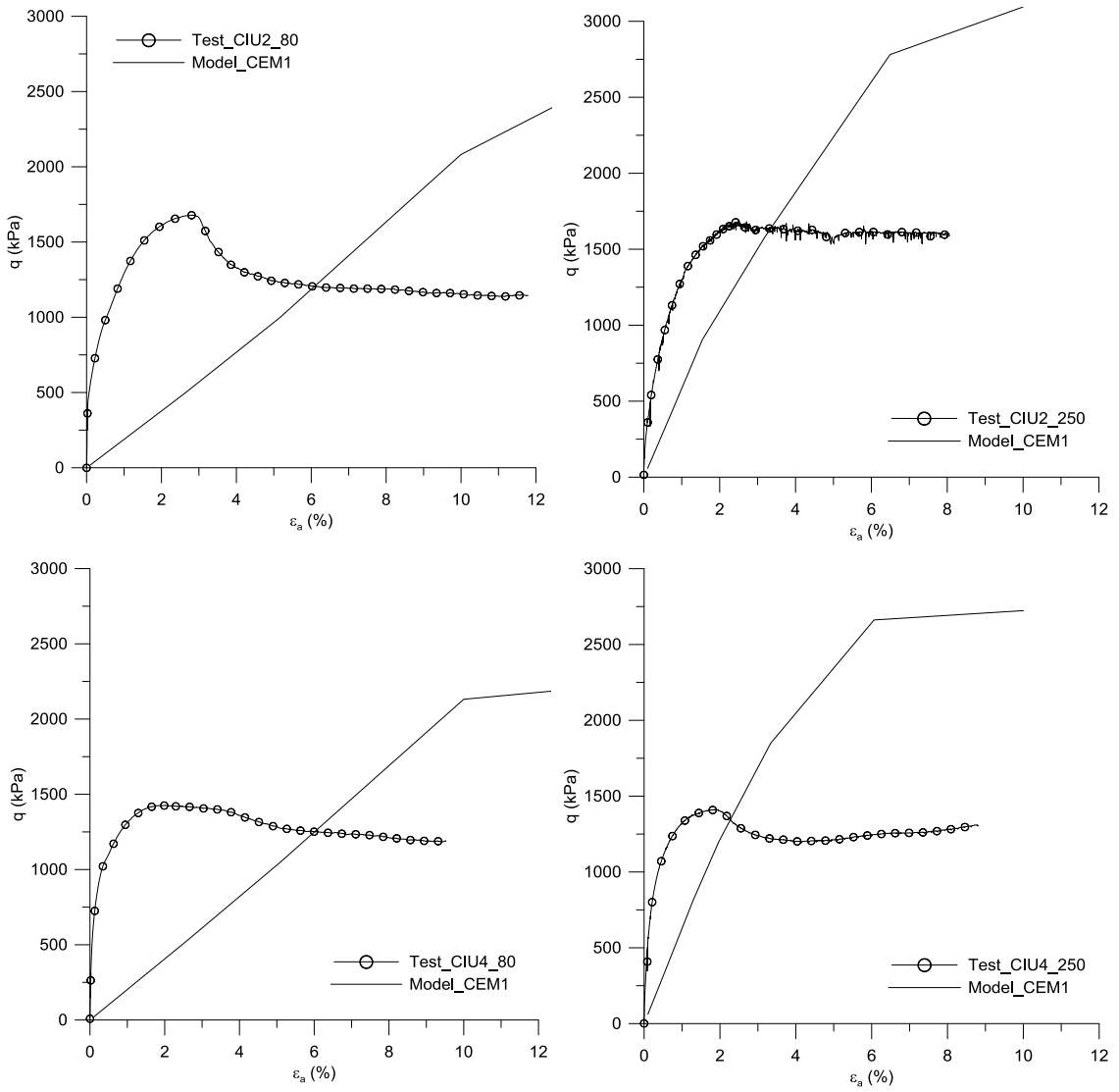

Figure 9.15 Calibration results with CEM 1 in undrained tests

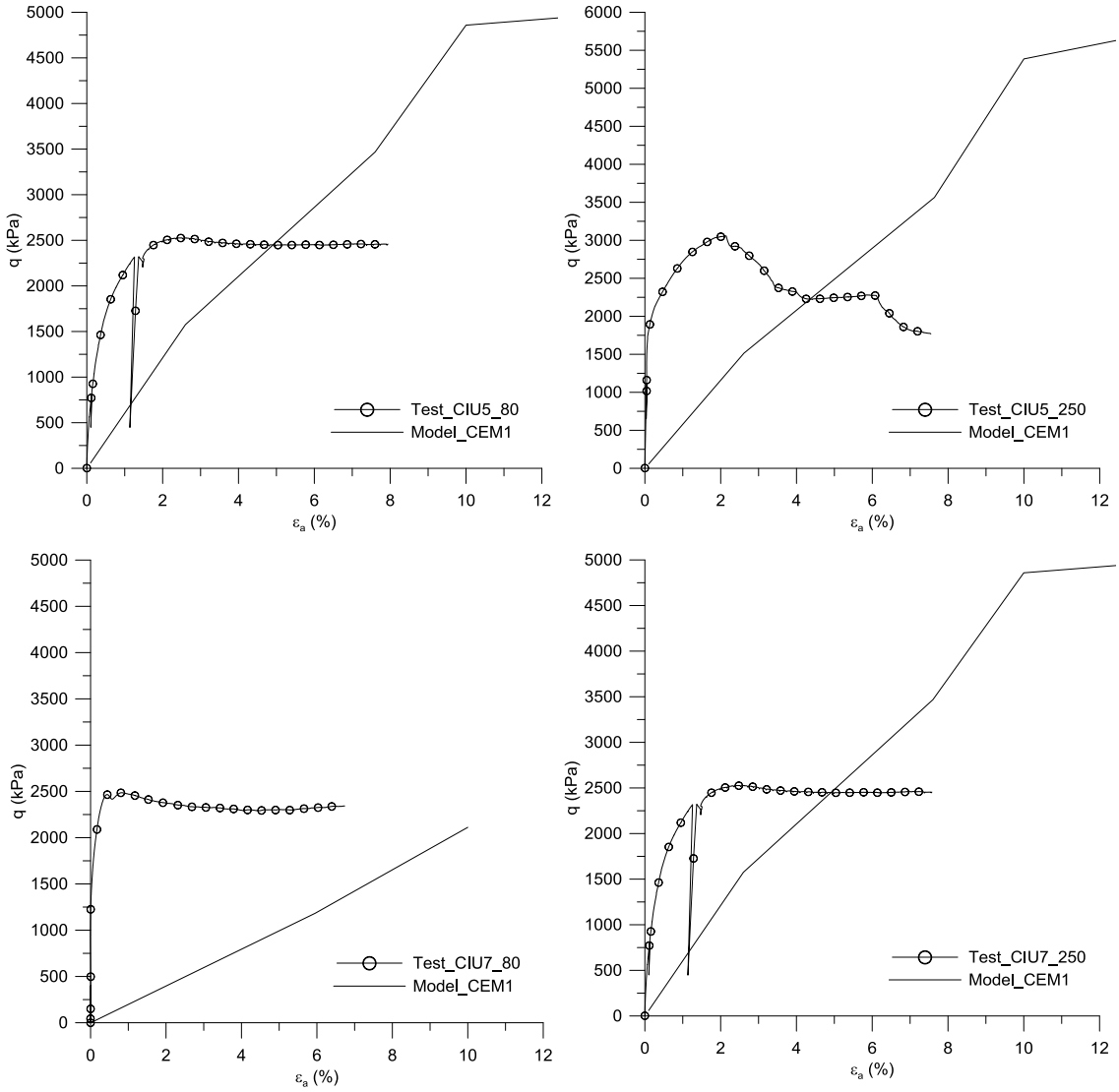

Figure 9.15 Calibration results with CEM 1 in undrained tests (cont.)

From the graphs related to the drained tests it can be concluded that the deviatoric stress at peak is relatively well simulated, conversely to the initial stiffness and, consequently, the axial strain at peak which are quite different in the test and in the simulation by CEM 1 model.

In the undrained tests, beyond these problems, the peak deviatoric stress of the model is much higher than the tests because the yield surface was calibrated for the drained tests.

As it was reported before, these results were obtained with a zero rate of bonding degradation. The parameters h_1 and h_2 only control the response of the soil after peak, so, considering that the problem in the reported results stands in the behaviour before peak and not after it, changing these parameters would not lead to a better adjustment.

Moreover, with this difference in the results it was not possible to calibrate them appropriately.

9.7 Limitations of the model

In the previous sections the cemented CASM model was calibrated according to its own "philosophy", starting by the uncemented parameters and then, keeping these unchanged, the calibration of the cemented parameters proceeded. Subsequently, this model assumes that most parameters (for example, controlling the shape of the yield surface or the slope of the swelling line) remain the same for both uncemented and cemented conditions.

The elastic behaviour of the model is controlled by the slope of the isotropic swelling line (k) and the Poisson ratio (ν). Considering that these parameters are the same in uncemented and cemented conditions it is not possible to reproduce the different initial stiffness values presented by a cemented material when compared to the same material in uncemented conditions. To account for this fact, Yu et al. (2007b) have proposed an expression for the calculation of bulk modulus (K) to introduce additional stiffness induced by bonding. Keeping the same symbols for the parameters already described, Yu et al. (2007b) formulation becomes as follows,

$$K = \frac{vp'}{k}\left(1 + \sqrt{\frac{p'_s b}{p'}}\right) \tag{9.16}$$

Note that when there is no bonding (b=0) this expression depends only on the slope of the swelling line, Poisson ratio and mean effective stress. Bearing this in mind, the previous relation can be used to introduce the effect of bonding on the elastic stiffness of cemented CASM by considering that the parameter k can be changed by cementation using equation (9.17),

$$\frac{1}{k_{cemented}} = \frac{1}{k_{uncemented}}\left(1 + \sqrt{\frac{p'_s b}{p'}}\right) \tag{9.17}$$

It should be noted that p', p'_s and b change during the test, while $k_{uncemented}$ is a fixed parameter, so it may be difficult to evaluate $k_{cemented}$ accurately. However, some simplifications may be introduced to provide an estimation of this value:

- if the initial tangent stiffness needs to be simulated the initial conditions can be used;

- if k is important in elastic conditions (up to peak), an average value can be obtained between peak and initial conditions. Note that if it is difficult to find the exact values of b and p'_s at peak (because they are calculated internally by the model and the output is not enough staged) they can be assumed to be constant up to the peak, assuming that only elastic strains were observed until this point.

Another limitation of the model concerns the undrained behaviour. From elasticity theory, it is known that in elastic and isotropic conditions an undrained stress-path (which has no volume change) is vertical in q against p' plot (Muir Wood, 2004). Consequently, if the model assumes that the behaviour is elastic up to the peak, the stress path will be vertical until it touches the yield surface. However, the test results do not show such marked behaviour, and even when they do (such as in CIU_30 of Figure 9.12), the stress-strain curve cannot be adjusted (Figure 9.11).

Finally, the tests results have exhibited a different peak deviator stress depending on the draining conditions which is not at all simulated by the model. For this reason, it was very difficult to adjust both types of tests.

Considering that these were the three main reasons that explain the distinct behaviour between the model and test results, it was decided to model only the drained tests, thus, removing the last two problems related to the undrained behaviour. Giving the great difference between the initial stiffness shown in the model and in the tests, the first approach based on the initial conditions was assumed. Subsequently, a new $k_{cemented}$ parameter was obtained for each conditions taking the corresponding p'_{s0}, b_0 and confining pressure (p'_0) according to equation (9.17).

The following graphs show the results obtained with this procedure (named CEM 2) which consists in using $k_{cemented}$ and keeping the remaining parameters as in Table 9.4. The graphs also include the k value used in each case.

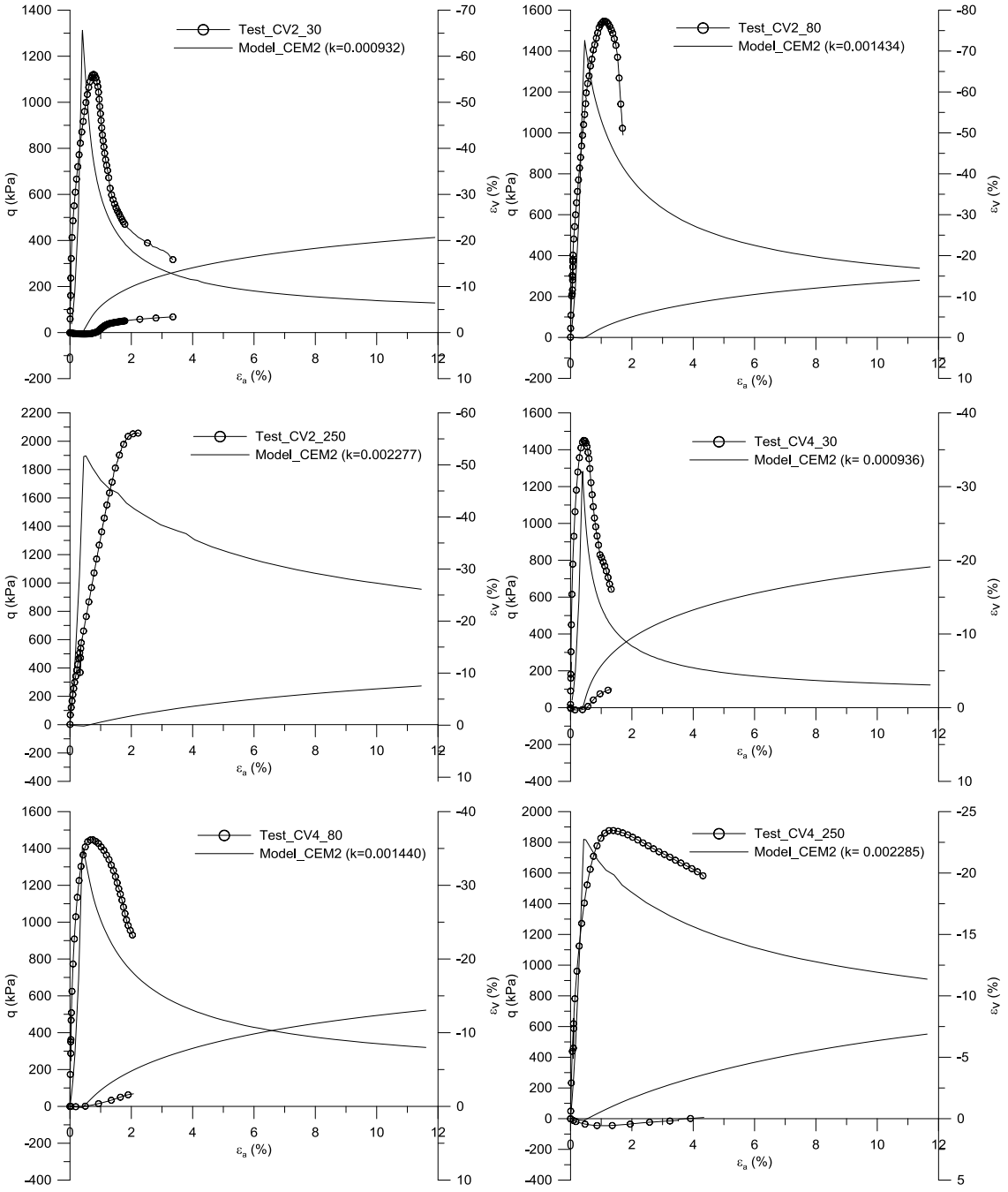

Figure 9.16 Calibration results with CEM 2 in drained tests

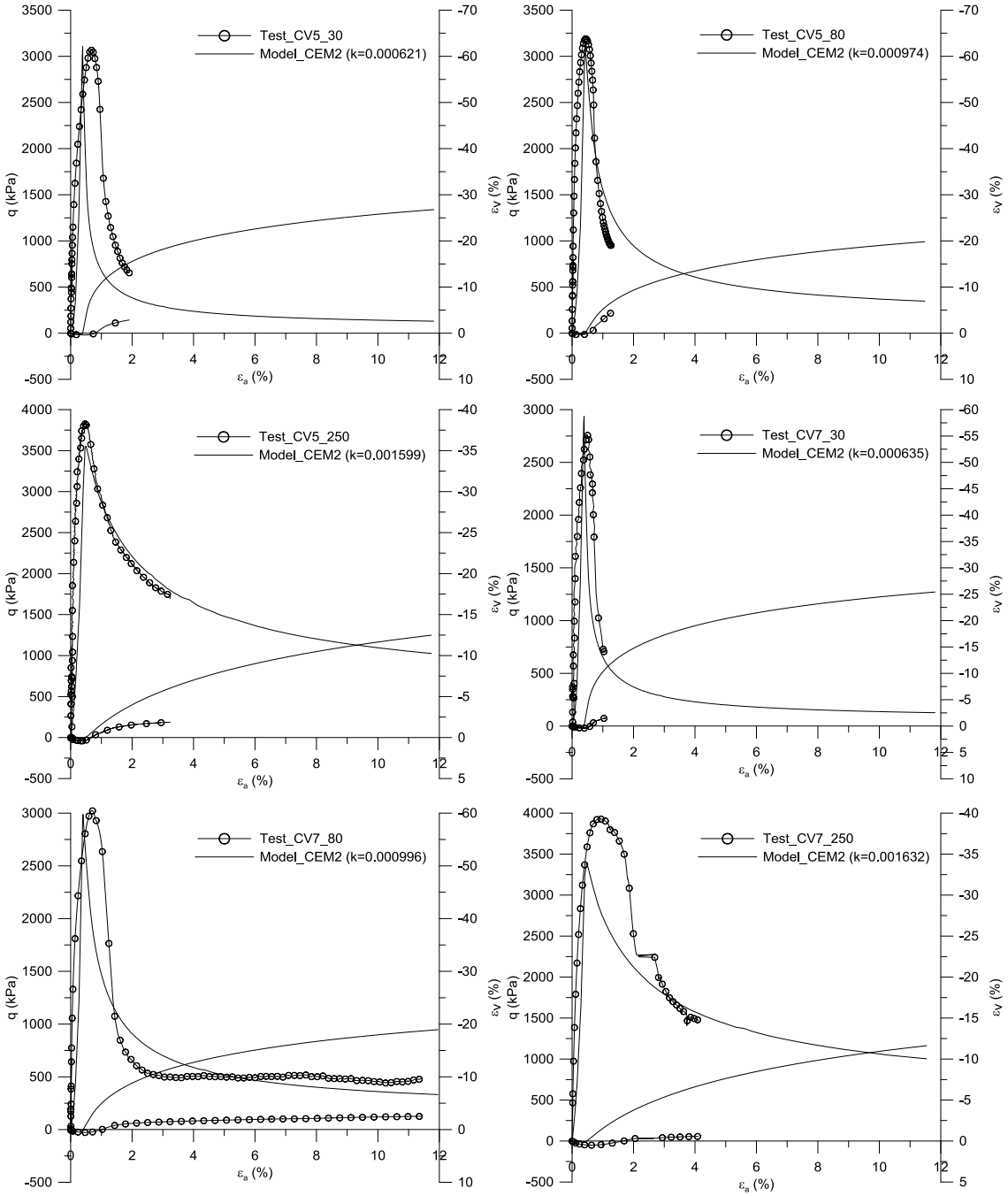

Figure 9.19 Calibration results with CEM 2 in drained tests (cont.)

The graphs of Figure 9.16 show that the results obtained by the CEM 2 parameters (with the initial stiffness adjusted by equation (9.17)) adjust rather well the stress-strain test results giving validity to the model. Still in the tests that had a reasonable adjustment with CEM1, like CV4_250, the calibration with CEM2 has shown an even better agreement between model and test results. This is mainly because the calculation of $k_{cemented}$ depends not only on the bonding (b_0) but also on the void ratio (by p'_{s0}) and confining pressure (p'_0)

while in CEM1 the same k value was used for all the tests irrespectively of the void ratio, cement content, or confining pressure.

However, the strain-volumetric curve is not so well adjusted, especially in the dilatant component of the constitutive behaviour, and thus, an attempt was made to calibrate the post peak behaviour by the degradation rate parameters h_1 and h_2. The following graphs show the results obtained with the same parameters as CEM2 but now with $h_1=h_2=2$, which will be called CEM3. Figure 9.17 clearly expresses that higher values of h_1 and h_2 lead to less accentuated dilatancy and faster reduction of deviatoric stress after peak which is attributed to a higher degradation rate of bonding. Therefore, in some cases the strain-volumetric curve may be better approached by CEM 3 or with higher values of h_1 and h_2, but at the same time the stress-strain curve become less adjusted.

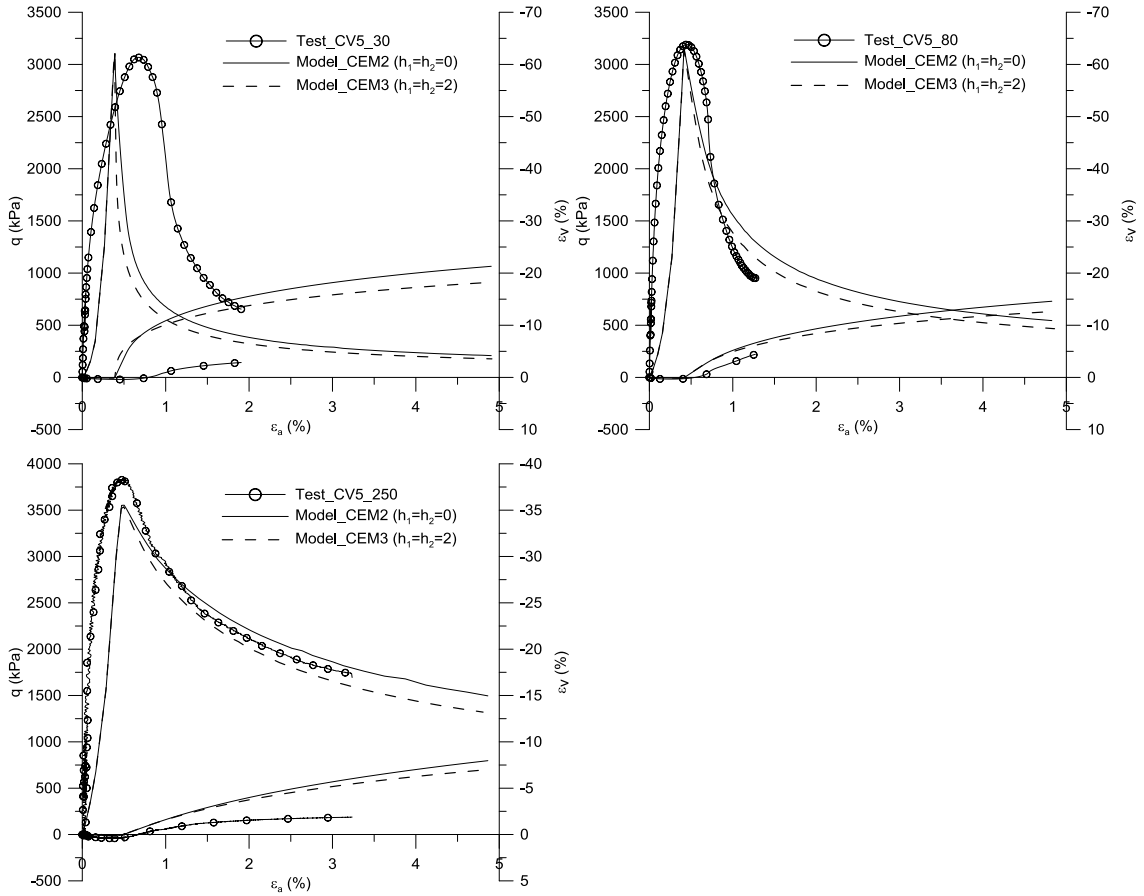

Figure 9.17 Comparison between calibration results with CEM 2 and CEM 3 in 5% drained tests

For that reason, another simulation (CEM 4) was performed considering that the rate of bonding degradation was only due to volumetric strains using $h_1=4$ and $h_2=0$. However, no difference was observed between CEM4 and CEM3 indicating that in this case the amount of volumetric and shear plastic strains should be equivalent. Considering these results

there is no great advantage in using h_1 and h_2 values greater than zero especially at lower confining pressures or, either, these values should be calculated according to each confining pressure.

9.8 Conclusions and Future developments

The contribution of the work presented in this chapter was to increase the knowledge if whether the constitutive model "Cemented CASM" could simulate the behaviour of Porto silty sand mixed with Portland cement. As reported previously, this model has only been tested in cemented clays, so it was important to know how a granular soil could be simulated and which parameters suited better.

On a first approach the simulation was not as good as expected due to some identified limitations of the model. However, some of these limitations were overcome improving in a great extent the adjusted results. This was performed mainly by using an expression of the literature to modify the elastic stiffness parameter k in cemented conditions, being the procedure easily implemented in the model which is suggested for next research programs.

Another interesting research line to follow would be to find correlations between the model parameters or initial values (for instance, p'_c and b) and the porosity/cement ratio ($n/C_{iv}^{0.21}$) like Arroyo et al. (2011) have done with Bergado's ratio (Lorenzo and Bergado, 2004; Bergado et al, 2006). Following Arroyo et al. (2011) this can be done either by triaxial or uniaxial tests results, however, careful should be taken in the unconfined compression tests in terms of draining conditions as they should probably be assumed to be near fully drained, in opposition to what was considered in cemented clays. These correlations would allow a much easier calibration of the model for other cementation degrees without any need of systematic and exhaustive laboratory tests for each specific mixture. Nevertheless, to have confidence in such correlations more experience is to be accumulated in the application of this model.

Chapter 10.
CONCLUSIONS

10.1 Conclusions

This work named “A general framework for the geomechanical characterisation of artificially cemented soil” was introduced in the first chapter as having three main goals that will be revisited in this section. The procedure for seeking those aims was an extensive experimental program over remoulded specimens of different mixtures of Porto silty sand with Portland cement.

The first goal presented in the first chapter was related to the influence of the several parameters involved in the strength and stiffness of soil-cement mixtures, mainly developed on Chapter 6, bearing in mind the present knowledge found in the literature and summarized on Chapter 3. In this part, a significant number of different tests was presented, being compressive and tensile strength as well as dynamic and static stiffness evaluation with seismic wave interpretation some of the most important topics analysed. Unconfined compression tests for several cement contents, initial void ratios and water contents were performed in a large number providing a good knowledge of the influence of each of these parameters on the unconfined compression strength. Consequently, the use of the porosity/cement ratio suggested by Consoli et al. (2007) adjusted by an exponent ($n/C_{iv}^{0.21}$) revealed to be very consistent and useful for the analysis of the unconfined compression strength, since a unique trend was obtained between this variable and $n/C_{iv}^{0.21}$. A relationship between indirect tensile and compressive strength of about 11% was found, provided by indirect tensile tests executed over specimens in similar conditions.

Seismic wave measurements were performed by means of bender elements, compression transducers, ultrasonic transducers and resonant column devices, some of these tests being performed over a wide range of mixtures. The high stiffness of these materials gave rise to some difficulties in seismic wave measurements. For instance, bender elements, which are generally very useful for shear (S) wave measurements, presented a difficult

interpretation in these materials since compression (P) and S waves' velocities were rather similar and therefore not always easy to distinguish. In opposition, compression transducers, generating only P waves, provided an excellent way to obtain accurate P wave velocities. The resonant column tests, although with questionable fixing conditions that may lead to misleading estimations of dynamic properties in these very stiff materials, gave quite reasonable results indicating that the random noise procedure studied by Camacho-Tauta (2011) may be more interesting to test these materials, due to the reduced distortion level, when compared to the ASTM standard procedure.

Nevertheless, a consistent procedure was used for S wave interpretation giving rise to a relationship between the maximum shear modulus (G_0) and the porosity/cement ratio $n/C_{iv}^{0.21}$ with a high correlation coefficient. The correspondent maximum Young Modulus (E_0) was compared to the initial tangent modulus obtained through the local strain instrumentation of unconfined compression tests (E_{ti}) by plotting them against $n/C_{iv}^{0.21}$ showing that, except for the absolute values, the trend is similar. These results gave consistency to the use of this ratio in artificially cemented materials to describe their behaviour both in strength and stiffness, instead of the cement content itself.

This was corroborated by Chapter 7 results on the static triaxial tests performed at low and high pressures over uncemented and cemented specimens. The isotropic compression tests presented in that chapter performed over cemented materials with different cement contents and void ratios, but only two different $n/C_{iv}^{0.21}$, were in agreement with the one-dimensional compression tests performed in oedometric cells in a constant rate of deformation, reported in Chapter 6. The results show that a single Normal Compression Line (NCL) is obtained for each $n/C_{iv}^{0.21}$ despite their cement content and initial void ratio. However, these NCLs do not join together with the uncemented NCL as it would be expected if all the cemented bonds were destroyed, indicating that uncemented behaviour could not be recovered. This was clear not only in the isotropic compression tests but also in the strength envelopes and in the stress-dilatancy analysis where M values resulted in different values for cemented (M=1.9) and uncemented conditions (M=1.4).

In terms of the strength parameters obtained in peak and ultimate conditions for cemented specimens, two different peak strength envelopes were obtained for each $n/C_{iv}^{0.21}$ ($n/C_{iv}^{0.21}$=36: ϕ'=30º and c'= 253 kPa; $n/C_{iv}^{0.21}$=29: ϕ'=39º and c'= 589 kPa) but a single ultimate strength envelope was achieved (ϕ'=47º). This value was significantly reduced when the high pressures tests were included (ϕ'=30) due to the degradation of the cemented bonds during consolidation to post yield pressures. However, this value is distinct of the angle of shearing resistance obtained in the uncemented tests (ϕ'=34º),

corroborating the idea that the cemented soil after testing (even to very high pressures) is distinct of the uncemented material. On the other hand, the uncemented angle of shearing resistance was also reduced at higher pressures possibly due to particle breakage. The strength envelope values of the cemented tests were obtained through a procedure based on the Mohr's circles analysis to solve the lack of representativeness of principle stress analysis due to non correspondence of the real localised shear locus. In fact, strain localisation is unavoidable in these very stiff materials, and consequently, the global stress-strain measurements are no longer representative of the conditions throughout the shearing process.

The definition of the Critical state line (CSL) in the volumetric space (v vs p') was also pursued. In uncemented conditions a possible line was defined, since the stress-strain behaviour presented by each uncemented test allowed the identification of the stress state of the tested specimens either on the wet or the dry side of critical state (as described in chapter 4). The tests were conducted up to high strain levels, so most of them should have reached states close to the critical state. In the cemented tests, this task was complicated by incomplete testing and strain localisation. The high pressure tests conducted over specimens with $n/C_{iv}^{0.21}=29$ revealed some interesting trend of the CSL at higher stresses but this is not totally compatible with the low pressure results which lead to the assumption of a curved CSL. However, it was not clear from the obtained results that this CSL is unique for each $n/C_{iv}^{0.21}$ at low pressures.

The second goal introduced in the first chapter comprised the identification of yield surfaces and the evaluation of the stress-dilatancy behaviour. The latter was already mentioned and tentatively understood due to its contribution to the interpretation of the different features between cemented and uncemented behaviour. The yield and state boundary surfaces were identified clearly by normalizing the test results for the effect of volume. For the yield surface, the results were normalised with respect to the uncemented NCL and a tentative yield surface was drawn following Coop and Airey's (2003) suggestion described in Chapter 4. The reason why this surface is not so well defined is the large difference between the consolidation stresses of the low and higher pressure tests, the latter being performed at consolidation stresses on their NCL and therefore, most of the interparticle structure has already been destroyed. For this reason, the yield surface is defined only by the low pressure shearing yield points and the high pressure isotropic yield points.

A third goal specified in the research programme was related to the soil-cement behaviour in cyclic conditions and this was developed in Chapter 8. The first approach was essentially based on the European standard for cyclic triaxial tests developed for unbound granular

materials - EN 13286-7 (CEN, 2004a), which was then considered to be inadequate in terms of the applied loads, strain limits and classification charts. This was concluded by comparing tests following the standard procedure with tests at a “higher” number of cycles and “lower” stress level than “those ranges specified in the standard”. In terms of the resilient behaviour, both types of tests showed that the resilient modulus becomes quite stable after a few number of cycles. On the other hand, the accumulated permanent deformation, which was quite constant and close to zero in the first tests, presented a significant increase when tested to a higher number of cycles.

These last tests performed drained and undrained, allowed a comparison between both conditions leading to some interesting conclusions. The undrained resilient modulus was always higher than the corresponding modulus obtained in drained conditions, which was considered to be the result of the volumetric effect with expression in the value of the observed Poisson ratio, on the Young Modulus. In terms of plastic deformation, undrained tests presented a much higher rate of accumulation of strains during the cycling process when comparing to the drained tests. It seems that in undrained conditions the resilient deformation is smaller and the permanent deformation is higher while in drained tests the opposite is observed.

The initial void ratio introduced a significant effect on both the resilient and plastic behaviour, as it would be expected, while the adjusted porosity/cement ratio that was considered very much representative of strength and stiffness in static tests was not so efficient in cyclic conditions. However, this might be related to the larger scatter in the results obtained in these tests mainly due to the low level of strain involved.

Finally, exceeding the initial objectives, this work was concluded with the calibration of a constitutive model. The cemented CASM, as it was named by the authors, is an extension of the well know Clay and Sand Model (CASM) developed by Yu (1998) based on the cemented formulation proposed by Gens and Nova (1993). This constitutive model has been recently applied with good success in natural structured clays (Gonzalez et al., 2007, 2009) and artificially cemented clays (Arroyo et al., 2011 and Ciantia et al., 2011), and, therefore, this work aimed at calibrate, for the first time, an artificially cemented granular soil. During calibration some limitations of the model were identified. The most important was that it admitted the same elastic parameters (k and υ) in uncemented and cemented conditions. To overcome this problem a new way to calculate the slope of the swelling line (k) in cemented conditions was applied based on the bulk modulus expression proposed by Yu et al. (2007b). The use of this procedure gave quite good results in the simulation of drained tests. Unfortunately, the simulation of the undrained tests was not so well

accomplished due to several reasons. It has been identified in Chapter 7 that the cemented tests strength envelope in drained and undrained conditions was different, the latter having a lower position in the stress space than the former. For this reason the same model could not adjust in the same way tests with such distinct behaviour. The drained tests were given preference because the undrained tests have shown another problem when uncemented tests were calibrated. The model assumes that no plastic strains are observed up to the yield surface (at peak) and thus, without volume change, the q vs p' stress-path is assumed to be vertical. However, this was not observed experimentally possibly due to small plastic strains since the very beginning. Therefore, the simulation of the undrained tests was very difficult.

Besides these limitations the Cemented CASM gave very promising results and it appears to be simple and very adapted to simulate the constitutive behaviour of these materials. Additionally, it can be implemented in user friendly software, such as PLAXIS®.

10.2 Future developments

In the previous section the most important conclusions were summarized along with a brief description of some parts of the work developed, becoming clear that some limitations were found that can be improved in other research works. In the same way, some conclusions lead to other research lines that could be explored in the future with great chances to solve some identified uncertainties, with low effort. For these reasons, in this section some outlines for future developments are highlighted.

Several tests were conducted for seismic wave measurements, although some of them proved to be more interesting than others. The use of compression transducers or ultrasonic transducers for P wave velocities is greatly encouraged in the evaluation of the stiffness degradation due to cyclic loads (using specimens with high curing time to assure bonding stabilisation), by one side, and performing distinct measurements in time to analyse the stiffness increase with curing.

The general framework attempted with the static triaxial tests experimental program would be greatly improved with more tests at intermediate confining pressures ideally just before isotropic yield. Also some more tests at high pressures could be performed in the other adjusted porosity/cement ratio ($n/C_{iv}^{0.21}$=36) to evaluate if the same conclusions taken on $n/C_{iv}^{0.21}$=29 are valid in other ratios, as it should be expected. These results would allow a more confident definition of the cemented yield and state boundary surfaces, whether it is unique or a set of surfaces for each cement content or adjusted porosity/cement ratio. The tests should be performed with the maximum possible deformation, so that critical state

may be identifiable, and with an accurate measurement of the void ratio, so the CSL in the v vs ln p' can be obtained. Investigation can be pursued to evaluate if a unique CSL can be obtained for each adjusted porosity/cement ratio just like the NCL and if it is curved towards the low pressures. The effect of particle breakage, for one side, and the formation of clusters with cementation and their shape and size evolution with confining pressure and shearing, would be much more clearly identified if microscopic analysis (such as SEM and else) are used in future research, that is, if nano properties are looked for.

In the cyclic tests, it is advisable that more tests with a great number of cycles, like the last tests performed in this cyclic experimental program, should be performed, which can be very useful to evaluate more realistically the evolution of these materials in long term conditions. The tests could be carried out in uncemented conditions and in others mixtures to provide data to a more comprehensive analysis.

In the calibration of the constitutive model it is greatly encouraged to implement the variation of the elastic stiffness with cementation, void ratio and confining pressure as proposed by Yu et al. (2007b). Finally, more research work could be carried out to find correlations between the model parameters or initial values (for instance, p'_c and b) and the porosity/cement ratio ($n/C_{iv}^{0.21}$) like Arroyo et al. (2011) have done with Bergado's ratio (Lorenzo and Bergado, 2004; Bergado et al, 2006). These correlations would allow a much easier calibration of the model for other cementation degrees without any need of laboratory tests.

REFERENCES

Acar, Y. and El-Tahir, A. (1986). Low strain dynamic properties of artificially cemented sands. Journal of Geotechnical Engineering, 112(11), 1001-1015.

ADIF (2006). Pliego de prescripciones técnicas tipo para los proyectos de plataforma. G108 Rellenos: Terraplenes, Pedraplenes y Cuñas de Transición (Technical specifications for railway platforms, In Spanish)

AFNOR (1992). NF P 11-300. Exécution des terrassements. Classification des matériaux utilisables dans la construction des remblais et des couches de forme d'infrastructures routières (Earthworks execution, soil classification for roads, In French), Association française de normalisation

AFNOR (1993). NF P 98-232-3 Détermination des caractéristiques mécaniques des matériaux traités aux liants hydrauliques (Evaluation of the mechanical characteristics of soils treated with hydraulic binders, In French), Association française de normalisation

AFNOR (1997). NF P 94-078 Sols: reconnaissance et essays - Indice CBR après immersion - Indice CBR Immédiat - Indice Portant Immédiate - Mesure sur échantillon compacté dans le moule CBR (CBR, CBR_i and IPI, In French), Association française de normalisation

Airey, D. W. (1993). Triaxial Testing of Naturally Cemented Carbonate Soil, Journal of Geotechnical and Geoenvironmental Engineering, 119(9), 1379-1398.

Alarcon-Guzman, A., Leonards, G. A. and Chameau, J. L. (1988). Undrained Monotonic and Cyclic Strength of Sands, Journal of Geotechnical Engineering, 114(10), 1089-1109.

Allman, M. and Poulos, H. (1988). Stress-Strain Behaviour of an Artificially Cemented Calcareous Soil, in Engineering for calcareous sediments, Balkema, Rotterdam, pp. 51-60.

Altuhafi, F., and Baudet, B. A. (2011). A hypothesis on the relative roles of crushing and abrasion in the mechanical genesis of a glacial sediment. Engineering Geology, (doi:10.1016/j.enggeo.2011.03.002).

Alvarado, G. (2007). Influence of late cementation on the behaviour of reservoir sands. PhD dissertation, Imperial College, London

Amaral, M. (2009). Evaluation of dynamic distortion modulus in soil-cement mixtures by pulse ultrasonic methods in the time domain and resonant modes by spectral analysis of Fourier series. MSc dissertation, Faculty of Engineering of the University of Porto (in Portuguese).

Amaral, M., Rios, S. and Viana da Fonseca, A. (2011). Yielding in isotropic compression of Porto silty sand. (submitted to ACTA Geotechnica Slovenica)

Arroyo, M., Ciantia, M., Castellanza, R. and Gens, A. (2011). A soft-rock model for cement-improved clays. Paper presented at the XV European Conference of Soil Mechanics and Foundation Engineering, Athens, Greece.

Asaoka, A., Nakano, M., Noda, T., Matsuo, M. (2001). The Decay of Structure and the Loss of Overconsolidation, in 5th International Conference on Soil Mechanics and Geotechnical Engineering, Istambul, 19-22.

ASTM (1996a). D 3999-91. Standard test methods for the determination of the modulus and damping properties of soils using the cyclic triaxial apparatus

ASTM (1996b). D 1633-96. Standard test method for compressive strength of molded soil-cement cylinders.

ASTM (1998a). D 2487-98 Standard practice for classification of soils and engineering purposes (Unified Classification System)

ASTM (1998b). D 5298-94 - Standard test method for the measurement of soil potential (suction) using filter paper. Annual Book of Standards, Vol. 04.09, ASTM International, West Conshohocken, PA, pp.156-161

ASTM (2000). D 4015-92 - Standard test methods for modulus and damping of soils by the resonant-column method. (1992, reapproved 2000).

ASTM. (2002). ASTM C597-02 - Standard Test Method for Pulse Velocity Through Concrete.

Atkinson, J. H. (2008). The Mechanics of Soils and Foundations, Taylor and Francis.

Baig, S., Picornell, M. and Nazarian, S. (1997). Low strain shear moduli of cemented sands. Journal of Geotechnical and Geoenvironmental Engineering, 123(6), 540-545.

Baudet, B. A. and Stallebrass, S. (2004). A Constitutive Model of Structured Clays, Géotechnique, 54(4), 269-278.

Been, K. and Jefferies, M.G. (1985). A state parameter for sands. Geotechnique 35(2), 99–112.

Bergado, D., Taechakumthorn, C., Lorenzo, G., and Abuel-Naga, H. M. (2006). Stress deformation behaviour under anisotropic drained triaxial consolidation of cement treated soft Bankok clay. Soils and Foundations, 46(5), 629-637.

Boey, C.F. (1990). Modelling of the behaviour of natural calcarenite. Ph.D. thesis, University of Sydney

Bolton, M. D. (1986). The strength and dilatancy of sands. Géotechnique 36(1), 65-78

Burland, J. B. (1990). On the compressibility and shear strength of natural clays. Géotechnique, 40(3), 329-378.

Burrow, M., G. Ghataora and D. Bowness (2004). Analytical track substructure design, International Seminar on Geotechnics in Pavement and Railway Design and Construction, Athens.

Camacho-Tauta, J. (2010). Evaluation of the small-strain stiffness of soil by non-conventional dynamic testing methods, PhD thesis submitted to Technical University of Lisbon, Portugal

Carrera, A., Coop, M.R. and Lancellotta, R. (2011) The Influence of grading on the Mechanical behaviour of Stava tailings. Géotechnique, (In Press).

Carvalho, J., Rios, S. and Viana da Fonseca, A. (2011). Elastic stiffness parameters of soil-cement mixtures from laboratory compression and shear wave velocity measurements. 5th International Conference on Earthquake Geotechnical Engineering, Santiago, Chile

Caspurro, I. and Dias, S. (2008). Experience in soil-cement application in the national road network. TRATCICA - Seminar on the treatment of materials with lime and cement for transport infrastructures (in Portuguese), Porto

Cavarreta, I., Coop, M., and O'Sullivan, C. (2010). The influence of particle characteristics on the behaviour of coarse grained soils. Géotechnique, 60(6), 413-423.

CEN (2003a). EN 13286-42 - Unbound and hydraulic bound mixtures. Test method for the determination of the indirect tensile strength of hydraulically bound mixtures, Comité Européen de Normalisation, Brussels

CEN (2003b). EN 13286-41 - Unbound and hydraulic bound mixtures. Test method for the determination of the compressive strength of hydraulically bound mixtures, Comité Européen de Normalisation, Brussels

CEN (2004a), EN 13286-7 - Unbound and hydraulically bound mixtures - Part 7: Cyclic load triaxial test for unbound mixtures, Comité Européen de Normalisation, Brussels

CEN (2004b), EN 13286-53 - Unbound and hydraulically bound mixtures - Part 53: Methods for the manufacture of test specimens of hydraulic bound mixtures using axial compression, Comité Européen de Normalisation, Brussels

CEN (2004c). CEN ISO/TS 17892-1 Geotechnical investigation and testing - Laboratory testing of soil - Part 1: Determination of water content (ISO/TS 17892- 1:2004), Comité Européen de Normalisation, Brussels

CEN (2006). EN 14227-10 - Mélanges Traités Aux Liants Hydrauliques - Spécifications - Partie10: Sol Traité Au Ciment, Comité Européen de Normalisation, Brussels

Chandler, R.J., Crilly, M.S. and Montgomery-Smith, G. (1992). A low cost method of assessing clay desiccation for low rise buildings. Proc. Institute of Civil Engineering, Vol.92(2), 82-89

Chang, T. S. and Woods, R.D. (1992) Effect of particle contact bond on shear modulus. Journal of Geotechnical and Geoenvironment Engineering, ASCE, 118(GT8), 1216-1233.

Cho, G. C., Dodds, J. and Santamarina, J. (2006). Particle shape effects on packing density, stiffness and strength: natural and crushed sands. Journal of Geotechnical and Geoenvironmental Engineering, 132(5), 591-602.

Ciantia, M., Arroyo, M., Castellanza, R. and Gens, A. (2011). The influence of jet-grout constitutive modelling in excavation analyses. Paper presented at the 7th International Symposium on "Geotechnical Aspects of Underground Construction in Soft Ground.

Clayton, C. R. I., Khatrush, S. A., Bica, A. V. D., and Siddique, A. (1989). The use of hall effect semiconductors in geotechnical instrumentation. Geotechnical Testing Journal, 12(1), 69–76.

Clough, G., Sitar, N., Bachus, R. and Rad, N. (1981). Cemented sands under static loading. Journal of the Geotechnical Engineering Division, 107799-817.

Consoli, N.C., Rotta, G.V. and Prietto, P.D.M. (2000). Influence of curing under stress on the triaxial response of cemented soils. Technical note. Géotechnique, 50(1), 99-105

Consoli, N.C., Vendruscolo, M. and Prietto, P. (2003) Behavior of Plate Load Tests on Soil Layers Improved with Cement and Fiber. Journal of Geotechnical and Geoenvironmental Engineering, 129(1), 96-101

Consoli, N.C., Rotta, G.V., Prietto and P.D.M. (2006). Yielding-compressibility-strengh relationship for an artificially cemented soil cured under stress. Tecnical Note. Géotechnique 56(1), 69-72

Consoli, N.C., Foppa, D., Festugato, L. and Heineck, K. (2007). Key Parameters for Strength Control of Artificially Cemented Soils, Journal of Geotechnical and Geoenvironmental Engineering, 133(2), 197-205.

Consoli, N.C., Viana da Fonseca, A., Cruz, R. C., and Heineck, K. (2009). Fundamental Parameters for the Stiffness and Strength Control of Artificially Cemented Sand, Journal of Geotechnical and Geoenvironmental Engineering, 135(9),1347–1353.

Consoli, N.C., Cruz, R. C., Viana da Fonseca, A. and Coop, M. (2011a). Influence of the voids-cement ratio on stress-dilatancy-strength behaviour of artificially cemented sand. Journal of Geotechnical and Geoenvironmental Engineering, ASCE (doi:10.1061/(ASCE)GT. 1943-5606.0000565)

Consoli, N.C., Viana da Fonseca, A., Cruz, R.C., Rios, S. (2011b) Void/cement ratio controlling tensile strength of cement treated soils. Géotechnique (accepted for publication)

Coop, M. (1991). “Computer control programme for high pressure triaxial apparatuses”, City University.

Coop, M. (2003). On the Mechanics of Reconstituted and Natural Sands, in Proceedings of Deformation Characteristics of Geomaterials, Swets and Zeitliager, Lisse.

Coop, M. and Atkinson, J. H. (1993). The Mechanics of Cemented Sands, Géotechnique, 43(1), 53-67.

Coop, M. and Airey, D.W. (2003). Carbonate Sands. Characterisation and Engineering Properties of Natural Soils. Swets and Zeitlinger, Lisse, Tan et al. (eds.), 1049-1086

Coop, M. and Wilson, S. M. (2003). Behavior of Hydrocarbon Reservoir Sands and Sandstones, Journal of Geotechnical and Geoenvironmental Engineering, 129(11),

Costa, C. (2008). Development of a monitoring system for control of triaxial tests of soils. MSc thesis presented to the Faculty of Engineering of the University of Porto (In Portuguese)

Cruz, R.C. (2008). The influence of key parameters on strength, stiffness and dilantancy of an artificially cemented sand. PhD dissertation presented to the Federal University of Rio Grande do Sul, Porto Alegre (in Portuguese)

Cruz, N. (2010). Modelling geomechanics of residual soils with DMT tests. PhD thesis presented to the Faculty of Engineering of the University of Porto.

Cuccovillo, T. and Coop, M. (1997). Yielding and Pre-Failure Deformation of Structured Sands, Géotechnique, 47(3), 491-508.

Cuccovillo, T. and Coop, M. (1998). "Automated Triaxial Apparatus for elevated pressures", In: Marr, W.A. and Fairhurst C.E. Eds., "Non-destructive and Automated Testing for Soil and Rock Properties", Proc. of the Symp. Nondestructive and automated testing for soil and rock properties, ASTM, San Diego. 231-246.

Cuccovillo, T. and Coop, M. (1999). On the Mechanics of Structured Sands, Géotechnique, 49(6), 741-760.

Dalla Rosa, F., Consoli, N. and Baudet, B. (2008). An Experimental Investigation of the Behaviour of Artificially Cemented Soil Cured under Stress, Géotechnique, 58(8), 675-679.

Dash, H.K., Sitharam, T.G. and Baudet, B. (2011). Influence of non-plastic fines on the response of a silty sand to cyclic loading. Géotechnique (in press)

Dif, W. (2007). Cyclic loadings on cemented soils cured under stress. Report of the Scientific Internship in the Department of Civil Engineering of the University of Porto

Dupas, J.-M., Pecker, A. (1979). Static and dynamic properties of sand-cement. Journal of Geotechnical Engineering Division, 105(3), 419-436.

Dyvik, R., and Madshus, C. (1985). "Lab measurements of Gmax using bender elements." *Proc., Advances in the Art of Testing Soils under Cyclic Conditions*, American Society of Civil Engineers, New York.

EP (2009). Caderno de Encargos Tipo Obra, Estradas de Portugal (Portuguese Institution for Roads, In Portuguese)

Fernandez, A. and Santamarina, J. (2001), Effect of Cementation on the Small-Strain Parameters of Sands, Canadian Geotechnical Journal, 38(1), 191-199.

Ferreira, C. (2008). The Use of Seismic Wave Velocities in the Measurement of Stiffness of a Residual Soil, PhD dissertation presented in the University of Porto

Ferreira, C., Viana da Fonseca, A. and Nash, D. (2011). Shear Wave Velocities for Sample Quality Assessment on a Residual Soil. Soils and Foundations, 51(4), IS-Seoul Special Issue

Feuerharmel, C., Gehling, W, Bica, A. (2006). The use of filter-paper and suction-plate methods for determining the soil-water characteristic curve of undisturbed colluvium soils. *Geotechnical Testing Journal 29*(5), 419-425.

Foppa, D. (2005). Análise de Variáveis-Chave no controle da Resistência Mecânica de Solos Artificialmente Cimentados. Dissertação de Mestrado. Universidade Federal do Rio Grande do Sul, Porto Alegre, Brasil.

Fortunato, E. (2008). Soil improvement: a high potential alternative. TRATCICA - Seminar on the treatment of materials with lime and cement for transport infrastructures (in Portuguese), Porto

Futai, M., Almeida, M. S. and Lacerda, W. A. (2004). Yield, strength and critical state conditions of a tropical saturated soil. Journal of Geotechnical and Geoenvironmental Engineering, 130(11), 1169-1179.

Gasparre, A. (2005). Advanced laboratory characterisation of London Clay. PhD dissertation presented to the University of London

Gasparre, A., Nishimura, S., Coop, M. R. and Jardine, R. J. (2007). The Influence of Structure on the Behaviour of London Clay, Géotechnique, 57(1), 19-31.

Gens, A. and Nova, R. (1993). Conceptual bases for a constitutive model for bonded soils and weak rocks. Geotechnical Engineering of Hard soils - Soft Rocks, Anagnostopoulos et al (eds). Balkema, Roterdam

Goldstein, J.I., Newbury, D.E., Echlin, P., Joy, D.C., Fiori, C., Lifshin, E. (1981). Scanning Electron Microscopy and X-Ray Microanalysis. A text for Biologists, Materials Scientists, and Geologists. Plenum Press, New York and London

Gomes Correia, A and Neves, J. (1999). Soil mixed with binders: mechanical and physic-chemical properties. Documentation for the discipline of Conception, design, construction and rehabilitation of roads, IST, Lisbon (In portuguese)

González, N. (2011). Development of a family of constitutive models for geotechnical applications. PhD dissertation submitted to Universitat Politècnica de Catalunya (UPC), Barcelona

González, N., Arroyo, M. and Gens, A. (2007). The effect of structure in pressuremeter tests in clay. Paper presented at the International Symposium on Numerical Models in Geomechanics (NUMOGX), Rhodes, Greece.

González, N., Arroyo, M. and Gens, A. (2009). Identification of bonded clay parameters in SBPM tests: a numerical study. Soils and Foundations, 49(3), 329-340.

Goto, S, Tatsuoka, F, Shibuya, S, Kim, Y-S, Sato, T (1991). A simple gauge for local small strain measurements in the laboratory. Soils and Foundations, 31(1), 169-180.

Gräbe, P. and Clayton, C. (2009). Effects of principal stress rotation on permanent deformation in rail track foundations Journal of Geotechnical and Geoenvironmental Engineering, 135(4), 555-565.

Greening, P.D, Nash, D.F.T. (2004) Frequency domain determination of G_0 using bender elements, ASTM Geotechnical Testing Journal, 27, 3, 1-7

Greening, P.D., Nash, D.F.T.; Benahmed, N.; Viana da Fonseca, A. and Ferreira, C., (2003) Comparison of shear wave velocity measurements in different materials using time and frequency domain techniques, Proceedings of Deformation Characteristics of Geomaterials, Lyon, France, 22-24 September, Lyon, France:Balkema, pp. 381-386.

GTR (2000). Guide des Terrassements Routières, Réalisation des remblais et des couches de forme (Technical guide for road earthworks, In French), LCPC

GTS (2000). Guide technique pour le traitement des sols à la chaux et/ou aux liants hydrauliques. Application à la réalisation des remblais et des couches de forme. (Technical guide for soils treated with lime and cement, In French), LCPC/SETRA.

Hamidi, A. and Haeri, S. (2008). Stiffness and deformation characteristics of a cemented gravely sand. International Journal of Civil Engineering, 6(3), 159-173.

Head, K. H. (1982). Manual of soil laboratory testing - Volume 2 - Permeability, shear strength and compressibility tests. Pentech Press limited

Henkel, D.J. and Gilbert, G.D. (1952). The effect of the rubber membrane on the measured triaxial compression strength of clay specimens. Géotechnique, Vol. 3, No.1

Hight, D.W. and Higgins, K.G. (1994). An approach to the prediction of ground movements in engineering practice: Background and application. Proc. Int. Symp. on Pre-Failure Deformation Characteristics of geomaterials – Measurement and Application. IS-Hokkaido, Sapporo, Vol. 2, pp.909–945.

Horpibulsuk, S., Miura, N. and Nagaraj, S. (2003). Assessment of Strength Development in Cement-Admixed High Water Content Clays with Abrams' Law as a Basis, Géotechnique, 53(4), 439-444.

Huang, J. T. and Airey, D. W. (1993). Effects of Cement and Density on an Artificially Cemented Sand, in Geotechnical Engineering of Hard Soils-Soft Rocks, Athens: Balkema, Rotterdam, pp. 553-560.

Idriss, I. M. and Boulanger, R. W. (2006). Semiempirical procedures for evaluating liquefaction potential during earthquakes. Soil Dynamics and Earthquake Engineering, 26(2–4), 115–130.

Ismail, M., Ferreira, C. and Fahey, M. (2004). Influence of the Cement Type on G_0 of a Carbonate Sand, in Advances in Geotechnical Engineering: Proceedings of the A.W. Skempton Memorial Conference.

Ismail, M., Joer, H., Sim, W. H. and Randolph, M. F. (2002). Effect of Cement Type on Shear Behaviour of Cemented Calcareous Soil, Journal of Geotechnical and Geoenvironmental Engineering, 128(6), 520-529.

Jardine, R.J. (1992). Some observations on the kinematic nature of soil stiffness. Soils and Foundations, 32(2), 111–124.

Jardine, R.J., St-John, H.D., Hight, D.W. and Potts, D.M. (1991). Some practical applications of a non-linear ground model. Proc. 10th European Conf. on Soil Mech. and Found. Engng., Florence, Vol. 1, pp.223–228.

Jiang, M. J., Yu, H. S., and Leroueil, S. (2007). A simple and efficient approach to capturing bonding effect in naturally microstructured sands by discrete element method. International Journal for Numerical Methods in Engineering, 69(6), 1158-1193.

Johnson (1986). Plastic Flow, residual stresses and Shakedown in rolling contact. Proceedings of the 2nd International Conference on Contact Mechanics and Wear of Rail/Wheel Systems, University of Rhode Island, Waterloo Ontario

Kasama, K., Zen, K. and Iwataki, K. (2006). Undrained shear strength of cement-treated soils. Soils and Foundations, 46(2), 221-232

Kavvadas, M. and Amorosi, A. (2000). A constitutive model for structured soils. Géotechnique 50(3), 263-273

Kent M F (1962). AASHO road test vehicle operating costs related to gross weight. Highway Research Board Special Report 73, pp. 149 –65

Khan, Z., Majid, A., Cascante, G., Hutchinson, D.J. and Pezeshkpour, P. (2006). Characterization of a cemented sand with the pulse-velocity method. Canadian Geotechnical Journal, 43, 294–309

Klotz, E. U., and Coop, M. R. (2002). On the Identification of Critical State Lines for Sands. Geotechnical Testing Journal, 25(3), 1-14.

Kongsukprasert, L., Tatsuoka, F., and Tateyma, M. (2005). Several Factors Affecting the Strength and Deformation Characteristics of Cement-Mixed Gravel., Soils and Foundations, 45, 107-124.

Konrad, J.-M. and Nguyen, Ph.D. (2006). The use of tangent stiffness to characterize the resilient response of unbound crushed aggregates, Canadian Geotechnical Journal, 43, 1117-1130.

La Rochelle, P., Leroueil, S., Trak, B., Blais-Leroux, L., Tavenas, F. (1988).Observational approach to membrane and area correction in triaxial tests. Advanced Triaxial testing of soil and rock, ASTM special technical publication 977, pp.715-731, ASTM Philadelphia

Ladd, R. S. (1978). Preparing test specimen using undercompaction. Geotechnical Testing Journal, 1(1), 16-23.

Lade, P. V. and Overton, D. D. (1989). Cementation effects on frictional materials. Journal of Geotechnical and Geoenvironmental Engineering, 115(2), 1373-1387.

Lambe, T.W. (1962). Soil stabilization. Cap. 4 of Foundation Engineering, G.A. Leonards Ed., Mc Graw-Hill

Lekarp, F., Isacsson, U., and Dawson, A., (2000a). State of art: I: Resilient response of unbound aggregates: Journal of Transportation Engineering, 127, 66-75.

Lekarp, F., Isacsson,U., and Dawson,A., (2000b) State of art. II: Permanent strain response of unbound aggregates: Journal of Transportation Engineering, 127, 76-83.

Leroueil, S. (2003). Behaviour and properties of natural soils and soft rocks. Characterisation and Engineering Properties of Natural Soils. Swets and Zeitlinger, Lisse, Tan et al. (eds.), pp. 29-254

Leroueil, S. and Vaughan, P. (1990). The General and Congruent Effects of Structure in Natural Soils and Weak Rocks, Géotechnique, 40(3), 467-488.

Li, D. and Selig, E.T., (1994). Resilient Modulus for Fine-Grained Subgrade Soils. Journal of Geotechnical Engineering, 120(6), 939-957.

Li, D. and Selig, E. T. (1996). Cumulative Plastic Deformation for Fine-Grained Subgrade Soils, Journal of Geotechnical Engineering, 122(12), 1006-1013.

Liyanapathirana, D. S., Carter, J. P., and Airey, D. W. (2005). Numerical Modeling of Nonhomogeneous Behavior of Structured Soils during Triaxial Tests. International Journal of Geomechanics, 5(1), 10-23.

LNEC (1971). E 243 Soils. Soil-cement (In Portuguese)

LNEC (1972a). E 264 - Soil-cement. Compression test. Specification of the National Laboratory of Civil Engineering, Lisbon (In Portuguese).

LNEC (1972b). E - 262 - Compactation tests, Specification of the National Laboratory of Civil Engineering, Lisbon (in Portuguese)

LNEC (1974) - E304 Road pavements. Soil-cement (In Portuguese)

Lohani, T.N., Kongsukprasert, L, Watanabe, K. and Tatsuoka, F.(2004) Strength and deformation properties of compacted cement-mixed gravel evaluated by triaxial compression tests. Soils and Foundations,Vol.44,Nº5,pp.95-108

Lopes, A.U.S (2007). Reforço no solo com cimento, para plataforma de comboios de alta velocidade (Soil treated with cement for high speed railway platforms, In Portuguese). Relatório de actividades de estágio de iniciação à investigação. Faculdade de Engenharia da Universidade do Porto.

Lorenzo, G. and Bergado, D. (2004). Fundamental parameters of cement-admixed clay - New Approach. Journal of Geotechnical and Geoenvironmental Engineering, 130(10), 1042-1050.

Lovelady, P.L. and Picornell, M. (1990). Specimen coupling in resonant column testing of cemented soils. In Dynamic elastic modulus measurement in materials, ASTM STP 1045, American Society for Testing and Materials, Philadelphia, Penn

Malandraki, V. and Toll, D. G. (1996). The definition of yield for bonded materials. Geotechnical Geological Engineering, 14(1), 67-82.

Marinho, F.A.M (1994). Shrinkage behaviour of some plastic clays. PhD Thesis, Imperial College, Imperial College, University of London

Marinho, F., Oliveira, O. (2006). The filter paper method revisited. Geotechnical Testing Journal. Vol.29, Nº3, pp.250-258Sibley and Williams (1990)

Matesic, L. and Vucetic, M., (2003). Strain-Rate Effect on Soil Secant Shear Modulus at Small Cyclic Strains. Journal of Geotechnical and Geoenvironmental Engineering, 129(6), 536-549.

Minguela (2008). Soils treated with cement. TRATCICA - Seminar on the treatment of materials with lime and cement for transport infrastructures (in Spanish), Porto

Mitchell, J.K. (1976) Fundamentals of soil behaviour, New York, Wiley

Momoya, Y., Sekine,E., Tatsuoka,F. (2005). Deformation characteristics of railway roadbed and subgrade under moving-wheel load. Soils and Foundations, Vol.45(4), 99-118

Muir Wood, D. (2004). Geotechnical Modelling. Spon Press, London

Novais-Ferreira (1981). On the compaction of roads. Seminar 249, LNEC, Lisboa (In Portuguese)

PCA (2005). Soil-Cement Technology for Pavements: Different Products for Different Applications, Portland Cement Association (www.cement.org/pavements accessed in 20/7/2009)

PG3 (2004). Pliego de prescripciones técnicas generales para obras de carreteras y puentes. Art. 512 - Materiales tratados con cemento (suelocemento y gravacemento). Art. 513 - Suelos estabilizados in situ (Technical specification for roads and bridges, Soils treated with cement, In Spanish) (Orden FOM 891/2004, de 1 de marzo, BOE 6-4-04)

Pinyol, N., Vaunat, J., and Alonso, E. (2007). A constitutive model for soft clayey rocks that includes weathering effects. Géotechnique, 57(2), 137-151.

Powell, M J, Potter, J F, Mathew, J. C, Nunn, T. (1984). The structural design of bituminous roads. Laboratory report 1132. Crowthorne, Transport and Research Laboratory

Qadimi, A. (2005). The cyclic response of a carbonate sand through critical state soil mechanics. PhD thesis submitted to The University of London (Imperial College Diploma)

Qadimi, A. and Coop, R. (2007). The Undrained Cyclic Behaviour of a Carbonate Sand, Géotechnique, 57(9), 739-750.

Rodrigues, C. (2003). Geotechnical characterization and study of the geomechanical behaviour of a granitic saprolite from Guarda. PhD Thesis, University of Coimbra. (in Portuguese)

Roscoe, K. H., Schofield, A. N. and Wroth, C. P. (1958). On the Yielding of Soils, Géotechnique, 8(1), 22-53.

Rotta, G.V. (2005). Behaviour of an artificially cemented soil cured under stress in isotropic and triaxial tests. PhD dissertation presented to the Federal University of Rio Grande do Sul, Porto Alegre (in Portuguese)

Rotta, G. V., Consoli, N. C., Prietto, P. D. M., Coop, M. R. and Graham, J. (2003).Isotropic yielding in an artificially cemented soil cured under stress.Géotechnique 53(5), 493-501

Rowe, P.W. (1962). The stress dilatancy relation for static equilibrium of an assembly of particles in contact. Proc. R. Soc. A 269, 500-527

SANRAL (2011). South African Roads Agency Limited. (http://www.nra.co.za/live/content.php?Category_ID=40) Accessed in 5/5/2011

Santamarina, J.C. (2001). Soil Behavior at the Microscale: Particle Forces. Proc. Symp. Soil Behavior and Soft Ground Construction, in honor of Charles C. Ladd – October 2001, MIT.

Schnaid, F., Prietto, P., Consoli, N. (2001). Characterization of cemented sand in triaxial compression. Journal of Geotechnical and Geoenvironmental Engineering, 127(10), 857-868.

Schofield, A. and Wroth, P. (1968). Critical State Soil Mechanics. McGraw-Hill, London, U.K.

Seed, H. B. and Idriss, I. M (1971). Simplified procedures for evaluating soil liquefaction potential. Journal of Soil Mechanics and Foundation Engineering, ASCE, 97, SM9, 1249-1273.

Sharma, S. (2004). Characterisation of cyclic behaviour of calcite cemented calcareous soils. PhD thesis submitted at The University of Western Australia, Perth

Sharma, S. S., and Fahey, M. (2003a), Evaluation of Cyclic Shear Strength of Two Cemented Calcareous Soils, Journal of Geotechnical and Geoenvironmental Engineering, 129(7), 608-618.

Sharma, S. S., and Fahey, M. (2003b), Degradation of Stiffness of Cemented Calcareous Soil in Cyclic Triaxial Tests, Journal of Geotechnical and Geoenvironmental Engineering, 129(7), 619-629.

Sharma, S., and Fahey, M. (2004), Deformation Characteristics of Two Cemented Calcareous Soils, Canadian Geotechnical Journal, 41, 1139-1151.

Sharp R. (1983). Shakedown analyses and the design of pavement under moving surface load. Ph.D. Thesis (University of Sydney)

Sharp R and Booker J. (1984) Shakedown of pavements under moving surface loads, Journal of Transportation Engineering, ASCE, 110(1), 1-14,

Sibley, J.W. and Williams, D.J. (1990). A new filter material for measuring soil suction, Geotechnical Testing Journal, 13(4), 381-384

Shipton, B. (2010). The Mechanics of Transitional Soils. PhD thesis presented to the University of London

Smith, P.R., Jardine, R.J., Hight, D.W. (1992). On the yielding of Bothkennar clay. Géotechnique, 40(2), 257-274

Sympatec (2008).Windox — Operating Instructions Release 5.4.1.0. Clausthal-Zellerfeld.

Tatsuoka, F., Jardine, R.J., Lo Presti, D.C.F., Di Benedetto, H. and Kodaka, T. (1997). Characterising the pre-failure deformation properties of geomaterials. Theme Lecture for Plenary Session No. 1. Proc. 14th Int. Conf. on Soil Mech. and Found. Eng., Hamburg, Vol. 4, pp.2129–2164.

Taylor, D.W. (1948). Fundamentals of Soil Mechanics, Wiley, New York

Taylor, R. N. and Coop, M. R. (1990). Stress path testing of Boom Clay from Mol, Belgium. Proc. Conf. on The Engng Geology of Weak Rock, University of Leeds, pp. 89-98.

Topa Gomes (2009). Elliptic shafts by the sequential vertical excavation method. The Porto metro case study. PhD dissertation presented to the Faculty of Engineering of the University of Porto (in Portuguese)

UIC (2008) - Code 719 R - Earthworks and track bed for railway lines, Union Internationale des Chemins de Fer

Vaughan, P. R. (1988). Characterising the mechanical properties of in-situ residual soil. Proc. 2nd Int. Conf. Geomechanics in Tropical Soils, Singapore Vol.2, pp. 469-487

Vaughan, P. R., Maccarini, M., Mokhtar, S.M. (1988). Indexing the engineering properties of residual soils. Quarterly Journal of Engineering Geology, Vol. 21, pp. 69-84.

Verdugo, R. and Ishihara, K. (1996). The steady state of sandy soils. Soils and Foundations, 36(2), 81–91.

Viana da Fonseca, A. (1988). Geotechnical characterization of a Porto residual soil from granite. Dissertation presented to the faculty of Engineering of the University of Porto to obtain the Master Degree in Structural Engineering (Report 130/88, NGR, LNEC, Lisboa) In Portuguese.

Viana da Fonseca, A. (1996) Geomechanics of Porto residual soil from granite. Project criteria for direct foundations. PhD Thesis. Porto University, In Portuguese

Viana da Fonseca, A. (1998). Identifying the reserve of strength and stiffness characteristics due to cemented structure of a saprolitic soil from granite. The Geotechnics of Hard Soils - Soft Rocks, Evagelista and Picarelli (eds), Balkema, Roterdam

Viana da Fonseca, A. (2003). Characterizing and deriving engineering properties of a saprolitic soil from granite, in Porto. Characterization and Engineering Properties of Natural Soils. Swets and Zeitlinger, Lisse, Eds. Tan et al., pp.1341-1378.

Viana da Fonseca, A. and Almeida e Sousa (2001). At rest coefficient of earth pressure in saprolitic soils from granite. XV ICSMFE, Istambul

Viana da Fonseca, A. and Coutinho, R. (2008). Characterization of residual soils. Paper presented at the Geotechnical and Geophysical Site Characterization, Taipé, Taiwan.

Viana da Fonseca, A., Matos Fernandes, M. and Silva Cardoso, A. (1997). Interpretation of a footing load test on a saprolitic soil from granite. Géotechnique, 47(3), 633-651

Viana da Fonseca, A., Carvalho, J., Ferreira, C., Santos, J.A., Almeida, F., Pereira, E., Feliciano, J., Grade, J. and Oliveira, A. (2006). Characterization of a profile of residual soil from granite combining geological, geophysical and mechanical testing techniques. Geotechnical and Geological Engineering, 24, 1307-1348

Viana da Fonseca, A., Ferreira, C., and Fahey, M. (2009). A Framework Interpreting Bender Element Tests, Combining Time-Domain and Frequency-Domain Methods. Geotechnical Testing Journal, 32(2).

Viana da Fonseca, A. Rocha, J., Tahar, G. (2011). Liquefaction assessment charts based on state and waves' velocities from static and cyclic triaxial tests on "Les Dunes" sands from Algers. 5th International Conference on Earthquake Geotechnical Engineering, Santiago, Chile

Walton, W.H. (1948). Feret's statistical diameter as a measure of particle size. Nature, 162, 329-330

Werkmeister, S. (2003). Permanent Deformatior Behaviour of Unbound Granular Materials in Pavement Constructions, PhD thesis, Technischen Universität Dresden.

Werkmeister, S., Dawson, A. and Wellner, F. (2001), Permanent Deformation Behavior of Granular Materials and the Shakedown Concept, Transportation Research Board, Washington, pp. 75-81

Werkmeister, S., Dawson, A. and Wellner, F. (2004). Pavement Design Model for Unbound Granular Materials, Journal of Transportation Engineering, 130, 665-674.

Werkmeister, S., Dawson, A. and Wellner, F. (2005). Permanent Deformation Behavior of Granular Materials and the Shakedown Concept, International Journal of Road Materials and Pavement Design, 32-52.

Yan, W. M., and Li, X. S. (2011). A model for natural soil with bonds. Géotechnique, 61(2), 95-106.

Yeoh, C.K. and Airey, D.W., (1994). Undrained cyclic loading of a cemented sand. Pre-failure Deformation of geomaterials, pp.95-100, Shibuya, Mitachi and Miura (eds), Balkema, Rotterdam

Yeoh, C.K. and Airey, D.W., (1998). Drained cyclic response of an artificially cemented calcareous sand, Proc. 2nd Int. Symp. on the Géotechnics of Hard Soils - Soft Rocks, Napoli, pp. 935-942.

Yoshinaka, R. and Osada, M. (1995). The Comparison between Dynamic and Static Strength of Soft Sedimentary Rocks, in Rock Foundation, ed. Y. Kiruchi, Balkema,pp. 109-114.

Yu, H. S. (1998). CASM: A Unified state parameter model for clay and sand. International Journal for Numerical and Analytical Methods in Geomechanics, 22, 621-653.

Yu, H. S., Khong, C. and Wang, J. (2007a). A Unified Plasticity Model for Cyclic Behaviour of Clay and Sand, Mechanics research communications, 34, pp.97-114.

Yu, H. S., Tan, S. M. and Schnaid, F. (2007b). A critical state framework for modelling bonded geomaterials. Geomechanics and Geoengineering, 2(1), 61-74.

Zhu, F., J. I. Clark, and M. J. Paulin (1995), Factors affecting at-rest lateral stress in artificially cemented sands, Canadian Geotechnical Journal, 32(2), 195-203.

APPENDIX A: EXPRESSIONS FOR MOULDING PARAMETERS

Before moulding the sample some previous calculations are needed to determine the right quantities of soil, cement and water to be mixed, which are based on the target values of the desired water content, cement content, and dry unit weight. In this appendix the expressions used in those calculations will be presented.

First, three previous notes should be introduced, as reported in chapter 6:

- the water content was defined as a percentage of the dry soil and cement;
- the cement content was defined as a percentage of the dry soil;
- the particle density was calculated by the weighted average of the particle density of the cement and soil in function of the quantities of soil and cement in the mixture following equation (A.1),

$$G_s^{mixture} = \frac{G_s^{soil} \times W_{soil} + G_s^{cement} \times W_{cement}}{W_{soil} + W_{cement}} \quad (A.1)$$

being,

- G_s the particle density (of soil, cement or mixture)
- W the weight (of soil or cement)

The procedure to calculate the amount of soil, cement and water, first assumes a certain mass of dry soil (W_{soil}) a little higher than what is really need for the mixture so as to provide some extra amount for the evaluation of moulding water content. Taking that amount of dry soil, the quantity of cement to introduce in the mixture is the easier to calculate as follows,

$$W_{cement} = cement\ content(\%)/100 \times W_{soil} \quad (A.2)$$

The quantity of water added to the mixture needs to take into account the hygroscopic water content (w_{hig}) already in the soil at the room temperature. The hygroscopic water content changes with the weather depending on the temperature and humidity of the air, and, for that reason, this value is measured periodically, ideally in the day before moulding.

The necessary quantity of water for the mixture, W_{water}^{add} is, thus, the difference between the theoretical water (derived from the water content), W_{water}^{theor}, and the hygroscopic water (W_{water}^{hyg}) so as,

$$W_{water}^{theor} = \left(\frac{w(\%)}{100}\right) \times (W_{soil} + W_{cement}) \quad (A.3)$$

$$W_{water}^{hyg} = (w_{hyg}(\%)/100) \times W_{soil} \quad (A.4)$$

$$W_{water}^{add} = W_{water}^{theor} - W_{water}^{hyg} \quad (A.5)$$

In order to keep the grain size distribution curve in the soil and in the mixture, and because the cement contributed to more fines in the soil, an equal quantity of soil fines equal to the amount of added cement was subtracted from the soil previously to the mixture. Therefore, to calculate the quantity of soil to be weighted for the mixture ($W_{soil}^{measured}$) the hygroscopic water has to be considered as well as the quantity of fines that will be removed, being,

$$W_{soil}^{measured} = (W_{soil} + W_{cement}) \times (1 + w_{hyg}(\%)/100) \quad (A.6)$$

Having the necessary quantities of soil, cement and water, mixing can start as described in section 6.2. The amount introduced in the mould is not the total sum of soil, cement and water ($W_{mixture}$) but the necessary quantity of mixture (W_{sample}) to obtain the target dry unit weight. The remaining mixture is used to measure the moulding water content as reported above.

Finally, some other parameters can be calculated being the most important for the present work the void ratio, porosity, volume of cement and volumetric cement content.

The void ratio can be calculated by the particle unit weight ($\gamma_s^{mixture}$) obtained from the particle density (equation (A.1)) and by the dry unit weight of the mixture (γ_d) according to the well know expression also reported in chapter 7,

$$\gamma_d = \frac{\gamma_s^{mixture}}{1 + e} \quad (A.7)$$

The porosity (n) is related by the void ratio as follows,

$$n = \frac{e}{1 + e} \quad (A.8)$$

The volume of cement (V_{cement}) was calculated from the particle unit weight of the cement (γ_s^{cement}) taking the mass of cement effectively inside the mould ($M_{cement} = W_{cement} * W_{sample}/W_{mixture}$),

$$V_{cement} = \frac{M_{cement}}{\gamma_s^{cement}} * \gamma_w \quad (A.9)$$

being, γ_w the unit weight of the water

The volumetric cement content (C_{iv}) is the ratio between the volume of cement and the volume of the sample (V_{sample}),

$$C_{iv} = \frac{V_{cement}}{V_{sample}} \quad (A.10)$$

APPENDIX B: MOHR CIRCLES EQUATIONS

The Mohr circle that represents the effective stress state in some stage of the test is defined by the maximum and minimum effective principal stresses (σ'_1 and σ'_3). In axial compression triaxial tests, the vertical stress increases while the radial stress remains constant, thus, the principal stresses are the vertical and horizontal stresses, which means that $\sigma'_1 = \sigma'_v$ and $\sigma'_3 = \sigma'_h$.

The center of the circle (a) positioned on the xx axis of the plot (τ, σ') is then,

$$a = \frac{\sigma'_V + \sigma'_H}{2} \quad \text{(B.1)}$$

And the radius (r) of the circle is,

$$r = \frac{\sigma'_V - \sigma'_H}{2} \quad \text{(B.2)}$$

Considering this Mohr circle, the pole is located in point (σ'_h ; 0) in the (τ, σ') plot. It is known that the shear plane failure is represented in a Mohr circle plot by the angle that a line starting from the pole does with the horizontal. Being so, the stresses on the shear plane failure are those which result from the intersection of the Mohr circle with the failure plane observed in the specimen as indicated by the point A on Figure A1.

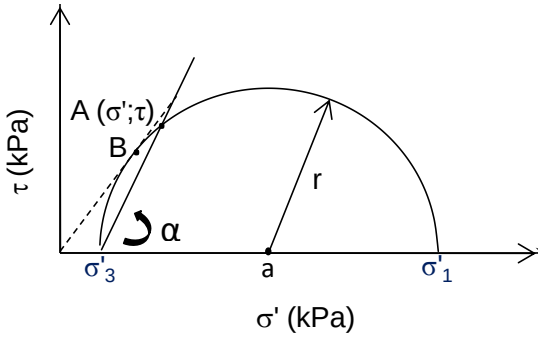

Figure A10.1 Mohr circle analysis

To solve the math part of the problem, the general equation of the circle is considered,

$$(x-a)^2 + (y-b)^2 = r^2 \quad \text{(B.3)}$$

where, (a , b) are the coordinates of the center of the circle and r is the radius.

In the case of the Mohr circles, b is equal to zero, remaining only,

$$(x-a)^2+(y)^2=r^2 \quad \text{(B.4)}$$

Having defined the circle, the other line representative of the shear plane failure has to be expressed. The slope (m) of this line is given by the angle of the shear plane failure observed in the sample (α), being m = tan (α). From this line, not only the slope is known but also the coordinates of the pole (σ'_h; 0) which is one point of this line.

If the general equation of a line is defined as,

$$y = m\,x + c, \quad \text{(B.5)}$$

then, $c = -\tan(\alpha)\,\sigma'_h$

so the equation becomes,

$$y = \tan(\alpha)\,x - \tan(\alpha)\,\sigma'_h = \tan(\alpha)\,(x - \sigma'_h) \quad \text{(B.6)}$$

Replacing this equation on the Mohr circle equation,

$$(x-a)^2+(\tan\alpha\,(x-\sigma'_h))^2=r^2 \quad \text{(B.7)}$$

$$x^2-2ax+a^2+x^2\tan^2\alpha-2x\,\sigma'_h\tan^2\alpha+\sigma'^2_h\tan^2\alpha=r^2 \quad \text{(B.8)}$$

$$x^2\,(1+\tan^2\alpha)+x(-2a-2\,\sigma'_h\tan^2\alpha)+a^2+\sigma'^2_h\tan^2\alpha-r^2=0 \quad \text{(B.9)}$$

which means that a 2nd degree equation has to be solved by the well known solution:

If an equation is $Ax^2 + Bx + C = 0$, then $x=\frac{-B\pm\sqrt{B^2-4AC}}{2A}$

Having obtained x (which will be in fact σ'), y can be easily determined by the equation of the line (equation (B.6)), and so the stresses on the plane τ and σ' are now calculated.

To draw the circles in Excel, y values are calculated through (B.10) equation given any x values,

$$(x-a)^2+(y)^2=r^2 \quad \text{(B.10)}$$

$y^2 = r^2-(x+a)^2$

$y = \sqrt{(r^2-(x-a)^2)}$

APPENDIX C: CRITICAL STATE *M* PARAMETER

The Mohr-Coulomb envelope can be defined by the following equation,

$$\boldsymbol{\tau_f = \sigma_f \tan(\emptyset') + c'} \quad \text{(C.1)}$$

Considering a Mohr circle defined by the maximum and minimum effective principal stresses, respectively σ'_{1f} and σ'_{3f}, that represent the stress state at some point at failure. The stresses (τ_f and σ_f') at the failure plane in that point result from the intersection of the Mohr-Coulomb envelope with the Mohr circle and can be written as function of the principal stresses as following:

$$\boldsymbol{\tau_f = \frac{\sigma'_{1f} - \sigma'_{3f}}{2} \cos \emptyset'} \quad \text{(C.2)}$$

$$\boldsymbol{\sigma'_f = \frac{\sigma'_{1f} + \sigma'_{3f}}{2} - \frac{\sigma'_{1f} - \sigma'_{3f}}{2} \sin \emptyset'} \quad \text{(C.3)}$$

On the other hand, the principal stresses can be easily expressed in function of the deviatoric stress q and mean effective stress p',

$$\boldsymbol{\sigma'_1 = \frac{2}{3} q + p'} \quad \text{(C.4)}$$

$$\boldsymbol{\sigma'_3 = p' - \frac{1}{3} q} \quad \text{(C.5)}$$

So, considering that q_f and p_f' are respectively the deviatoric stress and the mean effective stress at failure, equations (C.2) and (C.3) can be rewritten replacing σ'_{1f} and σ'_{3f} by equations (C.4) and (C.5) becoming,

$$\boldsymbol{\tau_f = \frac{q_f}{2} \cos \emptyset'} \quad \text{(C.6)}$$

$$\boldsymbol{\sigma'_f = \frac{q_f}{6} + p_f' - \frac{q_f}{2} \sin \emptyset'} \quad \text{(C.7)}$$

Finally, equations (C.6) and (C.7) can be applied on the Mohr-Coulomb envelope (equation (C.1)).

$$\frac{q_f}{2}\cos\emptyset' = (\frac{q_f}{6} + \mathrm{p'_f} - \frac{q_f}{2}\sin\emptyset')\tan\emptyset' + \mathrm{c'}$$

$$\frac{q_f}{2}\cos\emptyset' = (\frac{q_f}{6} + \mathrm{p'_f})\ \tan\emptyset' - \frac{q_f}{2}\frac{\sin^2\emptyset'}{\cos\emptyset'} + \mathrm{c'}$$

$$q_f\left(\frac{\cos\emptyset'}{2} - \frac{\tan\emptyset'}{6} + \frac{1}{2}\frac{\sin^2\emptyset'}{\cos\emptyset'}\right) = \mathrm{p'_f}\tan\emptyset' + c'$$

$$q_f\left(\frac{\cos^2\emptyset'}{2\cos\emptyset'} - \frac{\sin\emptyset'}{6\cos\emptyset'} + \frac{1}{2}\frac{\sin^2\emptyset'}{\cos\emptyset'}\right) = \mathrm{p'_f}\tan\emptyset' + c'$$

$$q_f\left(\frac{0.5\cos^2\emptyset' - \frac{1}{6}\sin\emptyset' + 0.5\sin^2\emptyset'}{\cos\emptyset'}\right) = \mathrm{p'_f}\tan\emptyset' + c'$$

$$\frac{q_f}{2}\left(\frac{\cos^2\emptyset' + \sin^2\emptyset' - \frac{1}{3}\sin\emptyset'}{\cos\emptyset'}\right) = \mathrm{p'_f}\tan\emptyset' + c'$$

$$\frac{q_f}{2}\left(\frac{1 - \frac{1}{3}\sin\emptyset'}{\cos\emptyset'}\right) = \mathrm{p'_f}\tan\emptyset' + c'$$

$$q_f = \mathrm{p'_f}\left(2\tan\emptyset'\frac{\cos\emptyset'}{1 - \frac{1}{3}\sin\emptyset'}\right) + \frac{2\cos\emptyset'}{1 - \frac{1}{3}\sin\emptyset'}c'$$

$$q_f = \mathrm{p'_f}\left(\frac{2\,\mathrm{sen}\,\emptyset'}{1 - \frac{1}{3}\sin\emptyset'}\right) + \frac{2\cos\emptyset'}{1 - \frac{1}{3}\sin\emptyset'}c'$$

After a few developments and multiplying all terms by 3, the equation of the strength envelope in terms of q' and p' is obtained.

$$\boldsymbol{q_f = \frac{6}{3 - \sin\emptyset'}(\mathrm{sen}\,\emptyset'\mathbf{p'_f} + cos\,\emptyset' c')} \qquad \text{(C.8)}$$

This line has a gradient M defined in triaxial compression as,

$$\boldsymbol{M = \frac{6\,\mathrm{sen}\,\emptyset'}{3 - \sin\emptyset'}} \qquad \text{(C.9)}$$

APPENDIX D: CEMENTED CASM EXPRESSION FOR P'$_S$

Cemented CASM model has a very particular way of defining the normal compression line of the uncemented material, herein called intrinsic compression line (ICL). The slope of the ICL (λ) is assumed to be equal to the critical state line, and it is introduced in the model as a parameter, but to define the line another point is needed usually introduced by N, the specific volume at p'=1kPa. However, in this model, N is not directly introduced as a parameter but it is computed internally through the relationship between p'$_s$ and e_0, as following:

$$p_s = exp\left(\frac{N - (1 + e_{0t}) - k\ln(p'_{0t})}{(\lambda - k)}\right) \tag{D.1}$$

where,

- N, λ and k have the meaning expressed in chapter 9 and illustrated in Figure C.1;
- e_{0t} and p'$_{0t}$ are the current void ratio and mean effective stress of the soil in a certain state (Figure C.1);

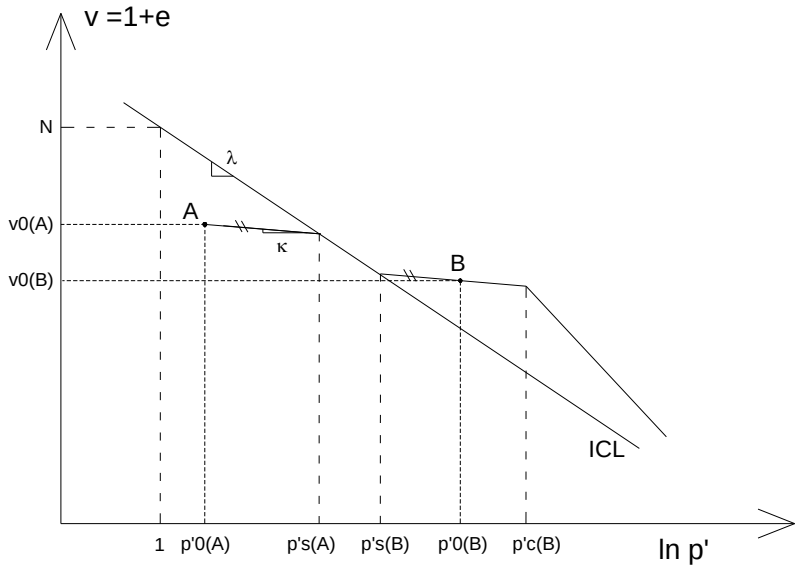

Figure C.1 Definition of p'$_{0t}$ and e_{0t}

The p'$_s$ is the value of p' derived from the intersection of the ICL and the swelling line that passes in the current point whose state is defined by (e_0; p'$_{0t}$) obtaining expression (D.1). The equation of the ICL is well know,

$$v = N - \lambda \ln p' \tag{D.2}$$

The swelling line assumes a generic form,

$$v = v_k - k \ln p' \tag{D.3}$$

where v_k is the specific volume at p'=1 kPa

In order to obtain the swelling line that passes in the point (e_0; p'_{0t}) the parameter v_k has to be computed replacing v and p' by ($1+e_{0t}$) and (p'_{0t}) as follows,

$$1 + e_{0t} = v_k - k \ln p'_{0t} \tag{D.4}$$

$$v_k = 1 + e_0 + k \ln p'_0$$

then, the swelling lines equation becomes.

$$v = 1 + e_{0t} + k \ln p'_{0t} - k \ln p' \tag{D.5}$$

The intersection of the ICL and the swelling line can be performed by equalizing them, recovering equation (D.1),

$$N - \lambda \ln p_s' = 1 + e_{0t} + k \ln p'_{0t} - k \ln p_s' \tag{D.6}$$

$$\lambda \ln p'_s + k \ln p_s' = -(1 + e_{0t}) - k \ln p'_{0t} + N$$

$$\ln p_s'(\lambda - k) = N - (1 + e_{0t}) - k \ln p'_{0t}$$

$$p'_s = \exp\left(\frac{N - (1 + e_{0t}) - k \ln p'_{0t}}{(\lambda - k)}\right)$$